DISSERTATION

PREPARATION, REGIOSELECTIVE CHEMISTRY, AND ELECTRONIC PROPERTIES OF

PERFLUOROALKYLFULLERENES

Submitted by

James B. Whitaker

Department of Chemistry

In partial fulfillment of the requirements

For the Degree of Doctor of Philosophy

Colorado State University

Fort Collins, Colorado

Fall 2013

Doctoral Committee:

    Advisor: Steven H. Strauss

    Eugene Chen
    Rick Finke
    Bob Williams
    John Ridley

ABSTRACT

PREPARATION, REGIOSELECTIVE CHEMISTRY, AND ELECTRONIC PROPERTIES OF

PERFLUOROALKYLFULLERENES

A systematic study of how various reaction parameters affect the product distribution of gas-solid reactions was carried out in a new reactor of local design. These reactions involve the trifluoromethylation of C_{60}, C_{70}, and the endohedral metallofullerenes $Sc_3N@C_{80}$ and $Y_3N@C_{80}$; and in particular, the reactions were optimized to favor $C_{60}(CF_3)_2$ and $C_{60}(CF_3)_4$. A new solution phase homogeneous perfluoroalkylation method was used to prepare a series of $1,7$-$C_{60}(R_F)_2$ compounds with different R_F chain lengths and branching patterns. A range of analytical methods including ^{19}F NMR and UV-vis spectroscopy, APCI mass spectrometry, and X-ray crystallography were used to structurally characterize the compounds. Cyclic voltammetry, DFT E(LUMO) calculations, and gas phase electron affinity (EA) measurements were used to determine the substituent effect of the R_F groups. The results conclusively showed that the solution phase $E_{1/2}$, calculated E(LUMO), and EA values— that are typically assumed to be correlated for a series of electron acceptors— are not always correlated. Several highly efficient and selective methods were developed for the further functionalization of selected trifluoromethyl fullerenes (TMFs). These new functionalized TMFs were structurally characterized using the aforementioned analytical techniques and the X-ray crystal structures of five new derivatized TMFs were determined. Analysis of the how these newly derivatized TMFs pack in a crystalline solid revealed fullerene density values that were in general twice that of reported fullerenes that pack in the same motifs. These derivatized TMFs also exhibited extended

networks of short C⋯C distances between fullerene cages of adjacent molecules that has been correlated to increased free charge carrier motilities in organic photovoltaic device active layers. The solution phase $E_{1/2}$ values of the most commonly used fullerene derivatives in OPV devices were measured under carefully controlled conditions and revealed that poor reporting of electrochemical conditions, mistakes interpreting electrochemical data, and fullerene impurities have combined to cause significant confusion about the reported electrochemical values in the literature. A preliminary study of 32 OPV devices fabricated with active layers containing perfluoroalkylfullerenes (PFAFs) indicated that (i) PFAFs can function as suitable electron acceptors in OPVs, and (ii) that a more detailed study examining the complex electronic interplay between the fullerene electron acceptor and polymer donor is warranted.

ACKNOWLEDGEMENTS

TABLE OF CONTENTS

LIST OF COMMONLY USED ABBREVIATIONS

abbrev.	full name
PFAF	Perfluoroalkylfullerene
TMF	Trifluoromethylfullerene
OPV	Organic Photovoltaic
HPLC	High Pressure Liquid Chromatography
NMR	Nuclear Magnetic Resonence Spectroscopy
UV-vis	Ultraviolet-visible Spectroscopy
APCI-MS	Atmospheric Pressure Chemical Ionization Mass Spectrometry
oDCB	*ortho*-Dichlorbenzene
DCM	Dichloromethane
EMF	Endohedral Metallofullerene
ICMA	Indene-C_{60} Mono-adduct
ICBA	Indene-C_{60} Bis-adduct
ICTA	Indene-C_{60} Tris-adduct
V_{oc}	Open Circuit Voltage
J_{sc}	Short Circuit Current Density
PCBM	Phenyl-C_{60}-Butyric Acid Methyl Ester
CV	Cyclic Voltammetry
LUMO	Lowest Unoccupied Molecular Orbital
DFT	Density Functional Theory
GTGS	Gradient Temperature Gas-Solid Reactor

Chapter 1

Synthesis and Functionalization of Perfluoroalkylfullerenes

Introduction

Due to the combination of high thermal stabilities,[1] reversible electrochemical behavior in solution,[2] and a broad range of first reduction potentials (0.73 V in the case of $C_{60}(CF_3)_n$ derivatives), perfluoroalkyl fullerenes (PFAFs) show considerable promise for practical applications in organic electronics.[2,3] Functionalization of PFAFs has also been shown to further tune their properties and allow complex molecular systems such as electron donor-acceptor diads.[4,5] However, despite the large number of publications on different synthetic methods for PFAF preparation, there are very few examples[6,7] that discuss the effects of various reaction parameters on the product distribution. The most common method of PFAF syntheses described in the literature relies on heterogeneous, high-temperature reactions between fullerenes and R_F precursors (e.g., $R_F I$ or $AgOOCCF_3$). The vast majority of these reported synthetic procedures yield mostly PFAFs with a higher number of substituents (six and more); the efficient large-scale preparation of PFAFs with two and four R_F groups has not been achieved. Their largely intact π-systems as well as their different physical, chemical, and electrochemical properties makes PFAFs with only two or four R_F groups an intriguing series of compounds that may be used to

elucidate basic chemical knowledge (see Chapter 2) as well as study how minor changes in molecular structure (i.e., the number and position of R_F groups) affect organic electronic devices such as organic photovoltaics (see Chapter 3).

Therefore, this chapter will describe the systematic study of how various reaction parameters affect the product distribution in two new fullerene perfluoroalkylation methods; a particular goal of these studies is the optimization of the reaction conditions to prepare fullerenes with lower numbers of R_F groups. In addition to perfluoroalkylation of C_{60} and C_{70}, the effect of various reaction parameters on the trifluoromethylation of endohedral metallofullerenes (e.g., fullerenes with metal atoms inside the cage) will be examined. This chapter will go on to describe several very efficient (>95%) and selective chemical methods of PFAF functionalization that resulted in the significant alteration of physical, chemical and electrochemical properties of the PFAFs.

1.1. Heterogenous Trifluoromethylation

1.1.1. Literature Methods of Fullerene Trifluoromethylation: In general, trifluoromethylation of fullerenes is not a selective process. To date, TMF preparation has been achieved exclusively by radical addition reactions of trifluoromethyl radicals to bare cage fullerenes that, in most cases, result in complex mixtures of products that vary in both molecular composition as well as the addition pattern of CF_3 addends within a given composition. Generation of $CF_3\cdot$ radicals has been achieved by either thermolysis of a suitable precursor or by photolysis of a benzene solution of C_{60} and CF_3I.[1,8-16] Photolysis is performed on a benzene

solution of C_{60} in the presence of CF_3I gas; however, this method is less desirable due to the formation of various $C_{60}(CF_3)_nH_m$ species present in the crude reaction mixture.[17] The more desirable method of radical formation involves heating suitable radical precursors: these are mainly trifluoroacetates of transition metals[7,11,12,15,18] and trifluoromethyl iodide. [1,8-10,13,14] In general, when salts of trifluoroacetates are used as the $CF_3\cdot$ source, the resulting crude product mixture contains a complex mixture of over 60 different substituted fullerenes that include numerous $C_{60}(CF_3)_nH_m$ compounds. Typically, the crude reaction mixture is sublimed at high temperature (ca. 350 to 550 °C) to remove the $C_{60}(CF_3)_nH_m$ derivatives (presumably by the decomposition). In most cases several sublimation cycles are necessary to remove all unwanted $C_{60}(CF_3)_nH_m$ compounds. However, due to the multiple sublimation cycles, the yield of TMFs is greatly diminished.

To avoid the formation of unwanted $C_{60}(CF_3)_nH_m$ compounds and concomitantly improve the yield of TMFs based on C_{60}, CF_3I gas is used as a radical source in a solvent free hot tube reactor[19] or in a sealed glass amoule.[18] Both methods yield a manageable mixture of products that may be separated into compositionally and isomerically pure products by HPLC. A major advantage of using CF_3I over trifluoroacetates such as $AgOOCCF_3$ is that due to the absence $C_{60}(CF_3)_nH_m$ products, additional sublimation step(s) are not necessary prior to HPLC separation.

In both methods that use CF_3I (hot tube reactor and sealed glass ampoule), only a limited number of reaction parameters can be adjusted thus making optimization and controlling the extent of trifluoromethylation very limited. For example, in the hot tube reactor, only the temperature and the size of the reactive zone can be changed. Likewise, in sealed glass ampoules, due to the presence of liquefied CF_3I, there is not a significant change of pressure of the trifluoromethylation agent. Moreover, scaling up sealed glass ampoules is challenging since a

small diameter of glass tube is required in order for the ampoule to have a sufficient strength to withstand the high internal pressure. This small diameter obviously limits the capacity of the reactor. Similarly, scaling up the hot tube method is not trivial since changing the diameter of the hot tube will significantly change both the heat profile across the tube and the residence time.

Therefore, neither the hot tube reactor nor sealed glass ampoules are well suited for precise and reliable control/tuning of multiple reaction parameters in a wide experimental range or for scaling up the reaction. To study fullerene trifluoromethylation in detail and achieve a deeper understanding of the process, it is advantageous to change several parameters (gas pressure, reaction temperature, hot zone geometry) in the widest possible range so that the effects of these parameters on the distribution of TMF products can be studied independently, ultimately leading to an optimized synthetic method for the large scale production of various TMFs.

1.1.2. Gradient Temperature Gas Solid Reactor (GTGS): To overcome the limitations of the earlier experimental fullerene trifluoromethylation approaches (hot tube reactions and sealed glass ampoules), namely poor control of reaction parameters and difficulty in scaling up, a gradient-temperature gas-solid (GTGS) reactor shown in figure 1.2 was designed by Dr. Igor Kuvychko and was subsequently studied in this work.

The GTGS reactor design allows for numerous reaction parameters to be easily adjusted. A wide range of CF_3 pressures ranging from 0.5 torr up to 820 torr can be maintained during the course of any given reaction. The reactor vessel is made from fused silica that can he heated to temperatures in excess of 700 °C. The large internal diameter of the reaction vessel (23 mm) allows for larger amounts (> 100 mg) of starting material to be used in each reaction. A water-cooled, cold-finger condenser can be positioned within the reactor vessel allowing for the

geometry of the reactive zone to be changed. All of these reaction parameters, and others such as the size of refractory brick and presence of copper metal for example, were explored and optimized during this work.

In general, heterogeneous perfluoroalkyl radical addition to the fullerene presumably begins with the formation of R_F radicals. Once R_F radicals are present, several elementary steps probably take place: (i) sublimation of C_{60}; (ii) perfluoroalklation of the surface layer of solid C_{60} (and further perfluoroalkylation of so-formed solid PFAFs); (iii) sublimation of PFAFs from the hot zone; (iv) perfluoroalkylation of the subliming C_{60} and PFAFs in the gas phase; (v) condensation of C_{60} and PFAFs from the gas phase into the cold zone; and (vi) condensation of C_{60} and PFAFs back into the hot zone.

1.1.3. Experimental Design and Characterization: Experiments were designed to test each reactor parameter independently (e.g., temperature, pressure of CF_3I, presence of Cu metal, reactor geometry/configuration, duration of reaction, type of starting material, and reaction scale). As such, in each experiment, only one parameter was adjusted while keeping the others the same; therefore, any differences in the product distribution can be attributed to the parameter that was being investigated. In each experiment, with the exception of when the reaction scale and the starting material were varied, small samples in the range of 3.9 to 4.9 mg of finely ground C_{60} were placed in a quartz thimble that was subsequently evacuated. After the reaction, all soluble material was dissolved in toluene and placed in a tared glass vial. The toluene was removed via Nitrogen stream and the mass of the crude material was determined. The primary characterization method of determining the crude product distribution was done by HPLC. Although HPLC chromatograms do not offer any inherent information regarding the extent of

addition and the addition patterns themselves, correlation of retention times to known TMF isomers and compositions in a given eluent and stationary phase allows for general conclusions about the product distribution to be made, specifically the extent of substitution and conversion of C_{60}. It is possible to extract information about the extent of CF_3 substitution from the HPLC chromatogram of the crude products because, in general, the more substituted fullerenes have a shorter retention time, while the less substituted fullerenes have a longer retention time. Bare cage C_{60} typically elutes last with a retention time of ca. 8 min under the specific conditions employed. Due to the short retention times of TMFs with the high likelihood of co-eluting compounds with this mobile phase, no assumptions will be made about the specific isomers formed during each experiment but will be limited to the extent of substitution and the conversion of C_{60}.

It was imperative to demonstrate good fullerene trifluoromethylation reproducibility to confirm that the differences between each experiment could be attributed to the differences in reaction parameters and not to irreproducibility in the GTGS reactor. Several trifluoromethylation experiments were carried out under the exact same conditions; in every case the composition of the crude material was identical. There were only slight variations observed for the extent of conversion between identical experiments. This observation is presumably due to slight variations in fullerene distribution across the bottom of the reactor. Additionally, after the reactions were complete, a small portion of material was found to be insoluble in toluene. This material was however soluble in 1,2-dichlorobenzene producing a characteristic purple color indicating unreacted C_{60} (HPLC analysis of this fraction confirmed that only C_{60} was present). This indicates that C_{60} did not decompose or polymerize, but rather underwent a morphological change that drastically decreased its solubility in select solvents. The implications

of this observation are that the apparent conversion of C_{60} estimated by HPLC might be artificially high and might be slightly variable between experimental runs.

1.1.4. Effect of CF$_3$I Pressure on TMF Distribution: A series of 6 experiments were conducted in order to determine what effect varying the pressure form 5 torr up to 410 torr of CF$_3$I gas has on the extent of substitution as well as overall conversion of C_{60}. All other experimental parameters were identical; the reaction times were all 30 min, the reaction temperature was set to 500 ± 5 °C (the temperature of the reaction inside the thimble will be used for the remainder of this work; the actual furnace temperature was 600 ± 5 °C), and a 10 mm spacer between the furnace and the cold plate was used. During the course of the experiment, the drop of CF$_3$I pressure was negligible. The 5 pressures used were 5, 15, 45, 135, and 410 torr. The HPLC chromatograms of each crude reaction mixture were directly compared to one another, shown in Figure 1.2 and clearly indicate that the pressure has a strong effect on the extent of substitution. The reactions carried out at the lower pressures of 5 and 15 torr are mostly comprised of $C_{60}(CF_3)_2$, $C_{60}(CF_3)_4$, and unreacted C_{60}. As the pressure increases, so too does the extent of substitution and the conversion of C_{60}.

These experimental observations are consistent with the idea that as the pressure of CF$_3$I gas increases, the number of reactive $CF_3\cdot$ does too. However, as the pressure of gas inside the reactor increases, so does the convection and thus the transport of C_{60} and TMFs out of the reactive zone. These two factors are working against one another with the increased number of radicals favoring a higher number of substitutions, while the increased convection/ lower residence time leads to lower numbers of substitution. It is clear, however, from the HPLC traces

7

that the dominant factor that is affecting the extent of trifluoromethylation is the number of radicals present, while the increased convection is a minor factor.

1.1.5. Effect of Temperature on TMF Distribution: Two different temperatures were used to determine how the temperature affected the product distribution of heterogeneous fullerene trifluoromethylation in the GTGS reactor. Two series of experiments were set up with the only difference between them being the reaction temperatures, which were 450 ± 5 °C for one series and 500 ± 5 °C for the other. For both series of experiments 6 pressures ranging from 5 torr up to 410 torr were used while all other parameters were held constant. Comparison of the HPLC chromatograms, shown in Figure 1.3, clearly demonstrates that increasing the temperature increases the conversion of C_{60} as well as the extent of substitution. This observation is presumably due to the higher temperature resulting in a greater concentration of $CF_3 \cdot$ in the reactive zone of the reactor as well as the increased sublimation rate of C_{60}. An additional series of experiments were conducted using the same pressures only at an elevated temperature of 570 ± 5 °C. Analysis of the resulting HPLC chromatograms indicates a lower conversion of C_{60} compared to the reaction conducted at the same pressure but at 500 ± 5 °C. Additionally, the higher temperature reaction led to slightly lower numbers of substitution. We suggest that this result is due to increased convection and transport of C_{60} and the TMFs out of the reactive zone leading to lower conversion and lower numbers of substitution. It is likely that increasing the temperature even higher would tilt the balance between high concentration of $CF_3 \cdot$ vs. transport out of the reactive zone, and therefore towards the latter resulting in low conversion and low numbers of substitution. Moreover, at temperatures much greater than 570 °C, C_{60} starts to undergo a morphological change and decomposition to insoluble carbonaceous material that

leads to a greatly diminished conversion. When temperatures lower than 500 °C are used, the reaction becomes prohibitively slow and the conversion is extremely low.

1.1.6. Size of the Reactive Zone: The length of the reactive or hot zone can be easily increased by insertion of a heat insulating brick in between the furnace and the cold plate. A series of two experiments were conducted using the same pressure range and temperature; for one series of experiments a large insulating brick (50 mm) was put in place while in the other series of experiments a small brick (10 mm) was used. As with previous experiments, all reaction parameters were kept constant for all experiments while 4 different pressures of CF_3I gas were used in 4 different reactions. Comparison of the HPLC chromatograms from these 4 experiments that were done with the corresponding experiments that were performed with the small heat insulating brick can be seen in Figure 1.4. The differences are more marked at the higher pressures of CF_3I gas of 15 and 45 torr and indicate a correlation between the larger reactive zone and a greater extent of substitution and conversion. The experiment with a CF_3I pressure of >45 torr was not conducted because the resulting product distribution would most likely have been all highly substituted cages with 10 and 12 CF_3 groups. This result is intuitively easy to understand: the larger reactive zone leads to C_{60} spending more time in the presence of reactive $CF_3\cdot$, ultimately increasing the extent of substitution.

Additional experiments were carried out with the large hot zone with each pressure of CF_3I only at higher and lower temperatures of 550 ± 5 °C and 450 ± 5 °C respectively. The HPLC chromatograms of three experiments conducted at the three different temperatures all with a CF_3I pressure of 45 torr are presented in a waterfall plot in Figure 1.5. It is evident from this plot that at the lowest temperature the conversion is poor with only $C_{60}(CF_3)_{2,4}$ present.

Conversion improves and the product distribution widens as the temperature is increased to 500 ± 5 °C. However, as the temperature is increased further, the conversion decreases and the product distribution becomes slightly more narrow. This trend can be explained as a function of the interplay between two competing factors: residence time in the hot zone and concentration of $CF_3\cdot$. As the temperature increases the concentration of $CF_3\cdot$ increases; however, the residence time decreases due to increased convection.

1.1.7. Presence of Copper Metal: Copper has been used to scavenge iodine and facilitate the dissociation of perfluoroalkyl iodides; however, it had not been previously used in a heterogeneous trifluromethylation of C_{60}.[20] Control experiments were conducted prior to employing Cu metal with a fullerene sample. It was determined by the visible formation of I_2 crystals on the side of the reactor that at 45 torr, with or without C_{60}, that CF_3I undergoes decomposition at ca. 450 °C. However, when an identical experiment was conducted, but now with Cu metal placed inside of the reactor, the formation of copper(I) iodide as a white solid was detectable at a lower temperature of 320 °C. This white powder was confirmed to be CuI by adding a large excess of aqueous ammonia; the resulting solution had a characteristic blue color indicating the presence of the $[Cu(NH_3)_4]^{2+}\cdot 4H_2O$ complex. A series of experiments were performed where C_{60} was mixed with a large excess of copper powder (ca. 300 mg) and allowed to react with various pressures of CF_3I gas in the GTGS reactor; as depicted in Figure 1.6, despite a very low reaction temperature of ca. 410 ± 5 °C, a high conversion of C_{60} was achieved. In contrast, a control experiment without copper powder, that was carried out under otherwise identical conditions, showed no signs of TMF formation. Even when the temperature is increased to 450± 5 °C the conversion of C_{60} in the absence of copper is very low. In addition

to improving the conversion, the crude product composition shifts toward a greater extent of fullerene substitution with up to 14 CF_3 groups on the cage as determined by APCI-MS. This result is likely due to the compounding effects of two factors: (1) an increased number of $CF_3\cdot$ due to the Cu promoter, and (2) the lower temperature resulting in slower transport of material out of the reactive zone that leads to higher numbers of substitution. Two additional trifluoromethylation experiments with copper metal were performed with CF_3I pressures of 5 and 15 torr in order to examine the effect of increasing the temperature to 500 ± 5 °C. In both cases the conversion was excellent and was comparable to the experiment performed at a lower temperature. Likewise, the product distributions were all similar.

1.1.8. Reaction Scale: One of the major disadvantages of previous fullerene trifluoromethylation methods is the lack of scalability. To determine if the conversion and product distribution was maintained during C_{60} trifluoromethylation using the GTGS reactor while scaling the reaction up, 3 experiments were setup with all reaction parameters held constant with the amount of starting material used increasing from 4.0 mg up to 10.8 and then up to 40.9 mg. The resulting HPLC chromatograms were normalized to the unreacted C_{60} peak so that the conversion could be directly compared. As can be seen in Figure 1.7, the conversion decreases as the amount of C_{60} starting material increases. During these large scale experiments a large amount of iodine vapor was present in the reactive zone and a large amount of I_2 crystals formed in the cold zone of the reactor. An experiment was conducted to determine if the presence of the iodine vapor was inhibiting the reaction and causing the low yield. When all the reaction parameters were held constant, with the exception of a liquid-cooled, cold-finger condenser was used in one reaction and not the other, the conversion was markedly different.

11

The cold finger visually suppressed the amount of I_2 vapors in the reactive zone and the conversion of C_{60} (based on the integrated intensities of the two reactions) showed that the reaction with the cold finger had a much greater conversion of 52% compared to 29% conversion without the cold finger in place. Determination of the conversion based on the integrated intensity can be seen in figure 1.8 and is only a rough approximation.

1.1.9. Reaction Time: One of the simplest reaction parameters to control is reaction time. In the GTGS reactor, where products condense in the cold zone since the concentration of $CF_3\cdot$ is very low, it should follow that as the reaction time increases so too should the conversion but the product distribution should be unaffected. To confirm this hypothesis, we set up a series of 5 experiments where we varied the pressure of CF_3I gas from 5 torr up to 135 torr and allowed the reaction to proceed for 90 min. We then compared the HPLC traces of the crude products from these 5 experiments to a different series of 5 experiments that were conducted at the same pressure and temperature, but where the reaction in these 5 experiments was stopped after 30 min. The results shown in Figure 1.9 clearly support our hypothesis that only the conversion is increased with the longer reaction times while the product distribution remains largely unaffected. Over the course of the 90 min reactions, the pressure of CF_3I gas did not significantly drop. However, in subsequent reactions when the time and scale were increased further in reactions that took place for >10 hours, a significant pressure drop was seen and had to be accounted for by periodically adding CF_3I gas to keep the pressure within 10 to 15 torr of the starting pressure. In every GTGS reaction conducted, some material that was not soluble in toluene was always present at the end of every reaction. However, this material was soluble in *o*-dichlorobenzene after 30 minutes of sonication. Analysis of this material by HPLC showed that

it was unreacted C_{60} suggesting that the C_{60} underwent a morphological change that greatly lowered its solubility in certain solvents. Due to this leftover material, no matter how long the reactions were allowed to proceed, quantitative conversion of C_{60} was never achieved. This leftover C_{60} could however be recycled once it had been solubilized in *o*-dichlorobenzene. In order to ensure that all solvent had been removed prior to trifluoromethylation, the recycled C_{60} was loaded into the GTGS reactor and heated with a heat gun under dynamic vacuum until the C_{60} started to sublime and condense in the cold zone of the reactor. After sublimation, the reactor was charged with CF_3I and the furnace was raised into position and the reaction was initiated. There was no noticeable decrease in conversion or change in product distribution when recycled C_{60} was used as opposed to fresh C_{60} from a manufacturer.

1.1.10. Trifluoromethylation Reactions with C_{70}: Two separate series of trifluoromethylation reactions were conducted with C_{70} as the starting material at two temperatures: 500 ±5 °C and 570 ±5 °C. For each temperature, 6 different pressures of CF_3I gas were used ranging from 5 torr up to 410 torr. Overall, C_{70} exhibits the same trends as C_{60} does only it is slightly less reactive. Unlike C_{60}, increasing the temperature from 500 °C to 570 °C does not greatly increase the conversion of C_{70} as was seen with C_{60}. If an even greater temperature than 570 °C is used, significant decomposition occurs resulting in very low yields and a large amount of insoluble carbonaceous material left over. As was seen with the trifluoromethylation of fullerene extract, Figure 1.12 shows that C_{70} is slightly less reactive than C_{60} under identical conditions. Direct comparison of these HPLC traces can give an approximate idea as to the relative reactivity of the two substrates; however, it is important to remember that C_{70} has a larger extinction coefficient than C_{60} and therefore the relative amounts of unreacted

C_{70} is artificially inflated when compared to unreacted C_{60}. Comparison within each HPLC trace clearly shows that the reaction with C_{60} had a greater conversion than the reaction with C_{70}. This observation can be explained by the presence of less reactive triple hexagon junctions around the equator of C_{70}. The sp^2 carbon atom where three hexagons meet is inherently less planer than the sp^2 carbon atom located where two hexagons and a pentagon meet. Due to the increased cage strain if one of these planer carbon atoms were to become a more tetrahedral sp^3 hybridized carbon, the carbon atoms located at triple hexagon junctions are less reactive toward radical addition. As shown in Figure 1.14, C_{60} does not have any triple hexagon junctions while C_{70} has 10 carbon atoms that lie at triple hexagon junctions; this difference explains the reactivity difference between the two substrates.

Overall, C_{70} can be trifluoromethylated in the GTGS reactor and $C_{70}(CF_3)_2$ can be selectively targeted. The conversion is poor but the C_{70} can be recycled. Additional experiments should be carried out to examine what effect the presence of copper metal has on the product distribution as well as the overall conversion.

1.1.11. Trifluoromethylation of Fullerene Extract: A less expensive alternative to using 99.98% C_{60} (which averages about $60 per gram) is using fullerene extract, (which is roughly $10 per gram). Fullerene extract is material that contains approximately 80% C_{60}, 20% C_{70}, and trace amounts of higher fullerenes. This material also contains trace amounts of solvent used to extract the soluble fullerenes from the carbonaceous soot that is produced during preparation with an arc discharge reactor.

Due to the solvent present in fullerene extract, it proved necessary to first heat the fullerene extract under dynamic vacuum until it starts to sublime. If this heating step was

skipped, then the conversion dropped to almost nothing. However, when the extract was heated first to remove the occluded solvent, then the conversion was the same as it is when 99.98% C_{60} was used.

Due to the lower reactivity of C_{70}, fullerene extract was used for the large scale preparation of $C_{60}(CF_3)_n$ where $n = 2$ and 4. The low pressure of CF_3I used for the selective synthesis of $C_{60}(CF_3)_{2,4}$ is insufficient to produce any $C_{70}(CF_3)_n$ compounds and, therefore, the HPLC isolation of all trifluoromethylatied C_{60} isomers was straight forward. In addition, unreacted C_{70} was isolated and could be recycled in subsequent C_{70} trifluoromethylation reactions. Complications may arise when higher pressures of CF_3I gas are used to prepare $C_{60}(CF_3)_n$, where $n > 4$, due to the formation of trifluoromethylated C_{70} compounds that co-elute with $C_{60}(CF_3)_n$, where $n > 4$, compounds under most HPLC conditions. This co-elution of C_{60} and C_{70} trifluoromethylated products makes HPLC isolation of pure $C_{60}(CF_3)_n$ isomers difficult. Overall, due to the lower cost, using fullerene extract is an attractive starting material for large scale preparation of $C_{60}(CF_3)_{2,4}$. Although not experimentally confirmed, fullerene extract may be used for preparation of more highly substituted $C_{60}(CF_3)_n$ compounds, but would involve a more demanding HPLC separation.

1.1.12. Trifluoromethylation of Endohedral Metallofullerenes: A total of 9 GTGS trifluoromethylation reactions were conducted with $Sc_3N@C_{80}$ that was acquired from Professor Stevenson at University of Southern Mississippi to determine how the reaction temperature, pressure of CF_3I gas, use of copper powder as a promoter, and presence of an inert buffer gas affected the conversion and the number of CF_3 groups on the cage.

Three different temperatures were examined: 450 °C, 500 °C, and 570 °C. From previous work with C_{60}, trifluoromethylation is very slow below temperatures of 450 °C and likewise temperatures above 570 °C result in very low yields primarily due to massive decomposition of the fullerene starting material. There were no significant differences in the product distribution between reactions conducted at 450 °C and 500 °C. The conversion appeared to be improved at 450 °C but due to the difficulties in recovering all material out of the reactor the conversion may be misleading. However, visual inspection of the thimble after each reaction showed there to be less insoluble material left over at the lower temperatures. Primarily for this reason, as well as the fact that there were no real differences in product distribution, 450 °C was chosen for the remainder of the experiments.

To study the effect of copper metal on the trifluoromethylation of endohedral metallofullerenes, two experiments were conducted under identical conditions: one with copper metal promoter and the other without copper metal present. As shown in Figure 1.15, the Cu metal greatly enhanced the conversion. The product distribution was slightly altered toward greater numbers of addition as well. This result was also true when trifluoromethylating C_{60}.

By far the most important reaction parameter in determining the conversion and extent of substitution is the pressure of CF_3I. Four experiments were conducted at different pressures ranging from 50 to 600 torr of CF_3I while keeping all other parameters constant. At pressures equal to or less than 50 torr the conversion is poor. However, as shown in Figure 1.16, when the pressure is increased to 75 torr, the conversion drastically improves. Interestingly, determined by APCI-MS, the products are all highly substituted cages with very small amounts of products with less than 8 CF_3 groups on the cages. Contrary to the trends with C_{60}, as the pressure is increased to 250 and ultimately 600 torr the conversion does not improve, but the product distribution

widens slightly leading toward less substituted cages. This effect is not very pronounced but can be explained by the increased convection, and therefore lower residence times, in the reactive zone. An additional experiment was conducted at the same total pressure of 600 torr; however, the gas was composed of 75 torr CF_3I and 525 torr dinitrogen gas. The product distribution of this reaction with the buffer gas, as shown in Figure 1.17 was almost identical to the reaction conducted at 600 torr CF_3I. This result indicates that the concentration of $CF_3\cdot$ at 75 torr is sufficient for high conversion and high substitution however at such a low pressure the convection out of the hot zone is not very rapid, which leads to longer residence times and more highly substituted cages. When the convection is increased by the addition of a buffer gas the product distribution widens slightly indicating shorter residence times in the reactive zone. When all these results are considered together it is presumable that the reaction proceeds to completion when pressures > 75 torr are used; however, at pressures less than 50 torr very little reaction takes place. It is therefore expected that pressures between 50 and 75 torr are used with an inert buffer gas to increase convection, thereby lowering residence times, then the extent of cage substitution could be decreased, which is a desirable result for their incorporation into polymeric beads.

Besides examining $Sc_3N@C_{80}$, additional experiments were carried out with the endohedral metallofullerene $Y_3N@C_{80}$. It is well known that the reactivities of endohedral metallofullerenes are very dependent on the nature of the trimetallic nitride metal cluster inside the cage.[21,22] We conducted 3 reactions at various pressures of CF_3I gas and compared the conversion of fullerene starting material as well as the extent of substitution between the two endohedral metallofullerenes. And, as can be seen in Figure 1.18, I determined that the reactivities of the two are very similar under identical reaction parameters. Additionally, one

reaction was conducted with $Y_3N@C_{80}$ that had been recovered from the previous reactions. This reaction with recycled $Y_3N@C_{80}$ gave identical results to the previous reactions with fresh starting material, indicating that in reactions with a low conversion, the material can be recovered and used again. This is noteworthy because the price of $Y_3N@C_{80}$ is four times higher than $Sc_3N@C_{80}$.

Experimental for Section 1.1

Reagents and Solvents. HPLC Grade toluene, heptanes (Fisher Scientific), and CH_2Cl_2 (Fisher Scientific) were used as received. C_{60} (99.9%, Term-USA), CF_3I, (SynQuest Labs), and copper powder (Fischer Scientific), $Sc_3N@C_{80}$ (from Prof. Stevenson at USM), and $Y_3N@C_{80}$ (from Prof. Stevenson at USM) were used as received.

Instruments. HPLC analysis and separation was done using Shimadzu liquid chromatography instrument (CBM-20A control module, SPD-20A UV-detector set to 300 nm detection wavelength, LC-6AD pump, manual injector valve) equipped with 10-mm I.D. × 250 mm Cosmosil Buckyprep column, Nacalai Tesque, Inc.). APCI mass spectra were recorded on 2000 Finnigan LCQ-DUO mass-spectrometer (CH_3CN carrier solvent, 0.3 mL min^{-1} flow rate, TMF sample injected as solution in toluene).

GTGS reactor. A heating element from a Corning hot plate was placed on top of a magnesia refractory brick and powered by a Variac autotransformer. The temperature was

measured with a K-type thermocouple and placed directly in between the thimble and heating element. A patch of 10 mm fused silica wool was used as the small spacer while a 50 mm magnesia refractory brick was used for the large spacer. Directly on top of the spacer was a water cooled 1.25 mm brass plate. The quartz thimble was attached via an Ace compression joint fitted with a Viton O-ring to a 1 L ballast volume to insure that the pressure of CF_3I does not significantly change during the course of each experiment. This ballast flask was connected to a gas handling manifold with a ½ inch Cajon joint to allow for the manipulation of CF_3I gas and vacuum. A 0-1000 torr range Baratron was used for pressure measurements.

Description of a typical GTGS experiment. A sample of starting material (C_{60}, C_{70}, or fullerene extract) was finely ground with a mortar and pestle and placed in the center of the quartz reactor thimble. Care was taken to evenly distribute the fullerene sample across the bottom of the thimble each time to ensure even heating and reproducibility. The thimble was put in place and the entire reactor was evacuated. The desired amount of CF_3I was then added. The preheated furnace assembly was then put in place insuring a rapid ramp up to the desired stable temperature that was complete within 5 min. Determined in a previous work, the temperature of the furnace averages about 100 °C greater than the reaction temperature inside of the thimble. For the remainder of this chapter, the temperature of the reaction will be used and not the set furnace temperature. After the desired amount of time the furnace was lowered. Once the reactor was cool to the touch, the system was evacuated to remove any unreacted CF_3I and side products such as C_2F_6. The interior of the thimble was then washed thoroughly with toluene and placed in a tared evaporation dish. The toluene was then removed with gentle heating (< 40° C) and an N_2 stream in order to remove any remaining I_2. To the dried crude fullerene material, ca. 8 mL of

HPLC grade toluene was added then transferred into a clean 10 mL volumetric flask and diluted up to the 10.0 mL mark. A 500 μL sample was analyzed by HPLC in a 100% toluene mobile phase with a flow rate of 5 mL/ min. In order to compensate for small differences between the amounts of C_{60} starting material, each HPLC trace was scaled to the amount of starting material used for each reaction.

1.2. Homogenous Fullerene Perfluoroalkylation

1.2.1. General Remarks. Extending the family of fullerene(R_F)$_n$ compounds beyond trifluoromethyl fullerenes (TMF) promises to elucidate fundamental questions about the electronic properties of fullerenes, which in turn may pave the way for practical applications of fullerenes in organic photovoltaic (OPV) devices.[23-27] It is reasonable to predict that fullerene(R_F)$_n$ compounds should be better electron acceptors than their parent fullerene due to the electron withdrawing nature of the R_F addends.[2,6] Moreover, by gradually adjusting the length and branching patterns of the R_F substituents, it is possible to introduce a new level of fine tuning of both the electronic and physical properties of fullerene(R_F)$_n$ compounds. Specifically, changing the R_F substituent should affect the solid state morphology of thin films comprised of a blend of fullerene(R_F)$_n$ compounds and a conjugated polymer; blends such as these comprise the active layer of OPVs. It is generally accepted that the performance of OPVs depends not only on the electronic properties of the materials but also on the morphology of the active layer of the device.[28-33]

This section will describe the development of a homogeneous perfluoroalkylation synthetic procedure that was used to extend the family of fullerene(R_F)$_n$ compounds beyond TMFs with the specific goal of preparing a series of 1,7-$C_{60}(R_F)_2$ compounds with a varying length and branching patterns of the R_F substituents. A comprehensive structural characterization by spectroscopic methods will also be discussed; a more in depth discussion of their electrochemical properties will be examined in Chapter 2.

1.2.2. Preparation of $C_{60}(R_F)_2$. Homogeneous perfluoroalkylation was used to prepare a series of 5 fullerene bis-derivatives: $C_{60}(n\text{-}C_3F_7)_2$, $C_{60}(i\text{-}C_3F_7)_2$, $C_{60}(n\text{-}C_4F_9)_2$, $C_{60}(s\text{-}C_4F_9)_2$, and $C_{60}(n\text{-}C_8F_{17})_2$. A typical experiment consisted of adding a solution of C_{60} dissolved in oDCB into a Pyrex glass ampoule that had been preloaded with excess Cu powder. The desired equivalents of R_FI were added via a gas-tight syringe. The solution was then diluted to 1 mL total volume and degased by 3 cycles of freeze-pump-thaw. The ampoule was then flame sealed under vacuum and placed in a preheated tube furnace and heated for 24 hours (Table 1.2.1 summarizes the experimental reaction conditions used to target $C_{60}(R_F)_2$ compounds). The reaction conditions and equivalents of the R_FI reagent has since been optimized and published by a coworker Dr. Igor Kuvychko.[27] The ampoule was then removed from the furnace and allowed to cool, it was then opened and the solvent was pumped away. The remaining dry residue was then analyzed by HPLC with a Cosmosil Buckyprep column. The main product was then separated by HPLC and analyzed by APCI mass spectrometry and ^{19}F NMR spectroscopy. The conversion and selectivity for each reaction were in general good; for example, in the case of preparing $C_{60}(i\text{-}C_3F_7)_2$ the conversion was 41% by integrated intensity with an 81% selectivity toward a single product. Figures 1.18 through 1.23 show the HPLC traces of the crude material from each reaction

conducted as well as the HPLC separation method used to isolate the main product. APCI-MS was then used to identify the HPLC fraction that contained $C_{60}(R_F)_2$. In most cases a second stage of HPLC separation was necessary to isolate the $C_{60}(R_F)_2$ to 98 mol%. The APCI mass spectra for each isolated $C_{60}(R_F)_2$ products are shown in figures 1.21 through 1.25.

Fluorine-19 NMR spectroscopy as well as UV-vis spectroscopy and single crystal X-ray diffraction were used to determine the addition patterns of the isolated $C_{60}(R_F)_2$ products. The ^{19}F NMR spectra for $C_{60}(n\text{-}C_3F_7)_2$, $C_{60}(i\text{-}C_3F_7)_2$, $C_{60}(n\text{-}C_4F_9)_2$, and $C_{60}(n\text{-}C_8F_{17})_2$ all indicate that the molecule has a mirror plane. For example, the ^{19}F NMR spectrum in figure 1.2.7 of $C_{60}(i\text{-}C_3F_7)_2$ has 2 multiplets at ca. $-\delta$ 72 ppm with integration values of 6; a singlet is also present in the spectrum at a chemical shift of $-\delta$ 172.9 ppm with an integration value of 2. The two multiplets have chemical shift values typical of the fluorine atoms bound to a primary carbon atom, while the singlet is typical of a single fluorine atom bound to a tertiary carbon atom. All this data indicates two equivalent $i\text{-}C_3F_7$ addends bound to the cage, but does not offer any proof as to the exact addition pattern, that is, there are numerous symmetric bis-isomers possible. Therefore, additional techniques other than ^{19}F NMR were necessary to unambiguously determine the addition pattern of each compound.

The X-ray crystal structure of $1,7\text{-}C_{60}(i\text{-}C_3F_7)_2$ had previously been determined in the Strauss group and published.[23] Therefore, the addition pattern of the $C_{60}(i\text{-}C_3F_7)_2$ prepared in this work could be confirmed by matching the ^{19}F NMR spectrum to the published spectrum. In this work, a single crystal of $C_{60}(n\text{-}C_3F_7)_2$ suitable for x-ray crystallography was grown from $CDCl_3$ and the structure, shown in Figure 1.26, was solved by Dr. Natalia Shustova. This crystal structure confirmed that the compound was the $1,7\text{-}C_{60}(n\text{-}C_3F_7)_2$ isomer, the same addition

pattern as in 1,7-$C_{60}(i\text{-}C_3F_7)_2$. Crystals of the other bis-fullerenes could not be grown in any of a number of different solvents and techniques attempted.

In order to confirm the addition patterns of the remaining compounds where X-ray crystal structures were unavailable ($C_{60}(n\text{-}C_4F_9)$, $C_{60}(s\text{-}C_4F_9)_2$, and $C_{60}(n\text{-}C_8F_{17})_2$), UV-vis spectroscopy was used. It has been demonstrated in the fullerene literature that there is a link between the electrochemical properties of derivatized fullerenes and their addition patterns.[2] It has also been shown that since the electronic properties are linked to the fullerene addition pattern, the electronic absorbance spectra are also indicative of the addition patterns.[34] The UV-vis absorbance spectra of the 5 different $C_{60}(R_F)_2$ compounds prepared in this work were measured in toluene. In addition, the spectra of the previously published 1,7-$C_{60}(CF_3)_2$ were also measured in toluene. As can be seen in table 1.2.2, the UV-vis absorbance spectra of all the $C_{60}(R_F)_2$ compounds recorded in this work are virtually identical. This confirms that they all have the same addition patterns and since three of the measured compounds have been structurally characterized by X-ray crystallography. Hence, it can be safely concluded that all the bis-fullerene derivitives prepared in this work have the same 1,7 addition pattern.

In addition to the five 1,7-$C_{60}(R_F)_2$ compounds that were synthesized for this work, several attempts were made to prepare 1,7-$C_{60}(t\text{-}C_4F_9)_2$. This very bulky t-$C_4F_9$ reagent was attractive because the demanding steric requirements of the tertiary butyl group may prevent 1,7 addition leading to other addition patterns and concomitantly, different electronic properties. Characterization by APCI-MS and ^{19}F and ^{1}H NMR spectroscopy indicated that $C_{60}(t\text{-}C_4F_9)H$ formed. Analysis of the UV-vis spectrum, shown in Figure 1.22, indicates, however, that the same 1,7 addition pattern was formed.

1.2.3. Exhaustive Perfluoroalkylation of C_{60} and C_{70}. A series of homogeneous perfluoroalkylation reactions were conducted to determine the maximum degree of addition of n-C_4F_9I, s-C_4F_9I, t-C_4F_9I, and $CF_2C_6F_5$ to C_{60} and C_{70}. Each ampoule was prepared with 200 equivalents of the R_FI and excess fine Cu powder in oDCB. The ampoules were heated to 180 °C (the ampoule containing $ICF_2C_6F_5$ was heated to 130 °C) for 24 hours. After the ampoules were allowed to cool, they were opened and the crude products were filtered and analyzed by APCI-MS. Table 1.2.3 shows both the maximum number of R_F groups observed in APCI-MS as well as the most abundant ions in the spectrum. The APCI-MS spectrum of $C_{60}(n$-$C_4F_9)_n$ shows the presence of H atoms on the cage. It is unclear whether or not these H atoms are from the synthesis or they are from the APCI-MS and since H atoms can be readily detached under MS conditions via cleavage from the solvent. A ^{1}H NMR was not obtained on the crude material. In addition, the APCI-MS of $C_{60}(CF_2C_6F_5)_n$ only shows the ions where n is equal to only odd numbers of addition, presumably due to fragmentation in the MS. This observation is not unexpected as it has been hypothesized that the $CF_2C_6F_5$ addend is more labile than the other R_F addends in this study. In support of this conjecture, thermal isomerization of $C_{60}(CF_2C_6F_5)_2$ has been experimentally observed (unpublished data).

Analysis of the APCI-MS data demonstrates that the size of the addend plays a primary role in determining the maximum extent of addition. As the steric bulk of the addend increases from C_2F_5 up to t-C_4F_9, the maximum observed number of additions drops from 16 down to 6. This trend of increased steric bulk leading to lower numbers of addition is also observed within the series of C_4F_9 addends that were prepared under identical reaction conditions. As the steric bulk increases from normal to secondary to tertiary the extent of addition decreases from 12 to 8 to 6.

This same trend is also seen when identical reaction conditions are used to exhaustively perfluoroalkylate C_{70}. As the steric bulk increases from perfluoro *n*-butyl to perfluoro *sec*-butyl, the maximum number of addition as observed by mass spectrometry decreases from 11 to 9.

Experimental for Section 1.2

Reagents and Solvents. The solvents were used as received and included toluene (Fisher Scientific; HPLC grade), n-heptane (Fisher Scientific; HPLC grade), acetonitrile (Fisher Scientific; HPLC grade), 1,2-dichlorobenzene (Acros Organics; ACS grade), and chloroform-d$_3$ (Chambridge Isotope Laboratories, Inc.; 99.9% D). The R_FI reagents used including $R_F = CF_3$, *n*-C_3F_7, *i*-C_3F_7, *n*-C_4F_9, *s*-C_4F_9, *n*-C_8F_{17}, C_6F_6 (SynQuest Labs) were used as received. The copper powder (Fisher Scientific; 325 mesh; electrolytic grade) and C_{60} (Term-USA, 99.9%) were also used as received.

Instrumentation. A Shimadzu HPLC system, including a control module (CBM-20A), UV-detector (SPD-20A), pump (LC-6AD), and a manual injector valve, was used for HPLC analysis and separation equipped with a semi-preparative Cosmosil Buckyprep column 10 mm I.D. × 250 mm from Nacalai Tesque Inc. Atmosphereic pressure chemical ionization mass spectrometery (APCI-MS) was conducted using an Agilent Technologies Model 6210 TOF spectrometer with an APCI source. The carrier solvent was acetronitrile with 1% toluene. Fluorine-19 NMR spectra were recorded on a Varian 400 MHz NMR spectrometer operating at 376 MHz frequency (the solvent was CDCl$_3$).

25

General Experiment. A stock solution of 14 mM C_{60} in oDCB was prepared and used for each experiment. A 500 μL aliquot was transferred to a new, home built, Pyrex glass ampoule with approximant dimensions of I.D. = 5.0 mm, Length = 140 mm, volume = 2.7 mL. Copper powder (c.a. 500 mg) was then added into the ampoule. The desired amount of R_FI reagent was added via a gas-tight syringe. The ampoule was then diluted with oDCB to a 1.0 mL total volume. The ampoule was then subjected to three cycles of freeze-pump-thaw using liquid nitrogen and flame-sealed under vacuum. The ampoules were heated to the desired temperature in a tube furnace. After heating, the ampoules were frozen in liquid nitrogen and opened. The crude reaction products were put under dynamic vacuum until dry. The dry residues were then dissolved in toluene, filtered and analyzed by HPLC, NMR spectroscopy, and APCI mass spectrometry.

1.3. Functionalization of Trifluoromethylfullerenes

1.3.1. Oxidation of 60-10-3. The PFAF $1,3,7,10,14,17,23,28,31,40-C_{60}(CF_3)_{10}$ (60-10-3) was the first PFAF to have its structure determined by X-ray diffraction.[9] Its addition pattern is shown in Figure 1.31, which also shows the remaining C=C bonds with distances shorter than 140 pm. Note that this addition pattern results in an *isolated* pentafulvene fragment composed of C atoms 2, 11, 12, 13, 29, and 30, the first of its kind in fullerene chemistry (a pentafulvene fragment that is *not* isolated from the rest of the fullerene π system was observed in the structure of $1,7,11,24-C_{60}(9\text{-fluorenyl})_4$ published in 1997[35]). The 1D ^{19}F NMR spectrum of 60-10-3 dissolved in $CDCl_3$ is shown in Figure 1.32. Its ten quartets, quartets-of- quartets (apparent

septets), or unresolved multiplets are due to through-space Fermi-contact $^{6,7}J_{FF}$ coupling of proximate CF_3 groups that share the same fullerene hexagon or pentagon. [9,36] The previously published spectrum of 60-10-3 was recorded in C_6D_6 solution,[9] and the two multiplets with chemical shift values $< \delta -62$ were accidentally isochronous in that solvent (these multiplets arise from the CF_3 groups that share the same pentagon). Selective decoupling experiments (the spectra shown in Figure 1.3.3) performed in this work revealed the specific addition-pattern NMR assignments for these two multiplets. When multiplet A, at $\delta -59.5$, was decoupled, multiplets e and h became sharper and better resolved, indicating that CF_3 group a shares hexagons with CH_3 groups e and h. When multiplet b, at $\delta -59.7$, was decoupled, multiplets g and j became sharper and better resolved, indicating that CF_3 group b shares hexagons with CF_3 groups g and j. Several errors were made in the NMR assignments in the previously published paper. The authors stated that multiplets d and e were coupled to one another, which the 1D and 2D spectrum published in the same paper (shown in Figure 1.3.4) indicated to be incorrect. An additional error in the assignments of multiplets d and e was made, which in the spectrum published in 2005 were severely overlapped. The correct NMR assignments are shown on the schlegel diagram in figure 1.33.

Prolonged exposure (many months) of oxygenated, tightly stoppered chloroform or toluene solutions of 60-10-3 to ambient light resulted in the formation of a new soluble species with a new set of multiplets, the spectrum of which is shown in Figure 1.34 (there was little or no loss of solvent to evaporation, and no precipitate formed, during this time). Assuming that the addition pattern of the CF_3 groups had not changed, the multiplets with the greatest chemical-shift changes belonged to the six CF_3 groups that surrounded the isolated fulvene fragment. Furthermore, the APCI mass spectrum shown in Figure 1.3.5, a purified sample of the new

compound indicated that its composition was $C_{60}(CF_3)_{10}(O)_2$ (60-10-3[O_2]). The separation of this new compound was accomplished using HPLC, as shown in Figure 1.36. The UV-vis spectrum was recorded in toluene and is shown in Figure 1.37.

The structure of 60-10-3[O_2] was determined by single-crystal X-ray diffraction, and is shown in Figure 1.3.8. It is only the third fullerene diepoxide to be structurally characterized (the first two are co-crystallized isomers of $C_{60}(O)_2(IrCl(CO)(PPh_3)_2)$[37]) and the first TMF diepoxide. In the discussion that follows, the cage C atom locants for 60-10-3[O_2] are, for convenience, the same as the locants for 60-10-3, although the IUPAC locants for 60-10-3 and 60-10-3[O_2] are different (using the same locants, the numbered formula for 60-10-3[O_2] is 1,3,7,10,14,17,23,28,31,40-$C_{60}(CF_3)_{10}(11,29:13,30$-$O)_2$, whereas the correct numbering for 60-10-3[O_2], which will not be used below, is 7,9,12,15,18,20,39,24,45,57-$C_{60}(CF_3)_{10}(1,2:3,4$-$O)_2$).

The two epoxide O atoms in 60-10-3[O_2] have been added to the conjugated C11–C29 and C13–C30 double bonds of the pentafulvene fragment in 60-10-3. These were $C(sp^2)$–$C(sp^2)$ bonds in 60-10-3 (136.0(3) and 136.5(3) pm long, respectively[9]) and are $C(sp^3)$–$C(sp^3)$ bonds in 60-10-3[O_2] (150.0(8) and 149.2(8) pm long, respectively). The four C–O distances in 60-10-3[O_2] range from 142.2(7) to 145.3(7) pm and are unexceptional. As expected, the C11–C12, C12–C13, and C29–C30 bonds are longer in 60-10-3[O_2] (148.9(8), 149.4(8), and 153.2(8) pm, respectively) than in 60-10-3 (1.465(3), 147.3(3), and 147.6(3) pm, respectively). The other cage C–C bonds in 60-10-3[O_2] and 60-10-3 are virtually the same. For example, the C2–C12 double bond is 133.5(8) pm in 60-10-3[O_2] and 134.4(3) in 60-10-3.

Ignoring the $CDCl_3$ solvates, the molecules of 60-10-3[O_2] are arranged in both a nearly-planar and a puckered pseudo-hexagonal array, as shown in Figure 1.39. Within the hexagonal arrays, the C_{60} centroid–centroid distances range from 980 to 1,810 pm. The corresponding

centroid–centroid distances in the structure of 60-10-3, which did not contain any solvent molecules, are similar and range from 1,017 to 1,417 pm.[9] As can be seen in figure 1.39, the stacking of the pseudo-hexagonal arrays in the third dimension is irregular and will not be discussed.

1.3.2. Attempts to Intentionally Oxidize 60-10-3[O_2]. Fullerene epoxidation has been well studied and many methods for the addition of up to 12 oxygen atoms to the cage of C_{60} have been observed.[37-40] A number of these methods were used to attempt to prepare 60-10-3[O_2] from pure samples of 60-10-3.

Photolysis in the presence of molecular oxygen. Samples of 60-10-3 were irradiated in the presence of diovygen for various amounts of time in solution. Several experiments were performed in both polar and non-polar oxygenated solvents including benzene, toluene, dichloromethane (DCM) and heptane in order to determine if the solvent played a role in oxidation. Additionally, THF was investigated as were several mixtures of solvents (acetonitrile: benzene and acetonitrile: heptane). Furthermore, a thin film of 60-10-3 was made from DCM and irradiated for 12 hours. After irradiation it was determined by ^{19}F NMR spectroscopy that 60-10-3 does not undergo oxidation in any of the above conditions.

Thermal Reaction with O_2. Several experiments were conducted to determine if 60-10-3 undergoes thermal oxidation. In a sealed glass ampoule, 60-10-3 was heated in the presence of dioxygen to 555 °C for various amounts of time. The resulting residue was dissolved and analyzed by ^{19}F NMR spectroscopy; the resulting spectrum indicated that no oxidation or decomposition took place.

In addition, several experiments were conducted to determine if oxygenated solutions of 60-10-3 in various solvents underwent oxidation at 80 °C. These solutions of 60-10-3 were heated to 80 °C until the solvent had fully evaporated. The residue was then analyzed by ^{19}F NMR spectroscopy and indicated that there was no oxidation or decomposition. Solutions of 60-10-3 in various solvents were also heated to reflux for 24 hours and analyzed by ^{19}F NMR spectroscopy. Again, the ^{19}F NMR spectra indicated that there was no oxidation or decomposition.

It has been shown in the literature that fullerene oxidation occurs more readily in more polar solvents.[1] Two solutions of 60-10-3 were prepared, the first was 50:50 benzene:acetonitrile and the second was in 100% CS_2. Both solutions were heated for 24 hours and analyzed by ^{19}F NMR spectroscopy. No oxidation or decomposition was observed in either one.

Ozonation. A mixture of O_2 and O_3 gas was prepared by passing dioxygen through a corona discharge supplied by a tesla coil. This mixture of O_2 and O_3 was bubbled through a room temperature toluene solution of 60-10-3 for 5 min. The resulting solution was analyzed by APCI-MS, HPLC and ^{19}F NMR spectroscopy (shown in Figure 1.31 to 1.33) and indicated a complex mixture of 60-10-3 and various oxides of 60-10-3. This result of a complex mixture of oxides is in accordance with the literature on C_{60} when it is treated with O_3.[38] Analysis of the ^{19}F NMR spectrum of the products reveals that there is very little starting material left after ozonation.

Reaction with *m*-chloroperoxobenzoic acid (mCPBA). The preferred method of fullerene oxidation due to simplicity and control over the extent of oxidation, is using the chemical oxidant mCPBA.[37] A pure sample of 60-10-3 was dissolved in a toluene solution of excess mCPBA and allowed to react for 12 hours. A complex mixture of oxides and toluene adducts of 60-10-3 were analyzed by HPLC, APCI-MS, and ^{19}F NMR spectroscopy as shown in

figures 1.34 to 1.36. It is clear that the toluene adducts were not an artifact from the APCI-MS conditions as the mobile phase used for the APCI-MS analysis was acetonitrile and a small amount of CDCl$_3$ in order to solubilize the products. Therefore, the only source of toluene was the reaction solvent. In addition to the 24 hour reaction times, shorter reaction times ($\leq$ 1 hour) were used to try and target lower numbers of oxidation and improve selectivity toward the desired 60-10-3[O$_2$] product. Analysis of the crude material from these shorter reactions showed no reaction indicating that even with a strong oxidizer such as mCPBA, the oxidation reaction proceeds slowly.

This slow oxidation has important practical implications as more fullerene derivatives find uses as components in organic electronic devices, for example, as electron acceptors in organic photo voltaics (OPV), or in organic field effect transistors (OFETs), their instability toward air may adversely affect the device performance. A recent report indicated that a fullerene (1,4-bis(dimethylphenylsilylmethyl)- [60]fullerene) that was used in the active layer in OPV devices underwent photo-oxidation in solution as well as in a thin film at room temperature over the course of several days.[41] It was also shown that as the percentage of oxidized fullerene in the active layer increased, the performance of the device deteriorated significantly.[41] The results of our study should warn researchers investigating new compounds for OPV devices on the necessity to investigate the stability of new materials toward oxidation. The fact that the TMFs investigated in this work do not undergo air oxidation in the solid state (in contrast to those molecules reported in reference[41]) suggests they belong to a potentially valuable class of air-stable organic molecules for practical applications.

General Remarks about 60-10-3 epoxidation. Numerous oxidation methods were employed to make 60-10-3 oxidize at a faster rate; including photolysis, ozonation, thermolysis, and the use of *m*CPBA as a chemical oxidant. All these attempts to prepare 60-10-3[O_2] selectively were unsuccessful indicating that diepoxidation of 60-10-3 is a kinetically very slow process. We propose that the reason for such low reaction rate is steric hindrance from the CF_3 groups that block the two fulvene endocyclic double bond addition sites. It is even more surprising that addition to the short exocyclic pentafulvene double bond or to one of the several less hindered double bonds on the cage of 60-10-3 does not occur at all. This observation adds credence to the hypothesis that the shorter double bonds in the fully isolated fulvene moiety are highly activated and may serve as a possible synthetic handle for further regiospecific functionalization of PFAFs that possess such a moiety on the fullerene core.

1.3.3. Oxidation of p^3-C$_{60}$(CF$_3$)$_4$. Multiple additions to fullerenes are notoriously difficult to perform regioselectively due to the presence of many reactive sites on the carbon cage. A fundamental understanding of reaction pathways via detection of intermediates in such reactions is paramount for further progress in new material developments for emerging applications. In polyadditions of bulky substituents to C_{60}, the most important closed-shell intermediate is a tetra-substituted molecule with a fulvene π-system, C_s-C$_{60}$X$_4$ (1) as shown on Figure 1.37. Formation of such short-lived species with a highly reactive exocyclic fulvene double bond is believed to explain high regioselectivity towards a hexakis derivative, with the skew pentagonal pyramid (SPP) addition pattern C_s-C$_{60}$X$_6$ (2). The cyclopentadienyl modes of addition are typical for organocopper chemistry,[42] amine additions and radical halogenations.[43] In only two cases was it was possible to experimentally observe the intermediate fulvene

fullerenes, $C_{60}X_4$, (1) when bulky X substituents (X = fluorene,[35] X_1 = 2-C_3F_7, X_2 = CF_3[24]) provided substantial sterical shielding to hamper further additions across the exocyclic fulvene double bond, for example, epoxidation of these compounds was not reported to occur. In this work, the X-ray crystal structure of C_s-$C_{60}(CF_3)_4$ was determined (60-4-2, see Figure 1.3.18 and ref.[2] for isomer notation); a rare example of the structurally characterized fulvene fullerene, and its unusual chemical properties. It belongs to a large family of perfluoroalkylfullerenes (PFAFs) that represent some of the most robust fullerene derivatives towards hydrolysis, thermal treatment and air oxidation. The only puzzling "black sheep in the family" has been the monoepoxide C_s-$C_{60}(CF_3)_4O$, abundantly and consistently present in the high-temperature trifluoromethylation products.[1] It was speculated earlier that the epoxide might originate from a hypothetical highly reactive intermediate C_s-$C_{60}(CF_3)_4$ (60-4-2);[1,44] however, until this work, it remained unknown when epoxidation occurs: during the reaction, or after exposure of the TMF product to air. Another interesting fact was that other TMFs did not seem to form epoxides at all. In this work, we were finally able to address these questions by isolating and determining the X-ray structure of this elusive trifluoromethylated fullerene and studying its reactivity towards various oxidants.

Compound 60-4-2 was produced using a recently described gradient-temperature-gas-solid (GTGS) reactor, where CF_3 radicals are produced by thermolysis of the CF_3I precursor in the presence of solid C_{60}.[44] The reaction of 250 mg of C_{60} with 10 torr of CF_3I at 480 °C yielded a brown solid product that was dissolved in $CDCl_3$ and immediately analyzed by ^{19}F NMR spectrometry. The spectrum showed signals due to 1,7-$C_{60}(CF_3)_2$ (60-2-1) (70%) and 1,4,9,12-$C_{60}(CF_3)_4$ (60-4-1) (12%); a third group of peaks at −δ 70.5 that belonged to a second most abundant TMF product (18%) did not match the ^{19}F NMR spectra of any known TMFs (figure

1.39). The atmospheric pressure chemical ionization mass spectrometry (APCI MS) analysis of this crude mixture only showed peaks with m/z values corresponding to C_{60}^-, $C_{60}(CF_3)_2^-$, and $C_{60}(CF_3)_4^-$ indicating that the new compound may be a bis- or tetrakis- TMF. This novel derivative was isolated using HPLC chromatography and was identified as 60-4-2 based on ^{19}F NMR and UV-vis spectroscopy (figure 1.3.18), APCI mass spectrometry and X-ray crystallography. The latter confirmed its addition pattern as a ribbon of edge-sharing p-$C_6(CF_3)_2$ hexagons as shown in figure 1.39.

Intentionally oxidizing 60-4-2. Three separate samples of 60-4-2 (A, B, and C) were prepared in order to determine what effect ambient light and polarity of the solvent has on the rate of oxidation. Sample A was dissolved in benzene-d_6 and was exposed to light for the duration of the experiment. Sample B was dissolved in 70:30 benzene-d_6: acetonitrile mixture and was kept in the dark, while sample C was dissolved in the same mixture of solvents but exposed to ambient light for the duration of the experiment. All samples were prepared at the same concentration and sealed in order to eliminate evaporation ensuring constant solvent composition. After 24 hours, sample C had undergone complete conversion to compound 60-4-O while samples A and B remained unchanged. Even after 17 days, samples A and B remained unchanged indicating that the oxidation of 60-4-2 requires both a polar solvent and ambient light. A control experiment was conducted to rule out the possibility that water was the source of the oxygen atom in the epoxide addend. Compound 60-4-2 was dissolved in a dry and degassed solution of 70:30 benzene-d$_6$: acetonitrile, exposed to ambient light and monitored by ^{19}F NMR spectroscopy (Figure 1.41). As expected, no oxidation product was visible after 24 hours. To the same solution, dry O_2 was introduced and the NMR tube was resealed and then monitored by ^{19}F

34

NMR spectroscopy every 15 min (the sample was exposed to ambient light). The % content of 60-4-2 steadily declined once the dry dioxygen was added. These experimental facts indicate that epoxidation mechanism of 60-4-2 observed here most likely involves photoinduced energy transfer (i.e., singlet oxygen as the reactive oxygen species, ROS), and not a single electron transfer, SET, as in the earlier reported epoxidations of tetraaminated[45] or pentaarylated[46] C_{60} in highly polar solvents that may occur in the dark.

To determine if 60-4-2 is the only C_{60}-TMF that undergoes oxidation in a polar solvent while exposed to ambient light in under 24 hours, three experiments were carried out with three TMFs with different numbers of CF_3 groups (60-2-1, 60-4-1 and 60-10-3, see Schlegel diagrams on Figure 1.3.20). These TMFs were chosen for two reasons: (1) varying the number of CF_3 groups on the cages from 2 to 10 allows us to determine if the number of CF_3 groups plays a role in the oxidation, and (2) to determine if the addition pattern of 60-4-2 plays a particular role, we choose another isomer of $C_{60}(CF_3)_4$, 60-4-1. These three different TMFs were dissolved in separate solutions of 70:30 benzene-d_6: acetonitrile and were exposed to ambient light for 24 hours. These conditions were identical to those for sample C from above. Fluorine-19 NMR spectroscopy revealed that there was no oxidation of any of the studied TMFs indicating that the number of CF_3 groups was not important, it was the addition pattern of 60-4-2 that lead to the increased reactivity with dioxygen.

Additional experiments were performed to determine if the high reactivity of 60-4-2 with O_2 is limited to solution phase reactions or if 60-4-2 would display similar reactivity as a solid. A solid sample of 60-4-2 was exposed to air and ambient light for 5 months. Upon examination of the resulting ^{19}F NMR spectrum, there was no evidence of compound 60-4-O. Furthermore, there

is no evidence of any other known TMF undergoing oxidation when left as a solid for up to 3 years, making them potentially attractive for practical applications.

When a thin film of 60-4-2 is heated to 120 °C for 20 min under a 20% O_2 atmosphere, 60-4-O formed with 100% conversion. Importantly, 120 °C is not sufficient temperature for sublimation ensuring that the reaction is between oxygen gas and solid 60-4-2. This same experiment was repeated with TMFs 60-2-1 and 60-10-3 with no observed oxidation. Interestingly, solid bare cage C_{60} does not undergo oxidation in a 20% oxygen atmosphere until it reaches 250 °C.[46] This result, along with our new data, confirm that 60-4-2 is more reactive with oxygen than any other known TMF as well as bare-cage C_{60}, even though part of the cage in 60-4-2 is covered with CF_3 groups.

To determine if the reactivity of 60-4-2 was limited to molecular oxygen, or if a chemical oxidant could be used to decrease the reaction time while maintaining the regioselectivity of oxidation, 60-4-2 was dissolved in toluene with 1.5 equivalents of m-chloroperbenzoic acid (mCPBA) and refluxed for 1 hour. The resulting product was examined with ^{19}F NMR spectroscopy revealing that complete conversion to compound 60-4-O took place (Figure 1.42). To eliminate the possibility that 60-4-2 was in fact reacting with dissolved oxygen in the refluxing toluene, a control experiment was run in which the same conditions were used only no mCPBA was used. No epoxide formation was observed in the resulting ^{19}F NMR spectrum after 1 hour of heating, indicating that the oxygen atom on the cage was from mCPBA and not from dissolved oxygen. As with previous experiments, other TMFs were studied under the same conditions. Fullerene 60-10-3 displayed no reactivity with 1.5 equivalents of mCPBA after 1 hour of reflux. Likewise, no reaction occurred when either 60-4-1 or 60-2-1 were heated to reflux in toluene with 1.5 equivalents of mCPBA. It is only when 10 equivalents of mCPBA are

reacted with 60-2-1 in refluxing 30:70 AcN:Benzene that there is any epoxide formation visible by ^{19}F NMR spectroscopy.

Just as 60-4-2 was found more reactive toward molecular oxygen than C_{60}, it is also more reactive toward mCPBA. The extent of C_{60} epoxidation varies depending on reaction time and amount of mCPBA used. Typically 10 to 30 equivalents of mCPBA are stirred in a toluene solution of C_{60} heated to 80 °C.[47] When 10 equivalents of mCPBA are reacted with C_{60} for 12 h, $C_{60}O$ is produced with a 15% yield (60% conversion of C_{60}). The remaining material consists of ca. 20% $C_{60}O_2$ and 25% insoluble material.[47] Increasing the equivalents of mCPBA to 30 will increase the number of oxygen additions up to 12. This is in stark contrast to the 1.5 equivalents necessary for complete oxidation of 60-4-2 in 1 hour.

Chemical oxidation of 60-4-2 is not limited to mCPBA. When ozone/oxygen mixture is bubbled through a room temperature toluene solution of 60-4-2 for 10 min while exposed to ambient light, complete conversion to 60-4-O takes place. The O_3/O_2 gas mixture was generated by passing a stream of O_2 gas through a corona discharge. When the same O_3/O_2 mixture is bubbled through a room temperature toluene solution of 60-10-3 for 5 min while exposed to ambient light, multiple oxide products are formed. Similar treatment of a toluene solution of C_{60} results in an unstable amber solution and a yellow brown amorphous precipitate; in solution $C_{60}O$ and numerous multiple oxide products were detected in accordance with the literature.[45,47]

Implications of oxidizing 60-4-2. It can now be explained why 60-4-O has been characterized previously while 60-4-2 has not. By far the most common method of isolation of TMF isomers is by HPLC separation. Presumably 60-4-2 that is present in the freshly prepared TMF mixtures undergoes oxidation to 60-4-O during a lengthy HPLC isolation. Our finding, that

oxidation of 60-4-2 can be avoided if care is taken to exclude ambient light as much as possible during isolation and any subsequent handling in solution, opens pathways for similarly light-sensitive fullerene derivatives to be successfully isolated and characterized.

1.3.4. Electrochemical Functionalization of $C_{60}(CF_3)_4$. Several experiments were conducted to take advantage of the unique addition pattern of 60-4-2 that creates a fulvene like moiety on the surface of the fullerene cage. As can be seen in Figure 1.44, the DFT predicted LUMO is localized by the CF_3 groups on the exohedral fulvene-like double bond. Therefore, as a dianion, the electron density should be localized on this now-activated double bond. In order to test this hypothesis, the 60-4-2 dianion was prepared by chemical reduction with K metal in a THF solution. One of three electrophiles, either BnBr, EtBr, or ICF_2COOEt, was then added to the dianion solution in a 10-fold excess in three separate reactions. The resulting reaction was then quenched with trifluoroacetic acid (TFA). Using ^{19}F NMR spectroscopy, APCI-MS, and HPLC the resulting crude material was characterized. In every case, APCI-MS indicated that one electrophile and one proton were successfully added to the cage. Analysis of the ^{19}F NMR spectrum and the HPLC chromatogram indicated that numerous isomers and or dimers formed during the reaction. However, due to the large number of products the crude material was not isolated or characterized further.

1.3.5. Regiospecific Functionalization of 60-4-2[O]. Since the synthesis and isolation of C_{60} in 1990, numerous reactions with C_{60} have been described and many thousands of fullerene adducts have been characterized. Reactions to further functionalize various fullerene derivatives has only recently begun to attract greater interest in order to prepare molecules for specific

applications, such as organic photovoltaics, and to gain a greater understanding of how different functional groups affect the physical and electrochemical properties of the molecule as a whole. In general, the reactive functional groups for most of these further functionalization reactions are not bound directly to the fullerene cage carbon atoms. One such example is the formation of water soluble C_{60} derivatives by conversion of carboxylic acid moieties into salts.[48] The successful transformation of functional groups attached directly to the fullerene cage carbon atom(s) has been very limited.

One such functional group that has served as a useful synthetic handle for further functionalization reactions are fullerene epoxides. Fullerene epoxides were among the first derivatized fullerenes found to exist and have since been used for numerous further functionalization reactions including the cleavage of fullerene cage bonds, acetalization reactions, and regiospecific addition of various halogens and nucleophiles that serve as synthetic handles themselves.[49-55]

In general, substitution of an epoxy group goes through a concerted S_N2 like mechanism where the initial step is a nucleophilic backside attack on one of the epoxy carbon atoms that opens the heterocycle.[53,56] However, such a backside attack is impossible because the closed fullerene cage occupies the entire backside of the epoxide group. Therefore, several groups have reported using Lewis acids in an S_N1' like mechanism to open the epoxide ring followed by nucleophilic attack.[53-55,57-60]

This section will describe the development of Lewis acid assisted epoxide opening reactions on a TMF epoxide. In addition, the structural characterization of the newly functionalized cages including several X-ray structures will be discussed. Lastly, a possible reaction pathway of Lewis acid assisted functionalization reactions will be presented.

1.3.6. Synthesis and Characterization. Gan et. al. was the first to report Lewis acid assisted functionalization of fullerene epoxides where they used a single equivalent of $FeCl_3$ to yield a vicinal hydroxyl chloride with an 85% yield.[51] The structure of this vicinal hydroxyl chloride was confirmed with single crystal X-ray crystallography. The remainder of the crude material, that was not the desired vicinal hydroxyl chloride product, consisted of starting material and a complex mixture of different isomers of phenylated fullerene cages (information from a private communication with Professor Gan).

Under similar conditions to those used by Gan et al. (the only difference being that they used a single equivalent of $FeCl_3$ while in this work an excess of $FeCl_3$ was used) a dry degassed benzene solution of 60-4-2[O] (henceforth referred to as compound **1**) was treated with excess anhydrous $FeCl_3$ for 30 minutes at room temperature followed by the addition of water; product **2**, shown in Scheme 1.46, was formed. This product forms with excellent yield (>95%) and 100% selectivity. The ^{19}F NMR spectrum of compound **2** showed two unresolved multiplets with a chemical shift of δ −67.2 and δ −68.4 ppm (shown in Figure 1.3.22) that arise due to the two pairs of CF_3 groups. Furthermore, the integrated intensity of these two signals were identical. The parent ion of compound **2** was also visible in the negative mode APCI mass spectrum. A single crystal suitable for single crystal X-ray diffraction was grown by slow evaporation of a saturated DCM solution of compound **2**. The X-ray crystal structure, solved by graduate student Eric Buckovsky as part of his graduate research, is shown in Figure 1.47 and confirms the initial structural assignment that was based off of the ^{19}F NMR spectrum and mass spectrometry.

By simply changing the reaction solvent and consequently the nucleophile from benzene to toluene, fluorobenzene, or iodobenzene while maintaining all other conditions, compounds **3**, **4**, and **5** are afforded, respectively (shown in figure 1.49). Remarkably, both compounds **3** and **4**

are produced with the same excellent yield and selectivity as compound **2**. The yield of compound **5** is slightly lower at 60%. The remaining 40% of the crude reaction material is compound **2**. The formation of compound **2** is due to an impurity of benzene that was present in the iodobenzene reagent (the presence of the benzene impurity was confirmed with ^{1}H NMR spectroscopy). The ^{19}F NMR spectra of compounds **3**, **4**, and **5**, as well as the ^{19}F NMR spectrum of compound **2**, were all very similar with two unresolved multiplets between −67 and −69 ppm. The ^{19}F NMR spectra of compounds **2**, **3**, **4**, and **5** are all shown in Figure 1.3.22. The similarity of the ^{19}F NMR spectra of these 4 different compounds indicates that they are structurally similar and all contain a mirror plane. The negative mode APCI mass spectra of these compounds all exhibit the parent ion minus a proton. The structures of **3** and **4** were confirmed by X-ray crystallography; good quality single crystals were grown by slow evaporation of concentrated DCM solutions. The structures of both molecules were solved by Eric Buckovsky as part of his graduate research and are shown in Figures 1.50 and 1.51.

In order to prepare the *cis*-chlorohydrin compound that is analogous to the compound produced by Gan et. al., the reaction solvent was changed to C_6F_6 while all other conditions remained the same. After 30 min the crude reaction material was worked up and analyzed by ^{19}F NMR spectroscopy indicating that only compound **6** was present. The isolated yield of compound **6** under these conditions was 98%. The structural assignment of compound **6** was based off of the ^{19}F NMR spectrum and APCI mass spectrometry. As was seen in the ^{19}F NMR spectra of the structurally analogous compounds **2**, **3**, **4**, and **5**, the ^{19}F NMR spectrum of compound **6** had two unresolved multiplets with chemical shifts of −68.5 ppm and −69.0 ppm. As discussed above, this similarity in chemical shift values between these compounds may indicate that they are structurally similar. Moreover, the presence of only two signals in the ^{19}F

NMR spectrum indicates that, like compounds **2**, **3**, **4**, and **5,** this new product contains a mirror plane. The APCI mass spectrum of compound **6** showed the mass of 1013 *m/z* which correlates to the mass of the molecular fragment $C_{60}(CF_3)_4OH$. The loss of the Cl atom in the APCI mass spectrum is not unexpected as the structurally similar *cis*-chlorohydrin compound $C_{60}R_4Cl(OH)$, prepared and characterized by Gan et. al. also underwent fragmentation via the loss of the Cl atom in APCI mass spectrometry.

Compound **6** is an interesting starting material for further functionalization reactions because it has been shown that this class of fullerenes with a *cis*-chlorohydrin moiety may be used for several base-induced reactions including intramolecular rearrangements and halogen replacement reactions with aromatic groups such as substituted phenols and anilines.[54]

In addition to vicinal hydroxyl chlorides, fullerenes with vicinal diols have been prepared by changing the Lewis acid from $FeCl_3$ to $B(C_6F_5)_3$. Fullerene vicinal diols have been used as convenient starting materials for carbon-carbon skeletal bond cleavage.[57-59] By cleaving fullerene skeletal bonds it is possible to "carve" holes in fullerenes large enough that small molecules such as methane and water can be encapsulated inside the fullerene cage.[55,60] When a DCM solution of **1** is treated with excess $B(C_6F_5)_3$ and heated to reflux for 10 minutes followed by an aqueous work up, the vicinal diol **7** is the only observed product with a moderate yield of 40%. The remaining material in the crude product mixture consists of starting material **1**. The structure of **7** was deduced from the ^{19}F NMR spectrum and APCI mass spectrometry that is shown in Figures 1.52 and 53.

When the reaction with excess $B(C_6F_5)_3$ was run for longer times while maintaining all other reaction conditions, compound **1** is converted to a novel fullerene boronate ester (**8**) with excellent yield. Compound **8** was isolated by flash chromatography and characterized by ^{19}F and

^{11}B NMR spectroscopy. The ^{11}B NMR spectrum only contained a singlet with a chemical shift of 16.7 ppm while the ^{19}F NMR spectrum contained 5 unresolved multiplets with integral values of 6:6:2:2:1 that correspond to the two pair of CF_3 groups bound to the cage and five fluorine atoms on the aromatic ring, respectively. Furthermore, the chemical shift values of these signals correlate well to the typical chemical shift values of fluorine atoms bound to sp^3 and aromatic carbon atoms. The structure of compound **8** was confirmed by single crystal X-ray diffraction and solved by the graduate student Eric Buckovsky. The X-ray structure of compound **8** is shown in Figure 1.54.

1.3.7. Possible Reaction Pathway of Lewis Acid Assisted Fullerene Functionalization Reactions. The reaction pathway for fullerene epoxide opening reactions was originally proposed by Gan et al.; however, the original reaction pathway needs to be expounded upon in light of this work.[51] As shown in Scheme 1.3.3 the initial step is presumed to be the coordination of $FeCl_3$ to the lone-pair electrons on the epoxide oxygen atom. This is followed by the cleavage of the epoxide-oxygen carbon bond resulting in the intermediates **1a** or **1b** depending on which epoxide-carbon bond was cleaved. However, the proposed intermediate **1b** contains an antiaromatic cyclopentadienyl cation moiety on the surface of the fullerene cage while **1a** does not. It is likely due to this destabilizing effect of the antiaromatic cyclopentadienyl cation moiety that only compounds with an OH group on the central pentagon are observed while compounds stemming from the proposed intermediate **1b** are not observed.

From the proposed intermediate **1a**, compound **6** is afforded upon addition of water. This pathway is only suitable in the absence of additional $FeCl_3$ and in the absence of a suitable nucleophile from the solvent. However, when excess $FeCl_3$ is present, in the case of the reactions

43

performed in this work, a Friedel-Crafts type reaction proceeds to form compounds **2**, **3**, **4**, and **5** depending on the nucleophile.

This proposed reaction pathway offers a hypothesis as to why the *cis*-chlorohydrin fullerene observed by Gan et al. was the main product while in this work the *cis*-arylhydrin is the main product. The reported synthetic procedure used only a single equivalent of FeCl$_3$ while in the work presented here an excess of FeCl$_3$ was used in each reaction. The presence of excess FeCl$_3$ results in the Freidel-Crafts reaction whereas without it, only compound **6** is possible. A control reaction that could be performed to confirm this proposed reaction pathway would be to repeat the procedure from the literature and use a single equivalent of FeCl$_3$ with compound **1**. If the major product is compound **6** then this reaction pathway is confirmed, if not, then an alternative pathway would need to be devised.

Information about the relative rates of the reaction steps in the proposed reaction pathway were examined. When an identical reaction is conducted in benzene with excess FeCl$_3$ and the reaction time is decreased from 30 min to 10 min, a mixture of 70% compound **2** and 30% compound **6** with no starting material is observed by ^{19}F NMR spectroscopy. By comparing the crude products from this shorter reaction to the products of the 30 min reaction where only compound **2** is observed indicates that the nucleophilic attack proceeds more slowly than the initial formation of the Lewis acid adduct.

The reaction pathway is presumably very similar when the Lewis acid is changed from FeCl$_3$ to B(C$_6$F$_5$)$_3$. The Lewis acid opens the epoxide ring followed by nucleophilic attack from adventitious water in the reaction solvent forming compound **7**. This is then followed by electrophilic attack from the excess B(C$_6$F$_5$)$_3$ forming 2 equivalents of C$_6$F$_5$H and compound **9.**

This hypothesis could be tested by treating compound **8** with B(C$_6$F$_5$)$_3$ or by monitoring the reaction progress by ^{19}F NMR spectroscopy.

Experimental for Section 1.3

Reagents and Solvents. All solvents were A.C.S. grade or better and were used as received without further purification unless otherwise stated. The 3-chloroperoxybenzoic acid (mCPBA) (Aldrich; 77% max with the remainder being 3-chlorobenzoic acid and water) was used as received. The O$_2$:O$_3$ mixture of gas was prepared by passing tech grade oxygen through a corona discharge generated with a tesla coil. The 60-10-3, 60-4-2, and 60-4-2[O] were prepared as previously described in the literature. The anhydrous FeCl$_3$ was prepared by reacting thionyl chloride with bulk FeCl$_3$ for 24 hours then removing the thionyl chloride by vacuum transfer. The solvents for each Lewis acid assisted epoxide opening reactions were dried by activated 3Å molecular sieves (activated by heating to 300 °C under vacuum for 24 hours) for 24 hours. Each solvent was analyzed by ^{1}H NMR spectroscopy to confirm purity and dryness prior to use. The iodo benzene contained ca. 10% benzene, all other solvents were pure by ^{1}H NMR spectroscopy. The trispentafluorophenyl borane was used as received and stored in a dry dinitrogen glove box with the water and oxygen content below 1 ppm. A ^{19}F NMR spectrum of the fresh B(C$_6$F$_5$)$_3$ was acquired quickly after received to confirm purity and dryness.

Instruments and Equipment: All thermal experiments were conducted on a hot plate or in a Lindber model 55035 tube furnace equipped with an external thermocouple. All photolysis

experiments were conducted in a photochemical safety cabinet equipped with a ventilation fan and a Hanovia #679A36 450 W Hg lamp placed in a water-cooled immersion well. The operating temperature was approximately 30 °C for the duration of each experiment. All HPLC analysis was performed on a Shimadzu HPLC system with a control module (CBM-20A), a UV-vis detector set to 300 nm (SPD-20A), pump (LC-6AD), and a manual injector. The HPLC column used was a semi-preparative 10 mm I.D. × 250 mm or a preparative 25 mm I.D. × 250 mm Cosmosil Buckyprep column from Nacalai Tesque, Inc. Fluorine-19 NMR spectra were recorded on a Varian 400 spectrometer operating at 376.5 MHz with a C_6F_6 internal standard referenced to δ −164.9 (solvent was $CDCl_3$). All APCI-MS were recorded in the negative ion mode on a Finnigan 2000 LCQ-DUO spectrometer. The sampels were injected as a 50:50 v:v toluene: acetonitrile mixture. The carrier solvent was acetonitrile.

X-ray Diffraction: Crystals of 60-10-3[O_2] were grown by slow evaporation from a saturated solution of chloroform-d_1. Crystals of **2**, **4**, **5**, and **9** were grown from slow evaporation of dichloromethane. Data sets were recorded on a Bruker Kappa APEX II CCD diffratometer equipped with a Mo Kα radiation source (graphite monochromator). Unit cell parameters were obtained from a least-squares fit to the angular coordinates to all reflections and intensities were integrated from a series of frames converting more than a hemisphere of reciprocal space. The structures were solved by using direct methods and refined (on *F2*, using all data) by a full-matrix, weighted least-squares process. All atoms were refined by using anisotropic atomic displacement parameters. Standard Bruker control and integration software (APEX II) was employed, and Bruker SHELXTL software was used for structure solution and refinement.

Reaction of 60-10-3[O₂] with Oxidizing Agents: A 1 mg sample of 60-10-3[O_2] was added to 50 mL of toluene and excess mCPBA was then added to a 100 mL round bottom flask. This solution was heated to reflux for 12 hours while light was excluded. After 12 hours had passed, the toluene was removed by vacuum. The mCPBA was removed by washing with petroleum ether 5 times. Ozonolysis was performed by bubbling a mixture of O_2 and O_3 gas from a home made apparatus through a toluene solution of 60-10-3[O_2] while exposed to light and air.

General Description of a Lewis Acid Assisted Epoxide Opening Reaction: Compounds **2**, **3**, **4**, **5**, **6**, and **7** were all prepared with identical procedures with the exception of the solvent which was dry/degassed (as previously described above) neat benzene, hexafluoro benzene, toluene, fluoro benzene, bromo benzene, and iodo benzene respectively. In a dry dinitrogen glove box with H_2O and O_2 less than 1 ppm, excess dry $FeCl_3$ was added to a reaction flask containing 60-4-2[O] and the solvent. The reaction flask was tightly stoppered and allowed to react for 30 min. After 30 min, the flask was removed from the glove box and excess distilled deionized water was added (typically 1 mL of water was used for the reaction scale conducted in this work). The now wet reaction was stirred for 10 min. After 10 min of stirring, the reaction mixture was placed under vacuum until dry. A mixture of 10:10:1 dichloromethane: petroleum ether: ethyl actetate (by volume) was added until all products dissolved. The mixture was then run through a silica gel column with the mobile phase being the same 10:10:1 dichloromethane: petroleum ether: ethyl actetate (by volume) solution. Only a single band (red to orange) eluted off the column. The ferric chloride remained behind in a dark band. The isolated product was then placed under vacuum and analyzed by ^{1}H and ^{19}F NMR spectroscopy and APCI-MS.

Conclusions

A general method for heterogeneous trifluoromethylation of various fullerene starting materials was developed and optimized for the large-scale production of trifluoromethyl fullerenes. Various reaction parameters including reaction temperature, pressure of CF_3I, presence of a Cu promoter, size of the reactive zone, time, and reaction scale were investigated and optimized for the production of both highly substituted fullerene cages as well as cages with two and four CF_3 groups. These results also demonstrate this method can be used on a wide variety of fullerene starting materials including both hollow and endohedral metallofullerenes, including the first example of the trifluoromethylation of $Y_3N@C_{80}$. Furthermore, a solution phase homogeneous perfluoroalkylation method was used to prepare a series of fullerene$(R_F)_2$ compounds with the same addition pattern, but with various chain lengths and branching patterns of the R_F groups.

The further functionalization of TMFs using oxidation and Lewis acid assisted epoxide opening reactions was also successfully carried out. Moreover, these further functionalization reactions were used to introduce a range of different adducts and were shown to be both highly efficient, with isolated yields greater than 95%, and also regiospecific. These reactions were used to prepare seven novel derivatized TMFs that were isolated and structurally characterized using a range of spectroscopic techniques. Data for five new crystal structures of derivatized TMFs were collected the main features of these structures was discussed. Lastly, experimental evidence was put forward to support a new Lewis acid assisted fullerene epoxide opening reaction pathway.
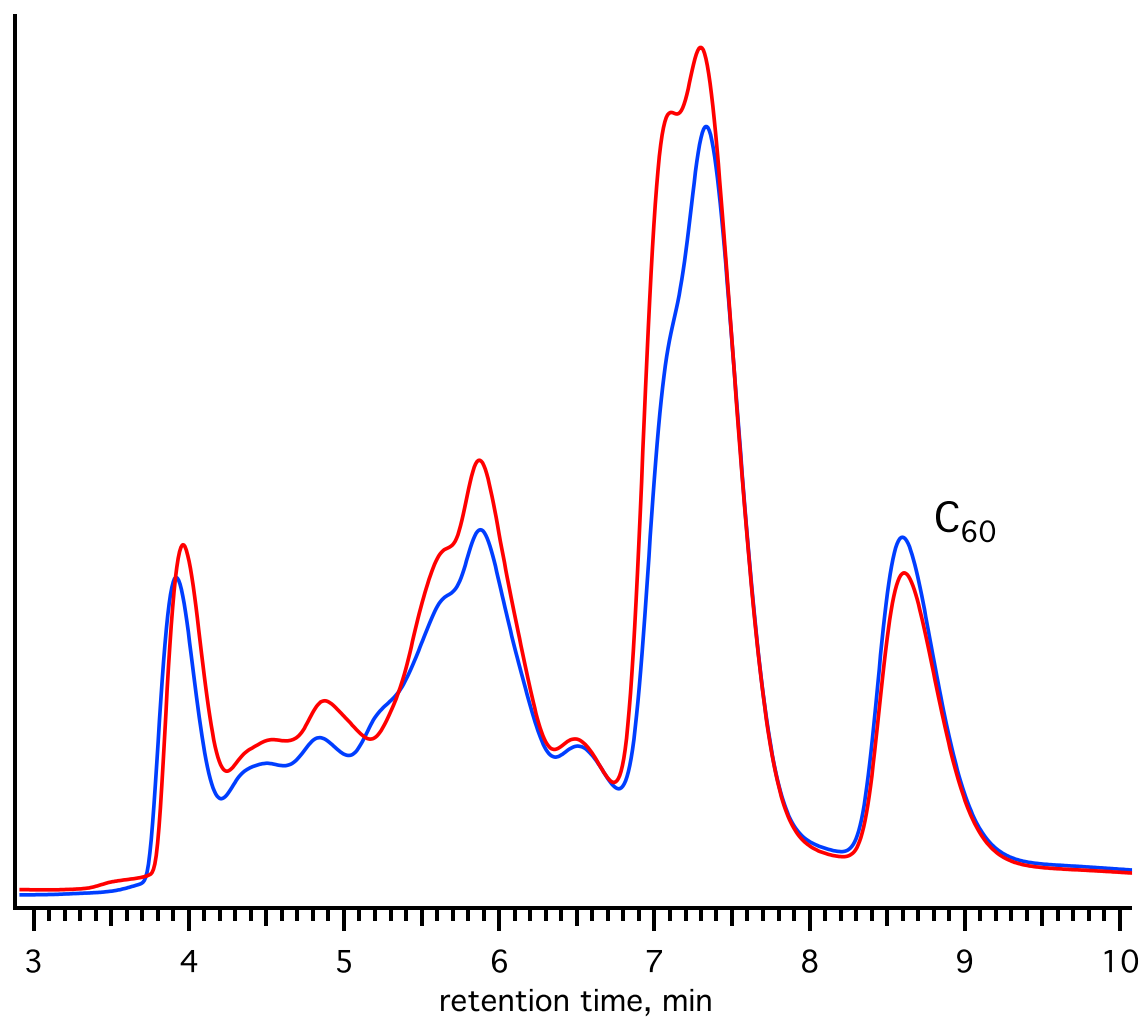
Figure 1.1. Two HPLC chromatograms of the crude products from identical trifluoromethylation reactions conducted at 500 °C with a CF_3I pressure of 45 torr. The HPLC mobile phase is 100% toluene with a flow rate of 5 mL/min.
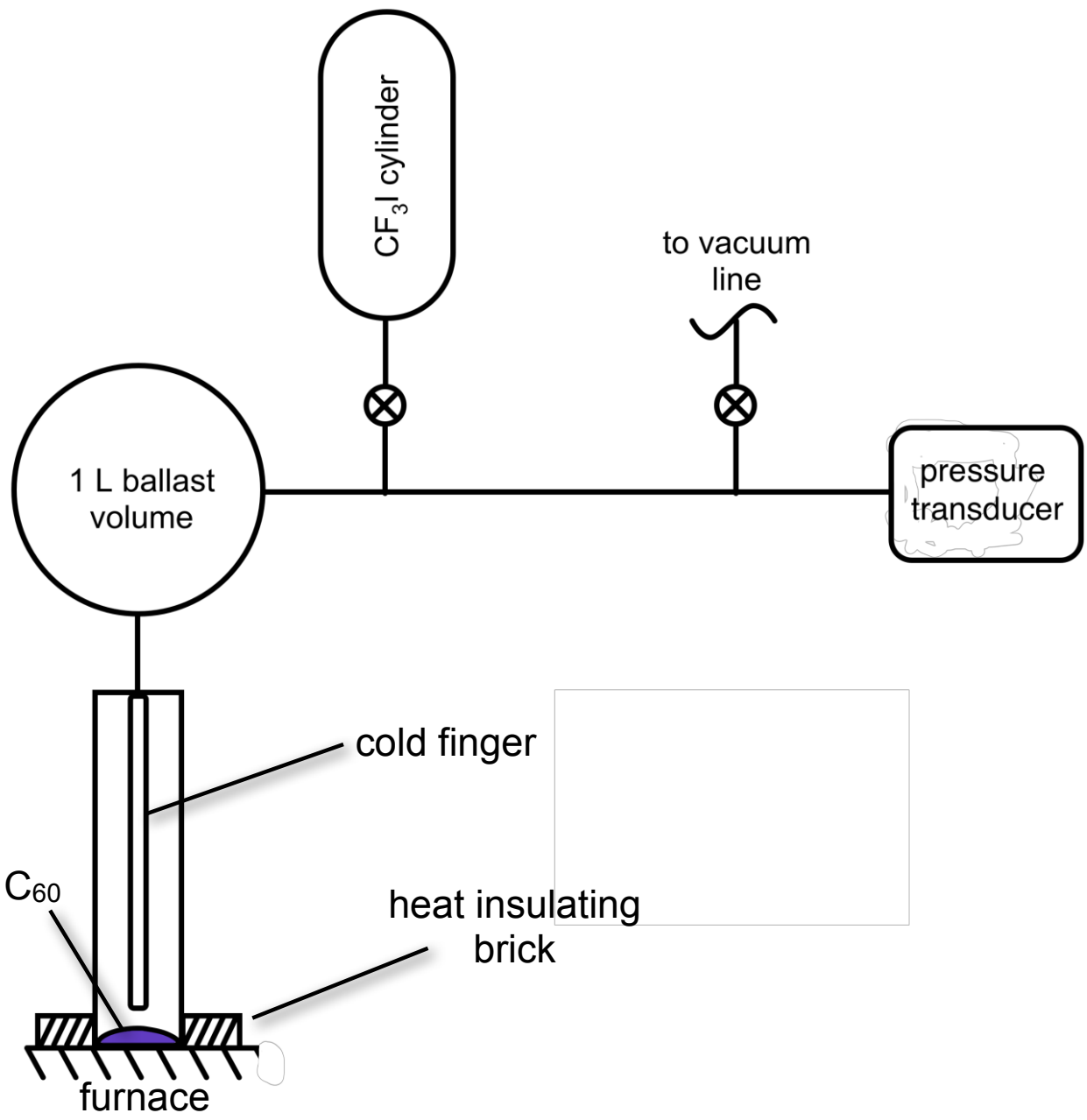
Figure 1.2. Schematic of the gradient temperature gas solid (GTGS) reactor.
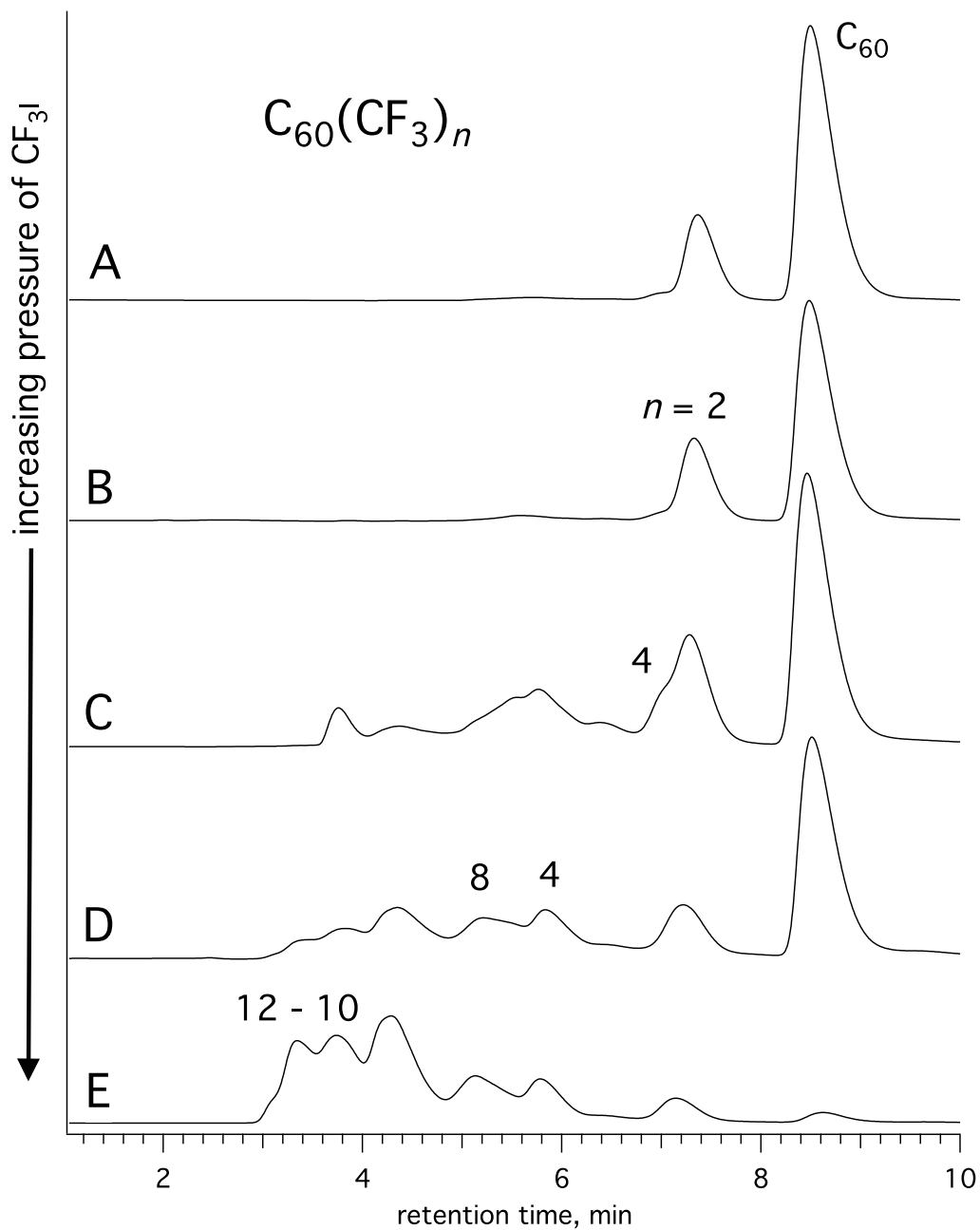
Figure 1.3. HPLC chromatograms in 100% toluene of the crude products from C_{60} trifluoromethylation reactions done at 500°C with a CF_3I pressure of (A) 5 torr, (B) 15 torr, (C) 45 torr, (D) 135 torr, and (E) 410 torr. Unreacted C_{60} elutes at 8.3 min. The HPLC parameters were identical for all 5 and consisted of 100% toluene mobile phase with a flow rate of 5 mL/ min.
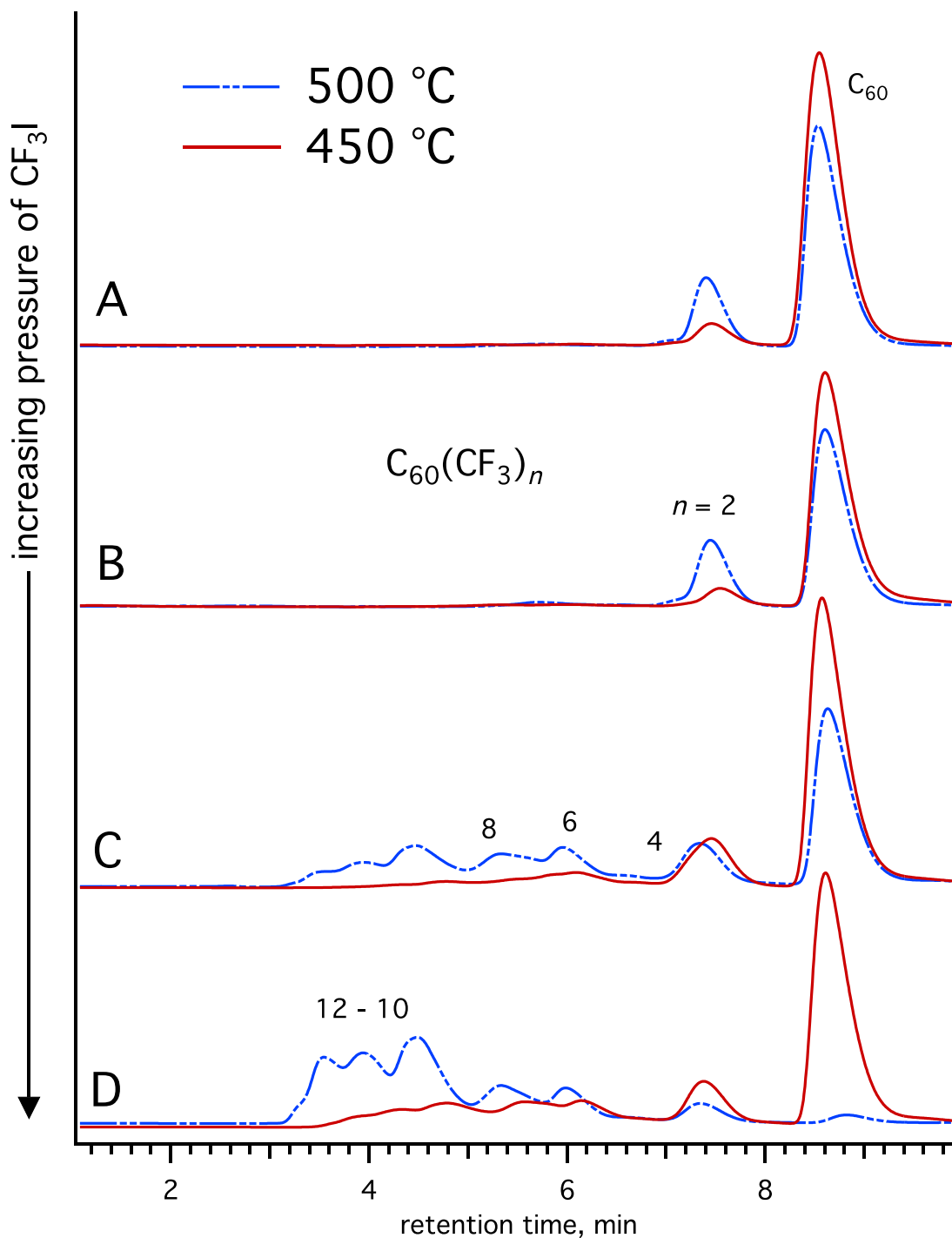
Figure 1.4. HPLC chromatograms in 100% toluene of the crude products from 8 different C_{60} trifluoromethylation reactions held at 450 °C (solid) and 500 °C (dashed) with CF_3I pressures of (A) 5 torr, (B) 15 torr, (C) 45 torr, and (D) 135 torr. Peak at 8.3 min is unreacted C_{60}.
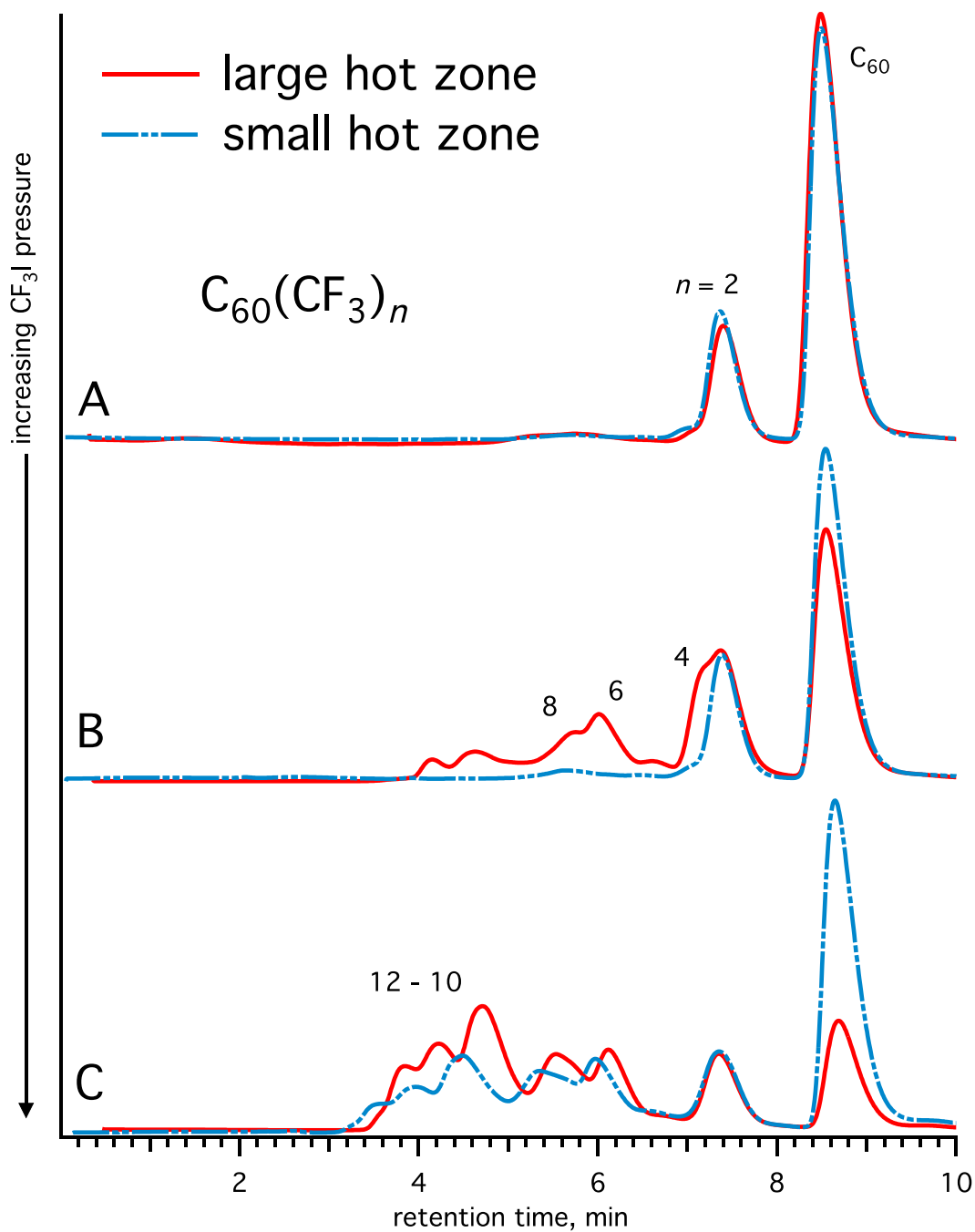
Figure 1.5. HPLC chromatograms in 100% toluene of the crude products from different C_{60} trifluoromethylation reactions carried out in the GTGS reactor at 500 °C fitted with a small hot zone (dashed) and a large hot zone (solid) with CF_3I pressures of (A) 5 torr, (B) 15 torr, and (C) 45 torr.

53
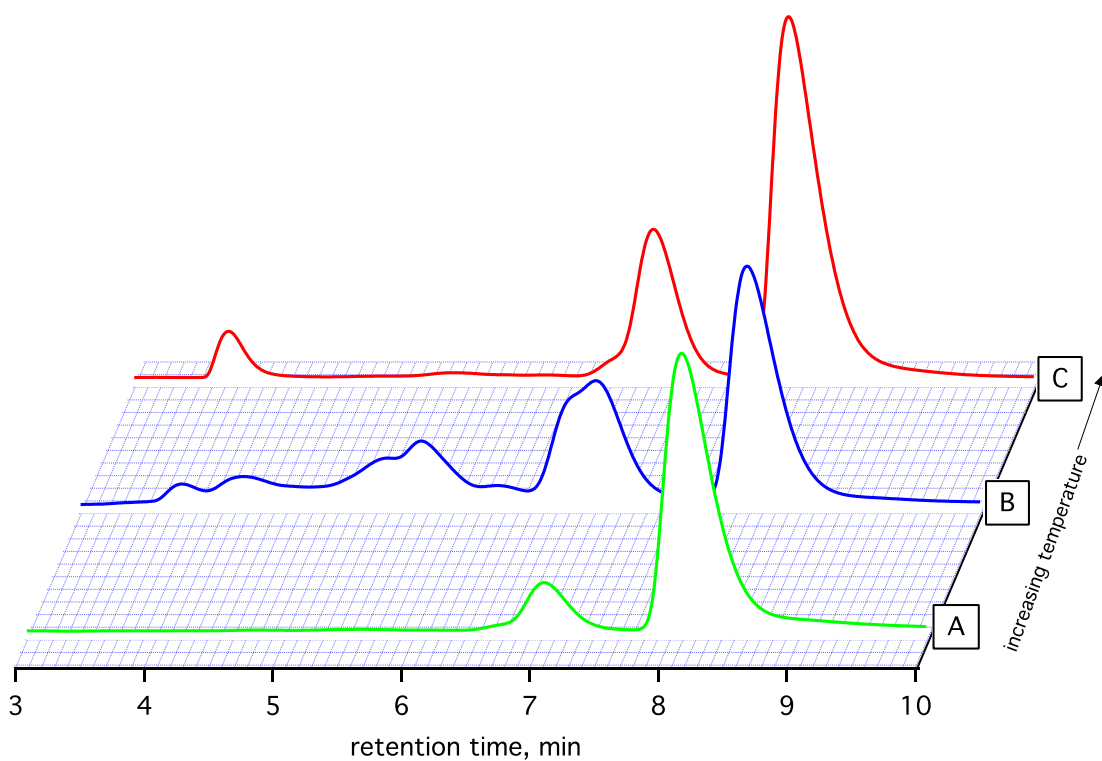
Figure 1.6. An HPLC waterfall plot of the crude material from three different C_{60} trifluoromethylation reactions all performed with 45 torr CF_3I gas. These three reactions were conducted at three different temperatures of (A) 450 °C, (B) 500 °C, and (C) 550 °C. The HPLC conditions were identical and consisted of 100% toluene with a flow rate of 5 mL · min^{-1}.
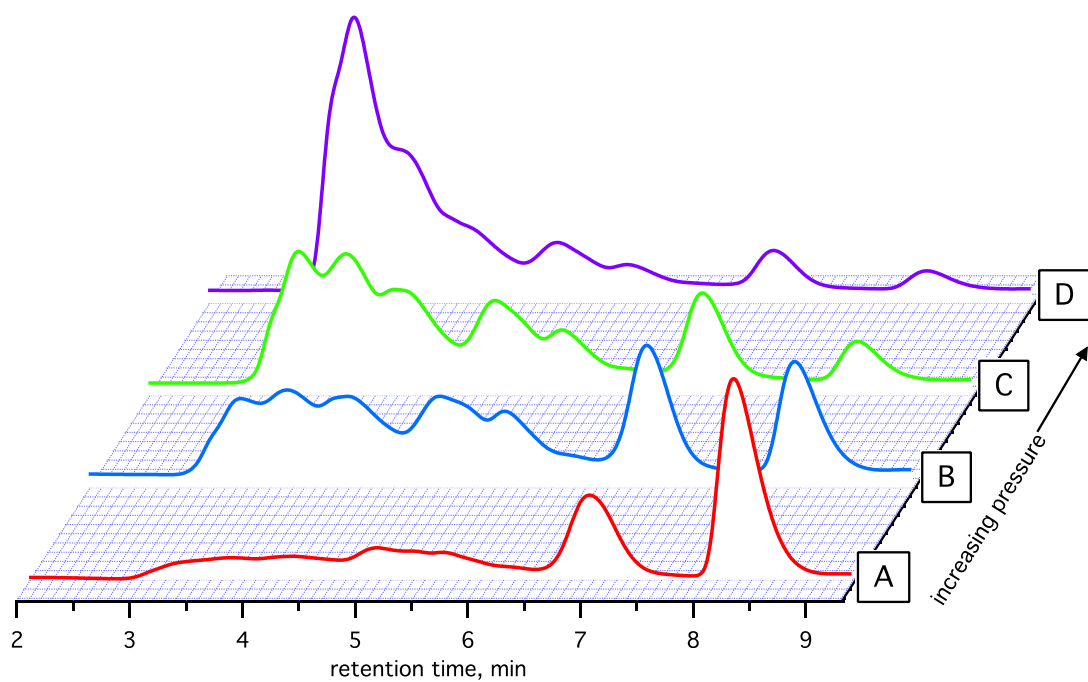
Figure 1.7. An HPLC waterfall plot of the crude products from 4 different C_{60} trifluoromethylation reactions performed in the presence of excess Cu metal with a CF_3I pressure of (A) 5 torr, (B) 15 torr, (C) 30 torr, (C) 135 torr, and (d) 410 torr.
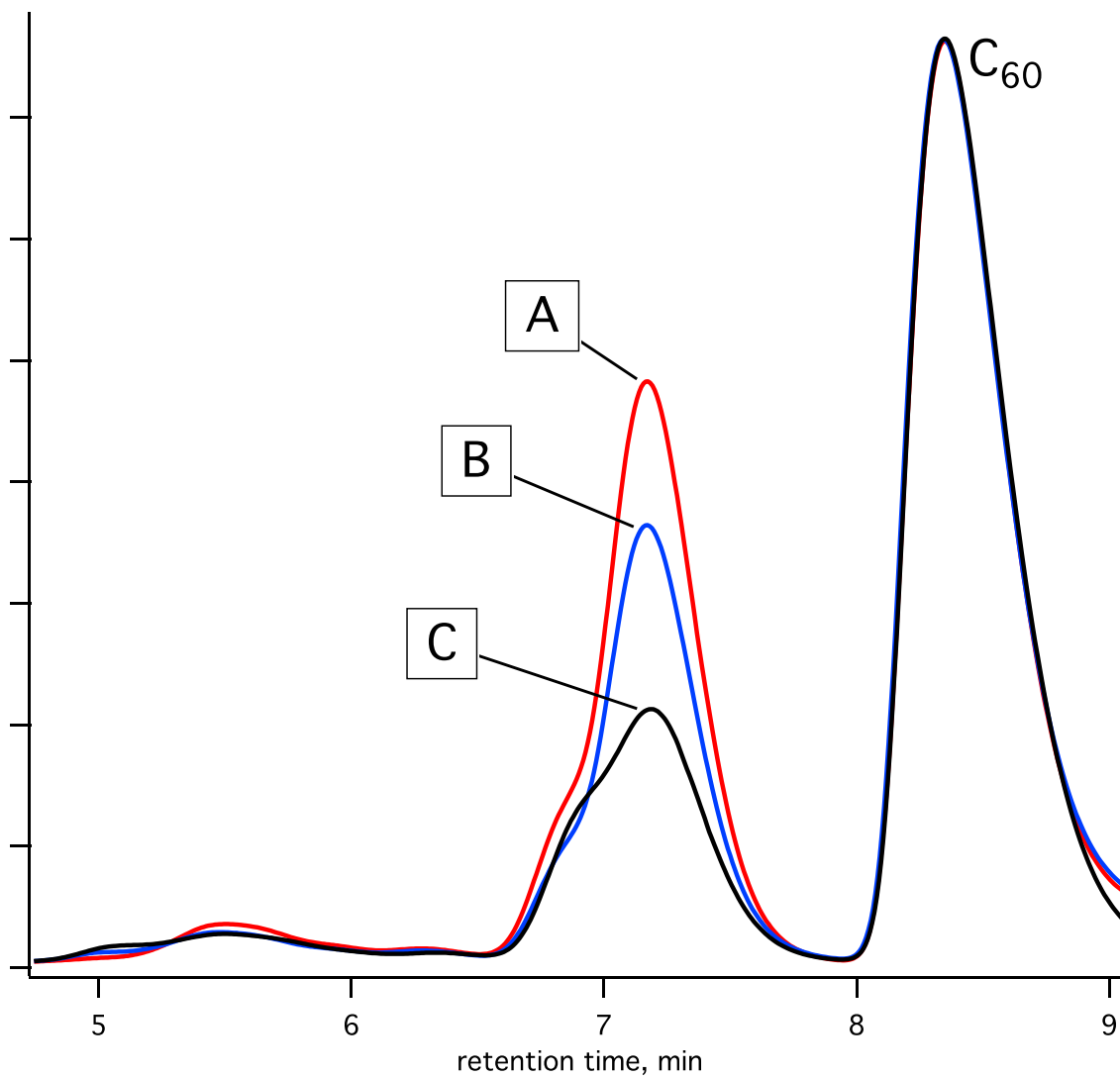
Figure 1.8. HPLC chromatograms of the crude products from three separate experiments conducted under the same conditions using different amount of C_{60} starting material (A) 4.0 mg, (B) 10.8 mg and (C) 40.9 mg. The HPLC chromatograms are normalized to the unreacted C_{60} peak that elutes at 8.3 min.
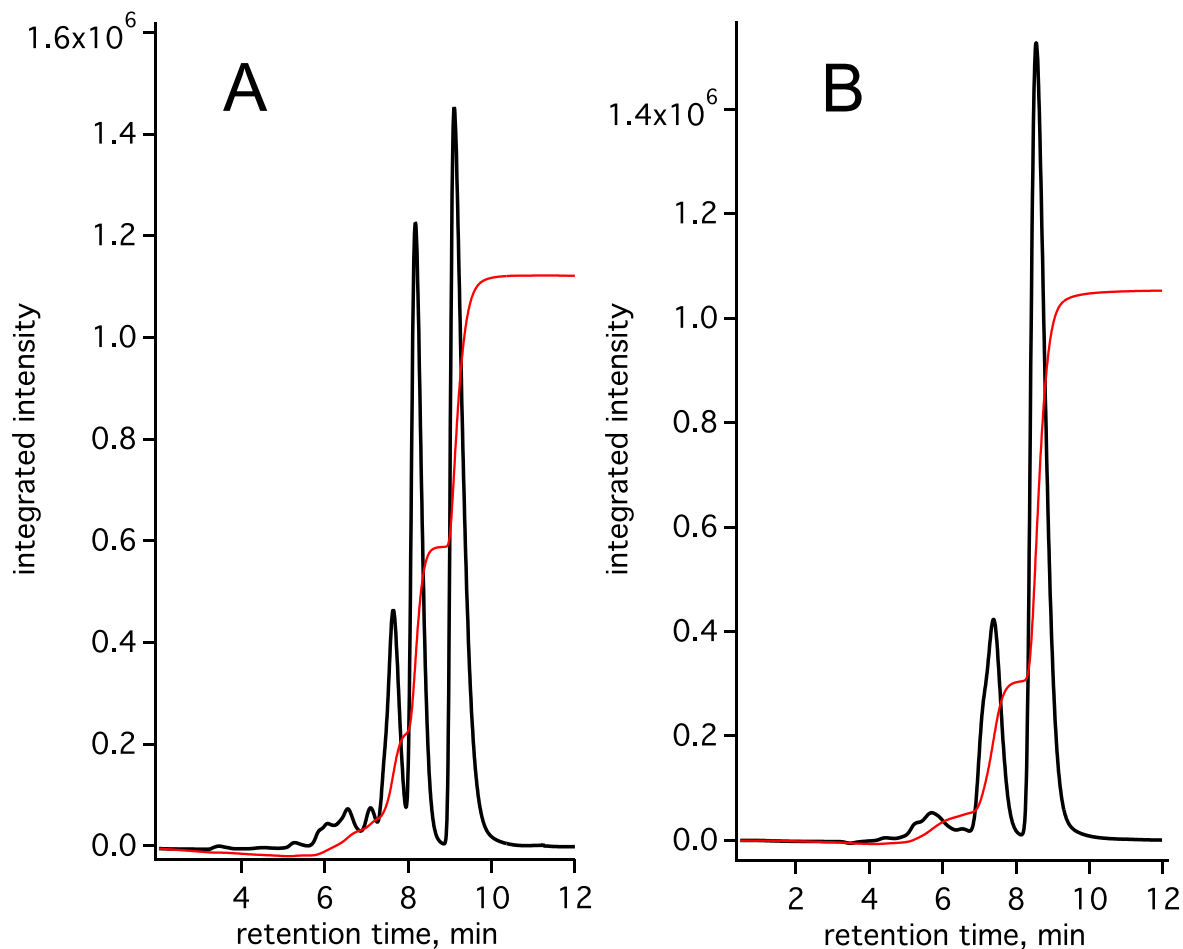
Figure 1.9. Determination of the conversion of C_{60} by integrated intensity from HPLC chromatograms of the crude products of trifluoromethylation reactions: (A) with a cold finger condenser in place resulting in a 52% yield and (B) without a cold finger condenser resulting in a 29% yield. Integrated intensity was divided by the total intensity and multiplied by 100% to determine the conversion of C_{60} into all $C_{60}(CF_3)_n$ products. The peak eluting at 9 min is due to C_{60} unreacted starting material.
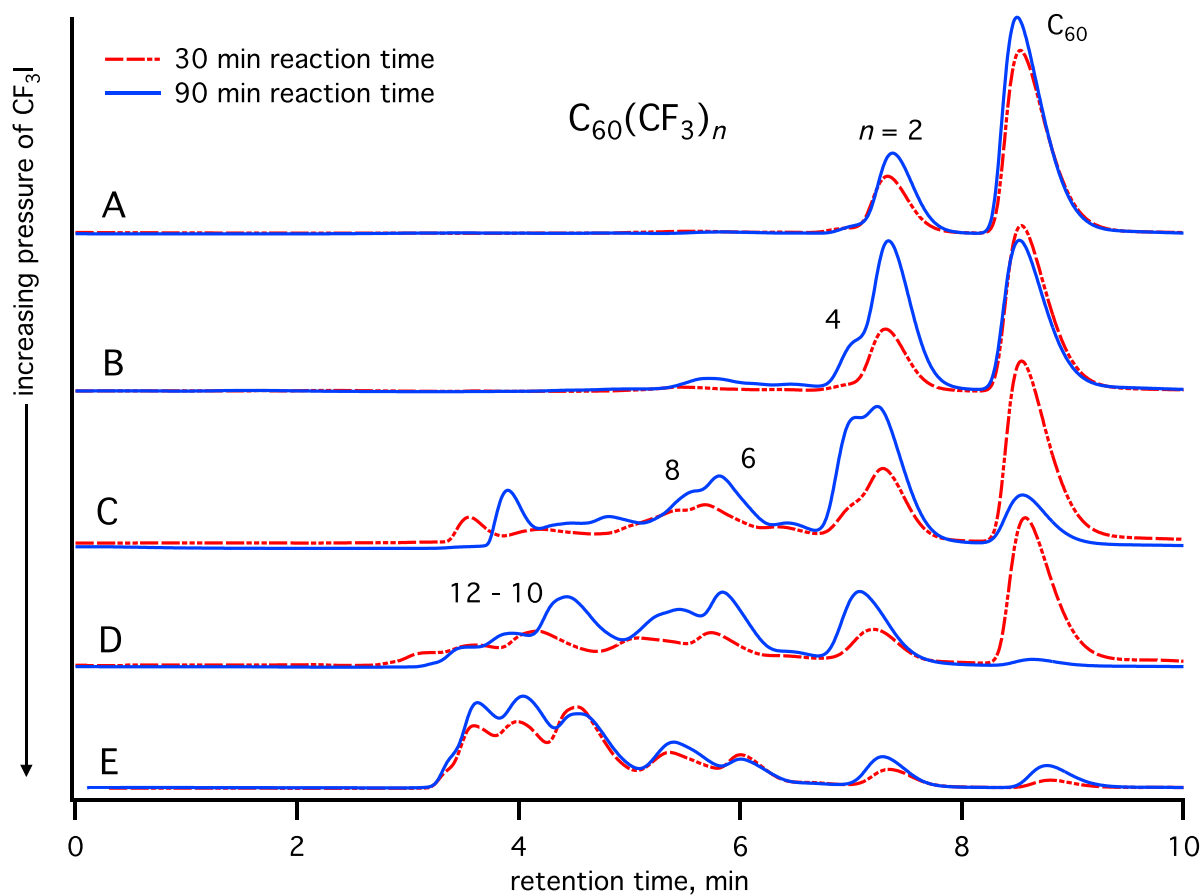
Figure 1.10. HPLC chromatograms of the crude products from 10 different C_{60} trifluoromethylation reactions with a total reaction time of 30 min (dashed) and 90 min (solid) and a total pressure of CF_3I gas of (A) 5 torr, (B) 15 torr, (C) 45 torr, (D) 135 torr and (E) 410 torr.
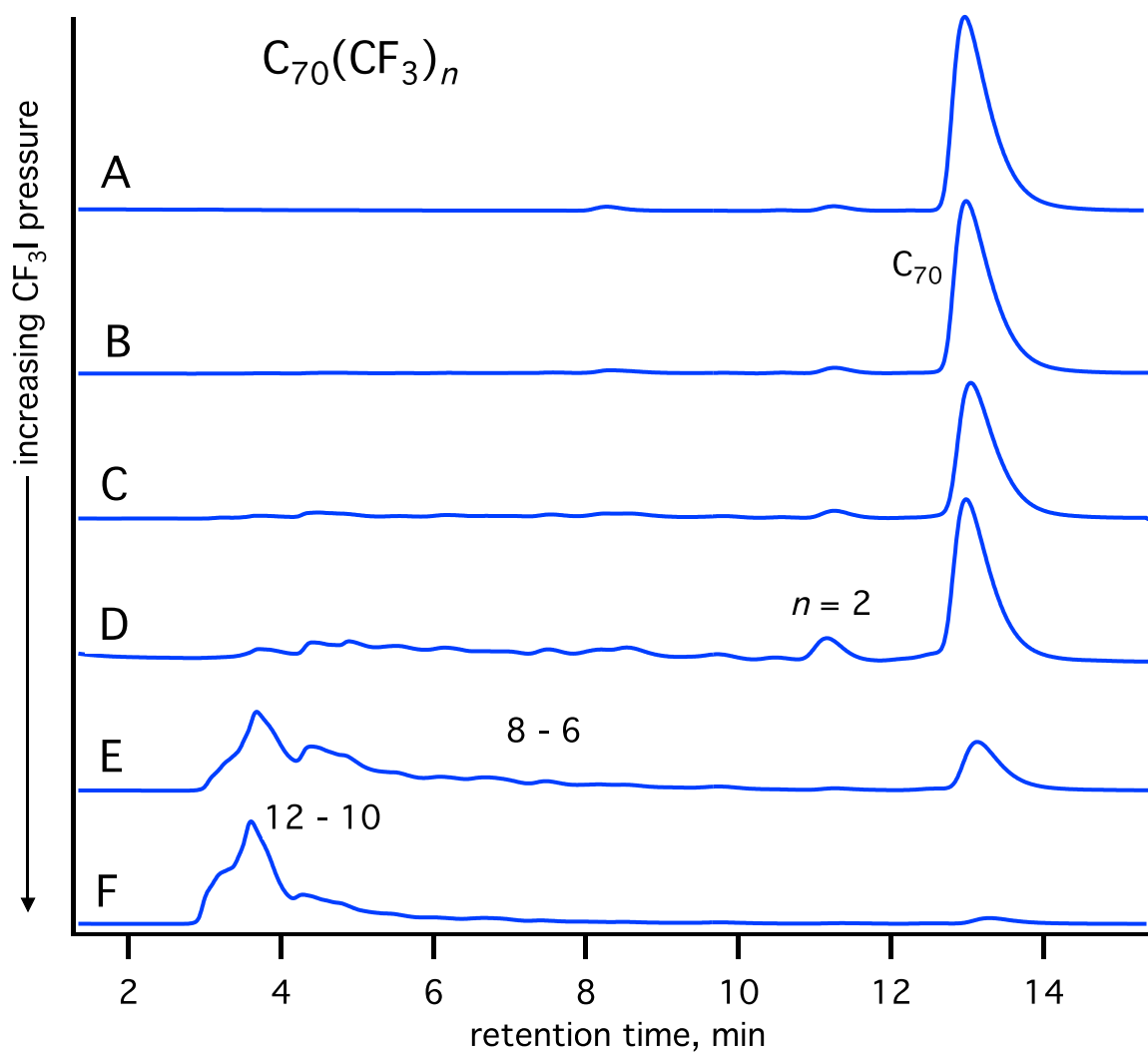
Figure 1.11. HPLC chromatograms of the crude products from 6 different C_{70} trifluoromethylation reactions conducted at 500°C in the GTGS reactor with a CF_3I pressure of (A) 5 torr, (B) 15 torr, (C) 30 torr, (D) 45 torr, (E) 135 torr, and (F) 410 torr. Unreacted C_{70} elutes at ca. 13 min.
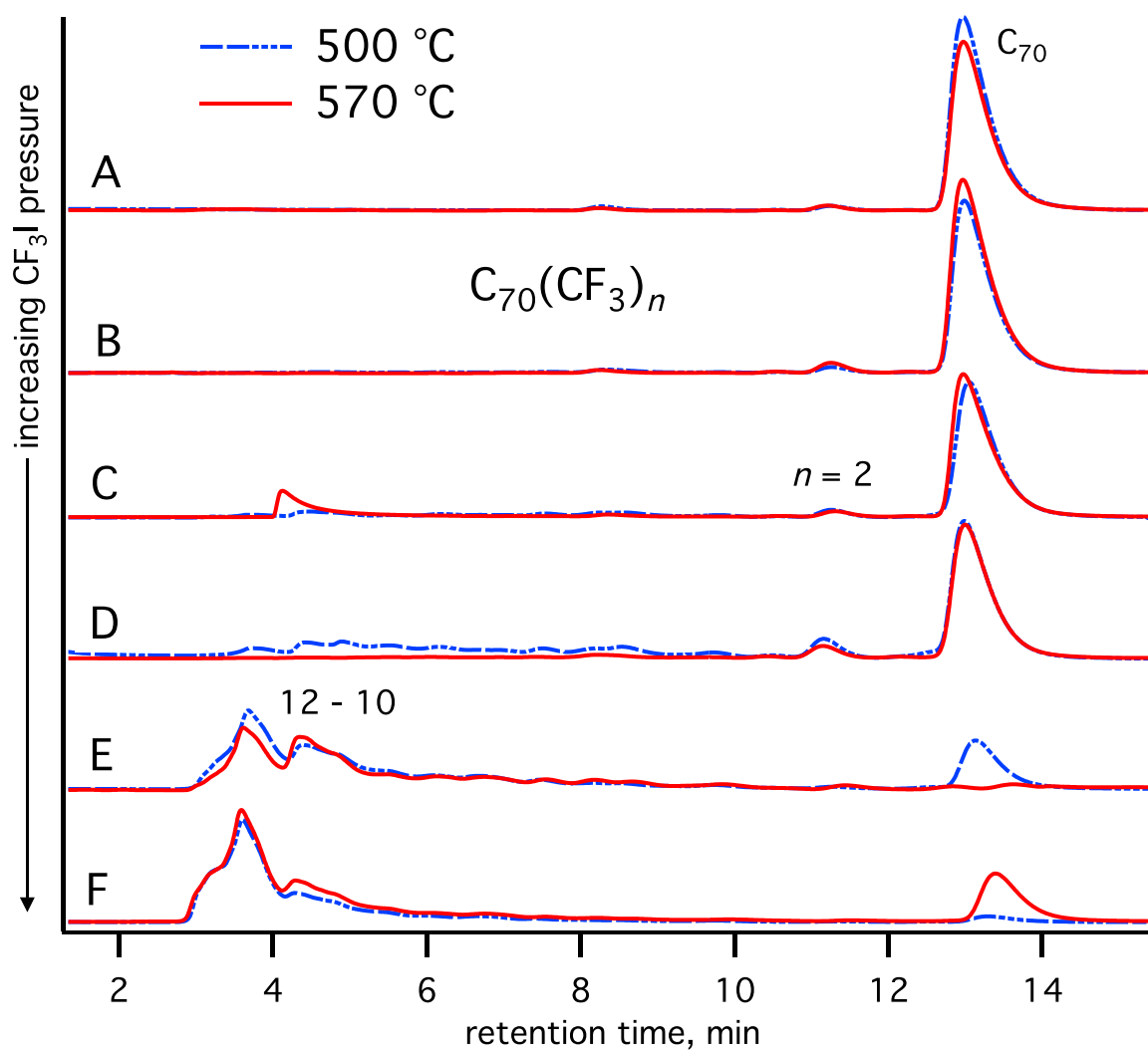
Figure 1.12. HPLC chromatograms of the crude products from a series of C_{70} trifluoromethylation experiments conducted in the GTGS reactor at 500 °C (dashed) and at 570 °C (solid) with various pressures of CF_3I gas of (A) 5 torr, (B) 15 torr, (C) 30 torr, (D) 45 torr, (E) 135 torr, and (F) 410 torr. Unreacted C_{70} elutes at ca. 13 min.
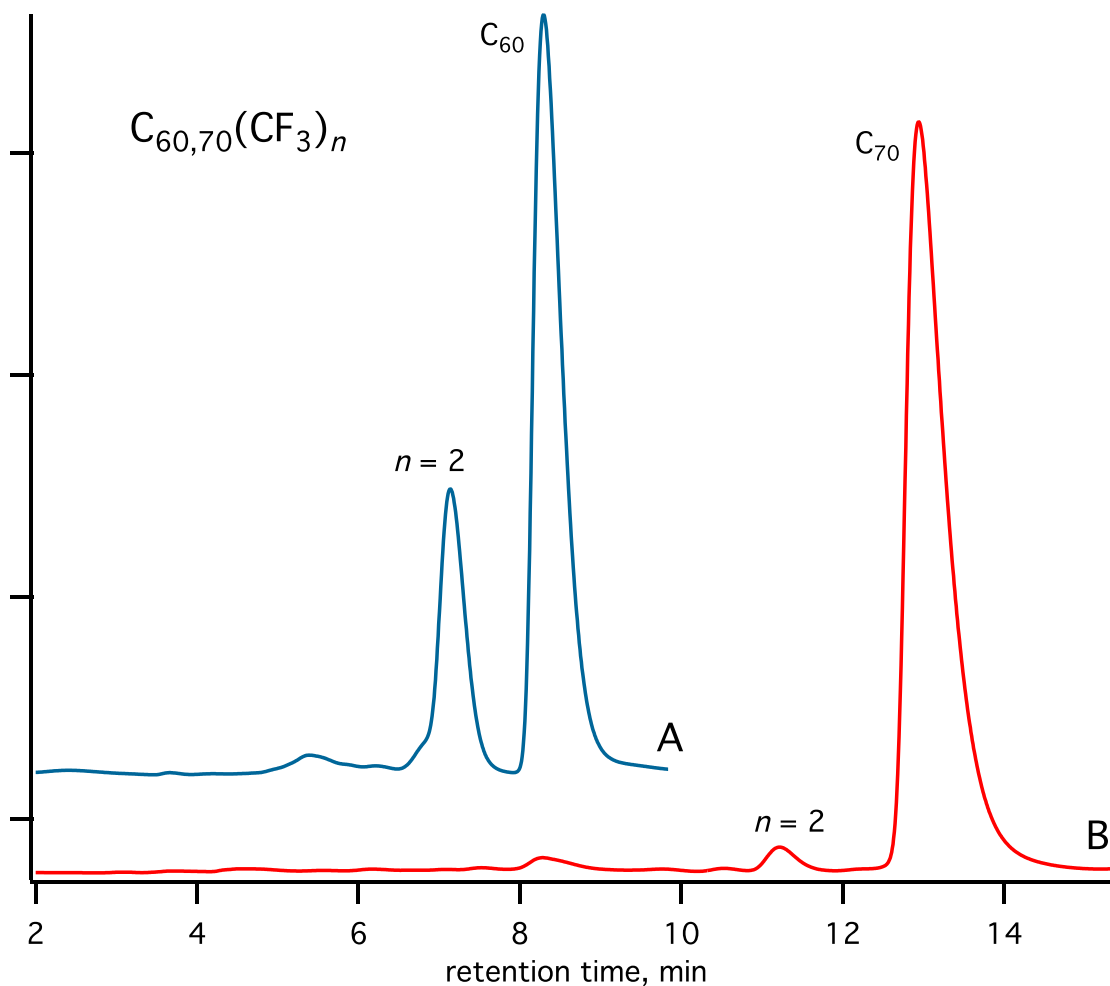
Figure 1.13. HPLC chromatograms of the crude products from two separate GTGS trifluoromethylation reactions under an identical temperature of 500 °C and with the same pressure of CF_3I gas of 15 torr only (A) used C_{60} as the starting material while C_{70} was used for reaction (B). The HPLC traces were normalized to the unreacted starting material.
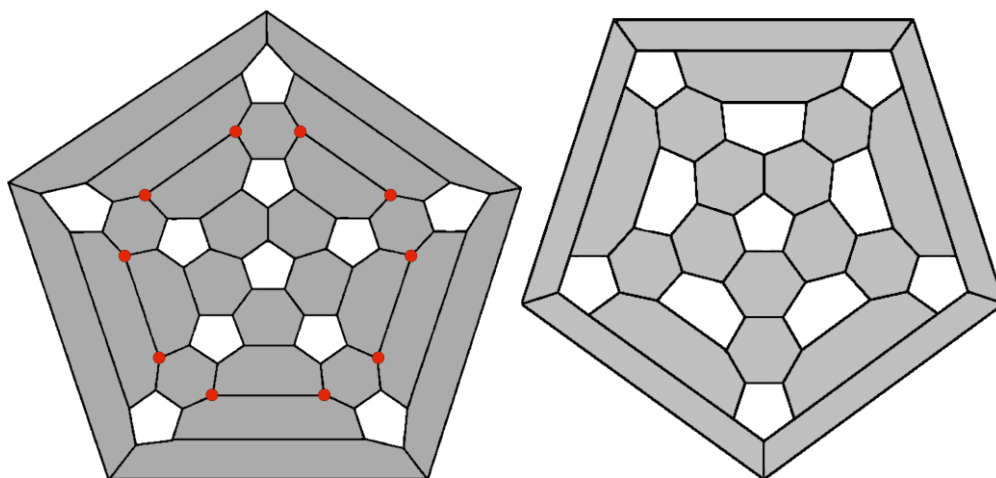
Figure 1.14. Schlegel diagrams of C_{70} (left) and C_{60} (right) with all the hexagons shaded in grey and the carbon atoms at the triple hexagon junctions highlighted in red.
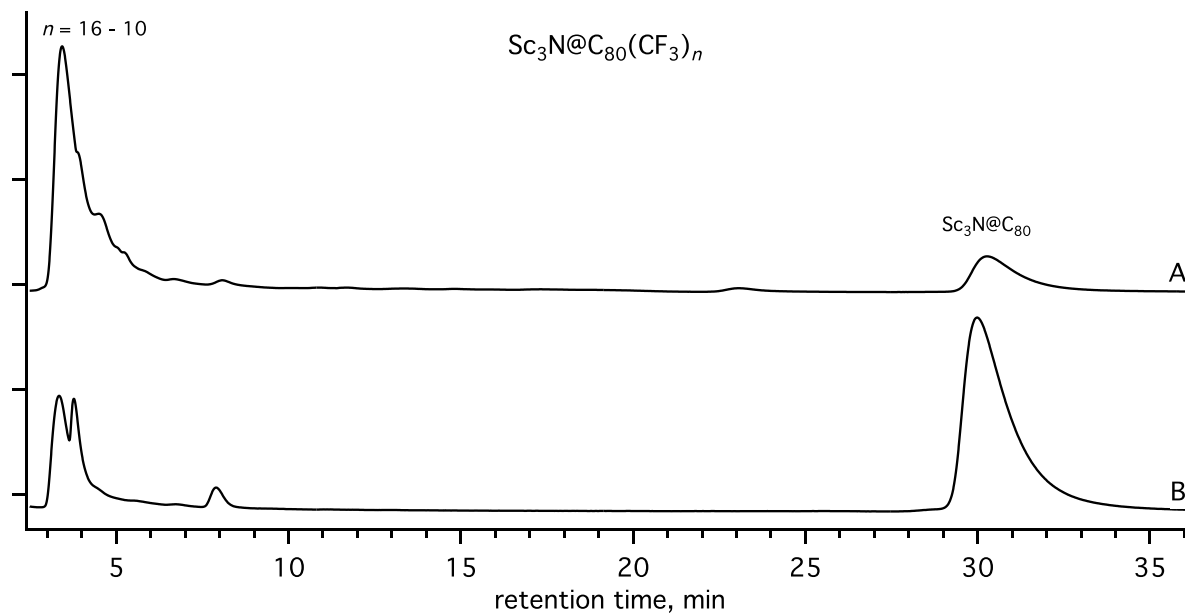
Figure 1.15. HPLC chromatograms of the crude products from two different GTGS trifluoromethylation reactions under identical conditions except that (A) was performed in the presence of copper powder while (B) was not. The peak with a retention time of ca. 30 min is the $Sc_3N@C_{80}$ starting material.
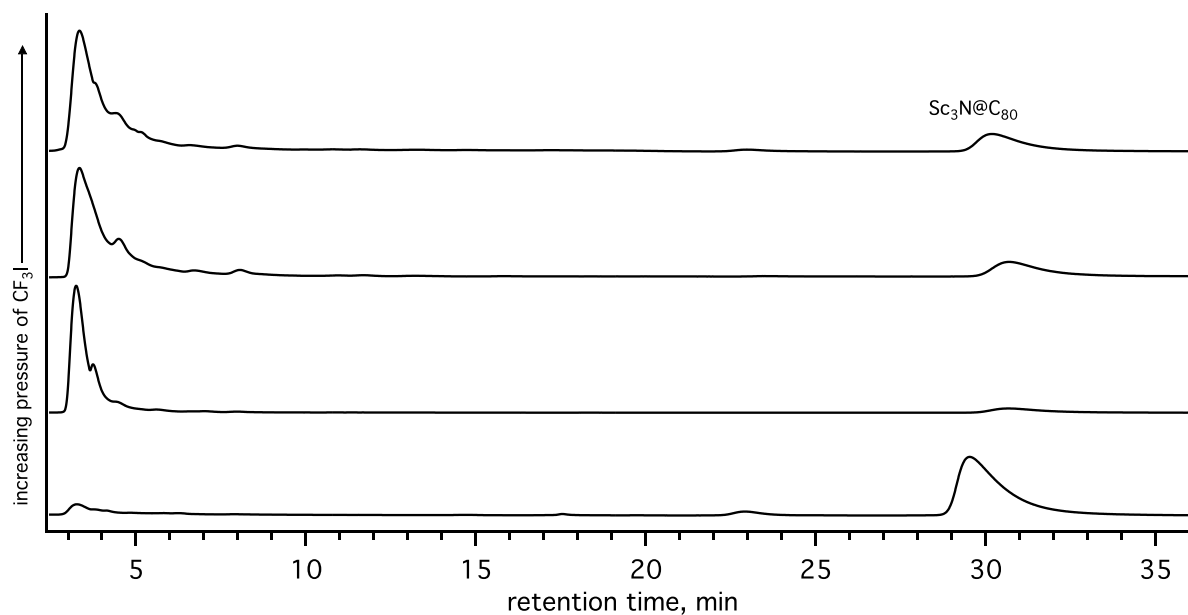
Figure 1.16. HPLC chromatograms of the crude products from a series of GTGS trifluoromethylation reactions with $Sc_3N@C_{80}$ for 5 hours at a furnace temperature of 550 °C in the presence of excess copper powder with (A) 600 torr CF_3I, (B) 250 torr CF_3I, (C) 75 torr CF_3I, and (D) 50 torr CF_3I. The peak at ca. 30 min is $Sc_3N@C_{80}$.
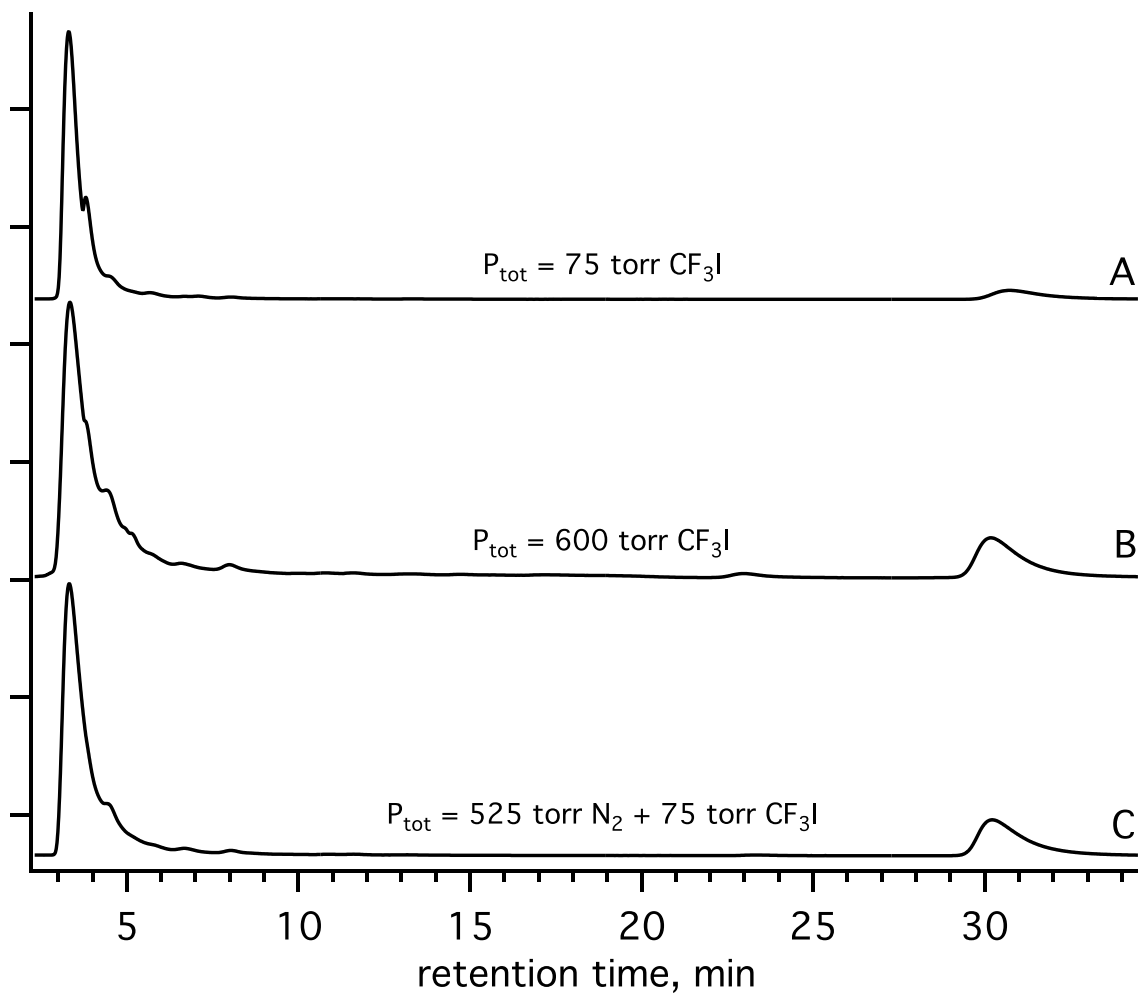
Figure 1.17. HPLC chromatograms of the crude products from three identical GTGS trifluoromethylation reactions with the only difference between them being the pressure of CF_3I in (A) was 75 torr (B) had a pressure of 600 torr while (C) was conducted at the same total pressure as (B) but the gas was composed of 75 torr CF_3I and 525 torr N_2. The peak with a retention time ca. 30 min is the unreacted starting material $Sc_3N@C_{80}$.
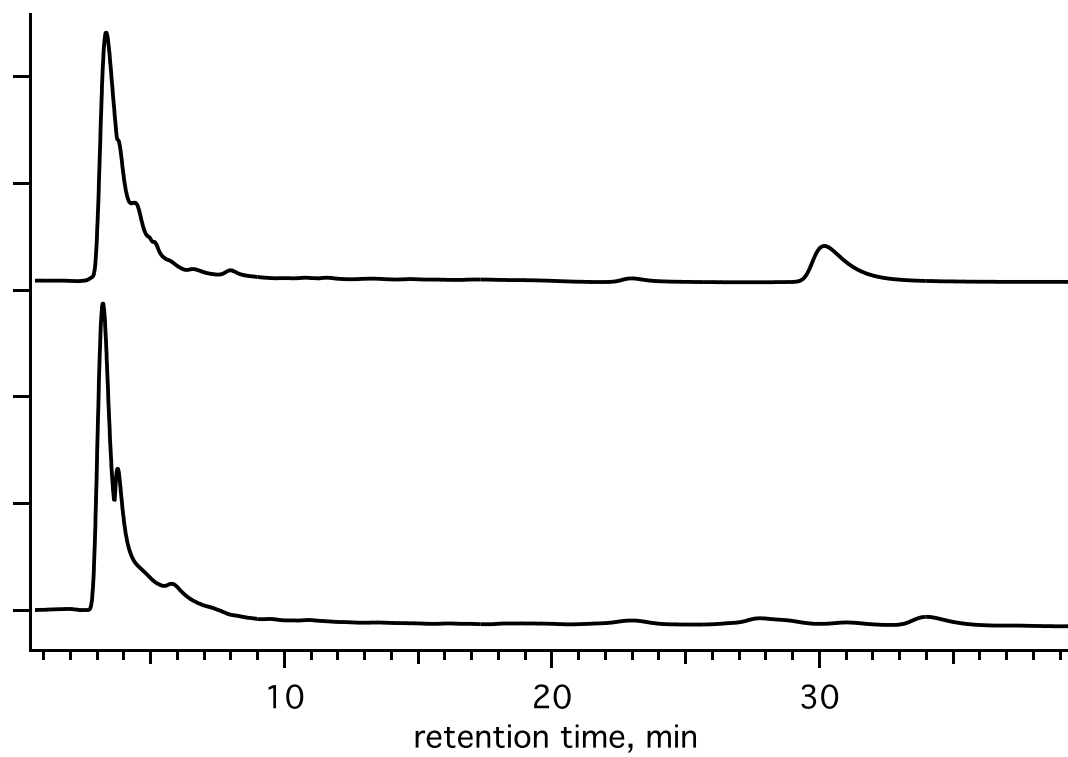
Figure 1.18. HPLC chromatograms of the crude products from two identical trifluoromethylation reactions with (top) $Sc_3N@C_{80}$ as the starting material and (bottom) $Y_3N@C_{80}$ as the starting material.

Table 1.1. Sealed ampoule reaction parameters used to prepare the series of $C_{60}(R_F)_2$ compounds studied in this section.

cmpd	R_FI equivalents	temp, °C	solvent	time, h
$C_{60}(n\text{-}C_3F_7)_2$	18	180	oDCB	24
$C_{60}(i\text{-}C_3F_7)_2$	18	180	oDCB	24
$C_{60}(n\text{-}C_4F_9)_2$	12	180	oDCB	24
$C_{60}(s\text{-}C_4F_9)_2$	8	180	oDCB	24
$C_{60}(n\text{-}C_8F_{17})_2$	6	180	oDCB	24
$C_{60}(CF_2 C_6F_5)_2$	2	130	oDCB	24
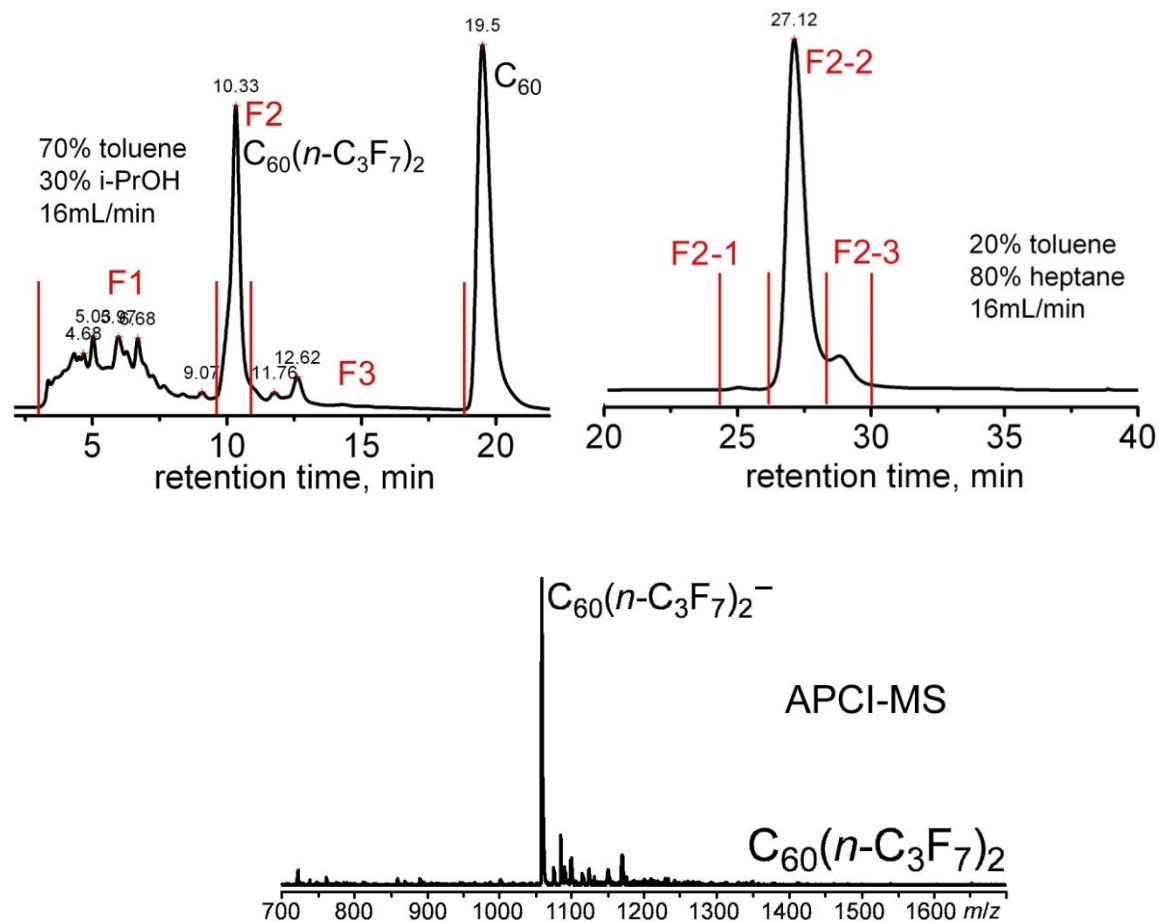
Figure 1.19. (Top from left to right) First and second stage HPLC separation of the crude reaction material containing $C_{60}(n-C_3F_7)_2$. (Bottom) APCI-MS of the isolated fraction F2-2.
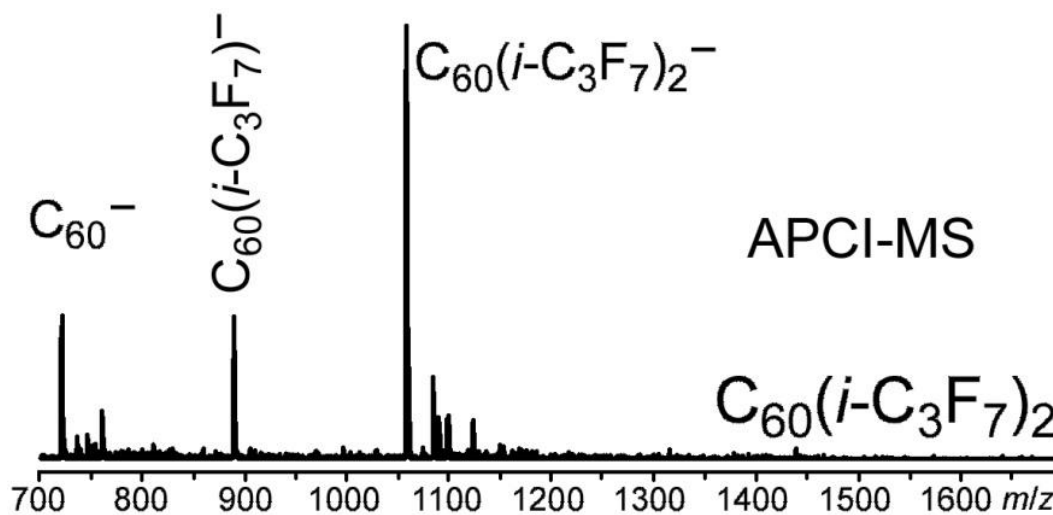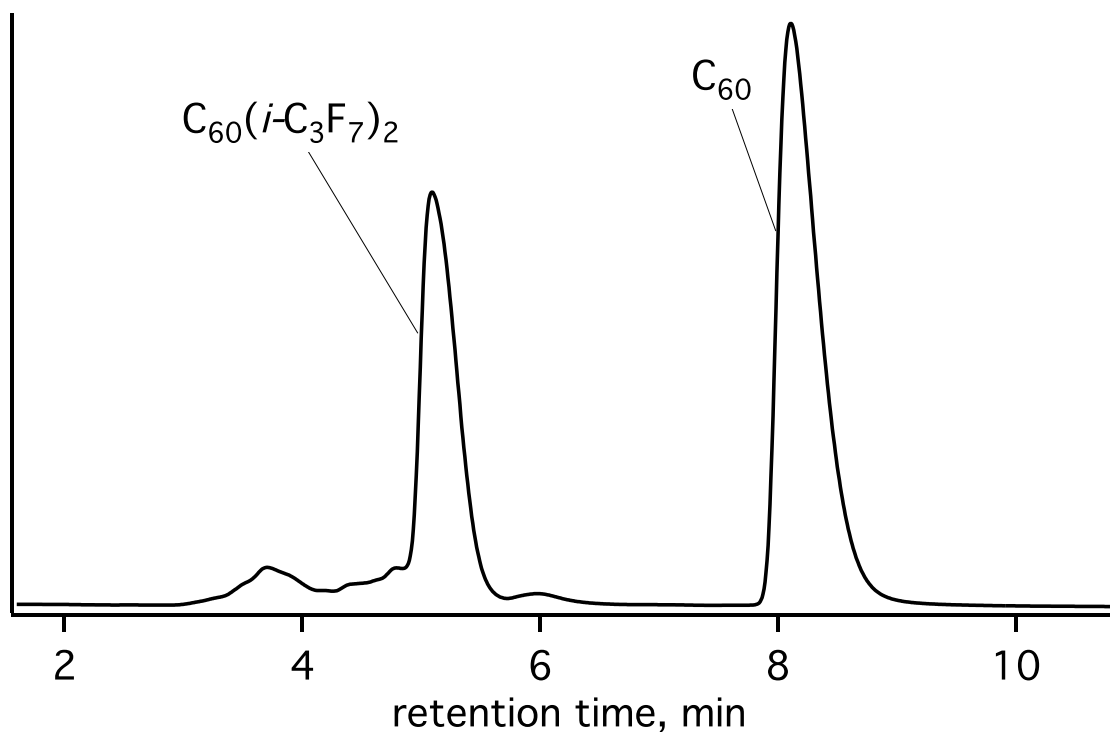
Figure 1.20. (Top) HPLC chromatogram of the crude products from a homogeneous sealed ampoule reaction of C_{60} and 18 equivalents of $i\text{-}C_3F_7I$ in oDCB for 24 h at 180 °C. The HPLC conditions are 100% toluene at 5 mL/min using a semi-preparative Cosmosil Buckyprep HPLC column. (Bottom) APCI-MS of the isolated compound $C_{60}(i\text{-}C_3F_7)_2$.
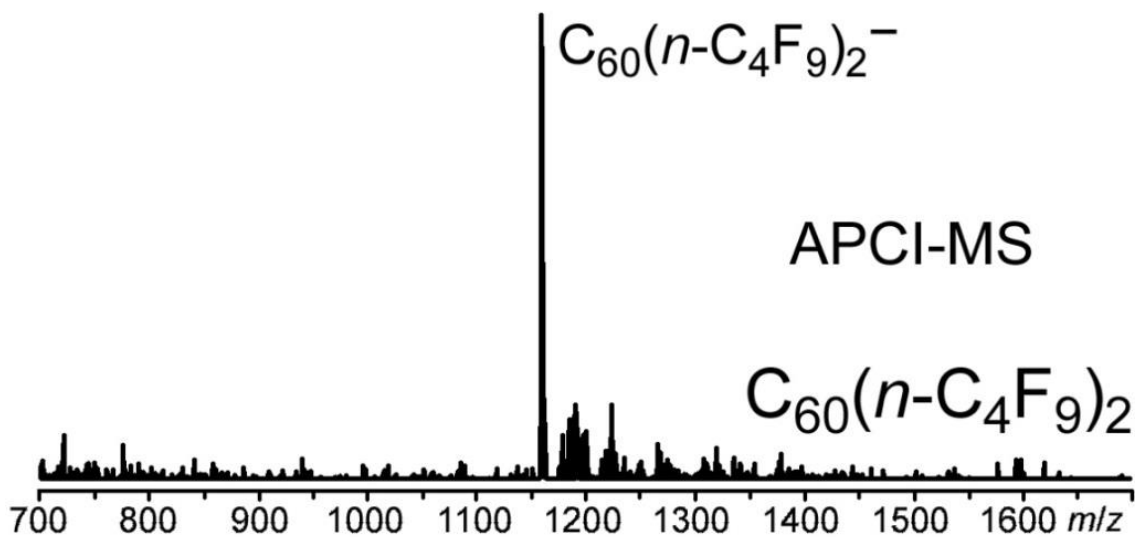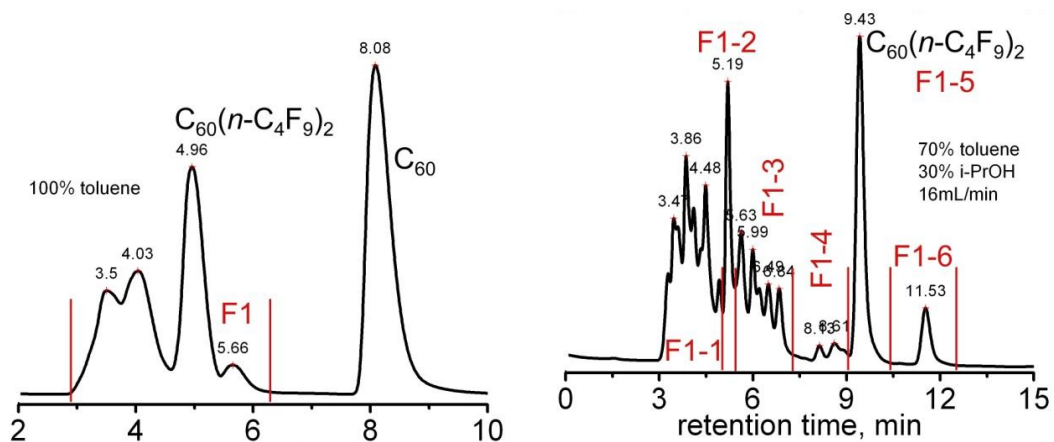
Figure 1.21. (Top from left to right) First and second stage HPLC separation of the crude reaction material containing $C_{60}(n\text{-}C_4F_9)_2$. (Bottom) APCI-MS of the isolated fraction F1-5.
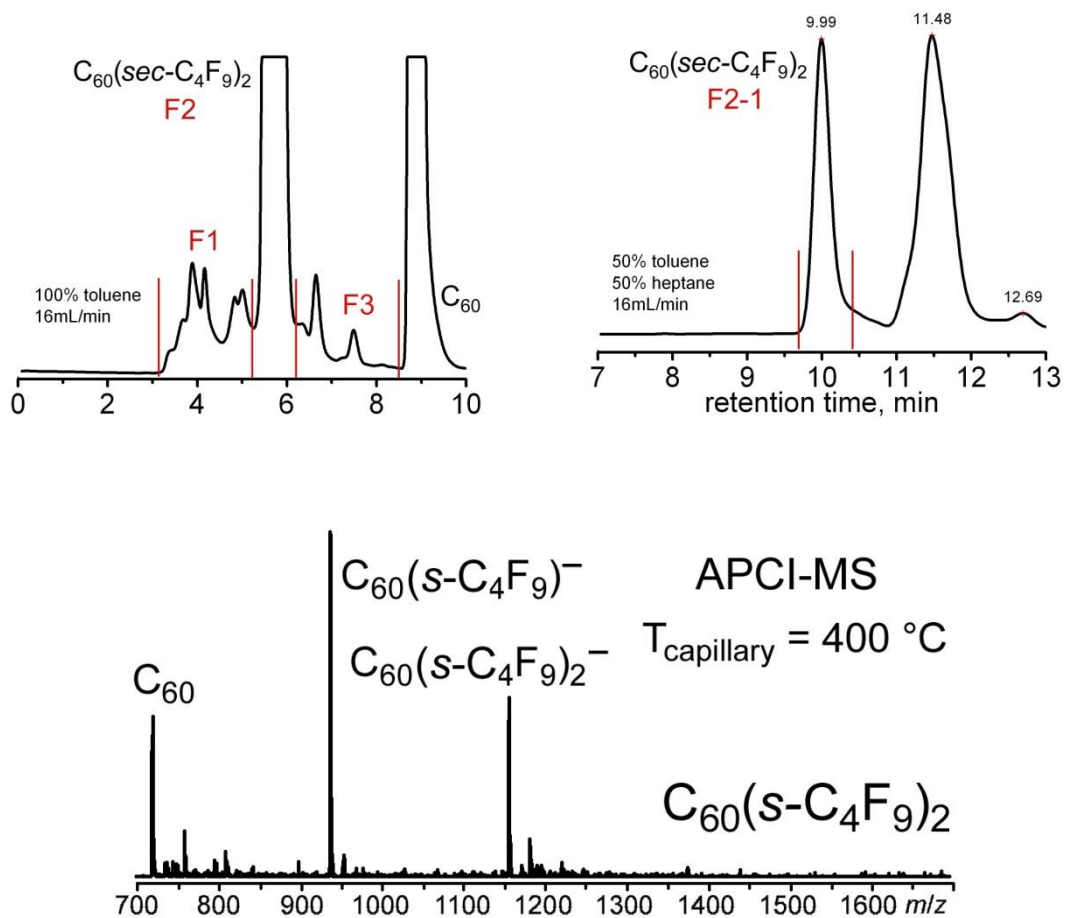
Figure 1.22. (Top from left to right) First and second stage HPLC separation of the crude reaction material containing $C_{60}(s\text{-}C_4F_9)_2$. (Bottom) APCI-MS of the isolated fraction F2-1.
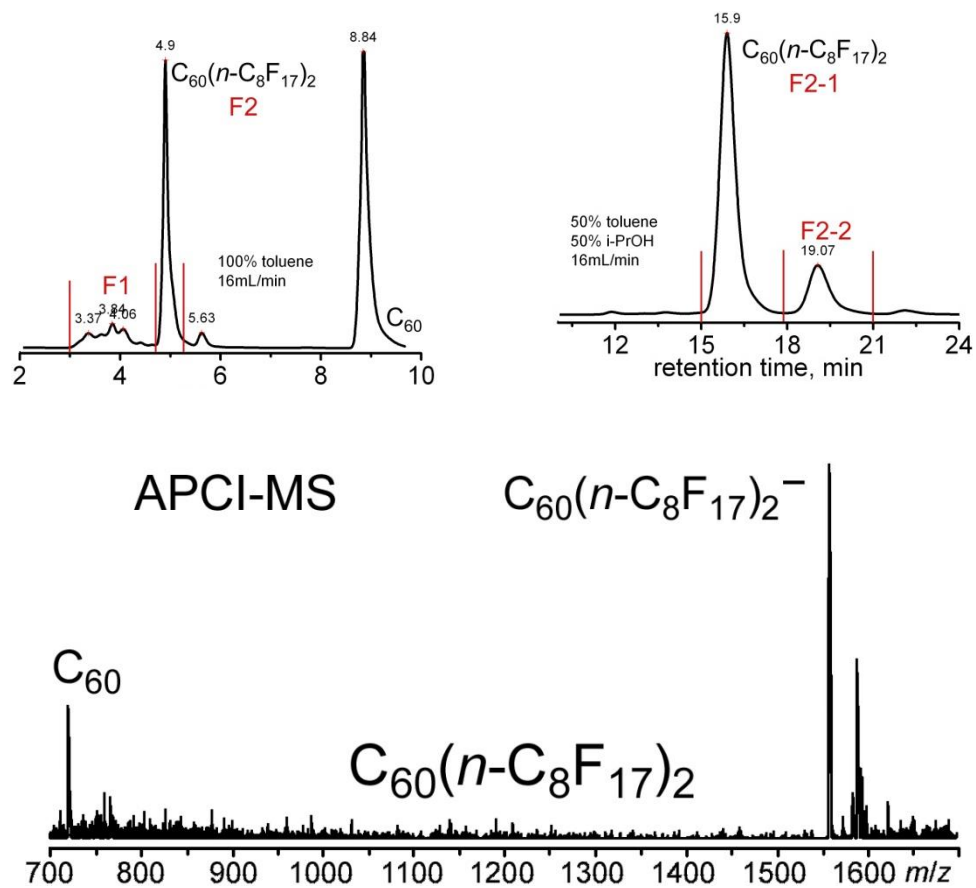
Figure 1.23. (Top from left to right) First and second stage HPLC separation of the crude reaction material containing $C_{60}(n\text{-}C_8F_{17})_2$. (Bottom) APCI-MS of the isolated fraction F2-1.
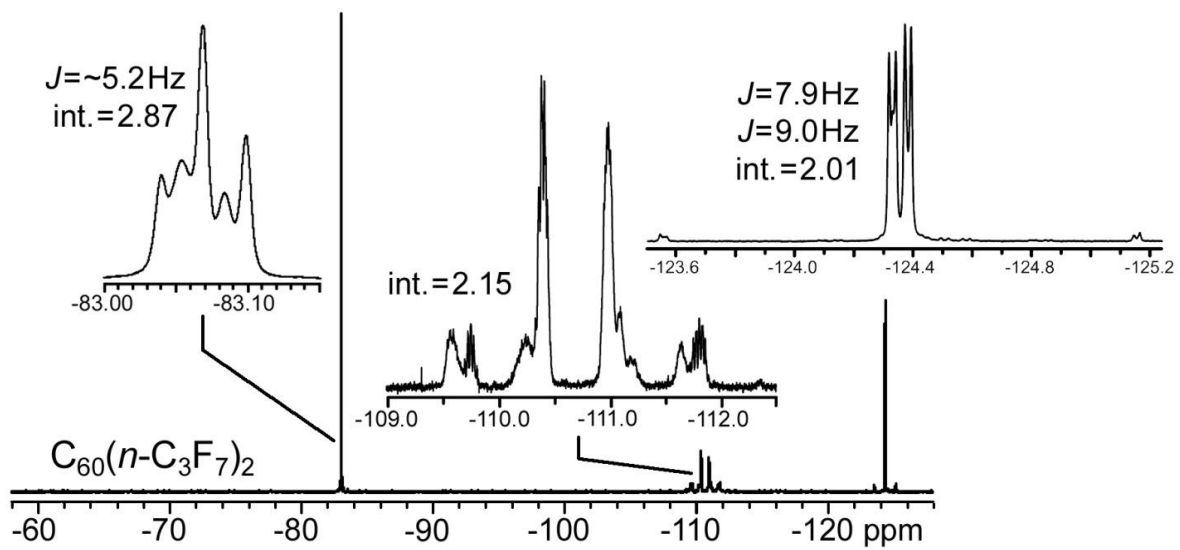
Figure 1.24. Fluorene-19 NMR spectrum of $C_{60}(n\text{-}C_3F_7)_2$ in $CDCl_3$.
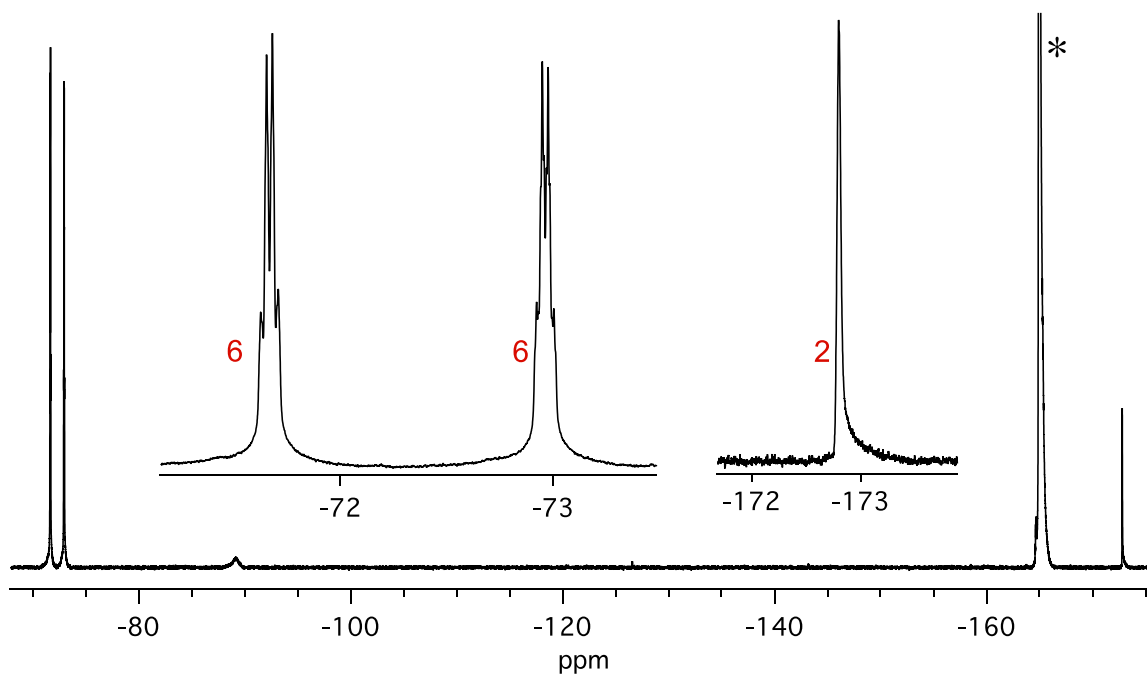
Figure 1.25. Fluorene-19 NMR spectrum of $C_{60}(i\text{-}C_3F_7)_2$ in $CDCl_3$.
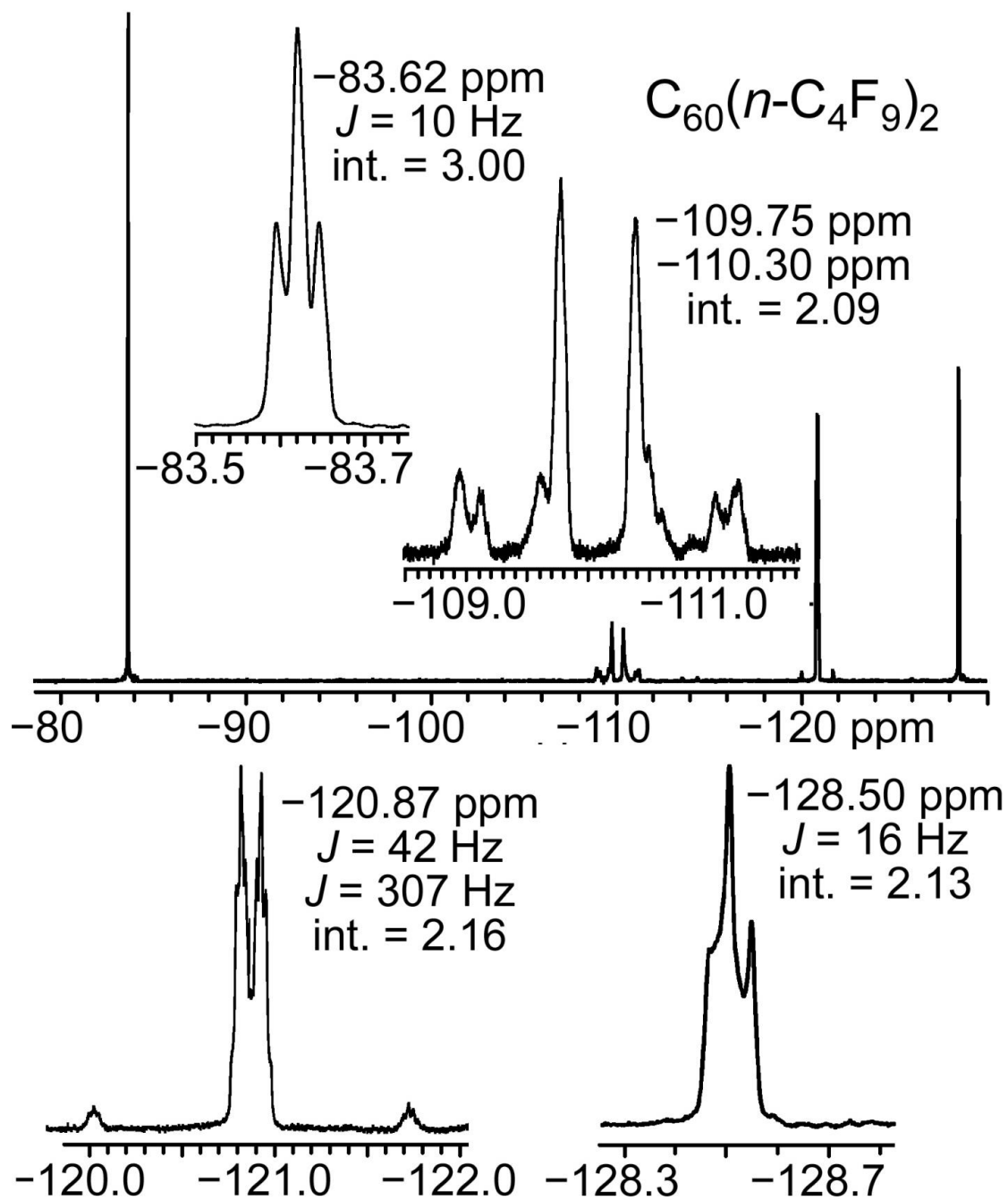
Figure 1.26. Fluorine-19 NMR spectrum of $C_{60}(n\text{-}C_4F_9)_2$ in $CDCl_3$.
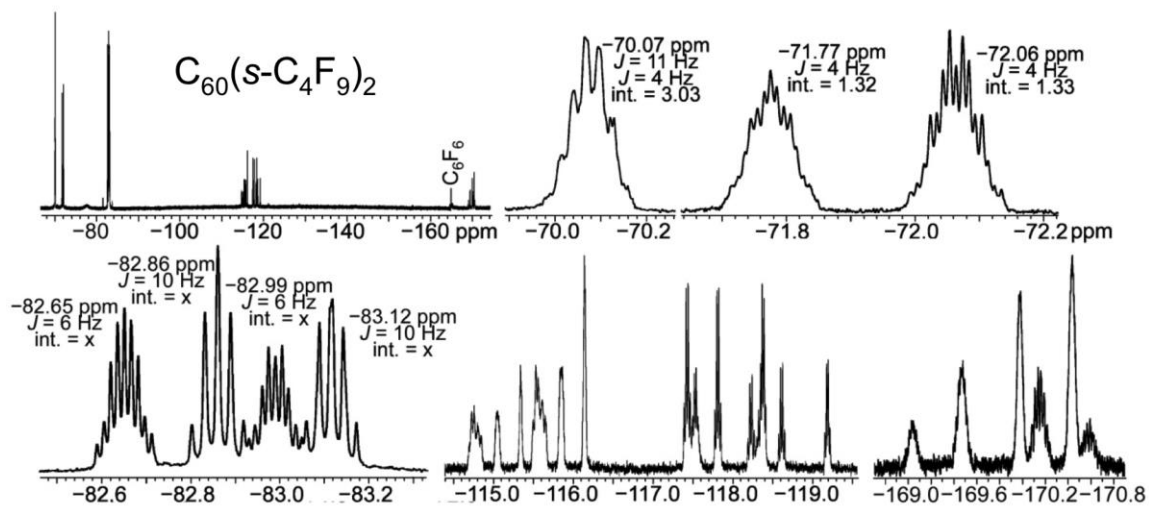
Figure 1.27. Fluorene-19 NMR spectrum of $C_{60}(s\text{-}C_4F_9)_2$ in $CDCl_3$
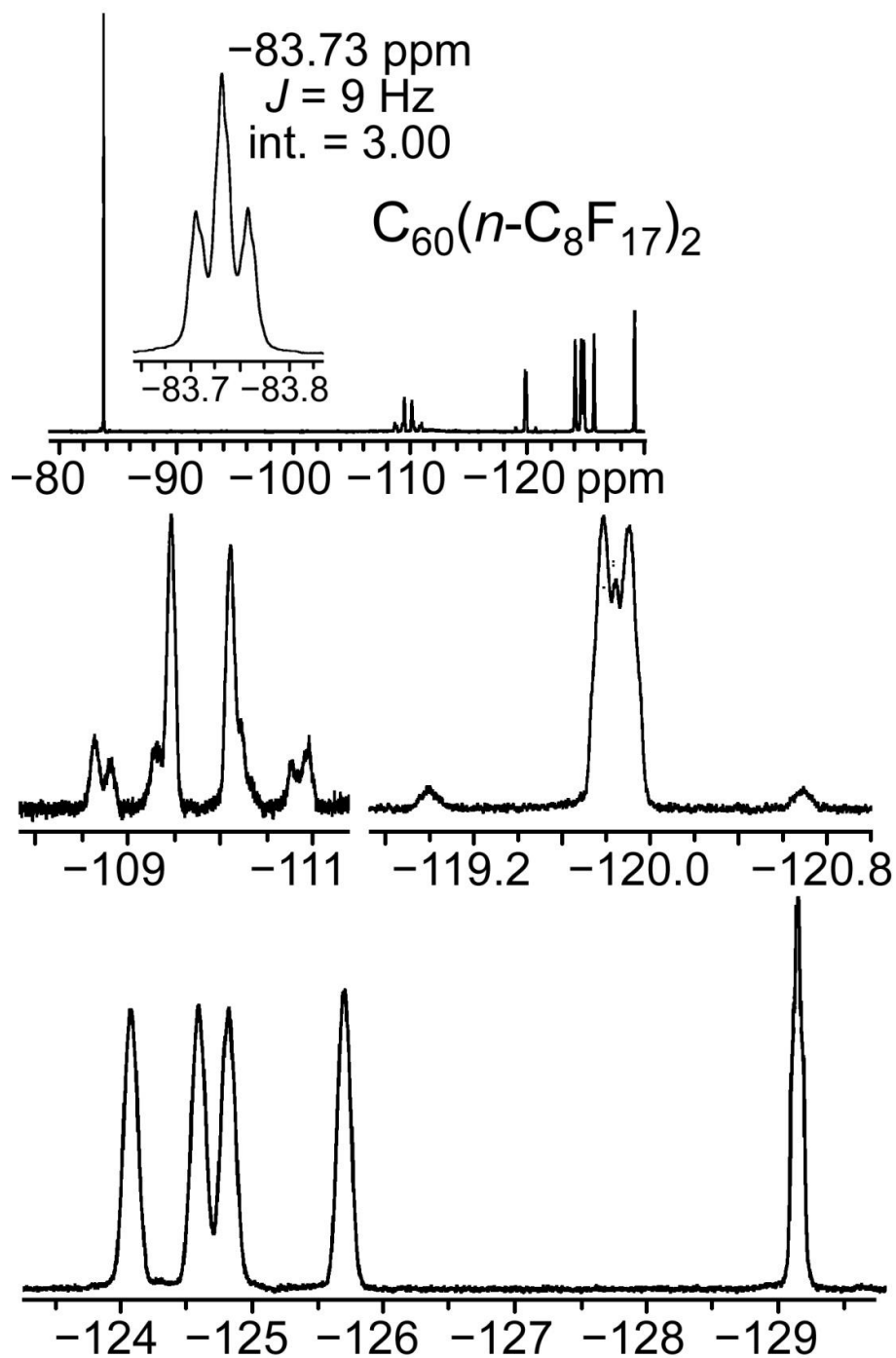
Figure 1.28. Fluorene-19 NMR spectrum of $C_{60}(n\text{-}C_8F_{17})_2$ in $CDCl_3$
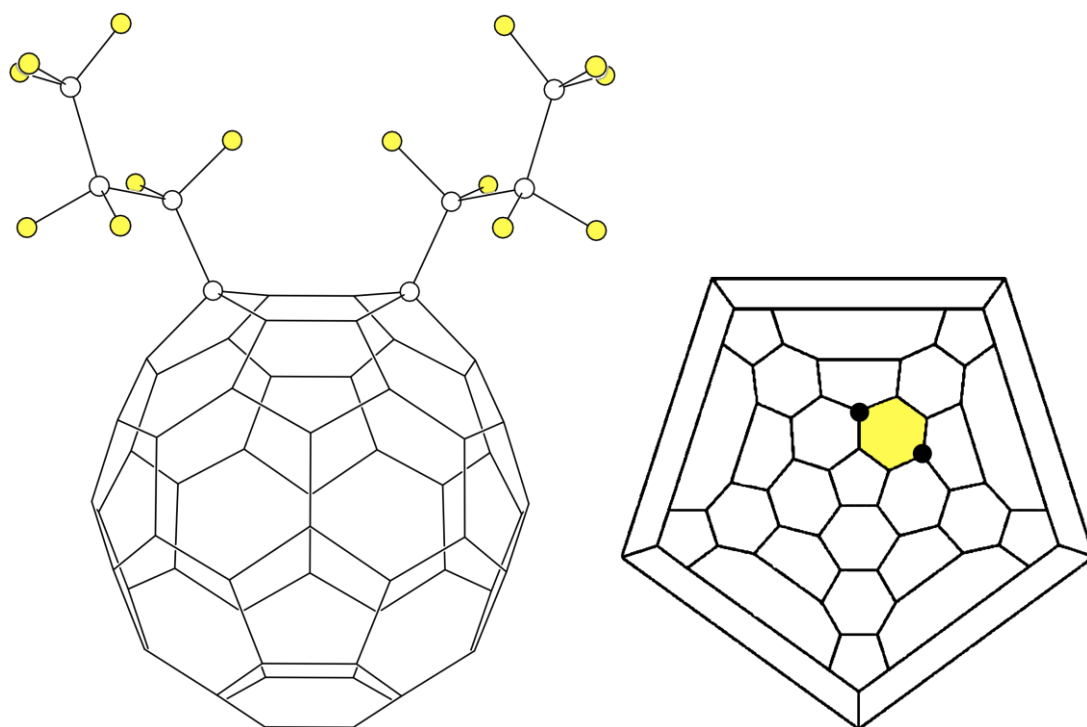
Figure 1.29. X-ray structure of $C_{60}(n\text{-}C_3F_7)_2$, the cage carbon atoms are represented by points. Right, Schlegel diagram showing the addition pattern of $C_{60}(n\text{-}C_3F_7)_2$.

Table 1.2.

			$R_F=$			
CF_3	C_2F_5	$n\text{-}C_3F_7$	$i\text{-}C_3F_7$	$n\text{-}C_4F_9$	$s\text{-}C_4F_9$	$n\text{-}C_8F_{17}$
328	327	329	328	328	327	328
445	448	447	445	447	445	447
529	535	532	475	532	476	536
565	561	565	534	570	534	568
602	601	602	565	598	567	599
633	630	631	604	632	603	627
662	657	659	628	659	629	660
693	692	692	691	692	691	692

The UV-vis peak maxima and minima (nm) of a series of seven $1,7\text{-}C_{60}(R_F)_2$ fullerenes recorded in toluene.
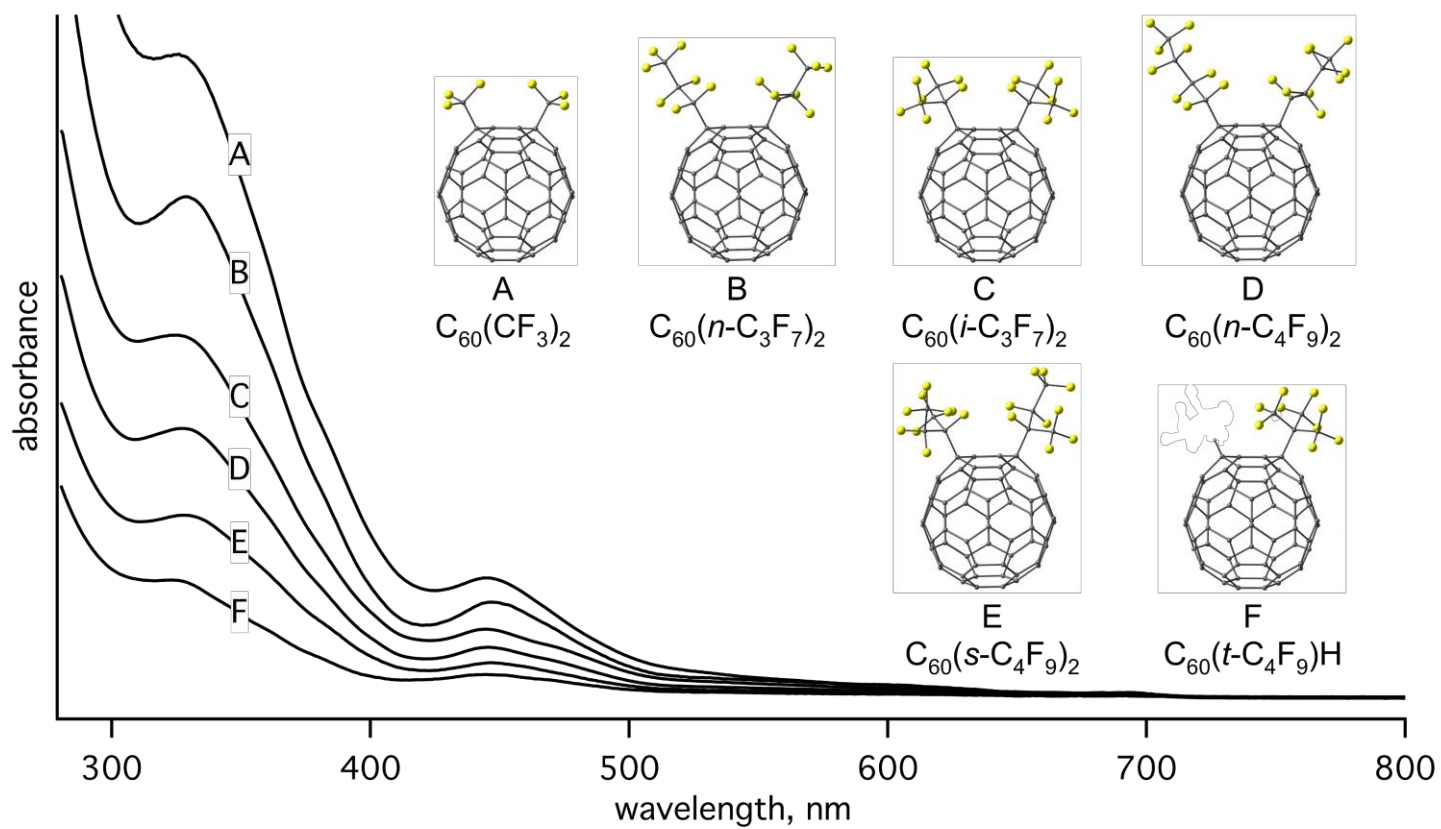
Figure 1.30. UV-vis spectra of a series of 1,7-$C_{60}(R_F)_2$ compounds that were recorded in toluene. The UV-vis spectrum of 1,7-$C_{60}(t$-$C_4F_9)$H recorded in toluene is also shown.

Table 1.3. APCI-MS Data for Exhaustive Homogeneous Perfluoroalkylation of C_{60}[a]

	$I(C_{60}(R_F)_nH_m)$[b]		$C_{60}(R_F)_nH_m$[c]	
R_F	n	m	n	m
C_2F_5[d]	14	0	16	0
n-C_3F_7[d]	10	0	12	0
n-C_4F_9	10	1	12	1
s-C_4F_9	6	0	8	0
t-C_4F_9	4	0	6	0
$CF_2C_6F_5$	11	0	13	0

[a] All data from this work unless otherwise noted. [b] Most abundant ion. [c] Highest observed addition. [d] Reference [24].

Table 1.4. APCI-MS Data for Exhaustive Homogeneous Perfluoroalkylation of C_{70}[a]

	$I(C_{70}(R_F)_nH_m)$		$I(C_{70}(R_F)_nH_m)$	
R_F	n	m	n	m
n-C_4F_9	9	3	11	0
s-C_4F_9	4	0	9	0
t-C_4F_9	0	0	0	0
$CF_2C_6F_5$	11	0	13	0

[a] All data from this work unless otherwise noted. [b] Most abundant ion. [c] Highest observed addition. [d]
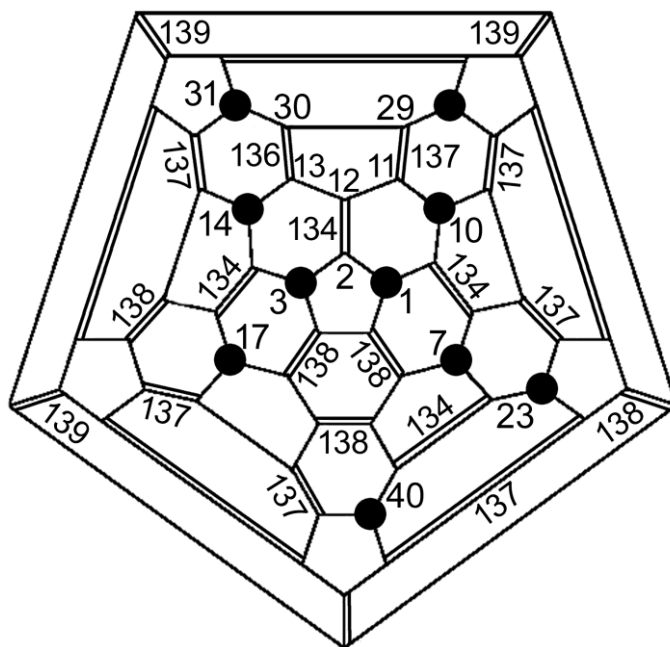
Figure 1.31. Schlegel diagram of the isomer of $C_{60}(CF_3)_{10}$ used in this work, 1,3,7,10,14,17,23,-28,31,40-$C_{60}(CF_3)_{10}$ (**II**). The black circles indicate the fullerene C atoms to which the ten CF_3 groups are attached. The one and two-digit numbers are IUPAC locants. The three digit numbers are, in pm, the fullerene C=C bonds shorter than 140 pm, and are taken from the X-ray structure of this compound reported in the literature[9] (note that three times the standard error for these bond distances is 0.9 pm).
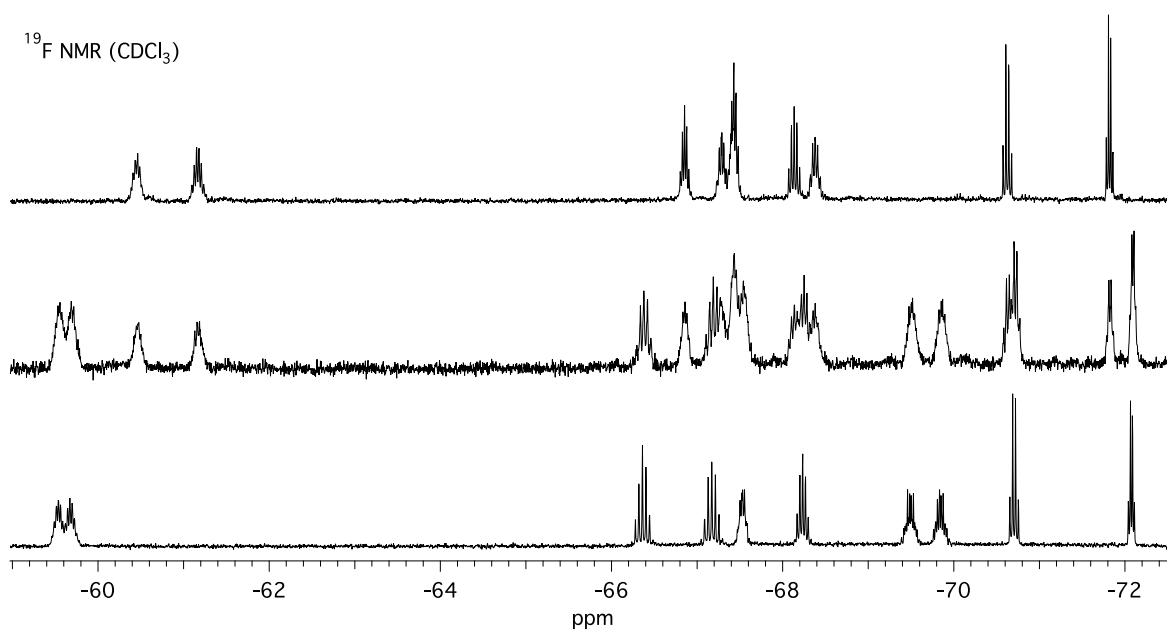
Figure 1.32. The 376.5 MHz ^{19}F NMR spectra of 60-10-3 (bottom), a sample of 60-10-3 exposed to air and ambient light for several months, which produced a mixture of 60-10-3 and 60-10-3[O_2] (middle), and a purified sample of 60-10-3[O_2] (top). The internal chemical shift standard was C_6F_6 (δ −164.9).
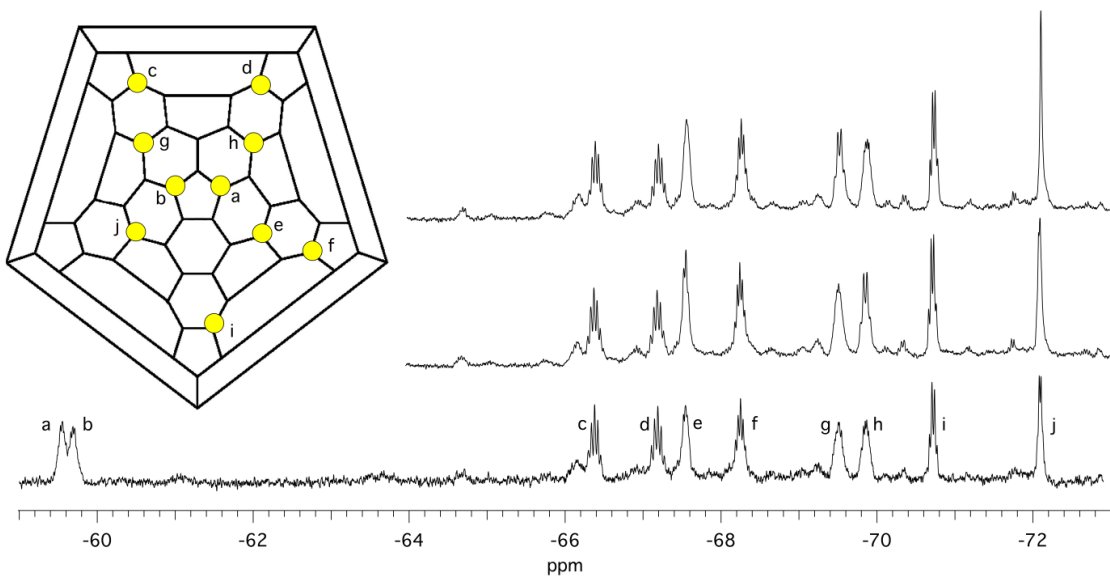
Figure 1.33. The 1D ^19F NMR spectrum of 60-10-3 in CDCl₃ (bottom). Selective decoupling ^19F NMR spectroscopy experiment on a sample of 60-10-3 dissolved in CDCl₃ where multiplet **a** was decoupled (middle) and when multiplet **b** was decoupled (top). Inset showing the correct NMR assignments on a schlegel diagram of 60-10-3.
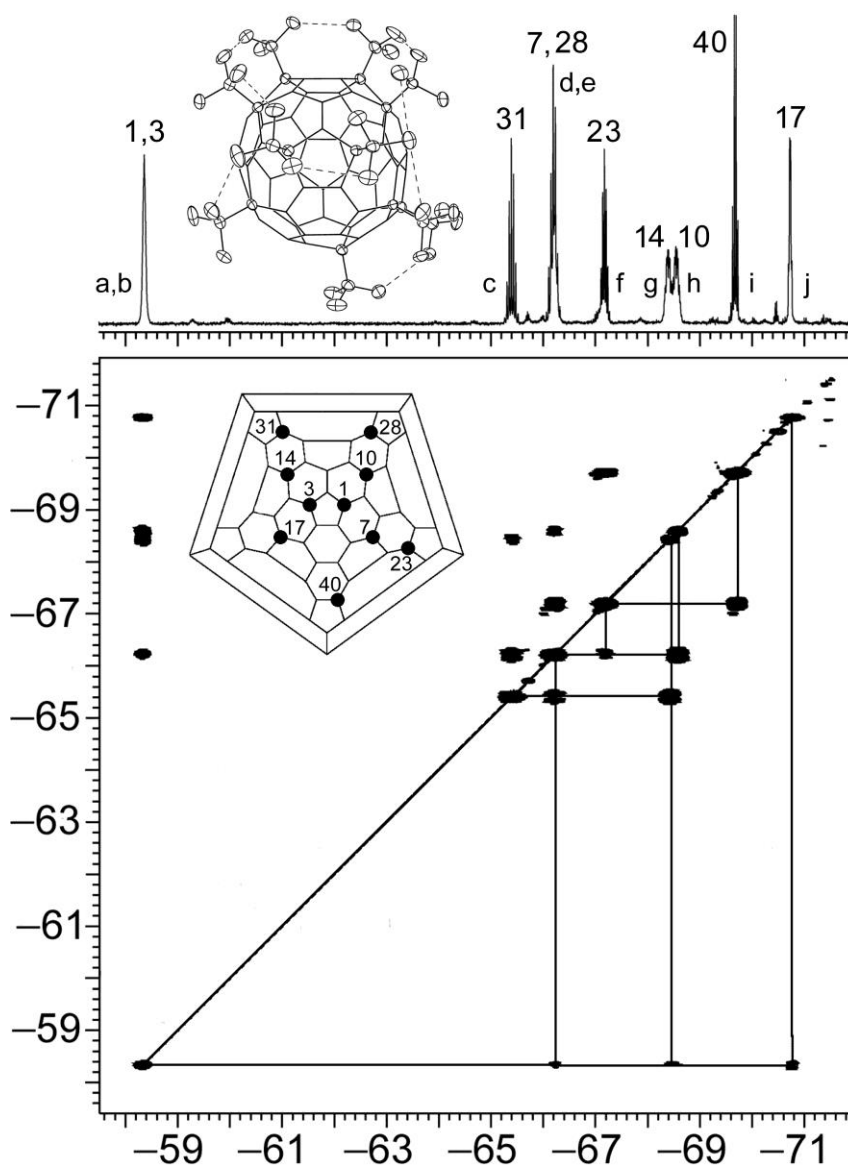
Figure 1.34. The 1D and 2D ^{19}F NMR spectrum of 60-10-3 in C_6D_6 from the literature with incorrect NMR assignments of a, b, d, and e.[9]
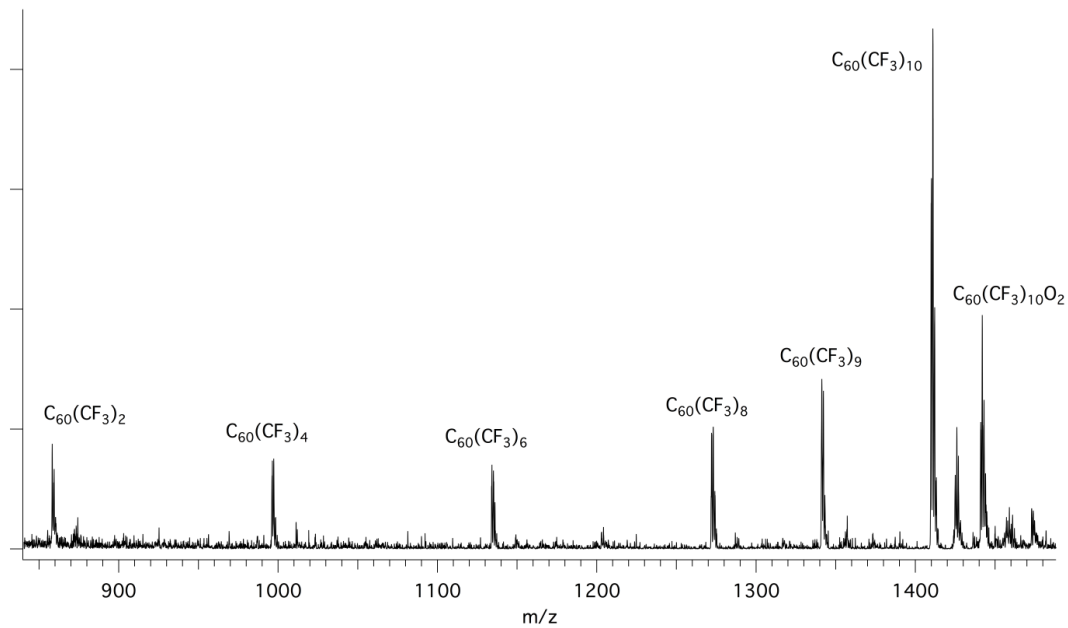
Figure 1.35. APCI-MS of $C_{60}(CF_3)_{10}O_2$ (compound **I**). The spectrum shows the parent ion at 1442 as well as the various fragments that result from the loss of each oxygen atom and the CF_3 groups.
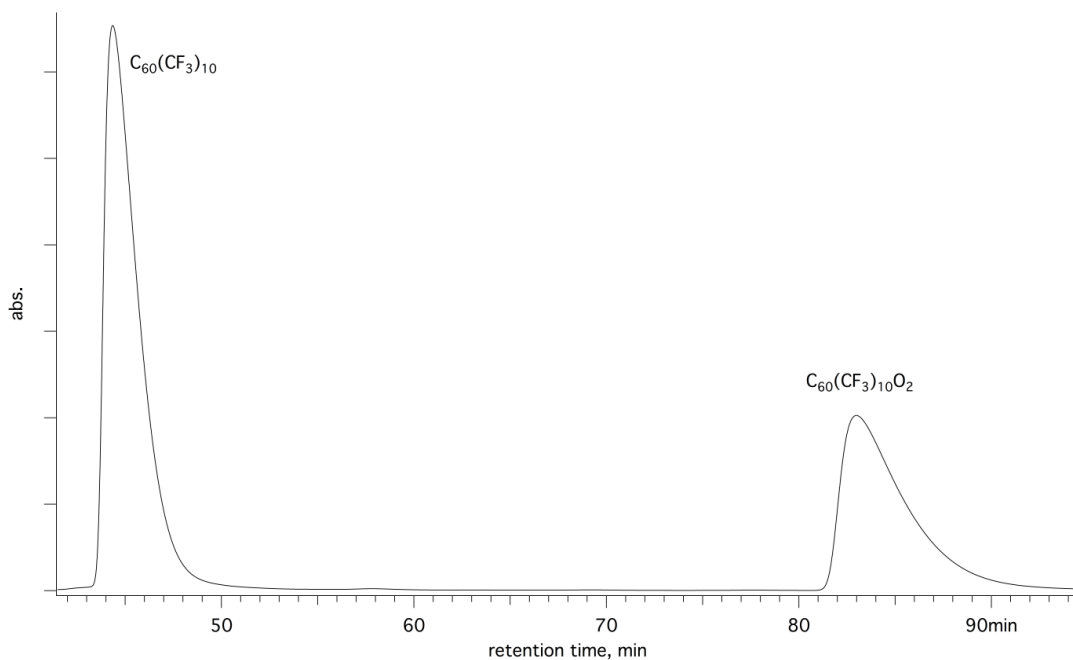
Figure 1.36. HPLC chromatogram of a mixture of 60-10-3 and 60-10-3[O_2] in 100% hexanes with a flow rate of 5 mL/ min. The retention time of 60-10-3[O_2] can be reduced to 6 min in 50:50 toluene: heptane.
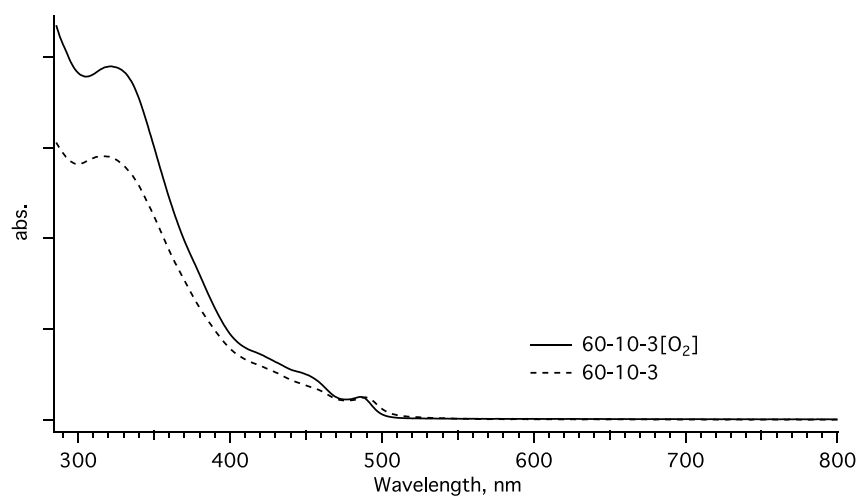
Figure 1.37. The UV-vis spectra of both 60-10-3 and 60-10-3[O_2] recorded in toluene.
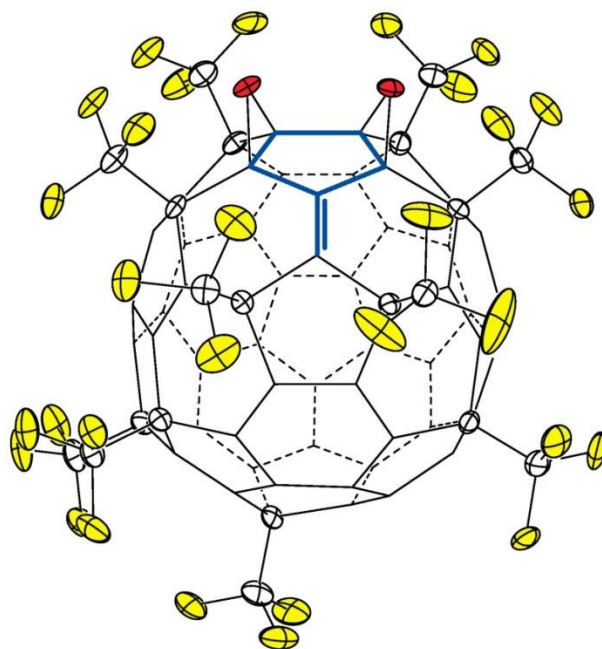
Figure 1.38. The structure of $C_{60}(CF_3)_{10}(O)_2$ (60-10-3[O_2]), with the former fulvene-like fragment highlighted in blue (50% probability ellipsoids for the O atoms, the CF_3 groups, and the cage C atoms to which the CF_3 groups are attached; the two molecules of $CDCl_3$ have been removed for clarity). The bond distance for the remaining C=C double bond in the former fulvene-like fragment is 133.5(8) pm.
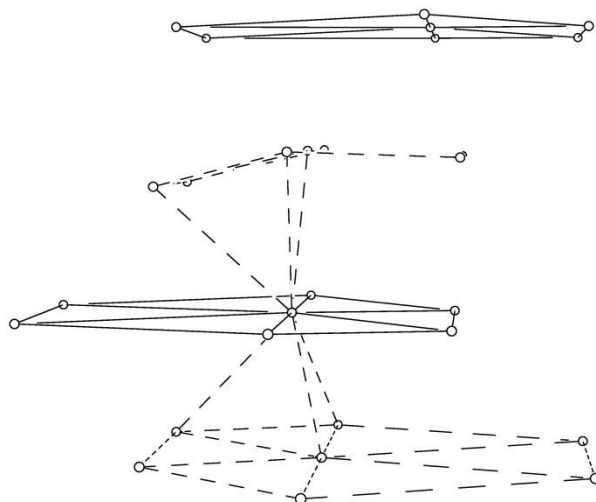
Figure 1.39. The packing of the C_{60} centroids in the structure of $C_{60}(CF_3)_{10}(O)_2$ (**I**). Note that there are nearly-planar and significantly puckered pseudo-hexagonal arrays that are stacked in a complicated fashion in the third dimension.
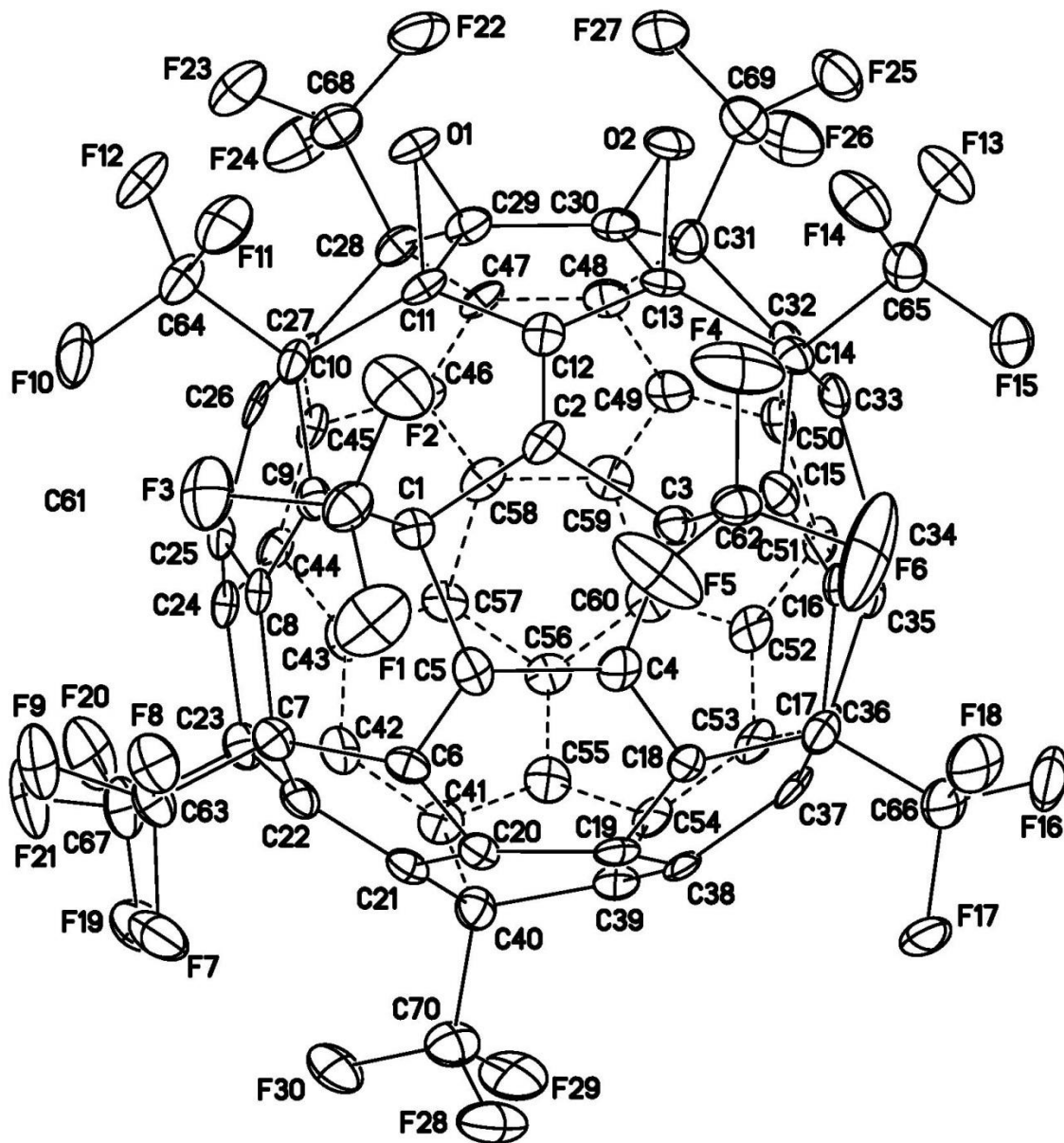
Figure 1.40. Numbered 50% probability thermal ellipsoid plot for $C_{60}(CF_3)_{10}(O)_2$

Table 1.5 Crystallographic data collection and structure refinement parameters for $C_{60}(CF_3)_{10}(O)_2 \cdot 2CDCl_3$

molecular formula	$C_{70}F_{30}O_2 \cdot 2(CDCl_3)$
formula weight	1683.45
crystal system	tetragonal
space group	$I4_1/a$
Z	16
color of crystals	yellow
unit cell dimensions (Å)	$a = 42.4640(19)$
	$b = 42.4640(19)$
	$c = 12.0696(6)$
data collection temperature, K	100(2)
final R indices, $[I > 2\sigma(I)]$	$R_1 = 0.0781$
	$wR_2 = 0.2555$
goodness-of-fit on F^2	1.270
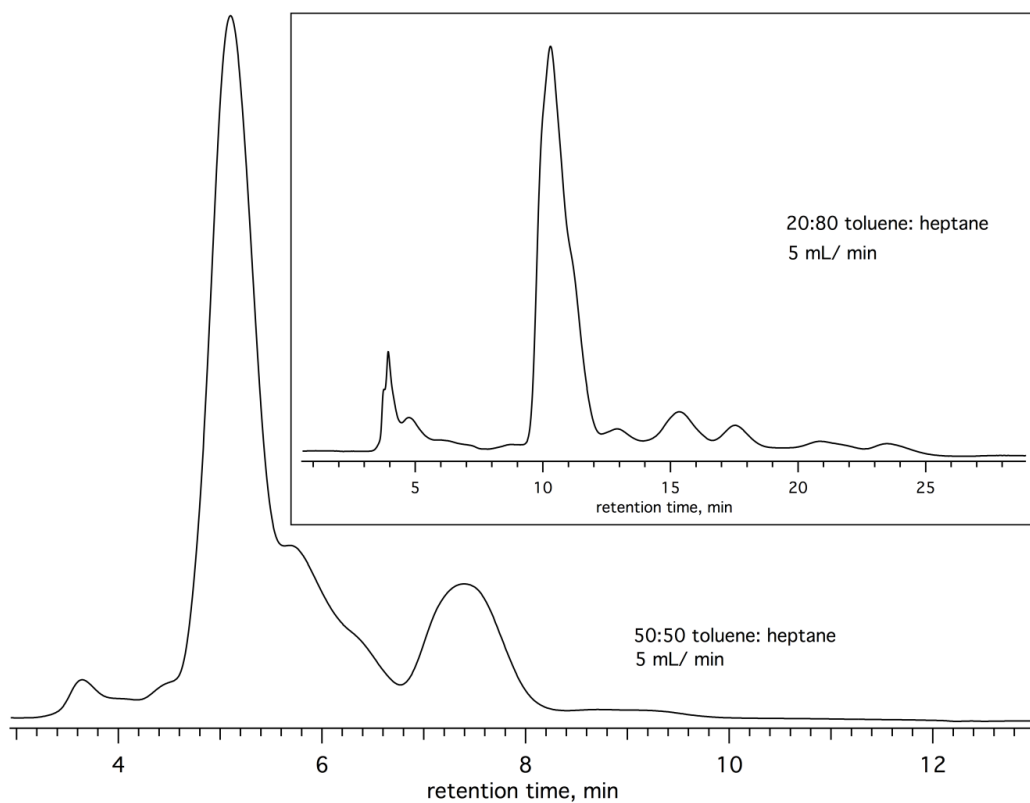
Figure 1.41. HPLC chromatogram of 60-10-3 after 10 min of reacting with O_3: O_2 gas mixture. Eluent is 50:50 (v:v) toluene: heptane, flow rate is 5 mL/min and monitored at 300 nm. Inset shows the largest peak in 20:80 toluene: heptane.
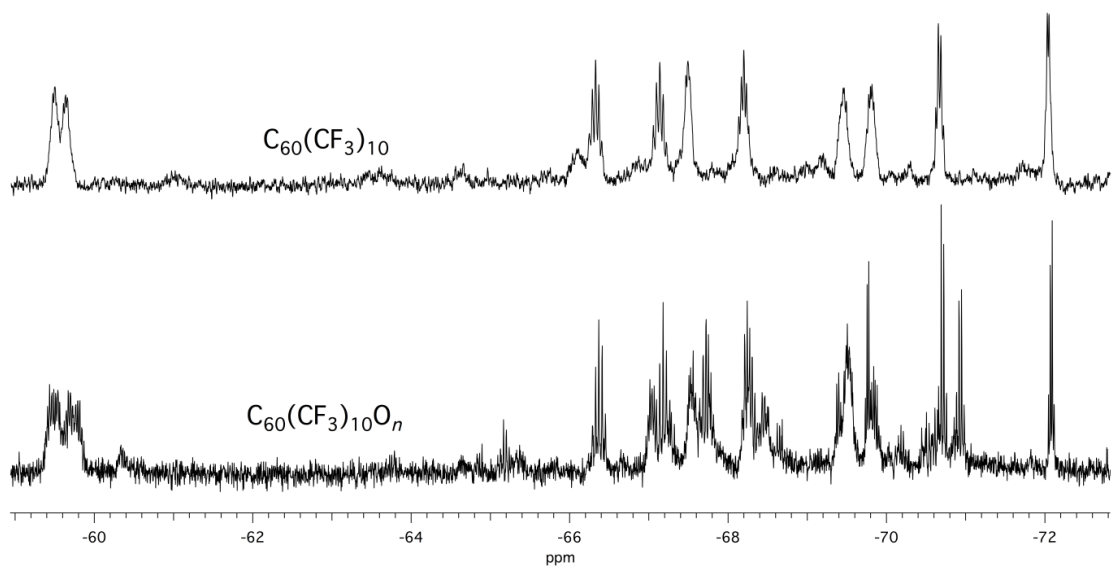
Figure 1.42. Bottom ^{19}F NMR spectrum shows the resulting mixture of oxides and starting material after the reaction of 60-10-3 and 10 min of O_3: O_2 gas mixture. The top ^{19}F NMR spectrum is compound 60-10-3 for reference. The solvent for both spectra is $CDCl_3$ and each spectrum has been referenced to an internal standard C_6F_6 with a chemical shift of $\delta -164.9$ ppm.
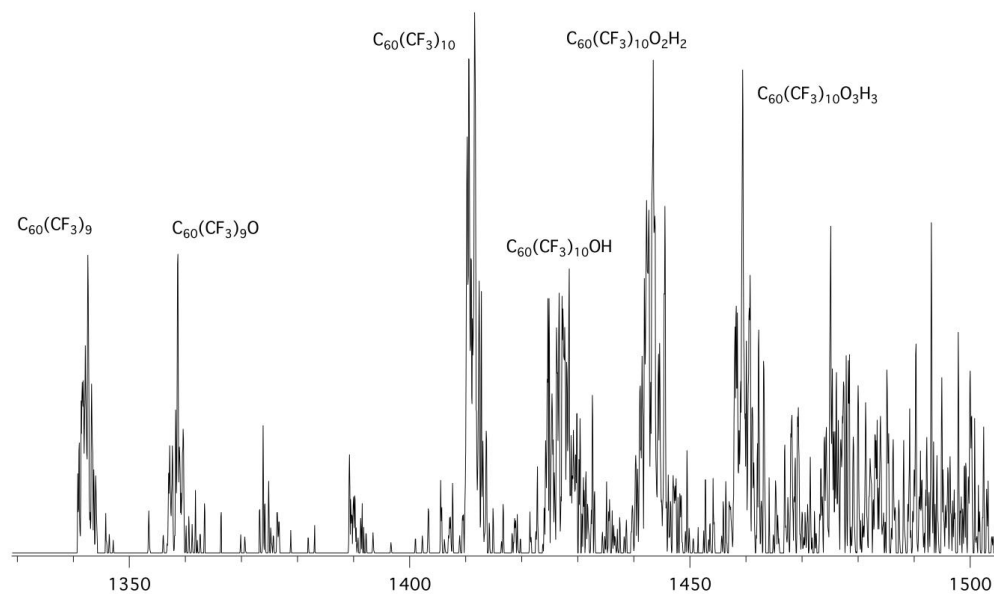
Figure 1.43. APCI-MS of the resulting mixture of various oxides, ozonides, and hydrogen atoms after 60-10-3 was treated with an O_3: O_2 gas mixture for 10 min.
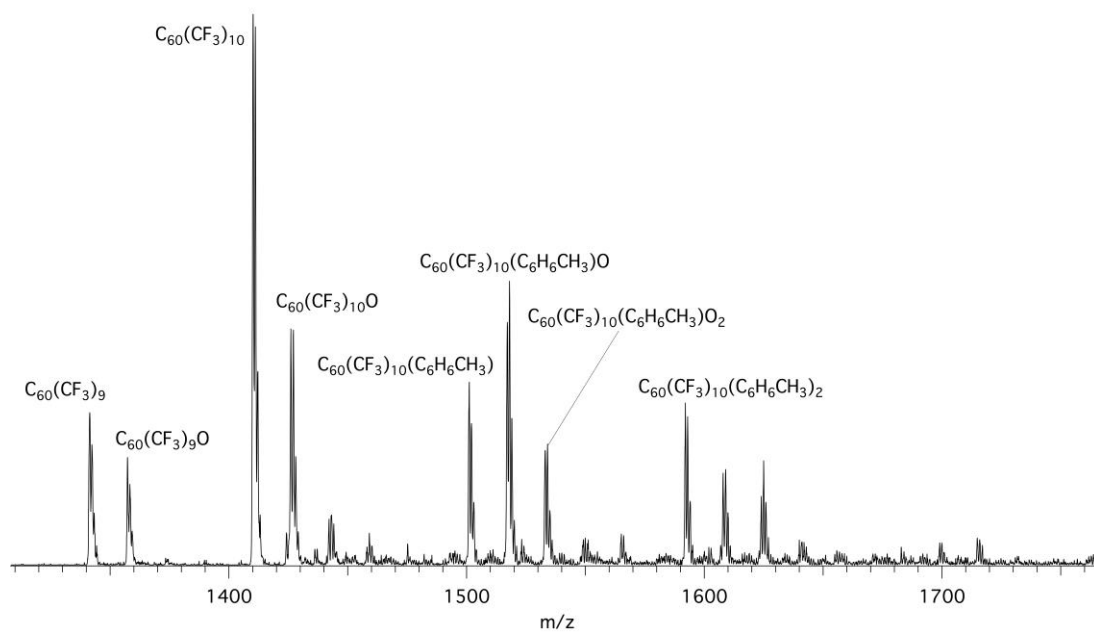
Figure 1.44. APCI-MS of the resulting oxides and toluene adducts from the reaction of mCPBA with 60-10-3. The mobile phase was acetonitrile and CDCl$_3$.
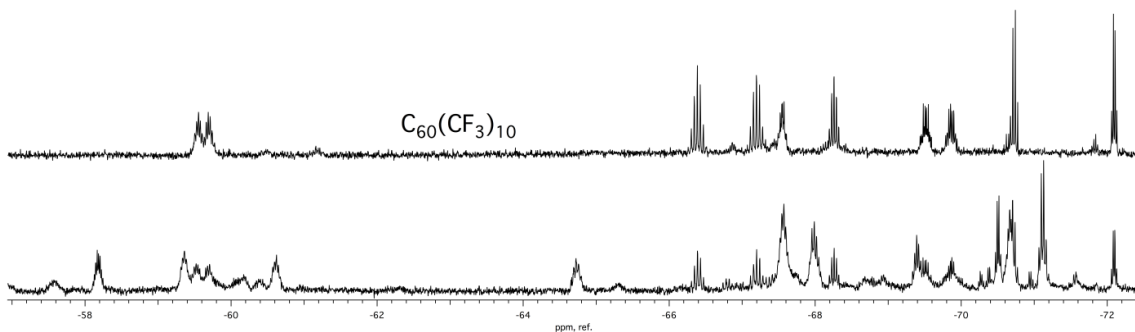
Figure 1.45. Fluorine 19 NMR spectrum of the resulting oxides and toluene adducts formed from the reaction of mCPBA with 60-10-3. Top spectrum is the starting material (60-10-3) for reference.
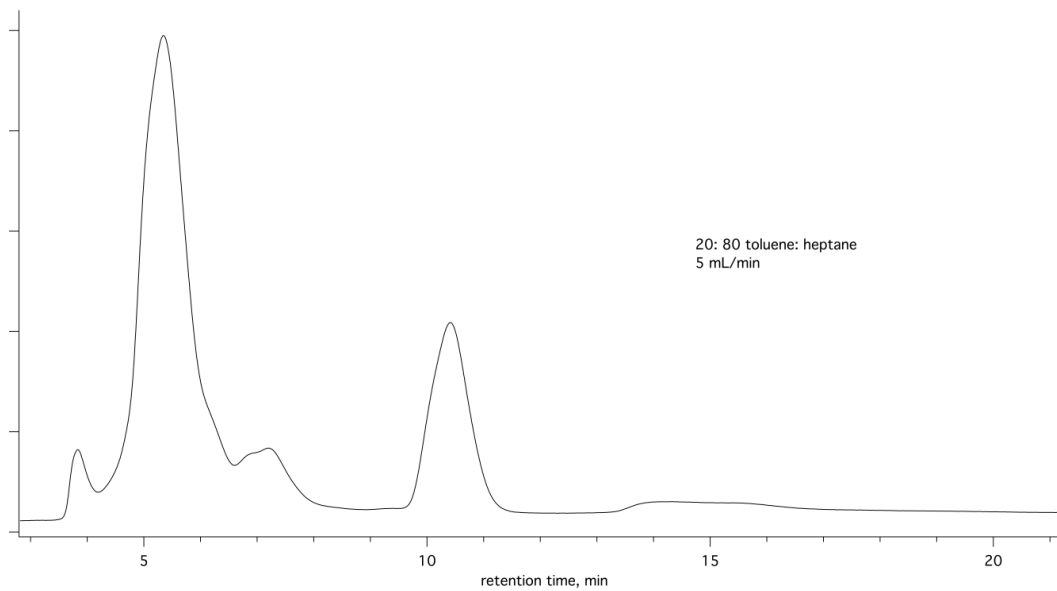
Figure 1.46. HPLC chromatogram of the resulting products from the reaction of mCPBA and 60-10-3. The mobile phase is 20:80 toluene: heptane with a flow rate of 5 mL/min.
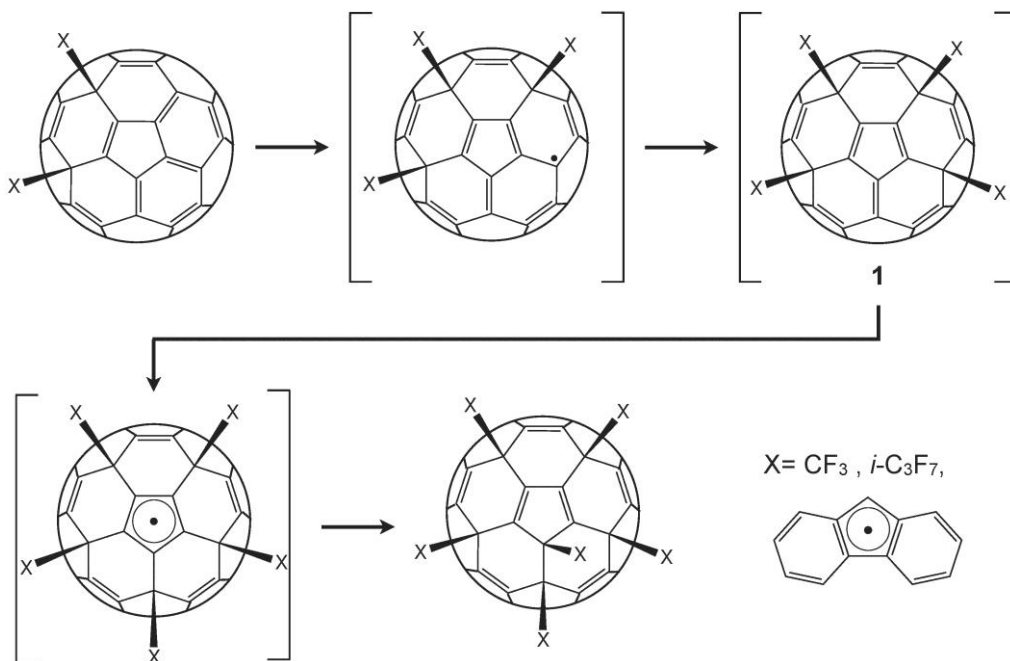
Figure 1.47. Proposed reaction pathway for the formation of the skew-pentagonal-pyramid addition pattern.
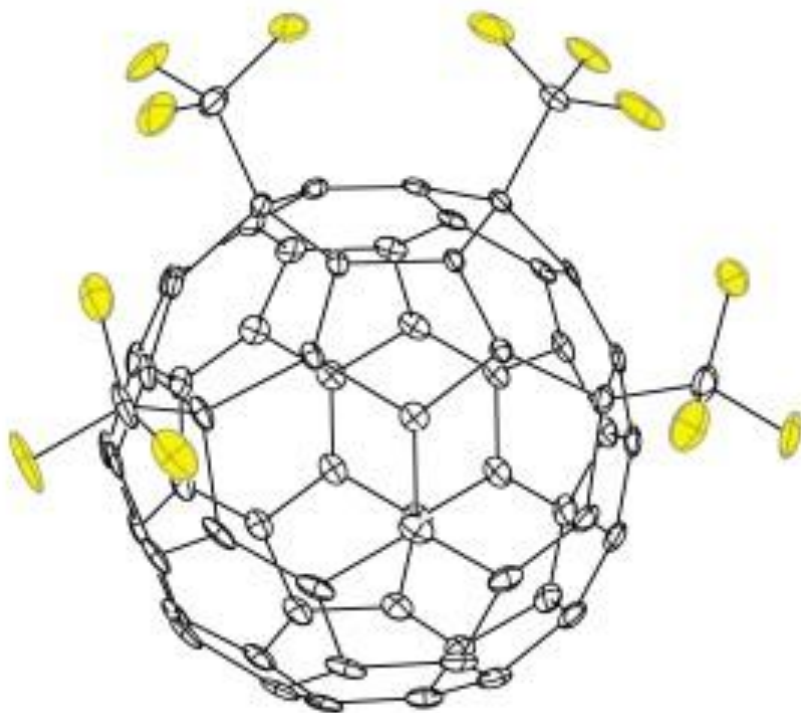
Figure 1.48. the 50% thermal ellipsoid plot of p^3-$C_{60}(CF_3)_4$.
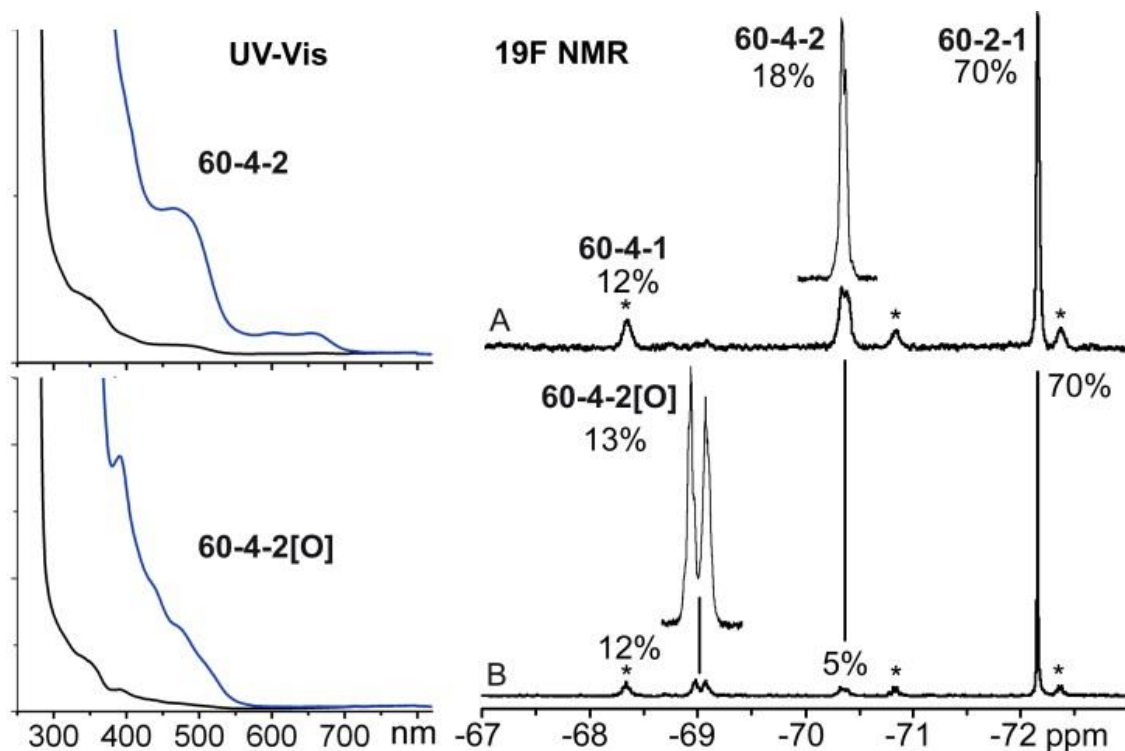
Figure 1.49. Right column: Fluorine-19 NMR spectra of the crude product of C_{60} trifluoromethylation in GTGS reactor under 10 torr of CF_3I and $T_{hot\ zone}$ = 480 °C. The top spectrum A was taken immediately after the dissolution of the crude TMF product in $CDCl_3$; the bottom spectrum B was taken using the same sample after two weeks under air. Asterisks denote peaks due to 60-4-1. The percentage abundance is calculated by normalizing the NMR peak intensity according to the number of fluorine atoms in the corresponding TMF. Left column: UV-vis spectra of 60-4-2 (top) and 60-4-O (bottom) recorded in toluene solution.

60-4-2
C_S-$C_{60}(CF_3)_4$

60-4-2[O]
C_S-$C_{60}(CF_3)_4O$

60-2-1
C_S-$C_{60}(CF_3)_2$

60-4-1
C_1-$C_{60}(CF_3)_4$

60-10-3
C_1-$C_{60}(CF_3)_{10}$
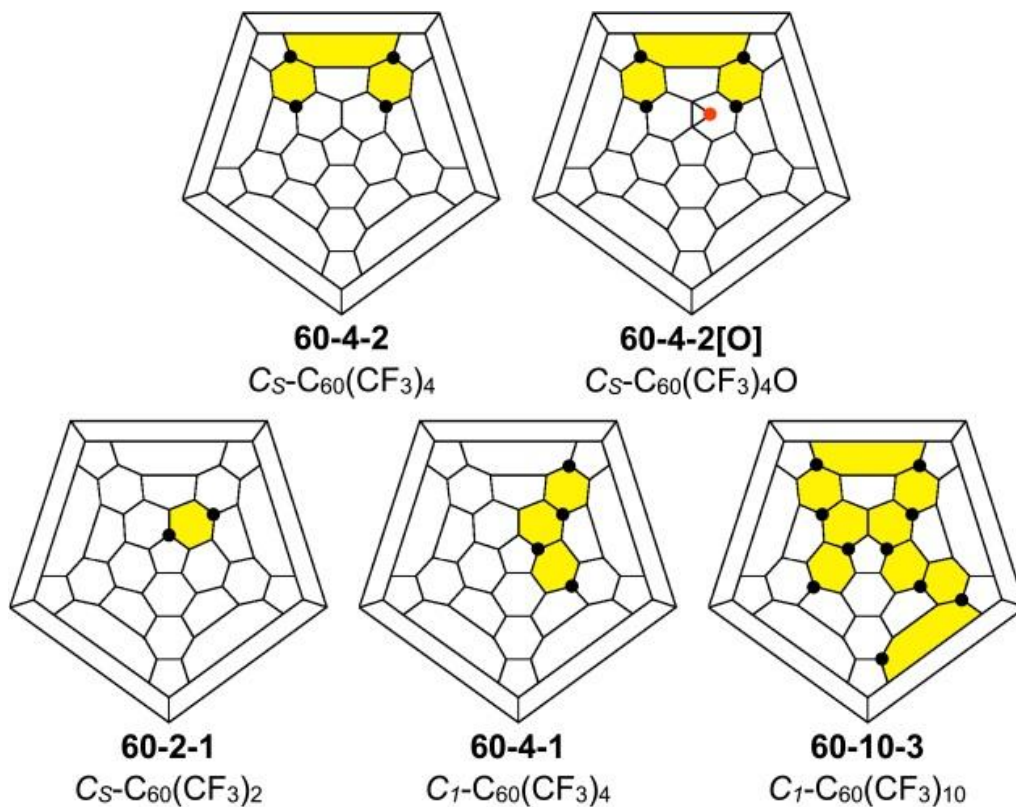
Figure 1.50. Schlegel diagrams of TMFs from this work with notations from ref.[8] Black circles denote CF_3 groups, yellow ribbons connect *para*-$C_6(CF_3)_2$ edge sharing hexagons.
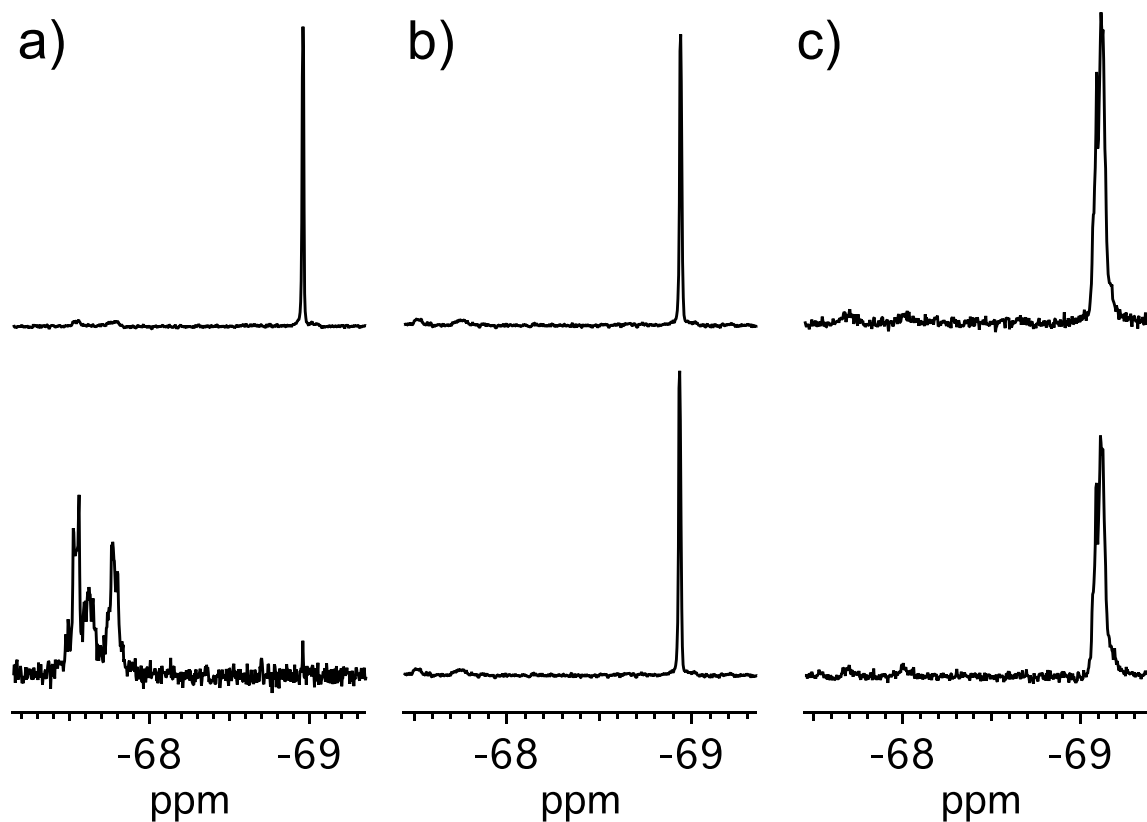
1.51. Fluorine-19 NMR spectra of three experiments (a) top: 60-4-2 dissolved in 70:30 benzene-d_6: acetonitrile; bottom: same sample after 24 hours exposed to ambient light. (b) top: 60-4-2 dissolved in 70:30 benzene-d_6: acetonitrile; same sample after 24 hours with ambient light excluded. (c) top: 60-4-2 dissolved in benzene-d_6; same sample after 24 hours exposed to ambient light. All samples contained internal standard C_6F_6 δ −164.9 ppm.
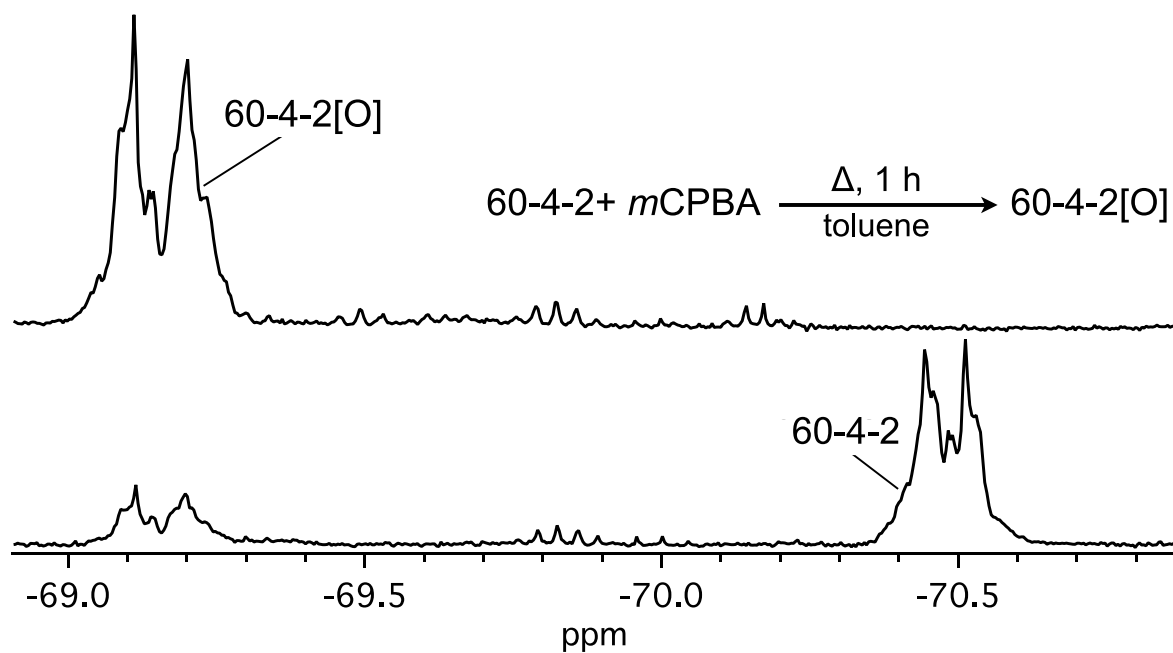
Figure 1.52. Fluorine-19 NMR spectra showing (bottom) the starting material 60-4-2 with a small amount of 60-4-2[O] present and (top) crude reaction products after reflux in toluene with 1 eq. mCPBA.
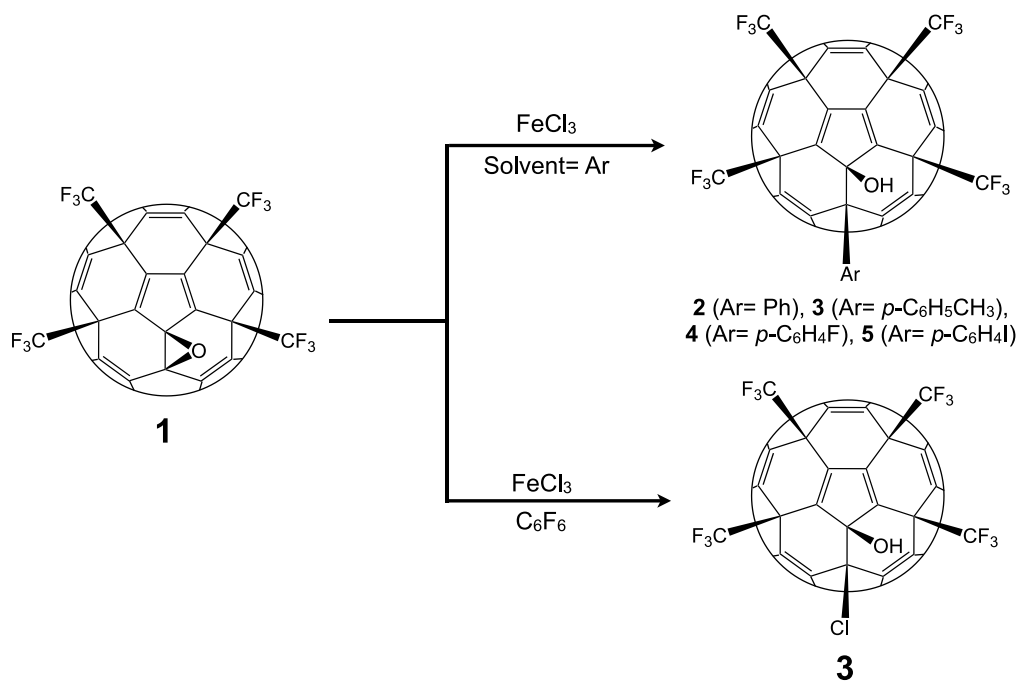
Figure 1.53. Scheme showing the various Lewis acid assisted epoxide opening reactions.
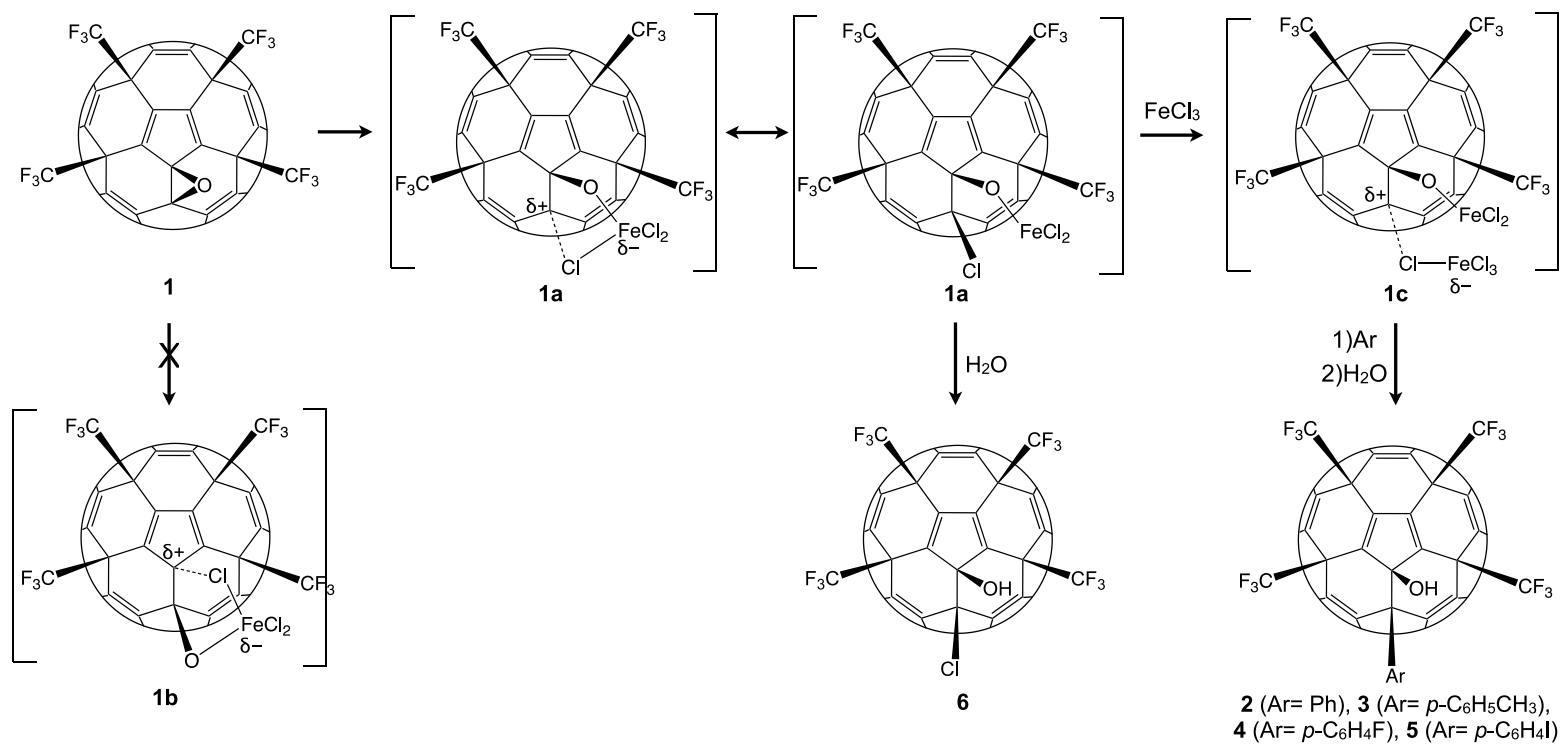
Figure 1.54. Proposed reaction pathway of the Lewis acid epoxide opening reactions.
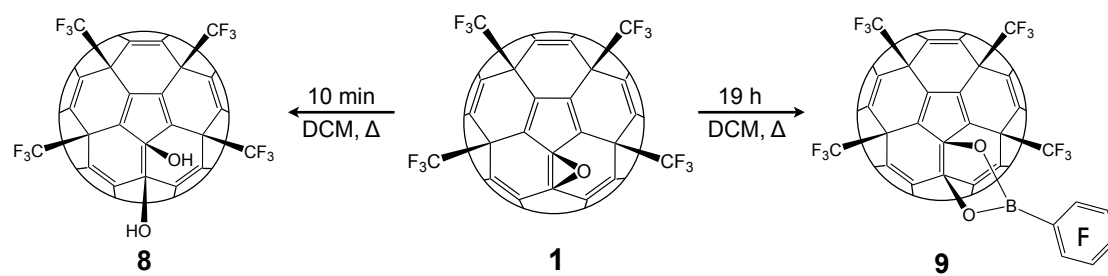
Figure 1.55. Products of using $B(C_6F_5)_3$ as the Lewis acid for epoxide opening reactions in DCM.
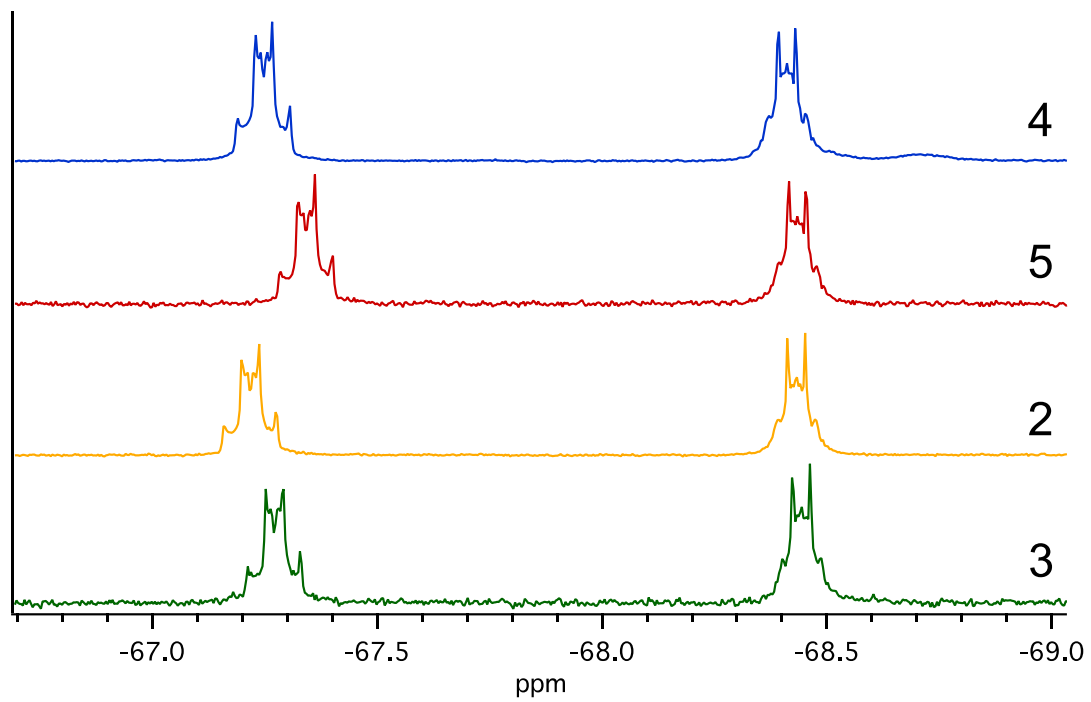
Figure 1.56. Fluorine-19 NMR spectra of compounds **2**, **3**, **4**, and **5** all recorded in CDCl$_3$..
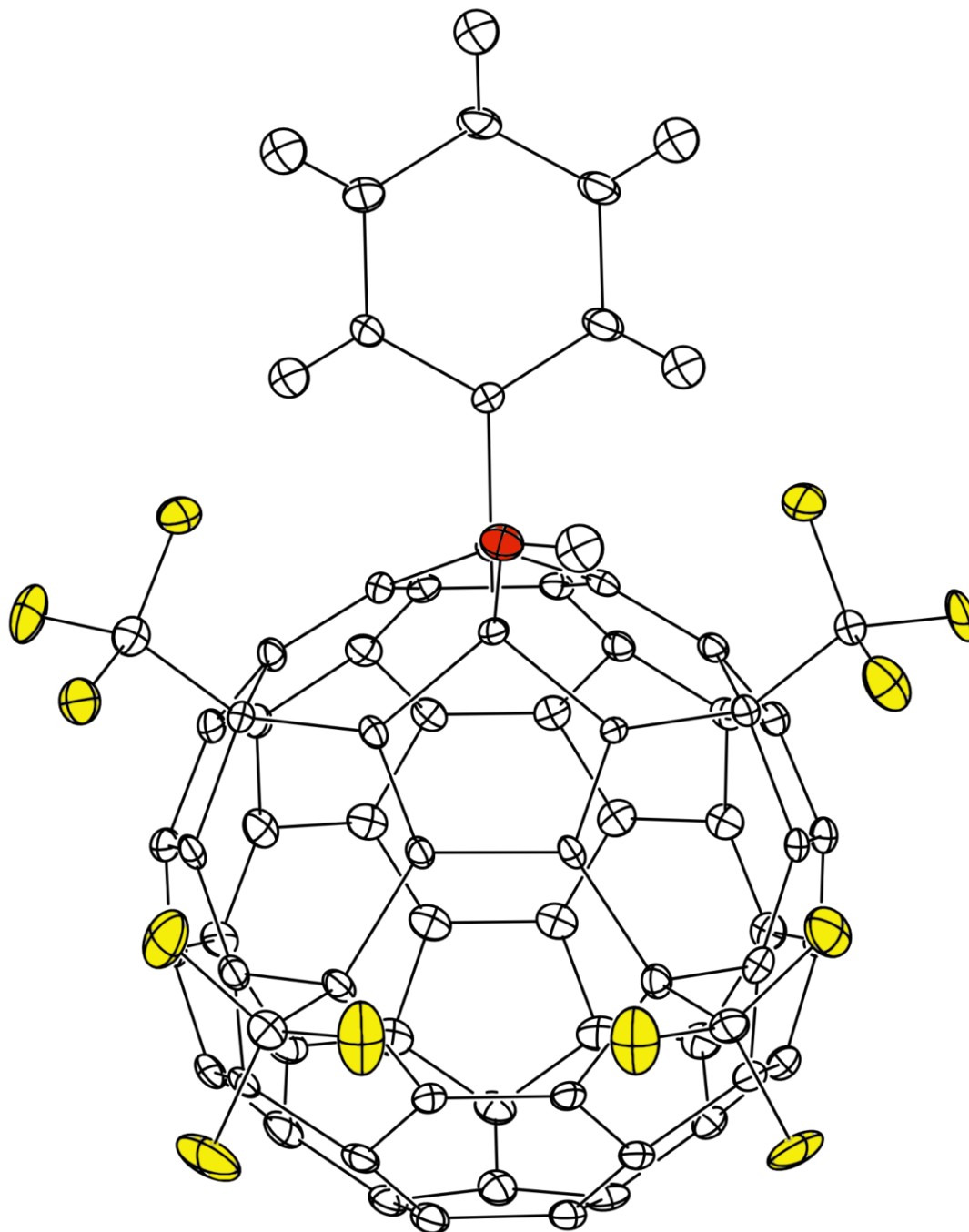
Figure 1.57. The 50% probability thermal ellipsoid plot of $C_{60}(CF_3)_4(C_6H_5)(OH)$.
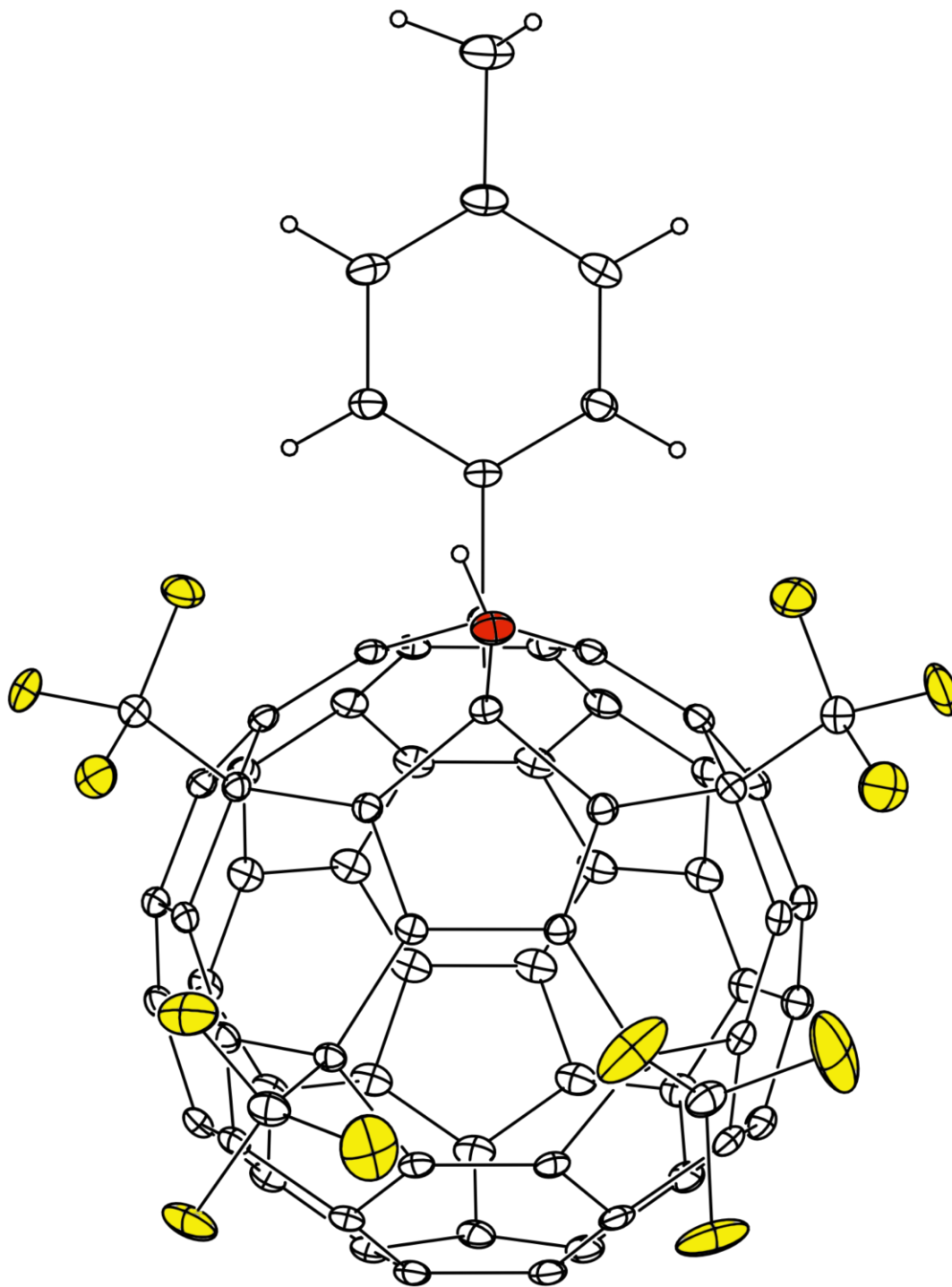
Figure 1.58. The 50% probability thermal ellipsoid plot of $C_{60}(CF_3)_4(C_6H_4CH_3)(OH)$.
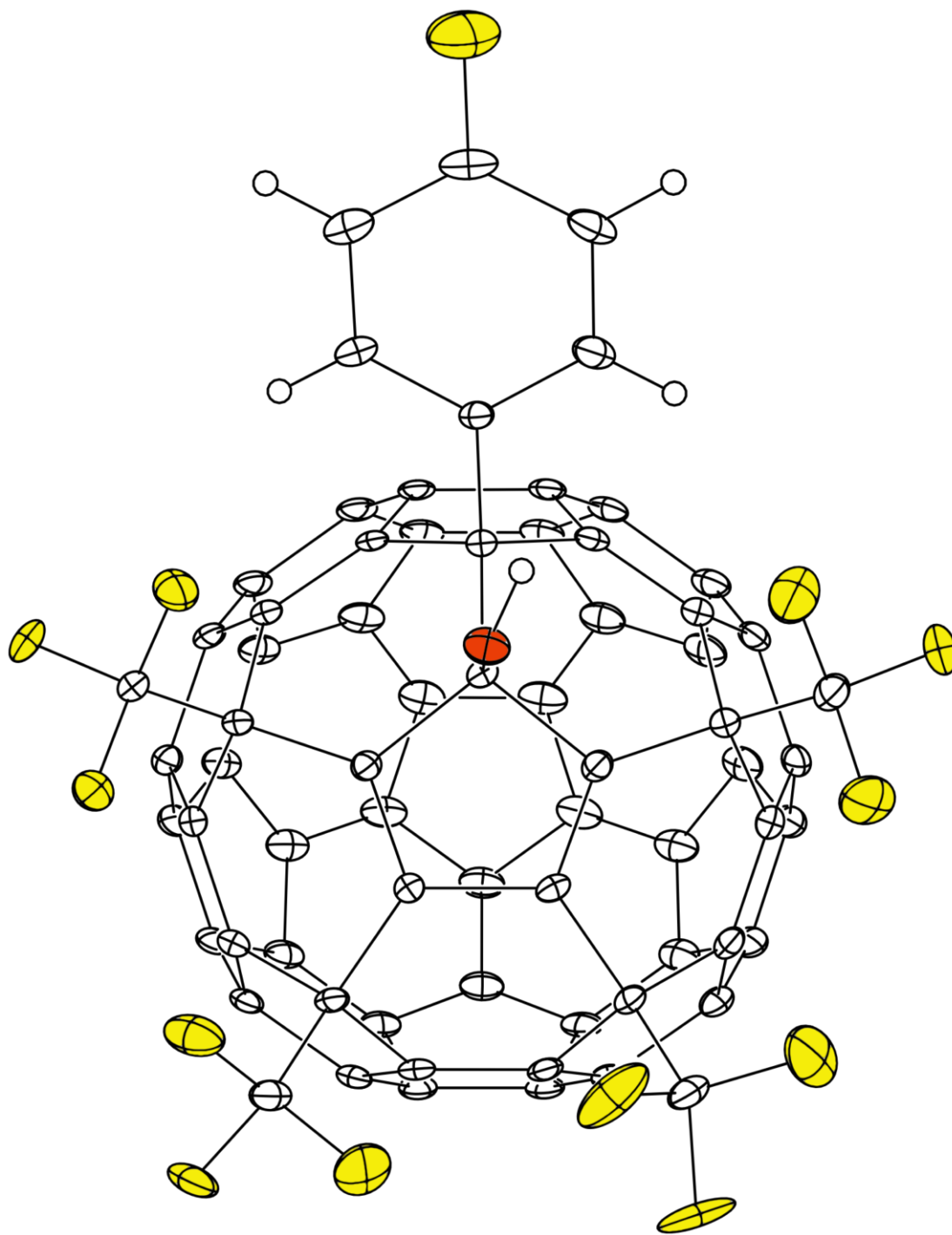
Figure 1.59. The 50% probability thermal ellipsoid plot of $C_{60}(CF_3)_4(C_6H_4F)(OH)$.
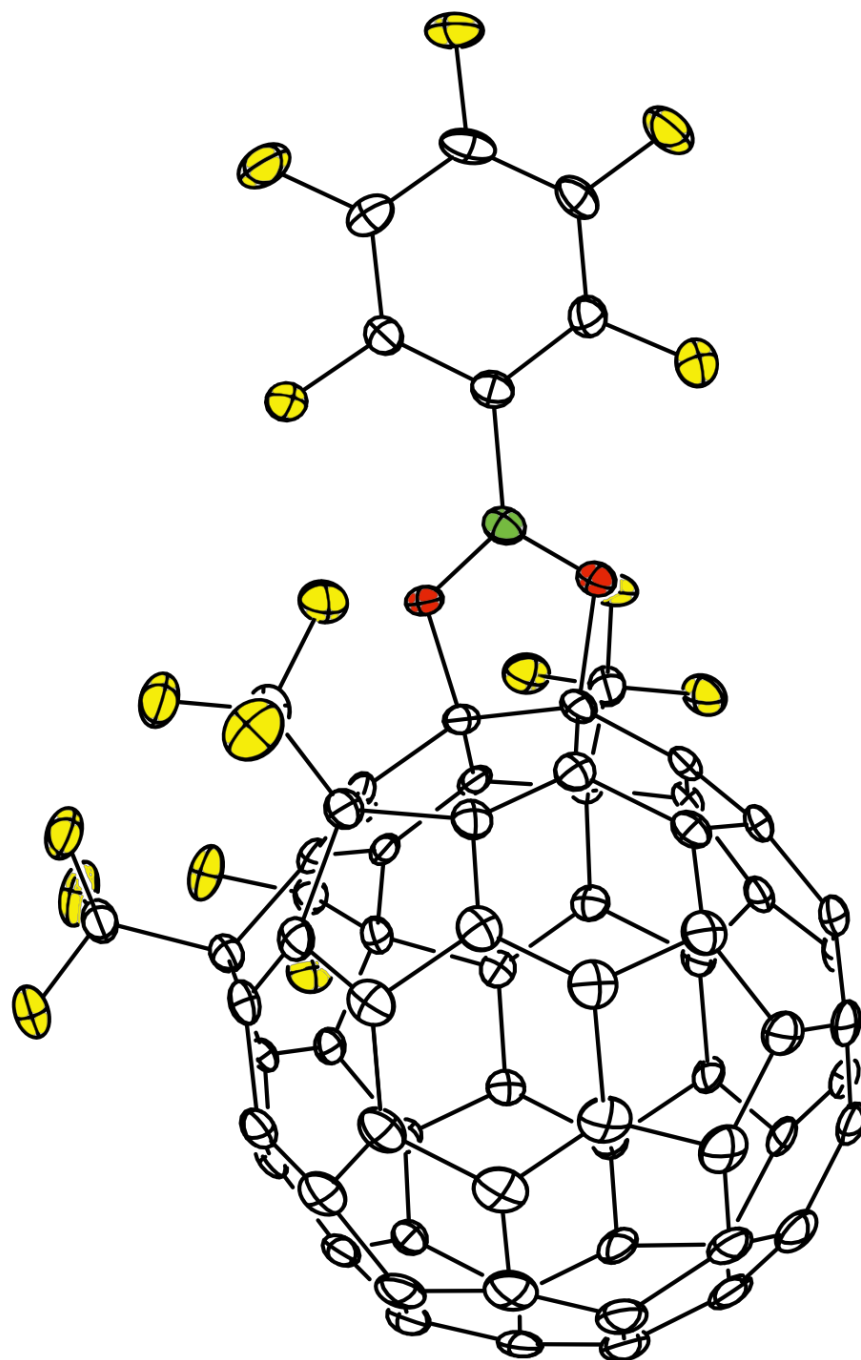
Figure 1.60. The 50% probability thermal ellipsoid plot of $C_{60}(CF_3)_4(O_2BC_6F_5)$.
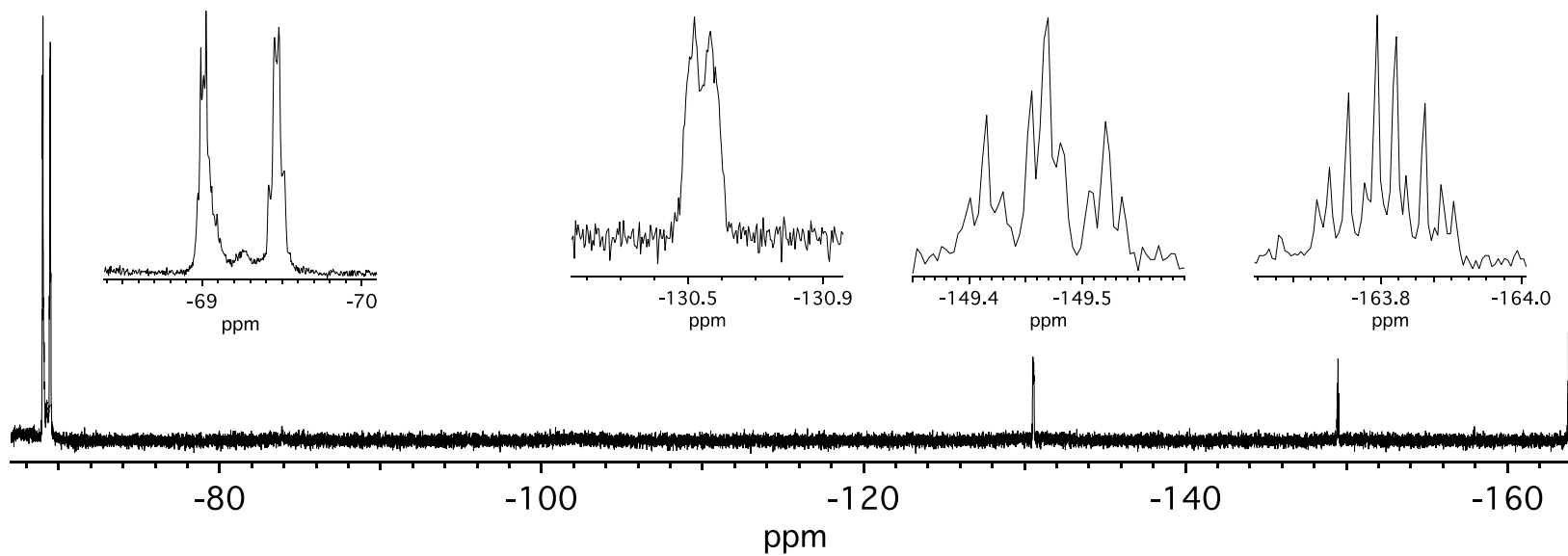
Figure 1.61. Fluorine-19 NMR spectrum of $C_{60}(CF_3)_4(O_2BC_6F_5)$ recorded in $CDCl_3$.
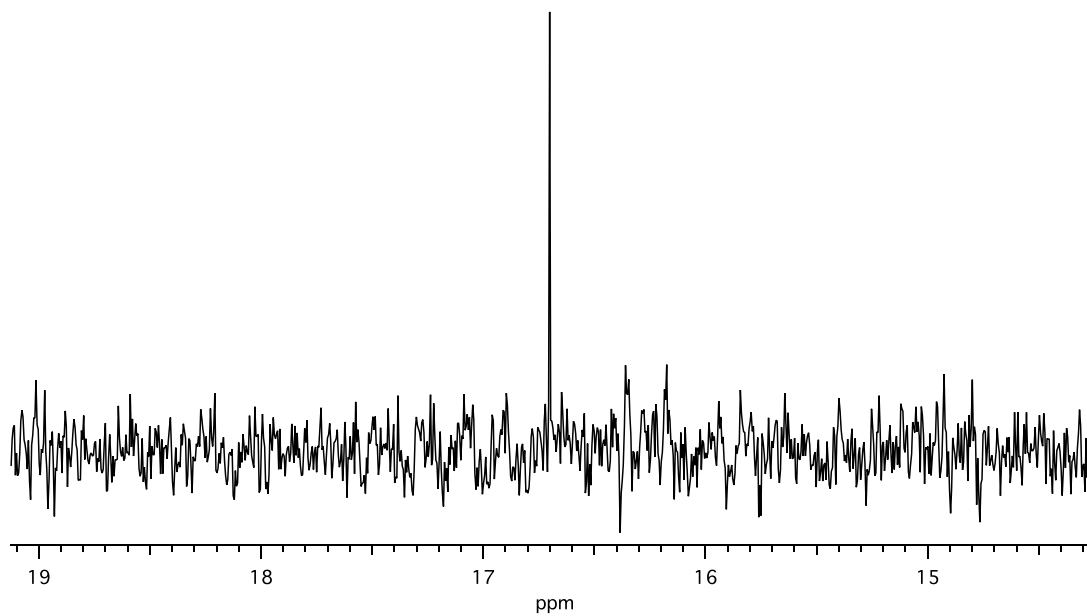
Figure 1.62. Boron-11 NMR spectrum of $C_{60}(CF_3)_4(O_2BC_6F_5)$ recorded in $CDCl_3$.
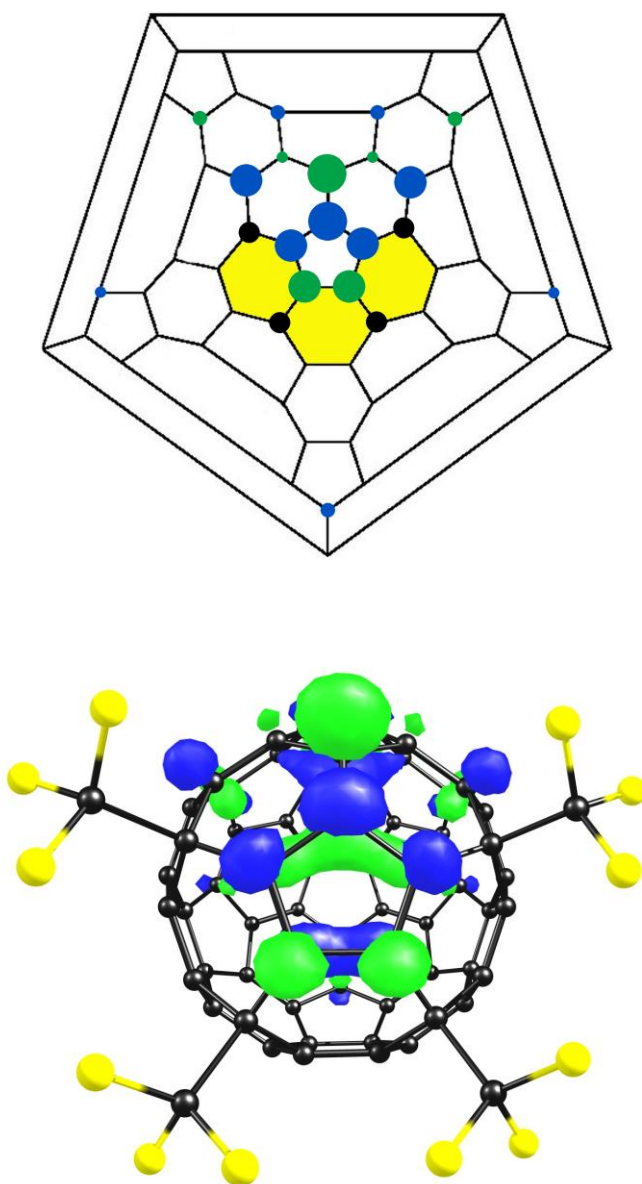
Figure 1.63. The DFT predicted LUMO of 60-4-2.

References

(1)   Kareev, I. E.; Shustova, N. B.; Kuvychko, I. V.; Lebedkin, S. F.; Miller, S. M.; Anderson, O. P.; Popov, A. A.; Strauss, S. H.; Boltalina, O. V. *J. Am. Chem. Soc.* **2006**, *128*, 12268–12280.

(2)   Popov, A. A.; Kareev, I. E.; Shustova, N. B.; Stukalin, E. B.; Lebedkin, S. F.; Seppelt, K.; Strauss, S. H.; Boltalina, O. V.; Dunsch, L. *J. Am. Chem. Soc.* **2007**, *129*, 11551–11568.

(3)   Popov, A. A.; Shustova, N. B.; Boltalina, O. V.; Strauss, S. H.; Dunsch, L. *ChemPhysChem* **2008**, *9*, 431–438.

(4)   Takano, Y.; Herranz, M. Á.; Martin, N.; de Miguel Rojas, G.; Guldi, D. M.; Kareev, I. E.; Strauss, S. H.; Boltalina, O. V.; Tsuchiya, T.; Akasaka, T. *Chem. Eur. J.* **2010**, NA–NA.

(5)   Takano, Y.; Herranz, M. Á.; Kareev, I. E.; Strauss, S. H.; Boltalina, O. V.; Akasaka, T.; Martin, N. *J. Org. Chem.* **2009**, *74*, 6902–6905.

(6)   Popov, A. A.; Kareev, I. E.; Shustova, N. B.; Lebedkin, S. F.; Strauss, S. H.; Boltalina, O. V.; Dunsch, L. *Chem. Eur. J.* **2008**, *14*, 107–121.

(7)   Dorozhkin, E. I.; Ignat'eva, D. V.; Tamm, N. B.; Goryunkov, A. A.; Khavrel, P. A.; Ioffe, I. N.; Popov, A. A.; Kuvychko, I. V.; Streletskiy, A. V.; Markov, V. Y.; Spandl, J.; Strauss, S. H.; Boltalina, O. V. *Chem. Eur. J.* **2006**, *12*, 3876–3889.

(8)   Goryunkov, A.; Kuvychko, I.; Ioffe, I. *Journal of Fluorine Chemistry* **2003**.

(9)   Kareev, I. E.; Kuvychko, I. V.; Lebedkin, S. F.; Miller, S. M.; Anderson, O. P.; Seppelt, K.; Strauss, S. H.; Boltalina, O. V. *J. Am. Chem. Soc.* **2005**, *127*, 8362–8375.

(10)   Troyanov, S. I.; Dimitrov, A.; Kemnitz, E. *Angew. Chem. Int. Ed.* **2006**, *45*, 1971–

(10)   Troyanov, S. I.; Dimitrov, A.; Kemnitz, E. *Angew. Chem. Int. Ed.* **2006**, *45*, 1971–
         1974.

(11)   Kareev, I. E.; Lebedkin, S. F.; Bubnov, V. P.; Yagubskii, E. B.; Ioffe, I. N.; Khavrel, P.
         A.; Kuvychko, I. V.; Strauss, S. H.; Boltalina, O. V. *Angew. Chem. Int. Ed.* **2005**, *44*,
         1846–1849.

(12)   Shustova, N. B.; Popov, A. A.; Mackey, M. A.; Coumbe, C. E.; Phillips, J. P.;
         Stevenson, S.; Strauss, S. H.; Boltalina, O. V. *J. Am. Chem. Soc.* **2007**, *129*, 11676–
         11677.

(13)   Troyanov, S. I.; Goryunkov, A. A.; Dorozhkin, E. I.; Ignat'eva, D. V.; Tamm, N. B.;
         Avdoshenko, S. M.; Ioffe, I. N.; Markov, V. Y.; Sidorov, L. N.; Scheurel, K.; Kemnitz,
         E. *Journal of Fluorine Chemistry* **2007**, *128*, 545–551.

(14)   Popov, A. A.; Tarábek, J.; Kareev, I. E.; Lebedkin, S. F.; Strauss, S. H.; Boltalina, O.
         V.; Dunsch, L. *J. Phys. Chem. A* **2005**, *109*, 9709–9711.

(15)   Fagan, P. J.; Krusic, P. J.; McEwen, C. N.; Lazar, J.; Parker, D. H.; Herron, N.;
         Wasserman, E. *Science* **1993**, *262*, 404–407.

(16)   Darwish, A. D.; Abdul-Sada, A. K.; Avent, A. G.; Lyakhovetsky, V. I.; Shilova, E. A.;
         Taylor, R. *Org. Biomol. Chem.* **2003**, *1*, 3102–3110.

(17)   Goryunkov, A.; Ioffe, I.; Kuvychko, I.; Yankova, T.; Markov, V.; Streletskii, A.; Dick,
         D.; Sidorov, L.; Boltalina, O.; Strauss, S. *Fullerene Nanot Carbon Nanostruct* **2004**, *12*,
         181–185.

(18)   Goryunkov, A. A.; Ignat'eva, D. V.; Tamm, N. B.; Moiseeva, N. N.; Ioffe, I. N.;
         Avdoshenko, S. M.; Markov, V. Y.; Sidorov, L. N.; Kemnitz, E.; Troyanov, S. I. *Eur. J.
         Org. Chem.* **2006**, 2508–2512.

(19)   Kareev, I. E.; Kuvychko, I. V.; Lebedkin, S. F.; Miller, S. M.; Anderson, O. P.; Seppelt, K.; Strauss, S. H.; Boltalina, O. V. *J. Am. Chem. Soc.* **2005**, *127*, 8362–8375.

(20)   Kareev, I. E.; Kuvychko, I. V.; Lebedkin, S. F.; Miller, S. M.; Anderson, O. P.; Strauss, S. H.; Boltalina, O. V. *Chem. Commun.* **2006**, 308.

(21)   Cardona, C. M.; Kitaygorodskiy, A.; Echegoyen, L. *J. Am. Chem. Soc.* **2005**, *127*, 10448–10453.

(22)   Shu, C.; Cai, T.; Xu, L.; Zuo, T.; Reid, J.; Harich, K.; Dorn, H. C.; Gibson, H. W. *J. Am. Chem. Soc.* **2007**, *129*, 15710–15717.

(23)   Shustova, N. B.; Kuvychko, I. V.; Peryshkov, D. V.; Whitaker, J. B.; Larson, B. W.; Chen, Y.-S.; Dunsch, L.; Seppelt, K.; Popov, A. A.; Strauss, S. H.; Boltalina, O. V. *Chem. Commun.* **2011**, *47*, 875–877.

(24)   Shustova, N. B.; Kareev, I. E.; Kuvychko, I. V.; Whitaker, J. B.; Lebedkin, S. F.; Popov, A. A.; Dunsch, L.; Chen, Y.-S.; Seppelt, K.; Strauss, S. H. *Journal of Fluorine Chemistry* **2010**, *131*, 1198–1212.

(25)   Kuvychko, I. V.; Shustova, N. B.; Avdoshenko, S. M.; Popov, A. A.; Strauss, S. H.; Boltalina, O. V. *Chem. Eur. J.* **2011**, *17*, 8799–8802.

(26)   Kuvychko, I. V.; Whitaker, J. B.; Larson, B. W.; Folsom, T. C.; Shustova, N. B.; Avdoshenko, S. M.; Chen, Y. S.; Wen, H.; Wang, X.-B.; Dunsch, L.; Popov, A. A.; Boltalina, O. V.; Strauss, S. H. *Chem. Sci.* **2012**, *3*, 1399–1407.

(27)   Kuvychko, I. V.; Strauss, S. H.; Boltalina, O. V. *Journal of Fluorine Chemistry* **2012**, *143*, 103–108.

(28)   Chiu, M.-Y.; Jeng, U.-S.; Su, M.-S.; Wei, K.-H. *Macromolecules* **2010**, *43*, 428–432.

(29)   Olson, D. C.; Lee, Y.-J.; White, M. S.; Kopidakis, N.; Shaheen, S. E.; Ginley, D. S.;

Voigt, J. A.; Hsu, J. W. P. *J. Phys. Chem. C* **2008**, *112*, 9544–9547.

(30)   Cardona, C. M.; Li, W.; Kaifer, A. E.; Stockdale, D.; Bazan, G. C. *Adv. Mater.* **2011**, *23*, 2367–2371.

(31)   Matsuo, Y. *Pure Appl. Chem.* **2012**, *84*, 945–952.

(32)   Coffey, D. C.; Larson, B. W.; Hains, A. W.; Whitaker, J. B.; Kopidakis, N.; Boltalina, O. V.; Strauss, S. H.; Rumbles, G. *J. Phys. Chem. C* **2012**, *116*, 8916–8923.

(33)   Nardes, A. M.; Ferguson, A. J.; Whitaker, J. B.; Larson, B. W.; Larsen, R. E.; Maturová, K.; Graf, P. A.; Boltalina, O. V.; Strauss, S. H.; Kopidakis, N. *Adv. Funct. Mater.* **2012**, n/a–n/a.

(34)   Kadish, K. M.; Gao, X.; Caemelbecke, E. V.; Suenobu, T.; Fukuzumi, S. *J. Phys. Chem. A* **2000**, *104*, 3878–3883.

(35)   Murata, Y.; Shiro, M.; Komatsu, K. *J. Am. Chem. Soc.* **1997**, *119*, 8117–8118.

(36)   Kareev, I. E.; Quiñones, G. S.; Kuvychko, I. V.; Khavrel, P. A.; Ioffe, I. N.; Goldt, I. V.; Lebedkin, S. F.; Seppelt, K.; Strauss, S. H.; Boltalina, O. V. *J. Am. Chem. Soc.* **2005**, *127*, 11497–11504.

(37)   Balch, A. L.; Costa, D. A.; Noll, B. C.; Olmstead, M. M. *J. Am. Chem. Soc.* **1995**, *117*, 8926–8932.

(38)   Heymann, D.; Weisman, R. B. *C. R. Chimie.* **2006**, *9*, 1107–1116.

(39)   Weisman, R. B.; Heymann, D.; Bachilo, S. M. *J. Am. Chem. Soc.* **2001**, *123*, 9720–9721.

(40)   Tajima, Y.; Takeuchi, K. *J. Org. Chem.* **2002**, *67*, 1696–1698.

(41)   Matsuo, Y.; Ozu, A.; Obata, N.; Fukuda, N.; Tanaka, H.; Nakamura, E. *Chem. Commun.* **2012**, *48*, 3878–3880.

(42)   Matsuo, Y.; Nakamura, E. *J. Am. Chem. Soc.* **2005**, *127*, 8457–8466.

(43)   Kuvychko, I. V.; Streletskii, A. V.; Popov, A. A.; Kotsiris, S. G.; DREWELLO, T.; Strauss, S. H.; Boltalina, O. V. *Chem. Eur. J.* **2005**, *11*, 5426.

(44)   Dorozhkin, E. I.; Goryunkov, A. A.; Ioffe, I. N.; Avdoshenko, S. M.; Markov, V. Y.; Tamm, N. B.; Ignat'eva, D. V.; Sidorov, L. N.; Troyanov, S. I. *European Journal of Organic Chemistry* **2007**, *2007*, 5082–5094.

(45)   Isobe, H.; Tomita, N.; Nakamura, E. *Org. Lett.* **2000**, *2*, 3663–3665.

(46)   Kennedy, R. D.; Halim, M.; Khan, S. I.; Schwartz, B. J.; Tolbert, S. H.; Rubin, Y. *Chem. Eur. J.* **2012**, 7418–7433.

(47)   Shustova, N. B.; Kuvychko, I. V.; Popov, A. A.; Delius, von, M.; Dunsch, L.; Anderson, O. P.; Hirsch, A.; Strauss, S. H.; Boltalina, O. V. *Angew. Chem. Int. Ed.* **2011**, *50*, 5537–5540.

(48)   Hirsch, A.; Brettreich, M.; Wudl, F. *Fullerenes: Chemistry and Reactions*; 1st ed. Wiley-VCH, 2005.

(49)   Creegan, K.; Robbins, J.; Robbins, W. *J. Am. Chem. Soc.* **1992**.

(50)   Shigemitsu, Y.; Kaneko, M.; Tajima, Y.; Takeuchi, K. *Chem. Lett.* **2004**, *33*, 1604–1605.

(51)   Huang, S.; Xiao, Z.; Wang, F.; Zhou, J.; Yuan, G.; Zhang, S.; Chen, Z.; Thiel, W.; Schleyer, P. V. R.; Zhang, X.; Hu, X.; Chen, B.; Gan, L. *Chem. Eur. J.* **2005**, *11*, 5449–5456.

(52)   Huang, S.; Yang, X.; Zhang, X.; Hu, X.; Gan, L.; Zhang, S. *Synlett* **2006**, *2006*, 1266–1268.

(53)   Tajima, Y.; Hara, T.; Honma, T.; Matsumoto, S.; Takeuchi, K. *Org. Lett.* **2006**, *8*,

3203–3205.

(54)   Jia, Z.; Zhang, X.; Zhang, G.; Huang, S.; Fang, H.; Hu, X.; Li, Y.; Gan, L.; Zhang, S.;

Zhu, D. *Chem Asian J* **2007**, *2*, 290–300.

(55)   Zhang, Q.; Pankewitz, T.; Liu, S.; Klopper, W.; Gan, L. *Angew. Chem. Int. Ed.* **2010**,

49, 9935–9938.

(56)   Blackett, B. N.; Coxon, J. M.; Hartshorn, M. P.; Lewis, A. J.; Little, G. R.; Wright, G.

J. *Tetrahedron* **1970**, *26*, 1311–1313.

(57)   Xiao, Z.; Yao, J.; Yang, D.; Wang, F.; Huang, S.; Gan, L.; Jia, Z.; Jiang, Z.; Yang, X.;

Zheng, B.; Yuan, G.; Zhang, S.; Wang, Z. *J. Am. Chem. Soc.* **2007**, *129*, 16149–16162.

(58)   Xiao, Z.; Yao, J.; Yu, Y.; Jia, Z.; Gan, L. *Chem. Commun.* **2010**, *46*, 8365.

(59)   Jiang, Z.; Zhang, Y.; Gan, L.; Wang, Z. *Tetrahedron* **2008**, *64*, 11394–11403.

(60)   Gan, L.; Yang, D.; Zhang, Q.; Huang, H. *Adv. Mater.* **2010**, *22*, 1498–1507.

(61)   *Organic Photovoltaics: Materials, Device Physics, and Manufacturing Technologies*;

Brabec, C.; Scherf, U.; Dyakonov, V., Eds. 1st ed. Wiley-VCH, 2008.

(62)   Shaheen, S. E.; Ginley, D. S.; Jabbour, G. E. *MRS bulletin* **2005**, *30*, 10–19.

(63)   Avdoshenko, S. M.; Ioffe, I. N.; Sidorov, L. N. *J. Phys. Chem. A* **2009**, *113*, 10833–

10838.

(64)   Ignat'eva, D. V.; Mutig, T.; Goryunkov, A. A.; Tamm, N. B.; Kemnitz, E.; Troyanov,

S. I.; Sidorov, L. N. *Russ Chem Bull* **2010**, *58*, 1146–1154.

(65)   Mutig, T.; Kemnitz, E.; Troyanov, S. I. *Mendeleev Communications* **2009**, *19*, 30–31.

(66)   Goryunkov, A. A.; Dorozhkin, E. I.; Tamm, N. B.; Ignat'eva, D. V.; Avdoshenko, S.

M.; Sidorov, L. N.; Troyanov, S. I. *Mendeleev Commun.* **2007**, *17*, 110–112.

(67)   Rispens, M. T.; Meetsma, A.; Rittberger, R.; Brabec, C. J.; Sariciftci, N. S.; Hummelen,

J. C. *Chem. Commun.* **2003**, 2116.

(68)   Kennedy, R. D.; Ayzner, A. L.; Wanger, D. D.; Day, C. T.; Halim, M.; Khan, S. I.;

Tolbert, S. H.; Schwartz, B. J.; Rubin, Y. *J. Am. Chem. Soc.* **2008**, *130*, 17290–17292.

(69)   Niinomi, T.; Matsuo, Y.; Hashiguchi, M.; Sato, Y.; Nakamura, E. *J. Mater. Chem.*

2009, *19*, 5804.

(70)   Haddon, R. C.; Brus, L. E.; Raghavachari, K. *Chem. Phys. Lett.* **1986**, *125*, 459–464.

(71)   Xie, Q.; Perez-Cordero, E.; Echegoyen, L. *J. Am. Chem. Soc.* **1992**, *114*, 3978–3980.

(72)   Dubois, D.; Kadish, K. M.; Flanagan, S.; Wilson, L. J. *J. Am. Chem. Soc.* **1991**, *113*,

7773–7774.

(73)   Echegoyen, L.; Echegoyen, L. E. *Acc. Chem. Res.* **1998**, *31*, 593–601.

(74)   Lichtenberger, D. L.; Nebesny, K. W.; Ray, C. D. **1991**, *126*, 203–208.

(75)   Xie, Q.; Arias, F.; Echegoyen, L. *J. Am. Chem. Soc.* **1993**, *115*, 9818–9819.

(76)   Feldberg, S. W. *Journal of Electroanal. Chem.* **2008**, *624*, 45–51.

(77)   Tsierkezos, N. G. *J. Solution Chem.* **2007**, *36*, 289–302.

(78)   Zheng, M.; Li, F.-F.; Ni, L.; Yang, W.-W.; Gao, X. *J. Org. Chem.* **2008**, *73*, 3159–

3168.

(79)   Hammett, L. P. *Chemical Reviews* **1935**, *17*, 125–136.

(80)   Hansch, C.; Leo, A.; Taft, R. W. *Chemical Reviews* **1991**, *91*, 165–195.

(81)   Charton, M. *J. Am. Chem. Soc.* **1975**, *97*, 1552–1556.

(82)   Marzilli, L. G.; Bayo, F.; Summers, M. F.; Thomas, L. B.; Zangrando, E.; Bresciani-

Pahor, N.; Mari, M.; Randaccio, L. *J. Am. Chem. Soc.* **1987**, *109*, 6045–6052.

(83)   Bunten, K. A.; Chen, L.; Fernandez, A. L.; Poë, A. J. *Coordination chemistry reviews*

2002, *233*, 41–51.

(84)   Brown, T. L.; Lee, K. J. *Coordination chemistry reviews* **1993**, *128*, 89–116.

(85)   Simón-Manso, Y. *J. Phys. Chem. A* **2005**, *109*, 2006–2011.

(86)   Agrafiotis, D. K.; Shemanarev, M.; Connolly, P. J.; Farnum, M.; Lobanov, V. S. *J. Med. Chem.* **2007**, *50*, 5926–5937.

(87)   Do, J. Y.; Park, S. K.; Ju, J. J.; Park, S.; Lee, M. H. *Optical Materials* **2004**, *26*, 223–229.

(88)   Espeso, J.; Lozano, A. E.; la Campa, de, J. G.; de Abajo, J. *Journal of Membrane Science* **2006**, *280*, 659–665.

(89)   Babazadeh, M. *J. Appl. Polym. Sci.* **2006**, *102*, 633–639.

(90)   Justin Thomas, K. R.; Lin, J. T.; Tao, Y.-T.; Chuen, C.-H. *Chem. Mater.* **2004**, *16*, 5437–5444.

(91)   Brabec, C. J.; Gowrisanker, S.; Halls, J. J. M.; Laird, D.; Jia, S.; Williams, S. P. *Adv. Mater.* **2010**, *22*, 3839–3856.

(92)   Lemal, D. M. *J. Org. Chem.* **2004**, *69*, 1–11.

(93)   Corvaja, C.; Farnia, G.; Formenton, G.; Navarrini, W.; Sandona, G.; Tortelli, V. *The Journal of Physical Chemistry* **1994**, *98*, 2307–2313.

(94)   Combellas, C.; Kanoufi, F.; Thiébault, A. *J. Phys. Chem. B* **2003**, *107*, 10894–10905.

(95)   Yuan, Z.; Li, J.; Xiao, Y.; Li, Z.; Qian, X. *J. Org. Chem.* **2010**, *75*, 3007–3016.

(96)   Li, Y.; Li, C.; Yue, W.; Jiang, W.; Kopecek, R.; Qu, J.; Wang, Z. *Org. Lett.* **2010**, *12*, 2374–2377.

(97)   Ruoff, R. S.; Kadish, K. M.; Boulas, P.; Chen, E. *The Journal of Physical Chemistry* **2001**, *99*, 8843–8850.

(98)   Djurovich, P. I.; Mayo, E. I.; Forrest, S. R.; Thompson, M. E. *Organic Electronics*

2009, *10*, 515–520.

(99)   Doubois, D.; Moninot, G.; Kutner, W.; Jones, M. T.; Kadish, K. *The Journal of Physical Chemistry* **1992**, *96*, 7137.

(100)   Dixon, D. A.; Matsuzawa, N.; Fukunaga, T.; Tebbe, F. N. *The Journal of Physical Chemistry* **1992**, *96*, 6107–6110.

(101)   Kuvychko, I. V.; Strauss, S. H.; Boltalina, O. V. In *Efficient Preparation of Fluorine Compounds*; Wiley: New York, 2013; pp. 9–11.

(102)   Bonifazi, D.; Enger, O.; Diederich, F. O. *Chem. Soc. Rev.* **2007**, *36*, 390.

(103)   Matsuo, Y.; Iwashita, A.; Abe, Y.; Li, C.-Z.; Matsuo, K.; Hashiguchi, M.; Nakamura, E. *J. Am. Chem. Soc.* **2008**, *130*, 15429–15436.

(104)   Kennedy, R. D.; Ayzner, A. L.; Wanger, D. D.; Day, C. T.; Halim, M.; Khan, S. I.; Tolbert, S. H.; Schwartz, B. J.; Rubin, Y. *J. Am. Chem. Soc.* **2008**, *130*, 17290–17292.

(105)   Pope, M.; Swenberg, C. E. *Electronic processes in organic crystals and polymers*; Oxford University Press, USA, 1999.

(106)   Sawamura, M.; Kawai, K.; Matsuo, Y.; Kanie, K.; Kato, T.; Nakamura, E. *Nature* **2002**, *419*, 702–705.

(107)   Bashilov, V. V.; Dolgushin, F. M.; Tumanskii, B. L.; Petrovskii, P. V.; Sokolov, V. I. *Tetrahedron* **2008**, *64*, 11291–11295.

(108)   Ignat'eva, D. V.; Ioffe, I. N.; Troyanov, S. I.; Sidorov, L. N. *Russ. Chem. Rev.* **2011**, *80*, 631–645.

(109)   Green, M. A.; Emery, K.; Hisikawa, Y.; Warta, W. *Prog. Photovolt: Res. Appl.* **2007**, *15*, 425–430.

(110)   Green, M. A.; Emery, K.; Hishikawa, Y.; Warta, W.; Dunlop, E. D. *Prog. Photovolt:*

Res. Appl. **2011**, *19*, 565–572.

(111)   Larson, B. W.; Whitaker, J. B.; Wang, X.-B.; Popov, A. A.; Rumbles, G.; Kopidakis, N.; Strauss, S. H.; Boltalina, O. V. *J. Phys. Chem. C* **2013**, *117*, 14958–14964.

(112)   Kang, H.; Cho, C.-H.; Cho, H.-H.; Kang, T. E.; Kim, H. J.; Kim, K.-H.; Yoon, S. C.; Kim, B. J. *ACS Appl. Mater. Interfaces* **2012**, *4*, 110–116.

(113)   He, Y.; Chen, H.-Y.; Hou, J.; Li, Y. *J. Am. Chem. Soc.* **2010**, *132*, 1377–1382.

(114)   Brabec, C. J.; Cravino, A.; Meissner, D.; Sariciftci, N. S.; Fromherz, T.; Rispens, M. T.; Sanchez, L.; Hummelen, J. C. *Adv. Funct. Mater.* **2001**, *11*, 374–380.

(115)   Li, G.; Shrotriya, V.; Huang, J.; Yao, Y.; Moriarty, T.; Emery, K.; Yang, Y. *Nat Mater* **2005**, *4*, 864–868.

(116)   Wang, J.-C.; Weng, W.-T.; Tsai, M.-Y.; Lee, M.-K.; Horng, S.-F.; Perng, T.-P.; Kei, C.-C.; Yu, C.-C.; Meng, H.-F. *J. Mater. Chem.* **2010**, *20*, 862.

Chapter 2

Electrochemical, Thermal, and Crystal Packing Properties

of Perfluoroalkyl Fullerenes

Introduction

The practical applications of perfluoroalkyl fullerenes, namely as electron accepting materials in organic electronic devices, largely depends on the electrochemical behavior that the fullerene$(R_F)_n$ compounds exhibit. Previous studies by the Strauss group demonstrated that, in general, PFAFs exhibit reduction potentials are anodically shifted when compared to their parent fullerene cage (i.e., they are generally easier to reduce than their parent fullerene), while also being dependent on the number, type, and addition pattern of the R_F groups.[2] However, to date there has never been a study of how the electrochemical properties change over a series of fullerene$(R_F)_n$ compounds where the number and addition pattern of the R_F groups is held constant, while the chain length and branching pattern of the R_F group is varied.

Another property that could prove to be critical for practical applications of PFAF is their thermal stability. High temperatures are sometimes used in the preparation of OPV devices to thermally evaporate and deposit thin films and in annealing steps to adjust the morphology of

the active layers.[29,61,62] With the exception of a few reports in the literature,[63-65] PFAFs are generally assumed to be thermally stable due to the high temperatures (typically in excess of 400 °C) that PFAFs are typically prepared.[1,20,66] However, there is very little experimental evidence to support this assumption and no systematic study has been conducted to examine at what temperature PFAFs undergo decomposition and how various PFAF parameters (e.g. the number and addition pattern of CF_3 groups) affect their thermal stability.

The solid state crystal packing motifs of fullerene derivatives has also been reported to have important practical implications for OPV devices.[46,67-69] Close fullerene cage distances (<10.5 Å) that extend in 2 and 3 dimensional networks have been suggested to improve free charge carrier motilities and have been linked to improved power conversion efficiencies of OPV devices.[68]

This chapter will explore the electrochemical behavior and the thermal stability of selected PFAFs. Specifically, the electrochemical properties of the series of $1,7-C_{60}(R_F)_2$ compounds described in chapter 1 will be examined. The electrochemical behavior of PFAFs with different addition patterns and with different addends measured in different solvents will be presented. Furthermore, a carefully controlled study to accurately determine to what temperatures PFAFs can be heated, before undergoing compositional or isomeric changes, as well as the isolation and structural characterization of the decomposition products will be discussed. The effects on the thermal stability of the number and addition pattern of CF_3 groups will also be explained. Lastly, the crystal packing motifs will be examined and the possible implications toward OPV devices will be explored.

2.1. Studies on the Electrochemical Properties

of Perfluoroalkyl Fullerenes

2.1.1. Introduction. Soon after the serendipitous discovery of C_{60}, theoretical predictions indicated that the lowest unoccupied molecular orbital (LUMO) of both C_{60} and C_{70} was energetically low lying and triply degenerate thus capable of accepting 6 electrons.[70] The experimental proof of this triply degenerate and energetically low-lying LUMO came in several steps. First, four reversible reductions were reported followed by the hexanion being observed in 1992.[71,72] In accordance with the theoretical predictions, the measured $E_{1/2}$ values were −0.98, −1.37, −1.87, −2.35, −2.85, and −3.26 V vs. $FcH^{0/+}$ when measured in a mixture of acetonitrile: toluene (1:5).[73] It was also theoretically predicted that the oxidation of C_{60} would be difficult to observe; whereas the gas phase ionization potential was measured to be ca. 7.6 eV.[70,74] In 1993 the first oxidation of C_{60} and C_{70} was electrochemically observed in 1,1,2,2-tetrachloroethane at a potential of +1.26 V and +1.20 V vs $FcH^{0/+}$ respectively.[72,75] Considering the difficulty of oxidizing C_{60}, PFAFs should be considerably harder to oxidize due to the electron withdrawing nature of the perfluoroalkyl addends. This is supported by DFT-predicted E(HOMO) values of selected PFAFs whereas many PFAFs exhibit low-lying E(LUMO) values indicating a good electron-accepting ability.

Interest in PFAFs stems primarily from their strong electron accepting properties that can vary greatly depending on the number, type and addition pattern of the perfluoroalkyl substituent.[2] In general, PFAFs exhibit quasi-reversible one electron reductions that are more positive than their parent fullerene.[2] It is generally accepted that the reduction potential of a fullerene derivative is largely dependent on the interplay of the nature, number, and how the

substituents are arranged on the fullerene cage.[2,73] On one hand, as the number of additions increases, the cage π system becomes more localized and broken up thus making the molecule harder to reduce. However, this effect is offset by the nature of the addend. If the addend is electron withdrawing, like perfluoroalkyl groups, then the cage becomes more electron deficient thus lowering the reduction potential. Furthermore, it has been shown that the addition pattern of the substituents is as important, if not more important than the nature and number of addends in determining the reduction potential.[2]

This section will discuss how the nature of the substituent, the addition pattern of the substituents, and the solvent affect the solution phase $E_{1/2}$ values of both perfluoroalkyl and perfluorobenzyl fullerenes. In addition, theoretical DFT calculations performed by Dr. Popov from the Leibniz Institute for Solid State and Materials Research as well as experimental electron-affinity values measured by Dr. Wang from Pacific Northwest National Laboratory will be used to expound on and substantiate the conclusions made about the electrochemical behavior of fullerene(R_F) derivatives.

Experimental for Section 2.1

Instrumentation, Solvents, and Reagents. All electrochemical experiments were controlled with a PAR 263 potentiostat/galvanostat at a scan rate of 100 mV/sec unless otherwise noted. Each experiment was conducted in a dinitrogen filled glove box (oxygen and water < 1 ppm). The electrolyte was N(n-Bu)$_4$BF$_4$, Fluka puriss grade dried under vacuum at 70 °C for 24 h. A 0.1 M solution of N(n-Bu)$_4$BF$_4$ in o-dichlorobenzene that had been freshly dried with 3Å

molecular sieves and vacuum distilled was used for each measurement. All solvents used for electrochemical measurements were confirmed to be dry by ^{1}H NMR spectroscopy. Both Fe(Cp*)$_2$ $^{+/0}$ and Fe(Cp)$_2$ $^{+/0}$ were used as internal standards. A three electrode, one compartment electrochemical cell was used. Both the working and auxiliary electrodes were platinum wires (0.5 mm diameter). A silver wire (0.5 mm diameter, Alfa Aesar Premion, 99.99%) served as the quasi-reference electrode.

Squarewave voltammetry was conducted with the following parameters unless otherwise stated: pulse hight and width were 0.05 V for 0.02 sec, the step hight was 4.0 mV, and the scan rate was 100 mV/sec.

2.1.3. General Remarks about Electrochemical Measurements. Electrochemical cell. For every electrochemical experiment conducted in this section, a home-built, three-electrode electrochemical cell was used. The working and counter electrodes were platinum wire with a diameter of 0.127 mm. They were constructed by slowly melting glass capillary tubes around platinum wire. The Pt wires extended out from the glass insulator approx. 2 mm. In theory, as the electrode area decreases so too do the faradaic and non-faradaic currents. This decrease in current is desirable in one respect because it decreases the voltage drop or iR drop of the electrochemical cell. However, in practice this advantage is offset by rapid electrode contamination; the seal between the platinum wire and glass insulator will leak over time resulting in electroactive material leaking into the upper section of the working electrode. This electroactive material, mainly fullerene material from previous electrochemical experiments, will result in reduction events that will interfere with the waves from the sample. This contamination effect can be minimized by routinely cleaning the entire electrode; however, this is impractical.

Therefore, in this work a larger electrode area was used because an electrode with a larger area will result in a larger current from the sample thereby making the current from any impurities in the upper section of the electrode not visible.

Due to solubility restrictions, fullerene electrochemisty is predominantly carried out in non-polar organic solvents. As such, the use of aqueous reference electrodes such as the saturated calomel electrode (SCE) should be avoided. Aqueous electrodes may introduce unaccounted for junction potentials and also leak water into the electrochemical cell, thereby changing the nature of the solvent. For the electrochemical experiments conducted in this work, a silver wire was used as a pseudo-reference electrode. This, however, is not a true reference electrode, so the internal standards ferrocene and decamethyl ferrocene were used in every electrochemical experiment conducted.

Cyclic Voltammetry. Cyclic voltammetry (CV) was the primary means of determination of the $E_{1/2}$ values. The $E_{1/2}$ values were determined by subtracting the peak cathodic potential (E_{pc}) from the peak anodic potential (E_{pa}) and dividing by 2. The extent of electrochemical and chemical reversibility was determined by examining the current peak-to-peak offset (ΔE_p) and the peak current ratio (i_{pa}/i_{pc}). In every case, the ΔE_p deviated from ideal Nernstian fast electron transfer kinetics of 0.06 V/ n where n is the number of electrons transferred. Typical values of ΔE_p were between 0.09 V and 0.12 V depending on the solvent. This large deviation from 0.06 V for a one-electron transfer is attributed to the uncompensated resistance of the solution and is in accordance with values from the literature.[76,77] In addition, ferrocene is considered to be reversible in the solvents used in this work and the ΔE_p of the ferrocene internal standard was in the same range as the fullerene derivative being examined. The other figure of merit used to

128

determine electrochemical and chemical reversibility was the peak current ratio. Ideally this ratio should equal unity and is scan rate independent. In every case, the peak current ratio of the fullerene derivative being examined was in the range of 0.9 to 1.0. However, to maintain rigorous electrochemical terminology, the term quasi-reversible will be used to describe the electrochemical reversibility of the fullerene derivatives in this work.

Squarewave Voltammetry. Squarewave voltammetry (SWV) is an improvement on staircase voltammetry where a square waveform is used instead of a linear-sweep waveform. The difference in the current directly after the step and before the next step is taken and plotted vs. the applied potential. The advantage of this method is that the background non-faradaic or charging current is effectively subtracted. This technique is primarily used when the concentration of the electroactive species is very low, usually in the nanomolar concentration range. However, in this work SWV was used to effectively extend the solvent window and to support the conclusions drawn from CV experiments, not due to a low concentration of fullerene. It is important to note that, unless a backward scan is done in conjunction with the forward scan, SWV cannot be used to determine the $E_{1/2}$ of a material because no information is given about the reversibility of the system.

Control Experiments. To determine the reproducibility of the electrochemical measurements, control experiments were conducted with C_{60}, $C_{60}(CF_3)_2$, and $C_{60}(n\text{-}C_4F_9)_2$. After several days, separate fresh solutions of these three compounds were prepared and the voltammograms of each were recorded. This process was repeated several times resulting in a total of 4 separate measurements for each of the three compounds spread out over the course of 2

weeks. The standard deviations of the separate $E_{1/2}$ values were then calculated to be 0.0036 resulting in an error of 0.0102 V at the 3σ confidence level. Additionally, once the voltammograms had been recorded, the solutions were stored in a dinitrogen filled glove box with the water and dioxygen content below 1 ppm. After the solutions had been stored for 5 days, the voltammogram was recorded again resulting in identical values within the error of the measurement. To ensure that the measured $E_{1/2}$ was not concentration dependent, the voltammogram of an oDCB solution of $1,7\text{-}C_{60}(n\text{-}C_4F_9)_2$ was recorded. This same solution was then diluted with oDCB electrolyte solution and measured once again. The $E_{1/2}$ values between the two measurements were the same within the experimental error of $\pm$ 10 mV.

Periodically, as a quality control measure for the electrochemical cell, fresh solutions of C_{60} were prepared and the voltammograms recorded. Every time the cell was checked with C_{60}, the measured reduction potential of C_{60} was always the same, within the experimental error of $\pm$ 10 mV, as the accepted value.

Solvent Considerations. Three solvents were used in this work: oDCB, DCM, and benzonitrile. These solvents were chosen primarily for their ability to solubilize both the fullerene being studied and the electrolyte $TBABF_4$. The other equally important consideration was that they are electrochemically inert solvents in the potential window used. There are several reports of benzonitrile undergoing a reaction with fullerene trianions, therefore when benzonitrile was used only the first two reductions were observed.[78]

Several reports in the literature have used mixtures of polar (to solubilize the supporting electrolyte) and non-polar (to solubilize the fullerene) solvents such as acetonitrile: toluene (1:5). This is in general a bad practice; mixtures of solvents should be avoided for electrochemical

measurements because maintaining the same ratio of solvents from batch-to-batch is difficult and may result in poor reproducibility of measurements if the solvent ratio changes from experiment to experiment or lab to lab.

2.1.4. Substituent Effects in Bis-Perfluoroalkylated Fullerenes on Electronic Properties. It had previously been established that the addition pattern of substituents on the fullerene cage was as important, if not more important, than the number and type of substituent.[2] However, it was unknown how changing the length or branching pattern of a given substituent type affects the electronic properties of the substituted fullerene. Substituent effects are of paramount importance in virtually all fields of fundamental and applied chemistry. Classical and modern examples can be found in organic chemistry (Hammett[79,80] parameters and Charton steric parameters[81]), inorganic chemistry (trans effect and trans influence[82]), organometallic chemistry (phosphine cone angles[83,84]), physical chemistry (linear free energy relationships and DFT[85]), biochemistry (protein tertiary structure[9]), medicinal chemistry (SAR maps[86]), polymer chemistry (nonlinear optics[87] and permeation properties[88] and glass transition temperatures[87-89]), and materials chemistry (stability and luminescent properties of electroluminescent devices[90] and light-to-power conversion efficiencies of fullerene-derivative-based OPV devices[91]).

Despite the importance of organofluorine chemistry in science and technology (e.g., nonstick coatings, membranes for electrochemical cells, low k dielectrics, solvents, blood substitutes, inhalation anesthetics, pharmaceuticals and agrochemicals, CFC replacements, and fluorous-technology separation methods)[92], there has never been a systematic study of the effects of a homologous series of perfluoroalkyl (R_F) groups on the electronic/electrochemical properties of a given substrate. The work in this section was undertaken to discover the links, if any,

between gas-phase electron affinities (EAs), first reduction potentials ($E_{1/2}$ values), and quantum-chemical predicted E(LUMO) values for a set of compounds with the same substitution pattern but with different electron-withdrawing R_F groups.

The Hammett σ_p values from the literature for CF_3, C_2F_5, n-C_3F_7, i-C_3F_7, and n-C_4F_9, only range from 0.48 (n-C_3F_7) to 0.54 (CF_3), whereas σ_p values for a list of hundreds of neutral substituents range from −0.70 to 1.35.[80] The $E_{1/2}(0/-)$ value for trans-$C_2(CF_3)_2(C_2F_5)_2$ is 60 mV more positive than for $C_2(CF_3)_4$, suggesting that for these two olefins the C_2F_5 group is more electron withdrawing than the CF_3 group.[93] In contrast, the $E_{1/2}(0/-)$ values for 7,24-$C_{70}(R_F)_2$, with $R_F=$ CF_3 or C_2F_5, only differed by 10 mV, which is within the uncertainty of the measurements, suggesting that C_2F_5 is not more electron withdrawing than CF_3, at least not for a large substrate such as C_{70}.[3] Furthermore, the cathodic peak potentials (note: not reversible $E_{1/2}$ values) for three p-$C_6H_4(CN)(R_F)$ derivatives were the same to within ±10 mV for $R_F=$ n-C_4F_9, n-C_6F_{13} and n-C_8F_{17}, suggesting no difference in electron withdrawing ability for these R_F groups.[94] In addition, two other electrochemical studies of R_F substituted perylene diimides found negligible differences in $E_{1/2}(0/-)$ values when comparing CF_3 vs. n-C_8F_{17}[95] or when comparing n-C_4F_9 vs. n-C_8F_{17}.[96] Consistent with this lack of an electronic difference for different R_F groups, a series of $Ir(acac)(CO)_2(R_F)I$ complexes with $R_F=$ CF_3, C_2F_5, n-C_3F_7, i-C_3F_7, and n-C_4F_9, and s-C_4F_9 [96] and a series of $CpMo(CO)_3(R_F)$ complexes with $R_F=$ CF_3, C_2F_5, and n-C_3F_7 each had the same average $\nu(CO)$ value to within ±2 or ±1 cm^{-1}, respectively. The results from the organometallic compounds provide experimental evidence that the formal charges on the metal centers and the CO ligands are independent of the PFA group. Do different R_F groups differ in their electron-withdrawing ability? Most of the results listed above indicate that the

answer is ''no'', but the $C_2(CF_3)_4$ and $C_2(CF_3)_2(C_2F_5)_2$ $E_{1/2}(0/-)$ values indicate that the answer is ''yes''. Clearly the question does not have a consistent answer.

Experimental $E_{1/2}$ Values of a Series of 1,7-$C_{60}(R_F)_2$ Compounds. To help answer the question, "do different R_F groups differ in their electron-withdrawing ability", the $E_{1/2}$ values of seven 1,7-$C_{60}(R_F)_2$ compounds were measured with cyclic voltammetry and squarewave voltammetry. The synthesis and structural characterization of these compounds were described earlier in Chapter 1. The set of seven R_F groups: CF_3, C_2F_5, n-C_3F_7, i-C_3F_7, n-C_4F_9, s-C_4F_9, and n-C_8F_{17} had never been compared together in this way, and the literature that did exist for a subset of the seven R_F groups did not give a consistent answer.

The results from the electrochemical measurements of the seven 1,7-$C_{60}(R_F)_2$ compounds are presented in Table 2.1 as well as in Figure 2.1. The cyclic voltammograms of each compound are shown in Figures 2.2 to 2.4. As can be seen, the measured $E_{1/2}$ values of each of the 7 compounds are the same within the error of the measurement. This seems to suggest that the electron withdrawing strength of the series of R_F groups are identical. However, this result may be misleading as the experimental $E_{1/2}$ is dependent on the EA of the molecule as well as the $\Delta\Delta G_{sol}$ according to the equation $E_{1/2} = \text{EA} - \Delta\Delta G_{sol} + E_{ref}$. It is possible that the changing EA (and thus the changing electron withdrawing strength of the substituent) might be perfectly offset by the $\Delta\Delta G_{sol}$ resulting in the observed $E_{1/2}$ of the compounds being identical.

Experimental and computational electron affinities (EAs). The experimental relative EAs, measured by a collaborator Dr. Wang from The Pacific Northwest National Laboratory, increase from 0.000 to 0.090 eV across the series of R_F substituents, and the DFT-predicted EA

values, calculated by Dr. Popov, increase from 0.000 to 0.075 eV. Although the range of EAs is less than 0.1 eV, the precision of the experimental EA measurements, ± 8 or ± 10 mV, allows three trends to be observed conclusively about the electron-withdrawing properties of these R_F groups when they are attached to $C(sp^3)$ atoms of substrates with extensive π systems. The first trend is that the relative DFT- predicted EAs match the experimental values extremely well; therefore, DFT-predicted EAs of related compounds for which experimental EAs are not available can be used with a high degree of confidence.

The second trend is that there is a monotonic increase in the experimental gas-phase EA for five of the seven 1,7-$C_{60}(R_F)_2$ compounds, from CF_3 (0.000 eV) to C_2F_5 (0.030 eV) to n-C_3F_7 (0.050 eV) to n-C_4F_9 (0.065 eV) to n-C_8F_{17} (0.090 eV). This strongly suggests, for at least this set of homologous fullerene compounds, that a primary perfluoroalkyl group becomes a stronger electron-withdrawing group as its chain length increases. The EAs are plotted another way in Figure 2.5, assigning an integer x-axis value to each R_F group equal to the number of C atoms in the chain (in Figure 2.1 the x-axis values are also integers but do not correspond to the number of C atoms in the chain). Figure 2.5 also includes DFT-predicted EAs for all other 1,7-$C_{60}(n$-$R_F)_2$ derivatives up to n-$R_F = n$-$C_{10}F_{21}$. The EA graph in Figure 2.5 demonstrates that the electron-withdrawing effect of primary R_F groups (including CF_3) increases approximately linearly from CF_3 to n-C_4F_9 and, thereafter, increases more slowly as it approaches what appears to be a constant value at n-$C_{10}F_{21}$ and beyond. The significance of this finding is not diminished by the relatively small increments in EA as the n-R_F chain becomes longer because the n-R_F groups are attached to a large substrate, and the orbital into which the extra electron is added (i.e., the LUMO of 1,7-$C_{60}(n$-$R_F)_2$) has large contributions from fullerene cage C atoms remote from the R_F groups. Furthermore, a difference in EA of 0.090 eV means that the equilibrium constant for

the gas-phase electron-transfer reaction $1,7\text{-}C_{60}(CF_3)_2^- + 1,7\text{-}C_{60}(R_F)_2 \rightleftharpoons 1,7\text{-}C_{60}(CF_3)_2 + 1,7\text{-}C_{60}(R_F)_2^-$ will be ca. 100 at 293 K. This is not an insignificant effect, albeit one which remains to be experimentally verified.

The third trend is that a primary R_F group appears to be more electron withdrawing than a secondary R_F group with the same number of C atoms. For $n\text{-}C_3F_7$ vs. $i\text{-}C_3F_7$, the difference is just barely statistically significant; for $n\text{-}C_4F_9$ vs. $s\text{-}C_4F_9$, the difference in EAs is 0.025 eV and the sum of the uncertainties is only 0.018 eV. These differences, which are mirrored by the DFT calculations, may be due to sterics as well as electronic effects. The X-ray crystal structures of $1,7\text{-}C_{60}(i\text{-}C_3F_7)_2$[23] and $1,7\text{-}C_{60}(n\text{-}C_3F_7)_2$[26] (discussed in Chapter 1) are known, but the two-fold C_{60} cage disorder precludes detailed comparisons of bond distances and angles. However, the DFT-optimized structures predict that the $C(sp3)\text{-}C(R_F)$ distances are 1.574/1.575 and 1.595/1.600 Å in the $n\text{-}C_3F_7$ and $i\text{-}C_3F_7$ structures, respectively; the corresponding distances are 1.575/1.576 and 1.599/1.599 Å for the $n\text{-}C_4F_9$ and $s\text{-}C_4F_9$ structures, respectively (and they are 1.575/1.576 Å for the DFT-optimized structure of $1,7\text{-}C_{60}(n\text{-}C_8F_{17})_2$). Furthermore, X-ray derived $C(sp3)\text{-}C(R_F)$ distances for ordered, precise structures of $C_{60}(R_F)$ compounds with para-$C_{60}(R_F)_2$ moieties also show that secondary R_F groups (i.e., $i\text{-}C_3F_7$)[23] form slightly longer bonds to the C_{60} cage (1.560(3)–1.590(3) Å; median 1.577(3) Å) than do primary R_F groups (i.e., C_2F_5; 1.540(3)– 1.554(4) Å; median 1.548(3) Å)).[20] For this type of PFA compound, therefore, at least one of the reasons that a secondary R_F group is a slightly weaker electron-withdrawing group than the corresponding primary R_F group is that the cage–R_F C–C distance is slightly longer for the secondary R_F group.

Experimental and computational $E_{1/2}$ values and comparisons to EAs for 1,7-$C_{60}(R_F)_2$ derivatives. The DFT-predicted $E_{1/2}$ values were determined by subtracting $\Delta\Delta G_{solv}$ for a given $1,7\text{-}C_{60}(R_F)_2/1,7\text{-}C_{60}(R_F)_2{}^-$ pair from the electron affinity of the neutral $1,7\text{-}C_{60}(R_F)_2$ derivative, where $\Delta\Delta G_{solv}$ is defined as $\Delta G_{solv}(1,7\text{-}C_{60}(R_F)_2) - \Delta G_{solv}(1,7\text{-}C_{60}(R_F)_2{}^-)$ and the dielectric medium used in calculating the ΔG_{solv} values is equivalent to that of oDCB (9.93 at 23 °C).

To make direct comparisons easier, the y-axes in Figure 2.1 and 2.5 for the EA, $E_{1/2}$ and $\Delta\Delta G_{solv}$ plots are the same size and cover the same range, 0.10 eV (0.00 to 0.10 eV) for the EA and $\Delta\Delta G_{solv}$ plots and 0.10 V (−0.05 to 0.05 V) for the $E_{1/2}$ plots. This is the first time that gas-phase EAs and $E_{1/2}$ values have been compared for the same series of homologous compounds for which (i) all of the EAs were determined with the same instrumentation in the same laboratory, (ii) all of the $E_{1/2}$ values were measured with the same equipment in the same laboratory and with the same batch of solvent, electrolyte and internal standard, (iii) the samples for EA and $E_{1/2}$ measurements were taken from the same purified batch of each compound, and (iv) the EA and $E_{1/2}$ values were measured with high precision and, just as importantly, with equal precision.

Both experimentally and computationally, it is absolutely clear that there is *no* correlation between the EAs and $E_{1/2}$ values for this set of compounds. The experimental $E_{1/2}$ values are the same for six of the seven compounds to within the experimental uncertainty (±10 mV), and the DFT-predicted $E_{1/2}$ values are the same to within ±5 mV (the experimental ''outlier'' is the s-C_4F_9 compound). The cause of this unexpected result is the fact that the changes in relative EAs and $\Delta\Delta G_{solv}$ values are equal both in sign and magnitude across the entire set of R_F groups that

were studied in this work (i.e., the slopes of the linear least-squares fits to the DFT-predicted EAs and $\Delta\Delta G_{solv}$ values in figure 2.1 are the same, so their differences are all essentially 0 V).

As discussed earlier, it is generally assumed that EAs and $E_{1/2}$ values measure ''the same property'' of a molecule (albeit in two different ways and in different phases) and should therefore be strongly correlated, especially for a homologous series of compounds. This has been shown to be true in a number of cases. For example, Ruoff et al. reported that a plot of adiabatic gas-phase EAs vs. $E_{1/2}$ for a series of 20 aromatic hydrocarbons has a linear correlation with a slope of 1.04.[97] Djurovich et al. reported that a plot of IPES-determined solid-state ''electron affinities'' for thin films of 20 organic semiconductors vs. $E_{1/2}$ has a linear correlation with a slope of 0.90.[98] Popov et al. reported that a plot of DFT-predicted gas-phase EAs vs. experimental $E_{1/2}$ for a series of 17 $C_{60}(CF_3)_n$ derivatives with even $n= 2– 12$ also has a roughly linear correlation, but with a slope of only 0.69.[2] It has been shown in this work that EAs and $E_{1/2}$ values do not always increase together; an EA vs. $E_{1/2}$ plot for the seven compounds studied in this work is essentially a horizontal line (i.e., the slope is ca. 0). Therefore, we have shown that it cannot be reliably assumed, a priori, that $E_{1/2}$ values can be used to predict EAs, even for a set of structurally nearly identical compounds. There is certainly not a simple one-to-one correspondence in every case. The slope of an EA vs. $E_{1/2}$ plot for a given set of compounds can vary from 0 (this work) to 0.69 (Popov et al.) to 0.90 (Djurovich et al.) to 1.04 (Ruoff et al.).

Computational E(LUMO) values and comparisons to EAs and $E_{1/2}$ values. The relative E(LUMO) values are also listed in Table 2.1 and are shown in Figures 2.1 and 2.5. There is only a weak correlation between the experimental or DFT-calculated EA values and the corresponding DFT-calculated E(LUMO).

First and foremost, changing the R_F substituent does have an effect on the E(LUMO) value of a 1,7-$C_{60}(R_F)_2$ compound. For the seven compounds shown in Figure 2.1, the LUMO has a progressively lower energy as R_F varies from CF_3 to C_2F_5 to i-C_3F_7 to n-C_3F_7 to s-C_4F_9 to n-C_4F_9 to n-C_8F_{17}. However, the difference in E(LUMO) for 1,7-$C_{60}(n$-$C_4F_9)_2$ and 1,7-$C_{60}(n$-$C_8F_{17})_2$ is only 2 meV. Consistent with the latter observation, the E(LUMO) values for the ten n-R_F compounds shown in Figure 2.5 become more negative from CF_3 to C_2F_5 to n-C_3F_7 to n-C_4F_9 but are virtually the same for compounds with n-C_4F_9 and longer n-R_F groups. Significantly, Figure 2.1 shows that there is no correlation between E(LUMO) and $E_{1/2}$.

For the seven compounds in Figure 2.1, the approximately linear rate of change in E(LUMO) is only one-third of the rate of change in EA. This dampening effect can be explained by the fact that E(LUMO) is calculated for the neutral molecule while the EA is the energy difference between the neutral molecule and the one-electron reduced anion. The EA includes the Coulomb repulsion between the extra electron and the electrons in the neutral molecule; the E(LUMO) does not. Significantly, therefore, as far as using calculated ΔE(LUMO) to predict ΔEA for an unknown set of structurally similar compounds is concerned, only the sign, but not necessarily the relative magnitude, of the two changes are commensurate. This should serve as a warning to scientists or engineers who would want to equate ΔE(LUMO) with ΔEA to explain differences in measured figures of merit for electrical, optical or magnetic materials and/ or devices.

2.1.5. Electrochemical Behavior of Selected PFAFs. Effect of Varying the Solvent on the $E_{1/2}$. It is well known that the $E_{1/2}$ is solvent dependent. [97,99] This fact can be explained by the simple relationship $E_{1/2} \cong EA - \Delta\Delta G_{sol} + E_{ref}$.[97] The quantity $\Delta\Delta G_{sol}$ is dependent on the solvent/

supporting electrolyte of the solution while the EA is an inherent characteristic of the molecule. Therefore by changing the solvent and thus the solvation energy, the $E_{1/2}$ will also change.

One of the main factors that affect the solvation energy is the dielectric constant of the solvent. In order to determine what effect the dielectric constant of the solvent has on the measured $E_{1/2}$ value of seven 1,7-$C_{60}(R_F)_2$ compounds with R_F = CF_3, C_2F_5, n-C_3F_7, i-C_3F_7, n-C_4F_9, s-C_4F_9 and n-C_8F_{17}, each compound was measured in two structurally similar solvents with very different dielectric constants. The two solvents chosen were oDCB and benzonitrile. Both solvents have an aromatic ring, however the dielectric constant of oDCB is 9.93 while the dielectric constant of benzonitrile is 26.0. The relative $E_{1/2}$ values are shown in Table 2.2. On average, the first reduction potential of every 1,7-$C_{60}(R_F)_2$ fullerene examined is 20 mV easier to reduce in benzonitrile than in oDCB with the experimental outlier being 1,7-$C_{60}(n$-$C_4F_8)_2$. The difference between the measured reduction potentials is just outside the error of the measurement of ±10 mV. Since the gas-phase EA of the molecule does not change no matter what solvent it is in, it must be that the $\Delta\Delta G_{sol}$ energy of each molecule is likely smaller in benzonitrile than it is in oDCB. It is probable that due to the more polar nature, benzonitrile acts as a better solvent to the monoanion than the less polar oDCB. This effect would manifest as a lower reduction potential. The fact that the differences in reduction potentials of the same molecule in different solvents are so small is not unexpected. It has been reported that in general fullerenes have very small $\Delta\Delta G_{sol}$ values due to the large volume of the molecule that can effectively diffuse the charge over a large area.[97] When the charge is spread over such a large area, the solvent contributions, such as solvent reorganization, are minimized. When the $E_{1/2}$ is determined in CH_2Cl_2 that has a dielectric constant of 9.80 that is similar to oDCB (9.93), there are no differences between the measured $E_{1/2}$ values that are greater than the uncertainty of the measurement. Again, this result

is not unexpected as the difference in the $\Delta\Delta G_{sol}$ values for each compound in these two solvents should be, and are, small.

Electrochemical Behavior of Perfluoroalkyl and Perfluorobenzyl Fullerenes with an H Atom on the Cage. Both $1,7\text{-}C_{60}(C_2F_5)_2$ and $1,7\text{-}C_{60}(n\text{-}C_4F_9)_2$ exhibited 4 quasi-reversible 1-electron reductions in oDCB and DCM. However, when one R_F group is replaced with a hydrogen atom resulting in $1,7\text{-}C_{60}(C_2F_5)H$ and $1,7\text{-}C_{60}(n\text{-}C_4F_9)H$, the reduction becomes irreversible even when high scan rates such as 10 V/sec are used. The voltammograms are shown in Figure 2.6. This irreversible electrochemistry is observed not only in oDCB but also in CH_2Cl_2 and benzonitrile. The exact reasons as to why these two compounds exhibit irreversible 1-electron reductions is unclear at this point; however, it has been shown that the fullerene–H bond dissociation energy is relatively low and that PFAFs with a hydrogen atom attached to the cage can be gas-phase superacids.[25] In addition, $1,7\text{-}C_{60}(CF_2C_6F_5)H$ undergoes annulation after reduction (the annulated product is shown in Figure 2.8). The annulated product, $C_{60}(CF_2C_6F_4)$, exhibits reversible redox properties with the $E_{1/2}{}^{0/-} = -10$ mV vs. $C_{60}{}^{0/-}$. The voltammograms of both $1,7\text{-}C_{60}(CF_2C_6F_5)H$ and $C_{60}(CF_2C_6F_5)$ are shown in Figure 2.7. Interestingly, the two voltammograms look almost identical. This is due to the fact that upon reduction, the $1,7\text{-}C_{60}(CF_2C_6F_5)H$ is converted into $C_{60}(CF_2C_6F_4)$ and 2 equivalents of F^- and H_2 according to the balanced equation:

$$2\ C_{60}(CF_2C_6F_5)H + 2\ e^- \longrightarrow 2\ C_{60}(CF_2C_6F_5) + 2\ F^- + H_2$$
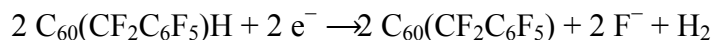
Coincidentally, the observed $E_{1/2}$ of the annulated product and the onset of reduction of the precursor are identical within the error of the measurement. This hypothesis that the hydrogen atom from $1,7\text{-}C_{60}(CF_2C_6F_5)H$ is removed upon reduction was substantiated by the

graduate student Long San, who also synthesized these compounds as part of his graduate research. To a solution of $1,7\text{-}C_{60}(CF_2C_6F_5)H$, he added 1 eq. of the chemical reductant $Co(C_6H_6)_2$ and observed the annulated product by ^{19}F NMR spectroscopy as a single product, with quantitative yield.

Effect of the Addition Patterns of Various PFAFs (other than TMFs). A previous electrochemical study conducted by the Strauss group indicated that for a given substituent type, (i.e., $R_F = CF_3$) the addition pattern is as important, if not more important than the number of addends or the addend type in determining the redox properties of the molecule.[2]

There are three main factors that affect the reduction potential (1) the number of addends, (2) the type of addends, and (3) the addition pattern of the addends and how they affect the position of the remaining double bonds on the cage. As the number of addends increases, the π system on the cage gets broken up and localized, typically making the reduction potential more negative. However, this effect can be offset if the addends are electron withdrawing such as R_F groups. The electron withdrawing nature of the R_F groups results in partial removal of electron density from the cage in effect making the reduction potential more positive. The third effect is the addition pattern of the addends and is just as important if not more important in determining the reduction potential. How the addition pattern affects the reduction potential can be explained by examining how the positions of the addends affect the remaining double bonds on the cage. Bare cage C_{60} does not have any double bonds in pentagons. When double bonds are forced to reside in pentagons by the addition of substituents, it results in destabilizing the cage by 35 kJ/mol.[100] It was shown in 2007 that the LUMO is anchored to non-terminal double bonds in pentagons (i.e., a double bond in a pentagon that has two neighboring sp^2 carbon atoms).[2] Popov

et. al. demonstrated that the presence and position of these non-terminal double bonds in pentagons lower the LUMO energy level, in effect making the molecule a stronger electron acceptor. The hypothesis from these observations is that the reduction of a fullerene molecule when the LUMO is localized on a non-terminal double bond in a pentagon will increase the electron density of that bond that will cause it to lengthen and thus making it closer to the length of a single C-C bond negating some of the destabilizing effect. This results in a lowering of the E(LUMO) and is manifested in a more positive $E_{1/2}$ value.

It was described in section 2.1.3 that in a series of 1,7-$C_{60}(R_F)_2$ derivatives changing the branching pattern and length of the perfluoroalkyl chain results in no measurable difference in the solution phase $E_{1/2}$ values. The conclusions that were drawn in that section were contingent on the series of fullerene$(R_F)_2$ compounds having the same addition pattern (and the same number of addends) so that the nature of the addend could be examined. In the case of $C_{60}(R_F)_2$ derivatives, only *para* addition has been observed; however, when the R_F groups are replaced with $CF_2C_6F_5$ two different isomers are observed.[101] Structural characterization including ^{19}F NMR spectroscopy, APCI-MS, and UV-vis spectroscopy indicated that the likely structures of the two isomers are 1,7-$C_{60}(CF_2C_6F_5)_2$ (*para* addition) and 1,9-$C_{60}(CF_2C_6F_5)_2$ (*ortho* addition). Both of these compounds exhibited quasi-reversible 1-electron reductions in *o*DCB, shown in figure 2.9, with $E_{1/2}$ values of 0.10 V for 1,7-$C_{60}(CF_2C_6F_5)_2$ and 0.00 V for 1,9-$C_{60}(CF_2C_6F_5)_2$ (both $E_{1/2}$ values are versus $C_{60}^{0/-}$). The experimental $E_{1/2}$ value of 1,7-$C_{60}(CF_2C_6F_5)_2$ is on average 40 mV harder to reduce than the series of 7 structurally homologous 1,7-$C_{60}(R_F)_2$ that were discussed above. This difference in the first reduction potential is presumably due to the lower electron withdrawing strength of $CF_2C_6F_5$ compared to the R_F groups.[80] When comparing the $E_{1/2}$ values of the two $C_{60}(CF_2C_6F_5)_2$ isomers, the *para* substituted isomer is 100 mV easier to

reduce than the *ortho* substituted isomer. In fact, the *ortho* substituted isomer has the same $E_{1/2}$ within the error of the measurement as the bare cage C_{60}. The hypothesis outlined above can be used to explain the difference in reduction potentials between the two isomers of $C_{60}(CF_2C_6F_5)_2$. When the two substituents add to the cage *ortho* to one another, a single double bond is removed from the cage. This minor change only slightly affects the delocalized π system. This disturbance makes the reduction potential more negative. However, this is offset by the slight electron withdrawing nature of the Bn_F groups. These two competing factors cancel each other out resulting in a reduction potential identical to bare cage C_{60}. However, substituents adding *para* to one another results in a non-terminal double bond in a pentagon. By applying the hypothesis outlined above it can be explained that the presence of this non-terminal double bond in a pentagon results in making the reduction potential more positive.

A collaborator, Dr. Natalia Shustova, prepared and structurally characterized several new $C_{60}(i\text{-}C_3F_7)_n$ derivatives where $n = 2$, 4 and 6.[23] Due to the steric bulk of the $i\text{-}C_3F_7$ groups, new addition patterns were observed. The structural characterization revealed that the two new $C_{60}(i\text{-}C_3F_7)_4$ compounds had an addition pattern that created 2 non-terminal double bonds in pentagons and the two new $C_{60}(i\text{-}C_3F_7)_6$ compounds had 3 non-terminal double bonds in pentagons. The Schlegel diagrams of the new compounds are shown in Figure 2.10. As measured in this work and partially by collaborator Dr. Popov in Dresden, all 4 new $C_{60}(i\text{-}C_3F_7)_n$ derivatives exhibited three reversible 1-electron reductions in *o*DCB. In accordance with the earlier hypothesis made about non-terminal double bonds in pentagons, the experimental $E_{1/2}$ values for both of the $C_{60}(i\text{-}C_3F_7)_4$ compounds were more positive than the $E_{1/2}$ value for *pmp*-$C_{60}(CF_3)_4$ that only has 1 non-terminal double bond in a pentagon. However, the $E_{1/2}$ values for both of the $C_{60}(i\text{-}C_3F_7)_6$ compounds were less positive than for an isomer of $C_{60}(CF_3)_6$ (60-6-1 also shown in Figure 2.10)

that has two *conjugated* non-terminal double bonds in a pentagon. Therefore, it appears that it is not only the presence of non-terminal double bonds in a pentagon, and their number in the molecule, but also the relative position of these bonds that dictates the reduction potential.

This hypothesis was substantiated by DFT calculated E(LUMO) values, performed by Dr. Alex Popov, on each of the structurally characterized fullerene(i-C$_3$F$_7$) isomers. A good correlation between the number and arrangement of non-terminal double bonds in pentagons was found. In addition, there was a good correlation between the calculated ΔE(LUMO) values and the $\Delta E_{1/2}$ values as can be seen in Figure 2.11. The good correlation between the DFT-calculated LUMO energies and $E_{1/2}$ potentials also provides further validation of the theoretical calculations and allows tentative predictions of reduction potentials for new fullerene addition patterns.

2.2. Crystal Packing Trends of Perfluoroalkyl Fullerenes

2.2.1. Introduction. There has been a lot of recent interest in establishing a link between the crystal packing structures of various fullerene derivatives and their performance in organic photovoltaic (OPV) devices. For example, Hummelen et. al. proposed that the efficiency of Phenyl-C$_{61}$-Butyric acid methylester (PCBM) based OPVs could be linked to the solvent used to fabricate the active layer.[67] This conclusion was partly based on the solvent-dependent crystal packing of PCBM where it was found that a three-dimensional network of short C$\cdots$C contacts between fullerene cages results when crystals are grown from chlorobenzene whereas a two-dimentional network forms when crystals are grown from oDCB. This analysis comported well with the observation that devices fabricated with chlorobenzene out-performed others made from

oDCB. This observation has since been expounded on by several groups that have ultimately ended at the same hypothesis that a higher fullerene density, and a greater number of short C⋯C contacts between fullerene cages, should facilitate electron transfer between fullerene molecules.[46,69,102-104] Rubin et al. described a large class of penta-substituted C_{60} fullerenes that pack in motifs that are solvent independent and described them as "self assembling" to form advantageous domains within the active layer of OPV devices.[46,68] One major drawback to the compounds described by Rubin et. al. was that the substituents were all very bulky which necessarily increased the C⋯C contacts between the fullerene cages that would disfavor the free charge carrier mobility.

The class of *spp*-$C_{60}(CF_3)_4(Ar)(OH)$ fullerenes (see Chapter 1) presented in this section are uniquely situated to shed light on the link between the extended solid state packing structures and the mobility of charge carriers in OPV active layers because of the small size of the CF_3 groups that allow for close packing and the Ar group that, through π-π interactions between the Ar group and the fullerene cage of the adjacent molecule, could facilitate molecular self assembly.

2.2.2. General Remarks. The crystal packing of compounds 2, 4, 5, 9, and 60-4-2 fit into one of two categories: stacked or dimeric (see Scheme 1.2.1 for molecular structures). The stacking motif is made up of individual molecules that form columns. Within each column, the fundamental relationship from one molecule to another can be defined by the angle Θ (°) between three fullerene centroids and the distance, in Å, from one fullerene centroid to its neighbor (S_D) as shown in Figure 2.13. The next level of packing complexity, the intercolumn distance is defined by the centroid to centroid distance between adjacent molecules in columns

that run in both a parallel (I_{Dp}) and anti-parallel (I_{Dap}) fashion also shown in Figure 2.13. This nomenclature has been used previously in the literature[46] and is sufficient to describe the relationship of molecules within each column as well as the relationship from column to column; it does not describe the relative orientations of the molecules to one another. This will be addressed in more detail as the individual crystal structures are discussed. The dimeric motif is composed of fullerene molecules that pair up into dimers where the centroid to centroid distance will be defined as D_D. At the next level of packing complexity, the dimers form layers also shown in Figure 2.13. As with the stacking parameters, the dimeric parameters do not describe the orientation of one molecule to its neighbor but will be discussed in a case-by-case basis.

In addition to these parameters, the fullerene density ρ_f ($\times 10^{-4}$ Å^{-3}) was calculated to describe the density of fullerenes within the crystal. This density has also been used in the literature to give an indication of the density of fullerene-to-fullerene π-π contacts within the crystal.[46] In the context of bulk heterojunction organic photovoltaics, a high ρ_F in the solid state should increase the electron mobility in the active layer resulting in devices with higher power conversion efficiencies.[46,105] The fullerene density was calculated by counting the number of fullerene cage carbon atoms contained in the unit cell then dividing by 60 carbon atoms /cage (in the case of C_{60}) to determine the number of fullerene cages per unit cell. This number of fullerene cages per unit cell was then divided by the volume of the unit cell to give the number of fullerenes per unit area or ρ_f.

2.2.3. Stacked Systems. This packing motif has generally been observed in pentasubstituted fullerenes with an *spp* addition pattern but has also been observed in a substituted azafullerene.[46,47,104,106,107] Both 60-4-2 and compound 9 pack in a stacked motif.

Furthermore, both systems display a column angle Θ of 180° or so called straight stacks. Although the crystals grown in this work were only grown from a single solvent, studies have been conducted that confirm that systems that display straight stacking tend not to pack in any other way, that is, the packing is solvent independent.[46] This observation that packing can be solvent independent may help control the nanoscale morphology of the active layers by self-assembly into nano-crystallites. Notably, amongst all the reported fullerene deriviatives that form the stacked motif, 60-4-2 has the shortest S_D distance of 10.141 Å and the highest fullerene density of 9.9×10^{-4} Å^{-3} (ρ_F) that is on average about twice that of other substituted fullerenes that pack in the same manner. Close interstack distances (I_D) between the fullerene centroids of 12.029 Å also comports with the high ρ_F. It is presumably due to the small size of the CF$_3$ groups on the cage, compared to the large penta-arylated fullerenes that typically display a stacking motif, that allow for such a high fullerene density and short S_D. Typically, as observed by Rubin *et al*., the straight stacked packing motif is strongly dependent on the presence of large substituents that create a deep socket for the neighboring fullerene cage to fit into.[46]

As previously mentioned compound 9 also displays a straight-stacking motif; however, it does not display the typical shuttle-cock type stacking where the bare side of the cage fits into the socket of an adjacent molecule.[47] Compound 9 forms straight stacks as shown in Figure 2.14 with the C$_6$F$_5$ aryl ring forming a π-π interaction (3.320 Å long) with the adjacent cage. This appears to be an important force because in 50% of the molecules, the C$_6$F$_5$ ring is rigorously coplanar with the BO$_2$C$_2$ heterocycle but in the other 50% the C$_6$F$_5$ ring is twisted by 42° so that it is parallel to the adjacent cage as shown in Figure 2.14. Both confirmations of the molecule display S_D distances of 12.221 Å.

2.2.4. Dimeric Systems. Compounds **2**, **4**, and **5** all pack in a dimeric motif where each molecule pairs up into dimers with the CF_3 groups pointing at each other as shown in Figure 2.13. The centroid-to-centroid distances (D_D) for compounds **2**, **4**, and **5** are 11.8, 12.085, and 12.006 Å respectively. These distances correlate to the bulkiness at the para-position on the aryl ring; as the bulkiness at the para position increases from H to F to a methyl group the D_D distance increases. The dimers form layers as shown in Figure 2.15 at the next level of packing complexity. These layers form 2D networks of close cage-cage contacts (close contacts defined as centroid to centroid distances of <10.5 Å) that could lead to improved free charge carrier motilities in the material.[46] As was seen in **60-4-2** and **9** that exhibit the straight stacking motif, compounds **2**, **4**, and **5** have ρ_F of 10.11, 8.82, and 9.16 $\times 10^{-4}$ Å^{-3} respectively that are almost twice the average ρ_F of many other derivatized fullerenes that pack in the same manner.

In summary, examining the crystal packing of compounds **60-4-2**, **2**, **4**, **5**, and **9** reveals that, presumably due to the small size of the CF_3 addends, these compounds exhibit very high fullerene densities in the crystalline state that are on average twice that of compounds that pack in the same manner. These high fullerene densities as well as networks of close contacts between adjacent cages in the crystal have been hypothesized to facilitate electron transfer through the dense fullerene network that ultimately may be correlated with increased efficiencies of OPV devices.[46,67,104] Future work on these compounds should include confirming that they exhibit the same packing motifs independent of the crystallization solvent as well as measuring the photo carrier dynamics of these compounds blended with a conjugated polymer.

2.3. Thermal Studies of Perfluoroalkylfullerenes and a Perfluoroalkylfullerene Epoxide

2.3.1. The Thermal Stability of $C_{60}(CF_3)_n$ where n= 2, 4, and 10. TMFs that had 2, 4, and 10 CF_3 groups were chosen in order to determine if the number of CF_3 groups on C_{60} affects the thermal stability of the molecule. Additionally, two different isomers of $C_{60}(CF_3)_{10}$ (60-10-2 and 60-10-3) were studied to determine if the addition pattern of CF_3 groups significantly affected the thermal stability of the molecules. Experiments were designed to determine at what temperature each one of the above mentioned TMFs could be heated to for 5 min before the composition began to change. Each experiment was conducted in a sealed and evacuated glass ampoule that was continually heated in a tube furnace and monitored by an external thermocouple. Visual inspection of each one of the ampoules once they had reached the set temperature of the furnace indicated that in every experiment all the material was in the gas phase as evidenced by a yellow vapor throughout the ampoule. After 5 min the ampoules were removed from the furnace and allowed to cool to room temperature. The residue inside the ampoules was then fully dissolved in 100% toluene and analyzed by HPLC chromatography. To rule out the possibility of a misinterpretation of the HPLC chromatograms due to TMFs co-eluting, the ^{19}F NMR spectrum of the crude material obtained after thermal treatment was recorded as well. By comparing the HPLC chromatogram as well as the ^{19}F NMR spectrum of the crude products after heating to the starting material, it was possible to determine at what temperature each TMF underwent decomposition. The compositions of 60-10-3, 60-10-2 and 60-4-1 began to change at temperatures above 300, 300, and 350 °C respectively while 60-2-1 was

stable to a temperature of 405 °C. Even after treatment at 450 °C for 5 min, 78% of the 60-2-1 remains intact while 20% was converted into bare cage C_{60}.

These results indicate an inverse relationship between the number of CF_3 groups on the cage and the temperature to which they are stable. What's more, that since the two isomers of $C_{60}(CF_3)_{10}$ were stable to the same temperature, it appears that the addition pattern of CF_3 groups does not affect the thermal stability as significantly as the number of CF_3 groups does. Overall, these results suggests that each one of the TMFs examined in this work, and likely many other TMFs that were not examined, are thermally stable in the context of many practical applications and synthetic procedures where temperatures do not exceed 300 °C for more than 5 min.

However, what happens when the TMFs are heated to the temperature where they begin to decompose for periods of time longer than 5 min? To answer this question, two additional experiments were carried out with longer heating times at the temperature that 60-2-1 begins to lose CF_3 groups. Two identical sealed and evacuated glass ampoules containing samples of 60-2-1 were heated to 405 °C. One ampoule was heated for 15 min while the other was heated for 24 hours. The HPLC chromatograms from these two experiments are shown in Figure 2.15. The results reveal the drastic effect of time of heating; there was no observable decomposition or loss of CF_3 groups to the sample heated for 15 min while the sample that was heated for 24 hours underwent significant (63%) decomposition to C_{60}. This indicates that at 405 °C, 60-2-1 slowly loses CF_3 groups. This loss of CF_3 groups occurs at a slow enough rate that after 15 min, there is no observable change in the HPLC chromatogram of the heated 60-2-1 sample vs. the non-heated starting material.

2.3.2. Possible Decomposition Pathways of 60-10-3. A set of 4 separate experiments was conducted where identical samples of 60-10-3 were heated in sealed glass ampoules at 300, 400, 450, and 500 °C for 5 min each. As was discussed before, visual inspection of each one of the ampoules after they had reached the set temperature of the furnace (i.e., 300, 400, 450, and 500 °C) confirmed that in each case all the material was in the gas phase as evidenced by a yellow vapor filling the entire ampoule. After 5 min the ampoules were removed from the furnace and placed on the lab bench where they were allowed to cool to room temperature. The solid material inside the ampoules was then fully dissolved in 100% toluene and analyzed by HPLC chromatography. The resulting HPLC chromatograms of the crude material after heating are shown in Figure 2.16 In addition to HPLC analysis, the main components of the crude material were isolated and subsequently analyzed by APCI-MS and ^{19}F NMR spectroscopy that allowed for identification of the main products in the crude product mixture.

As stated above, 60-10-3 did not undergo any compositional changes when heated to 300 °C for 5 min as evidenced by there being no change in the HPLC chromatogram of the resulting material from the starting material or there being any change in the ^{19}F NMR spectrum of the material after heating when compared to the ^{19}F NMR spectrum of the starting material. However, as the temperature is increased from 300 to 400 °C, 60-10-3 disproportionation begins to occur. Analysis of the HPLC chromatogram in conjunction with APCI-MS data on each one of the main fractions indicates that both the loss *and* addition of CF$_3$ groups occurs after 5 min at 400 °C. The crude product mixture is primarily composed of 60-10-3 starting material and $C_{60}(CF_3)_n$ where n = 12, 10, and 8. When the temperature is increased further to 450 °C for 5 min, the composition of the products becomes primarily $C_{60}(CF_3)_2$ along with some bare cage C_{60} and small amounts of $C_{60}(CF_3)_{n>2}$. When 60-10-3 is heated to 500 °C for 5 min the

151

composition of the products becomes primarily C_{60} with some $C_{60}(CF_3)_2$. The HPLC chromatograms of these experiments are shown in Figure 2.16.

The presence of $C_{60}(CF_3)_{12}$ in the experiment where 60-10-3 was heated to 400 °C for 5 min necessarily means that CF_3 groups are being added to the cage during this thermal treatment. Importantly, the only source of the CF_3 groups is other TMFs. There are two likely pathways for the addition of these CF_3 groups to 60-10-3: (1) homolytic cleavage of the CF_3-to-cage bond leaving a $CF_3\cdot$ and a TMF radical with an odd number of CF_3 groups, followed by subsequent CF_3 radical attack on another TMF molecule, and (2) intermolecular transfer of a CF_3 group from one TMF to another that results in two TMF radicals. The experimental evidence in this work, as well as that in the literature does not support one of these hypothesis over the other. However, several theoretical calculations have concluded that the intermolecular transfer of a CF_3 group must be accompanied by an inversion when transferred from one TMF to another.[63] The activation energy for this transfer was calculated to be greater than 210 kJ/mol even in the most favorable conditions where the products were 1,7-$C_{60}(CF_3)_2$ and bare cage C_{60}. The authors went on to state that this activation energy barrier was essentially equivalent to sequential detachment and reattachment of a CF_3 group. Therefore, there is no energetic advantage to either mechanism based on the theoretical calculations.

In addition to TMFs with 12 CF_3 groups, there were also several isomers with 10 CF_3 groups bound to the cage besides the starting material 60-10-3 that also had 10 CF_3 groups. The experimental evidence in this work is corroborated by experimental evidence from several other papers where TMFs were heated to similar temperatures.[64,65,108] There are 3 likely hypotheses as to how this isomerism occurs. First, unimolecular isomerism or rearrangement of one isomer of $C_{60}(CF_3)_{10}$ into another could occur. An alternative hypothesis is that a TMF with 10 CF_3 groups

undergoes the loss of one or several CF_3 groups followed by the addition of the same number of CF_3 groups that was previously lost at another location on the cage. Finally, similar to the latter hypothesis only with the opposite order of steps, a TMF with 10 CF_3 groups undergoes the addition of one or more groups and then the subsequent loss of different CF_3 groups resulting in a different isomer of $C_{60}(CF_3)_{10}$. Theoretical calculations have been done on the energetics of unimolecular CF_3 migration and determined that only 1,2 shifts of CF_3 groups were more energetically favorable to complete bond dissociation followed by reattachment at a different site.[63] It is only when the product of the 1,2 CF_3 shift results in an isomer that is roughly 200 kJ/mol more stable than the starting isomer is the activation barrier low. However, this mechanism cannot be applicable to the observations made in this work because the starting material has been calculated to be one of the more stable isomers of $C_{60}(CF_3)_{10}$. Moreover, in this study, each of the main products after the thermal treatment was structurally characterized and in no case were the addition patterns of the other isomers with 10 CF_3 groups accessible by 1,2 shifts of CF_3 groups from the addition pattern of the starting material. Therefore, it seems unlikely that unimolecular migration of CF_3 groups can account for the experimentally observed isomers of $C_{60}(CF_3)_{10}$ but based on experimental evidence it cannot be ruled out as a possible mechanism.

As was discussed above, based upon mass spectrometric data of the products, it is certain that CF_3 groups are both being added to and lost from cages. By applying the systematic method of addition/removal of CF_3 groups and vise versa it is possible to account for all of the isomers that were experimentally observed and shown in Figure 2.17 For example, starting out with 60-10-3 it is possible to arrive at 60-10-2 by simply removing 2 CF_3 groups yielding 60-8-1 followed by the subsequent addition of two $CF_3 \cdot$ to form 60-10-2. Likewise, the two main

153

isomers of $C_{60}(CF_3)_8$ can be attained from 60-10-3 by going through the stable intermediates 60-8-1 and 60-6-1 that are experimentally known to be in the reaction mixture.

2.3.3 Thermal stability of the TMF Epoxide $C_{60}(CF_3)_4O$. The thermal stability of the TMF epoxide p^3-$C_{60}(CF_3)O$ (60-4-2[O]) was examined to determine if the epoxide can be removed by thermal treatment. Prior to heating, the starting material was prepared by adding a small amount of 60-4-1 to 60-4-2[O] to serve as an internal standard for ^{19}F NMR spectroscopy. This addition of 60-4-1 was an ideal internal standard for ^{19}F NMR spectroscopy for several reasons. First, as discussed above, 60-4-1 is thermally stable to at least 50 °C higher than the experimental temperature used. This means that the signal from 60-4-1 will be the same before and after heating. Second, the ^{19}F NMR signal from 60-4-1 has a chemical shift of $-\delta$ 68.5 which is close to, but not overlapping the signal arising from 60-4-2[O]. By adding the internal standard prior to heating, the ^{19}F NMR spectrum of the starting material could be recorded and directly compared to the spectrum of the material after heating.

This mixture of 60-4-2[O] with a small amount of the thermally stable internal standard 60-4-1 was heated to 300 °C for 30 min in a sealed and evacuated glass ampoule as previously described. By comparing the ^{19}F NMR spectrum of the material prior to heating to the spectrum after heating it was determined that the integrated intensity of the signal arising from 60-4-2[O] decreased by 55% relative to the internal standard. A new signal with a chemical shift of $-\delta$ 70.5 appeared with an integrated intensity 45% of the original 60-4-2[O]. This new signal exactly matched the ^{19}F NMR spectrum of the compound p^3-$C_{60}(CF_3)_4$ (60-4-2) which is simply the starting material 60-4-2[O] without the epoxide. Moreover, in the spectrum after heating, the sum of the integrals from both the 60-4-2 and 60-4-2[O] equals the integrated intensity of the 60-

4-2[O] signal in the starting material. It is clear from this experiment that after heating 60-4-2[O] for 30 min to 300 °C in a sealed and evacuated glass ampoule that 45% of the starting material undergoes de-epoxidation to form 60-4-2 as shown in figure 2.18. As further proof that this reaction is simply the removal of the epoxide from 60-4-2[O], when the products of the thermal heating experiment that was conducted at 300 °C for 30 min are sealed in an ampoule containing 0.20 atmospheres of O_2 gas and heated to 120 °C for 1 hour, the starting material of 60-4-2[O] with the internal standard is fully recovered. Moreover, the integral of the signal that arises from the 60-4-2[O] relative to the internal standard is the same as it was in the ^{19}F NMR spectrum of the starting material prior to heating.

Conclusions

The results in this chapter conclusively show that a series of seven 1,7-$C_{60}(R_F)_2$ compounds have statistically different electron affinities (EA), at the ±10 meV level of uncertainty, but virtually identical first reduction potentials, at the ±10 mV level of uncertainty. The lack of a correlation between EA and $E_{1/2}$, and between E(LUMO) and $E_{1/2}$, for such similar compounds is unprecedented and suggests that explanations for differences in figures of merit for materials and/or devices that are based on equating easily measurable $E_{1/2}$ values with EAs or E(LUMO) values should be viewed with caution, especially when the range of values of these parameters are small.

The experimental evidence from the study of the thermal stabilities of selected TMFs indicate that TMFs are thermally stable. In many cases, TMFs are thermally stable to

temperatures that exceed 300 °C for an extended period of time. It was also convincingly shown that the greater the extent of CF_3 addition to C_{60}, the lower the thermal stability with $C_{60}(CF_3)_2$ exhibiting the highest thermal stability of all the TMFs studied in this work. This study also shed some light on the possible decomposition pathway of the TMF 60-10-3 and gave irrefutable experimental evidence of both the removal and transfer of CF_3 groups between different molecules at elevated temperatures.

Lastly, the crystal packing of 5 different fullerene derivatives synthesized and characterized structurally in this work was examined revealing that some of the highest reported fullerene densities and shortest $C \cdots C$ contacts between fullerene cages reported to date. These results comport well with the literature that suggests that the small size of the CF_3 groups allows them to pack efficiently and form multi-dimentional networks of close $C \cdots C$ contacts between fullerene cages. These findings argue for further studies of the transport properties of these and related compounds and their applications in optoelectronics.
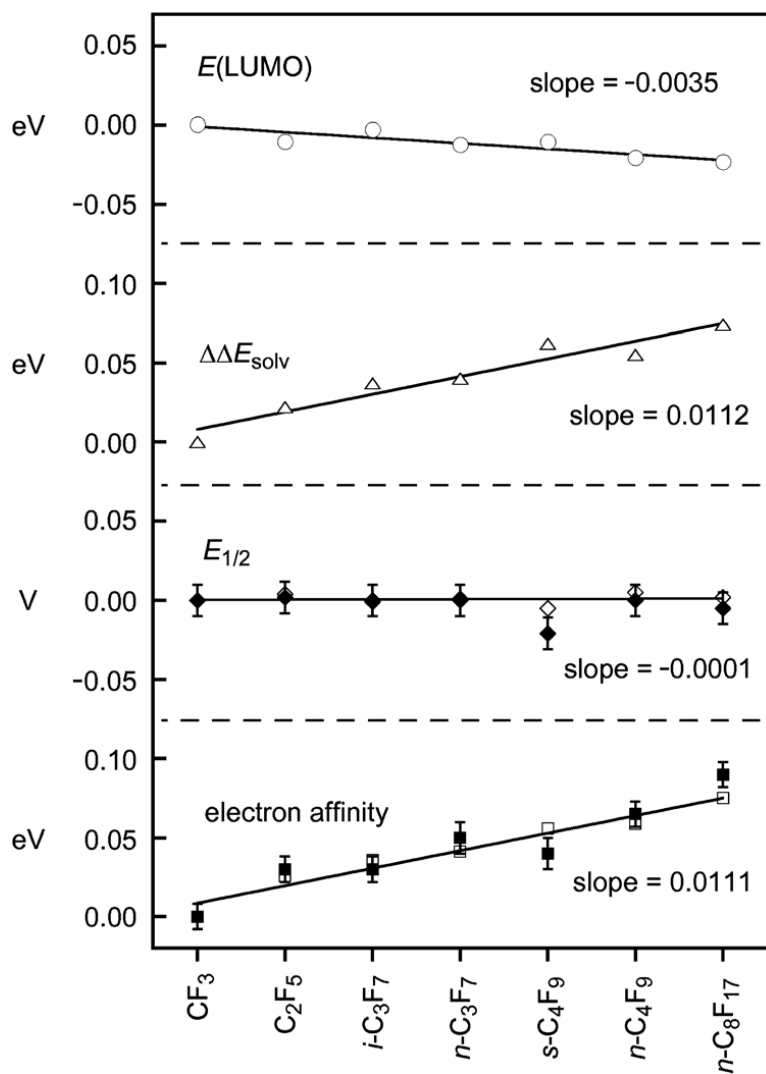
Figure 2.1. Plots of the data listed in Table 2.1 for 1,7-$C_{60}(R_F)_2$ compounds. The solid data points are experimental values (uncertainties shown as error bars); the hollow data points are DFT-predicted values. The lines are linear least-squares fits to the DFT-predicted results. Note that each plot has a y-axis interval of 0.10 eV or V, either from 0.00 to 0.10 or from "0.05 to 0.05. The slopes were derived by assigning each R_F group an x- axis value of successive integers as follows: $CF_3 = 1$, $C_2F_4 = 2$, etc.
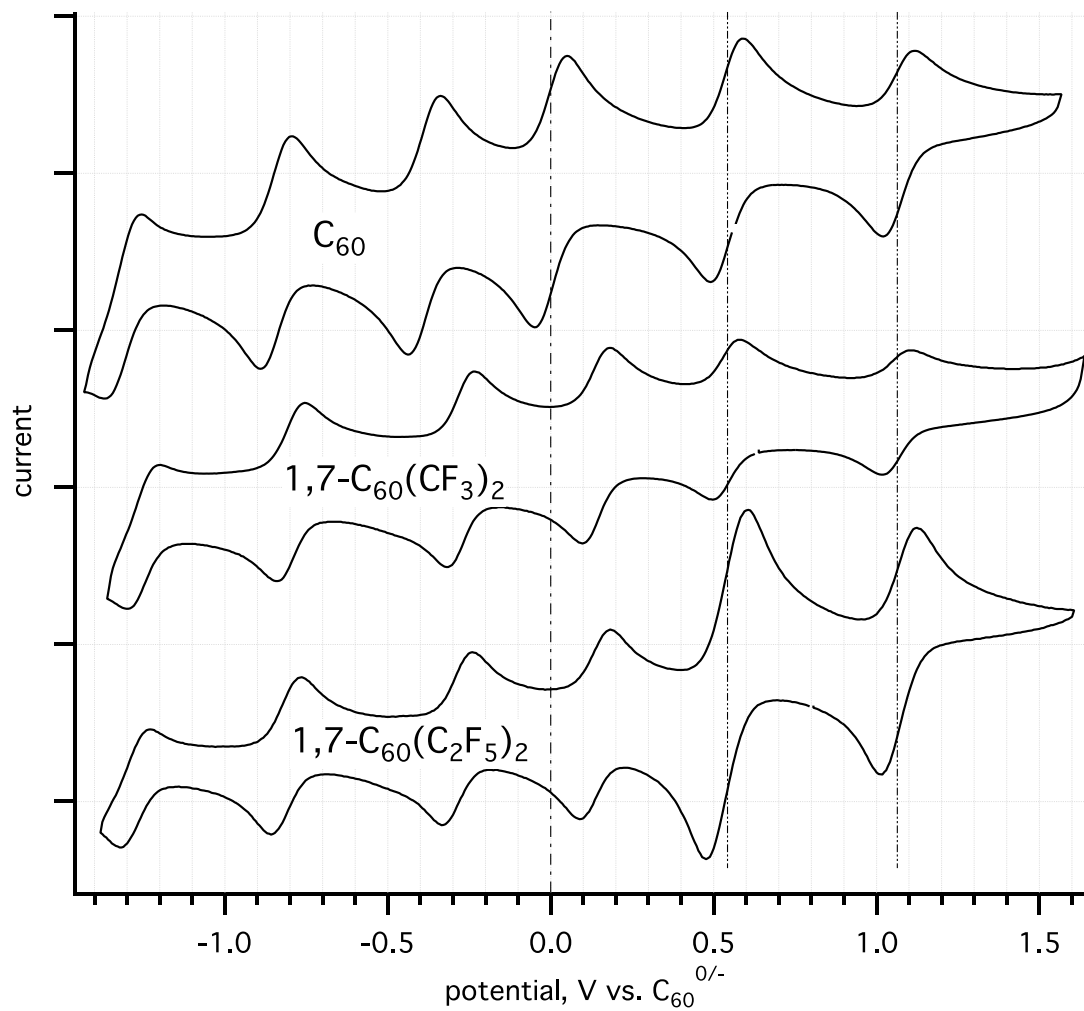
Figure 2.2. Cyclic voltammograms recorded in oDCB at a scan rate of 100 mV/sec. The supporting electrolyte used was TBABF$_4$. Both FcH and FcMe were used as internal standards, their $E_{1/2}$ values are indicated with the far left vertical dashed line and the second to the left dashed vertical line respectively. The potential has been referenced to $C_{60}^{0/-}$.
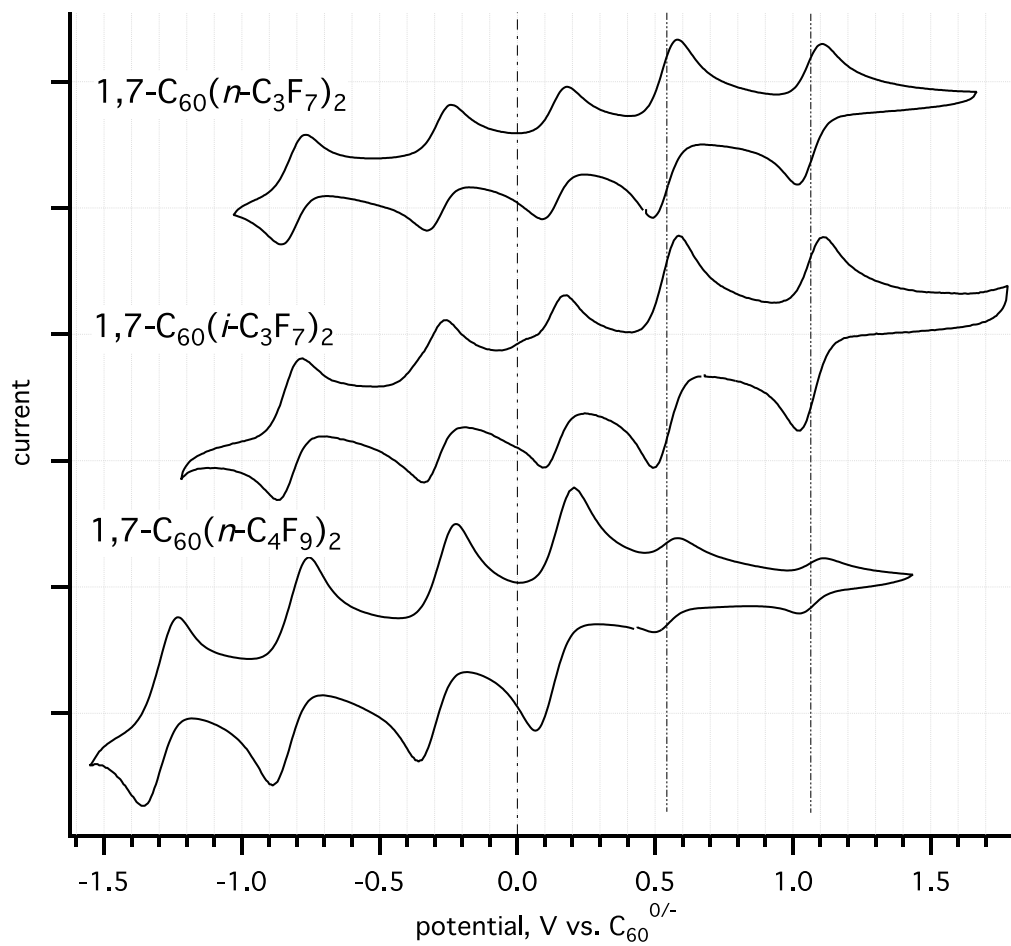
Figure 2.3. Cyclic voltammograms recorded in oDCB at a scan rate of 100 mV/sec. The supporting electrolyte used was TBABF$_4$. Both FcH and FcMe were used as internal standards, their $E_{1/2}$ values are indicated with the far left vertical dashed line and the second to the left dashed vertical line respectively. The potential has been referenced to C$_{60}$$^{0/-}$.
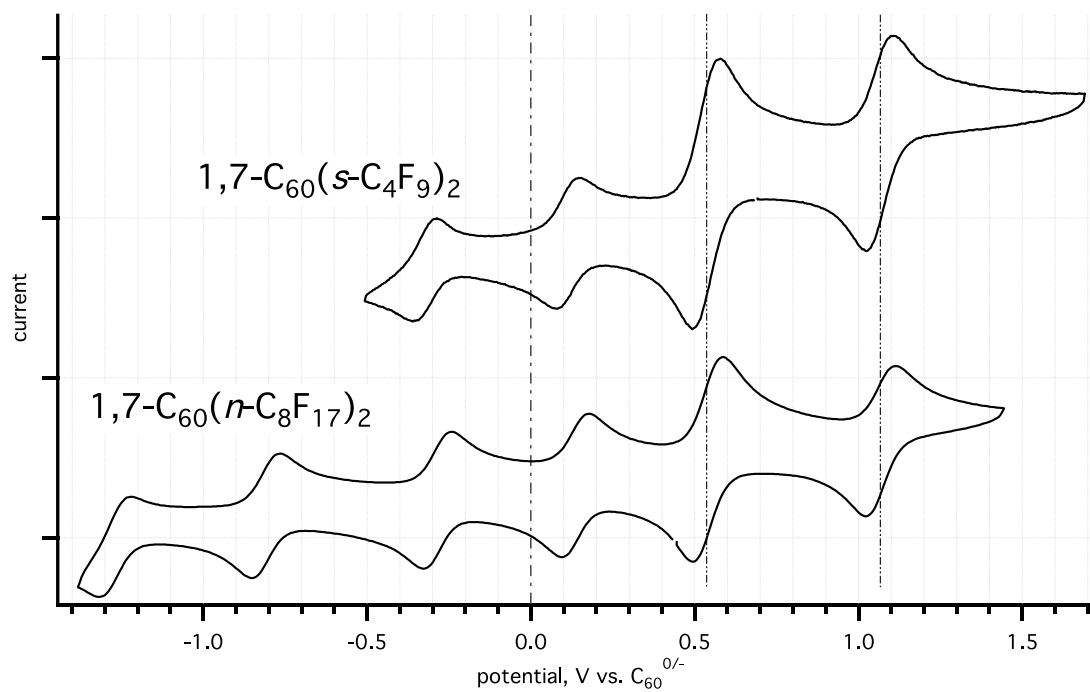
Figure 2.4. Cyclic voltammograms recorded in oDCB at a scan rate of 100 mV/sec. The supporting electrolyte used was TBABF$_4$. Both FcH and FcMe were used as internal standards, their $E_{1/2}$ values are indicated with the far left vertical dashed line and the second to the left dashed vertical line respectively. The potential has been referenced to $C_{60}^{0/-}$.

160
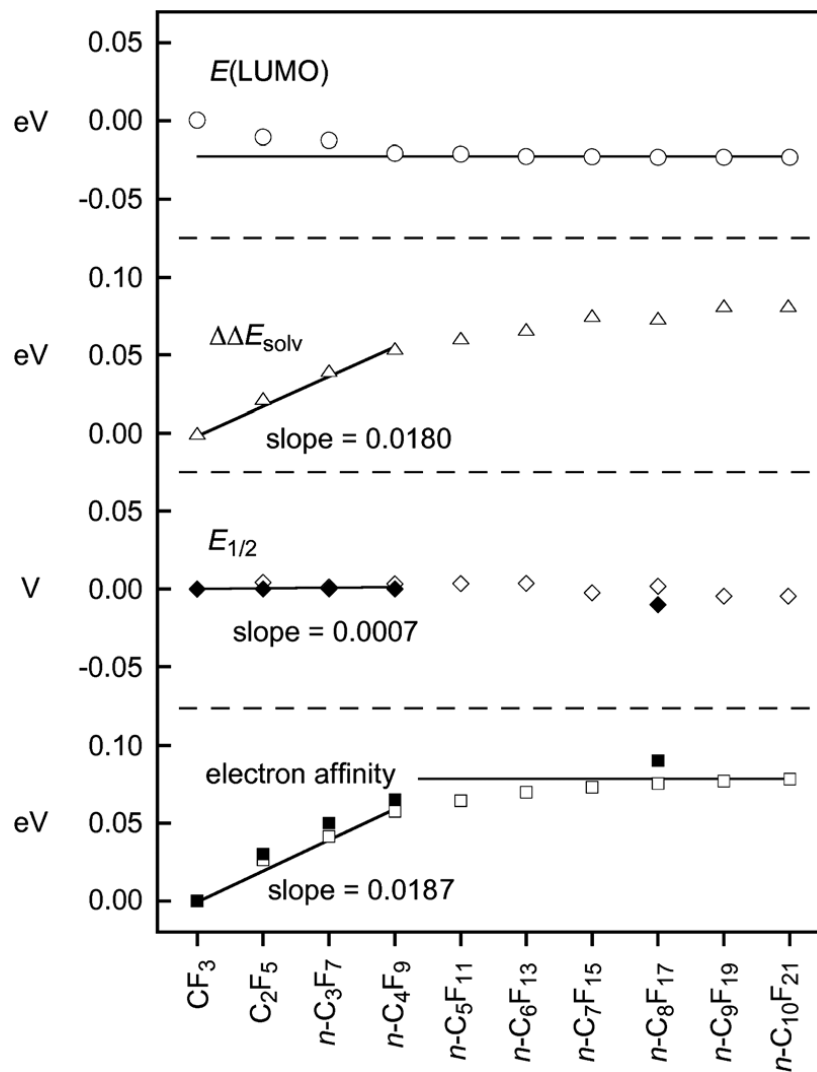
Figure 2.5. Experimental and DFT-predicted values of several parameters for 1,7-$C_{60}(R_F)_2$ compounds with $R_F = CF_3$ and primary R_F groups. The solid data points are experimental values; the hollow data points are DFT-predicted values. The lines with designated slopes are linear least squares fits to the DFT-predicted results for the first four compounds. The slopes were derived by assigning each R_F group an x-axis value equal to the number of C atoms in the chain. The solid horizontal line in the electron affinity and E(LUMO) graphs are visual aids and have no other significance.
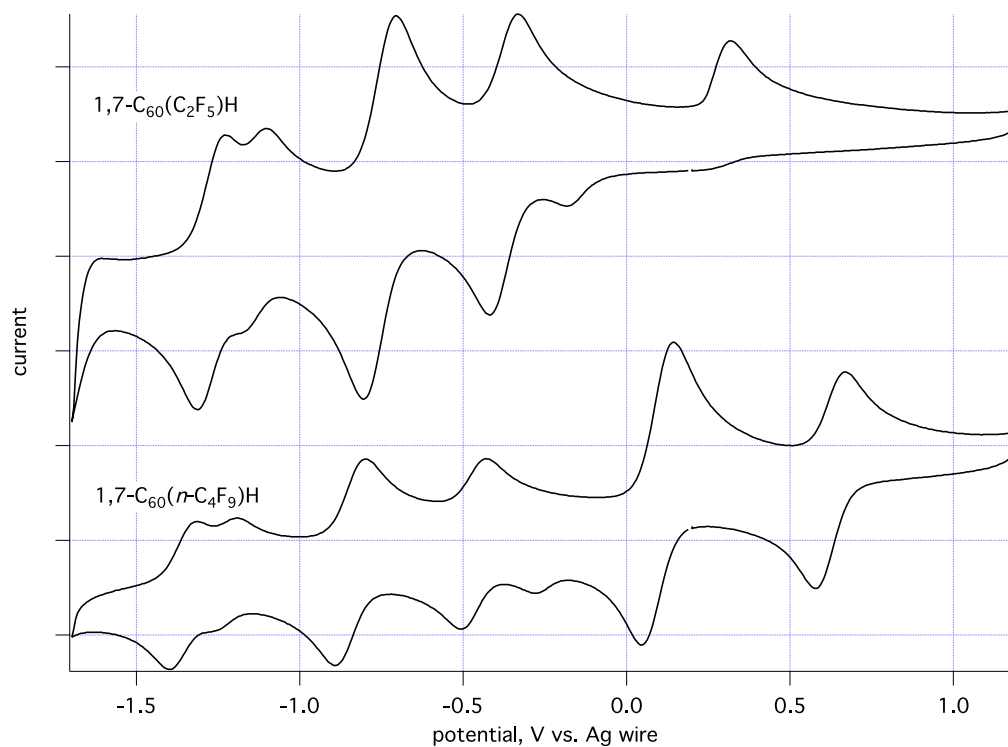
Figure 2.6. Cyclic voltammograms of the electrochemically irreversible (measured in oDCB with TBABF$_4$ as the supporting electrolyte) compounds 1,7-C$_{60}$(C$_2$F$_4$)H and 1,7-C$_{60}$(n-C$_4$F$_9$)H. The scan rate used was 100 mV/sec. Both FcH and FcMe were used as internal standards for the voltammogram of 1,7-C$_{60}$(n-C$_4$F$_9$)H (bottom).
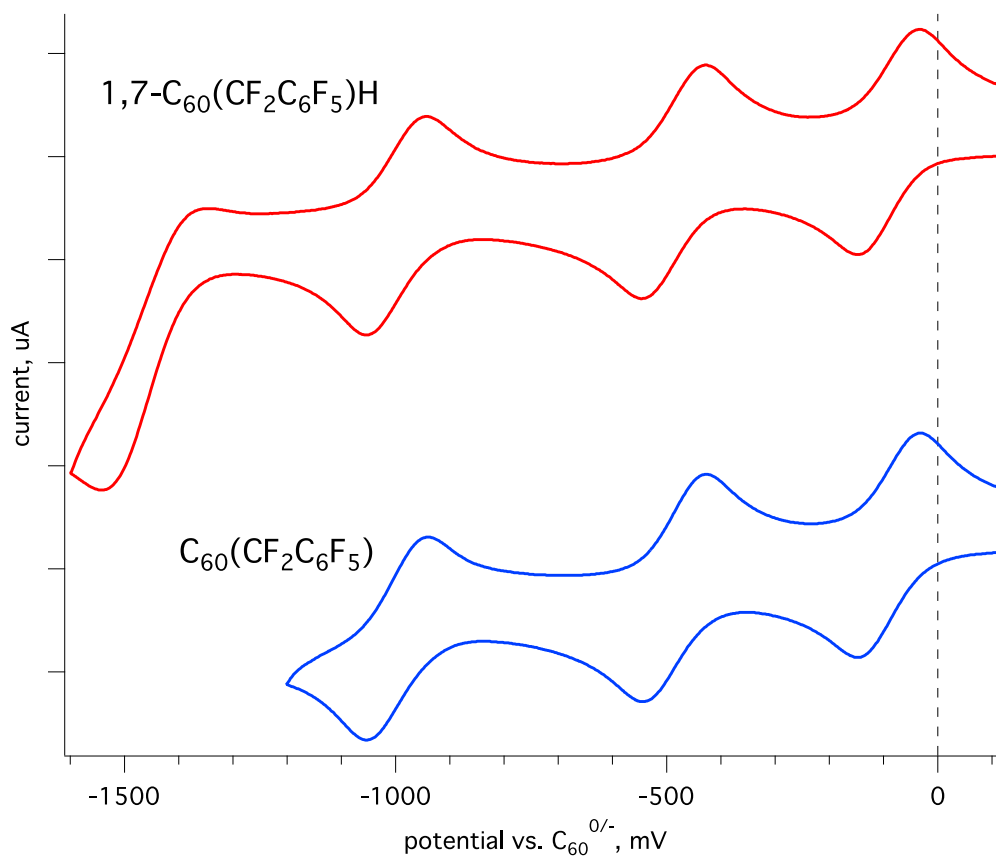
Figure 2.7. Cyclic voltammograms recorded in oDCB for $1,7\text{-}C_{60}(CF_2C_6F_5)H$ (top) and $C_{60}(CF_2C_6F_5)$ (bottom). The scan rate was 100 mV/sec and the supporting electrolyte was $TBABF_4$. The potential is referenced to $C_{60}^{0/-}$.
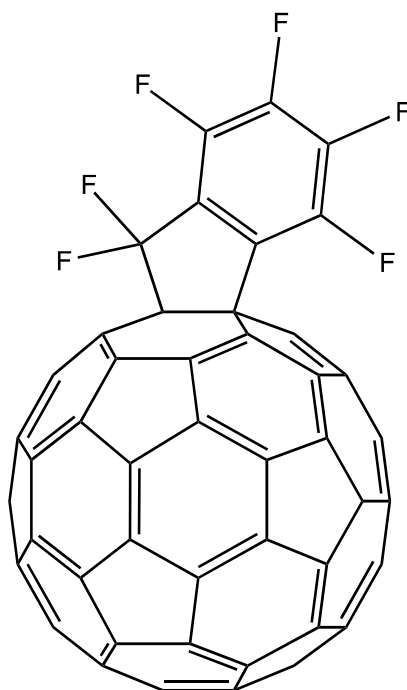
Figure 2.8. Drawing of the annulated product $C_{60}(CF_2C_6F_4)$ formed after the reduction of $C_{60}(CF_2C_6F_5)H$ according to the balanced equation: $2\ C_{60}(CF_2C_6F_5)H + 2\ e^- \longrightarrow 2\ C_{60}(CF_2C_6F_5) + 2\ F^- + H_2$
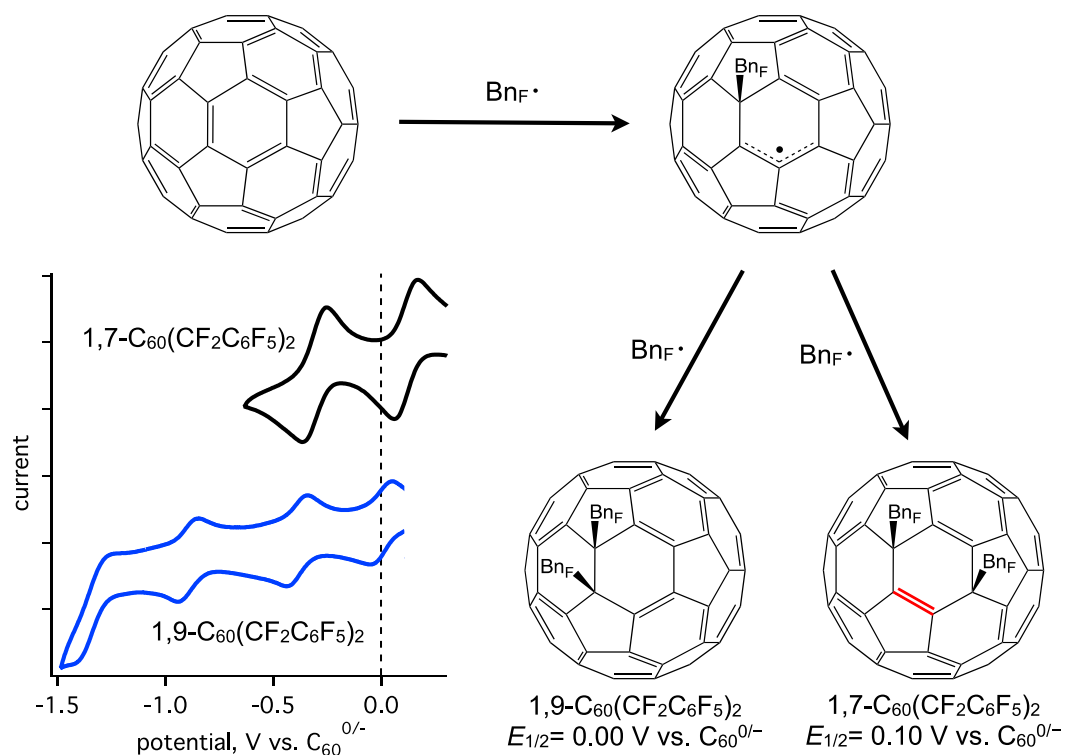
Figure 2.9. Cyclic voltammograms recorded in oDCB for 1,7-$C_{60}(CF_2C_6F_5)_2$ (top) and 1,9-$C_{60}(CF_2C_6F_5)_2$ (bottom). The scan rate was 100 mV/sec and the supporting electrolyte was TBABF$_4$. The potential is referenced to $C_{60}^{0/-}$. Also shown is a general reaction pathway showing the formation of the two isomers of $C_{60}(CF_2C_6F_5)_2$. The red double bond (bold) is the non-terminal double bond in a pentagon.
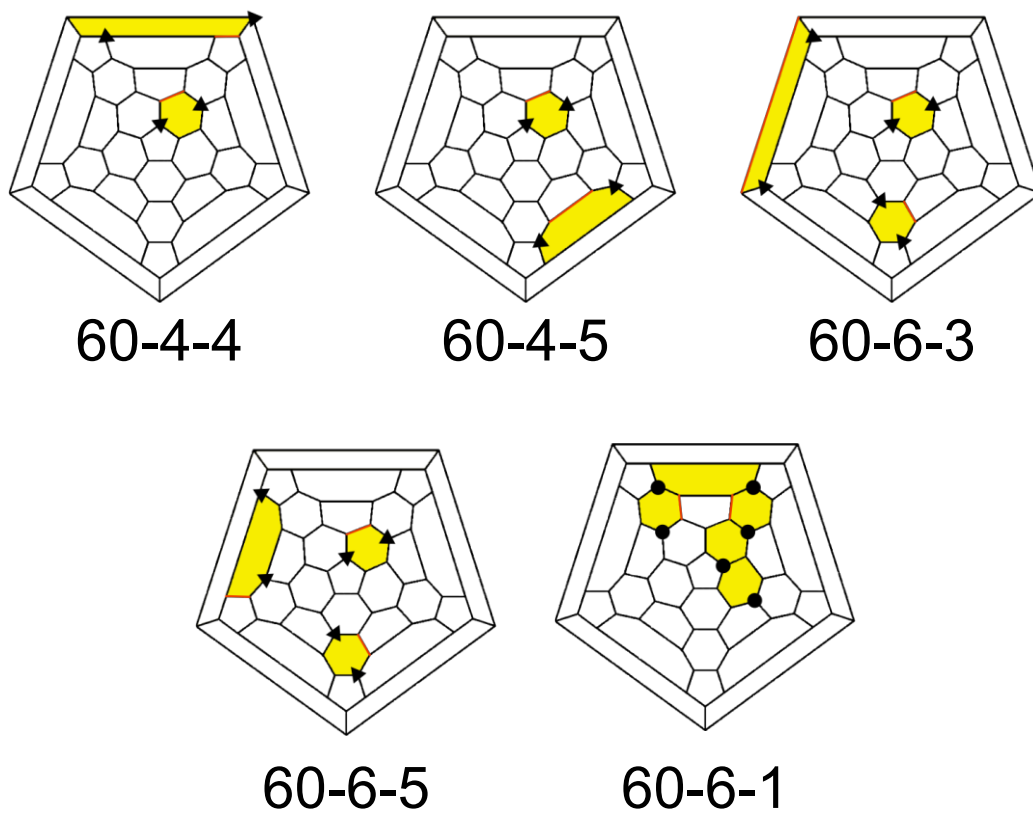
Figure 2.10. Schlegel diagrams of various PFAFs. Black triangles represent i-C_3F_7 groups while black circles represent CF_3 groups.
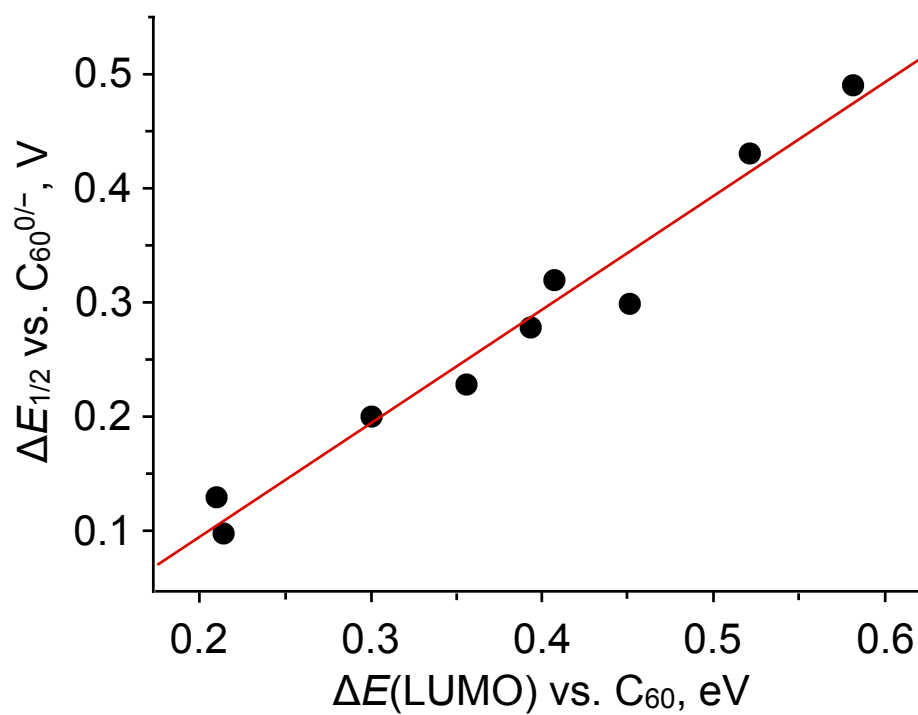
Figure 2.11. Plot of the ΔE(LUMO) vs $\Delta E_{1/2}$ for $C_{60}(i\text{-}C_3F_7)_n$ compounds.
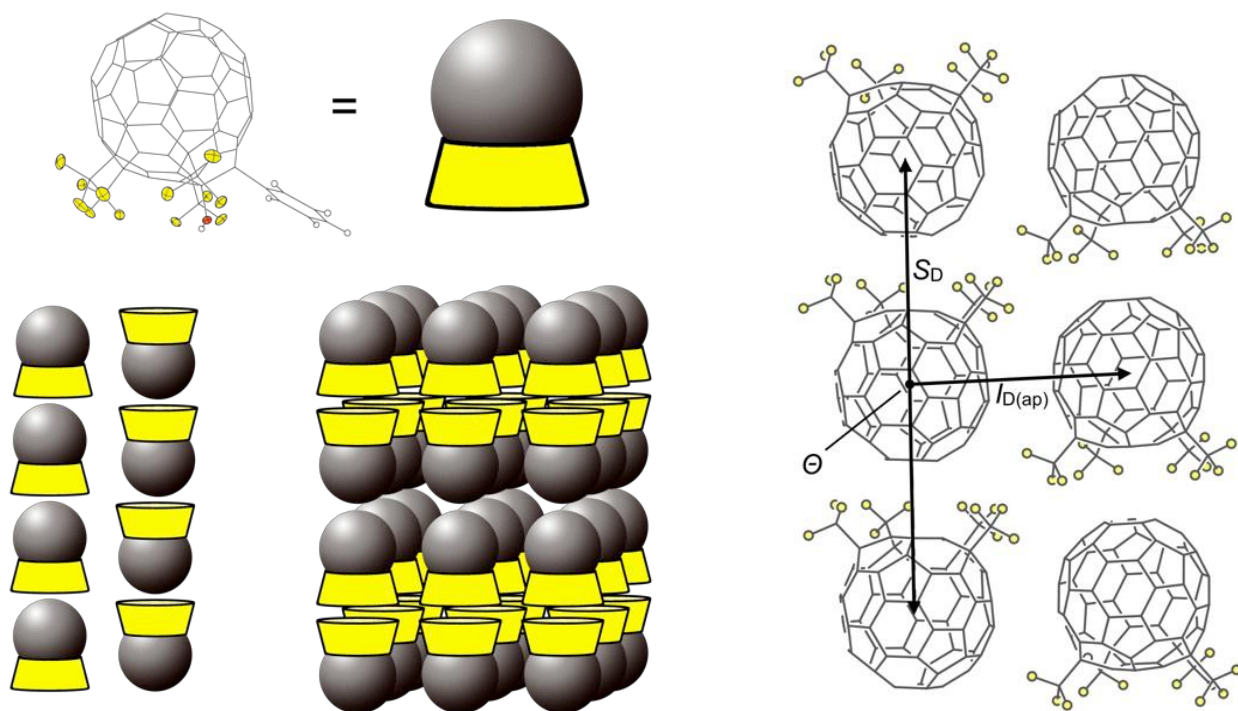
Figure 2.12 Top. A pictorial representation of the two packing motifs observed: straight stacked (left) and dimeric (right). Bottom, crystal packing of p^3-$C_{60}(CF_3)_4$ showing the figures of merit measured from the centroids of the fullerene cages.
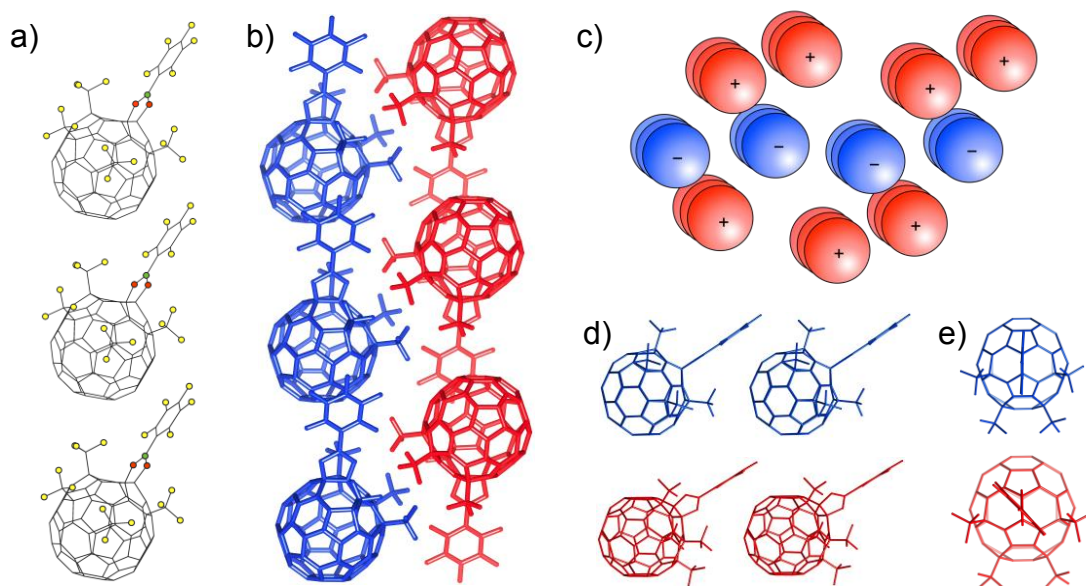
Figure 2.13 a) a single straight stack of compound 9. b) two stacks running in an anti-parallel fashion. c) viewing down the stack axis where red stacks are composed of molecules with a 42° torsion angle along the B-C bond and blue stacks composed of molecules where the rings are rigorously coplanar. The + and – indicate parallel and anti-parallel stacks. d) view perpendicular to the B-C bond. e) view down the B-C bond axis.
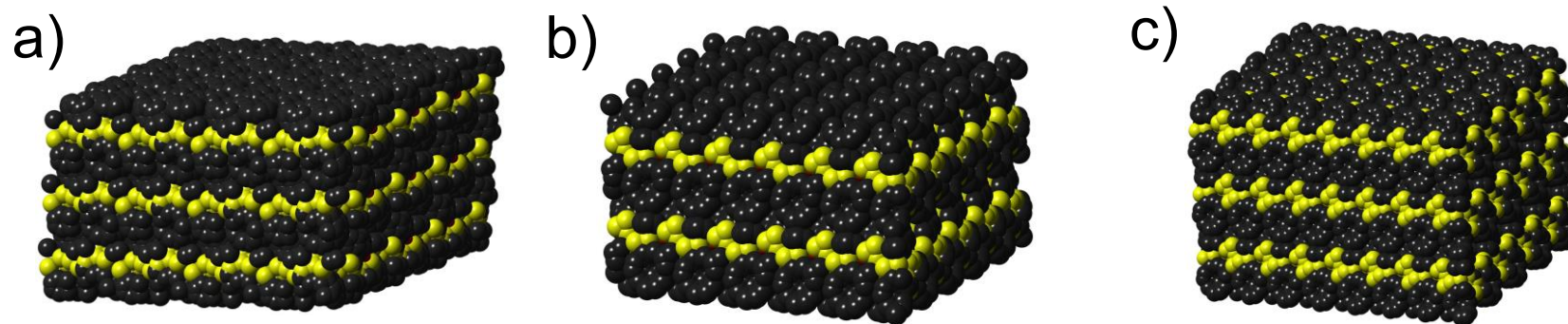
Figure 2.14 Representations showing a cut away of the crystal packing of (a) $C_{60}(CF_3)_4(C_6H_5)(OH)$, (b) $C_{60}(CF_3)_4(C_6H_4CH_3)(OH)$, and (c) $C_{60}(CF_3)_4(C_6H_4F)(OH)$. Carbon atoms are colored dark grey, fluorine atoms colored yellow, oxygen atoms colored in red.
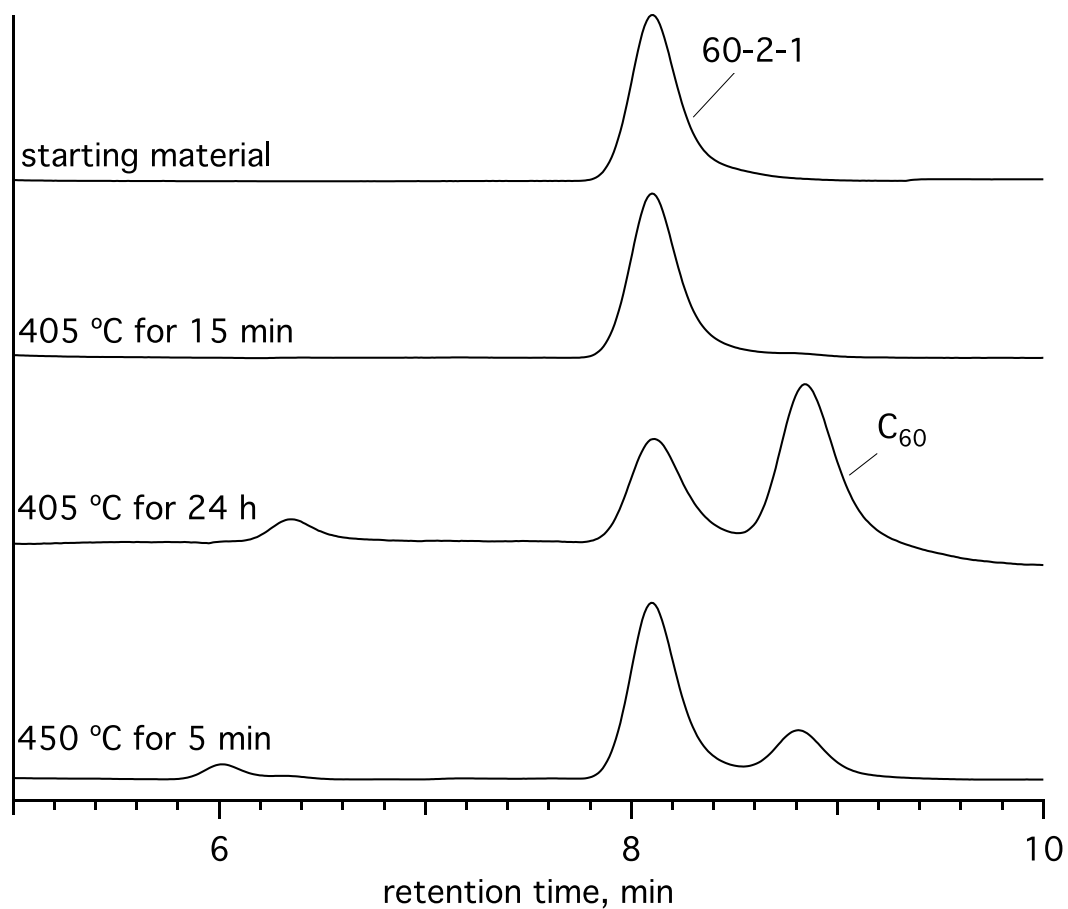
Figure 2.15. HPLC chromatograms in 100% toluene of the crude material from thermal stability experiments of 60-2-1 conducted at 405 °C for 15 min, 405 °C for 24 hours, and 450 °C for 5 min. The HPLC chromatogram of the starting material 60-2-1 is also shown for reference.
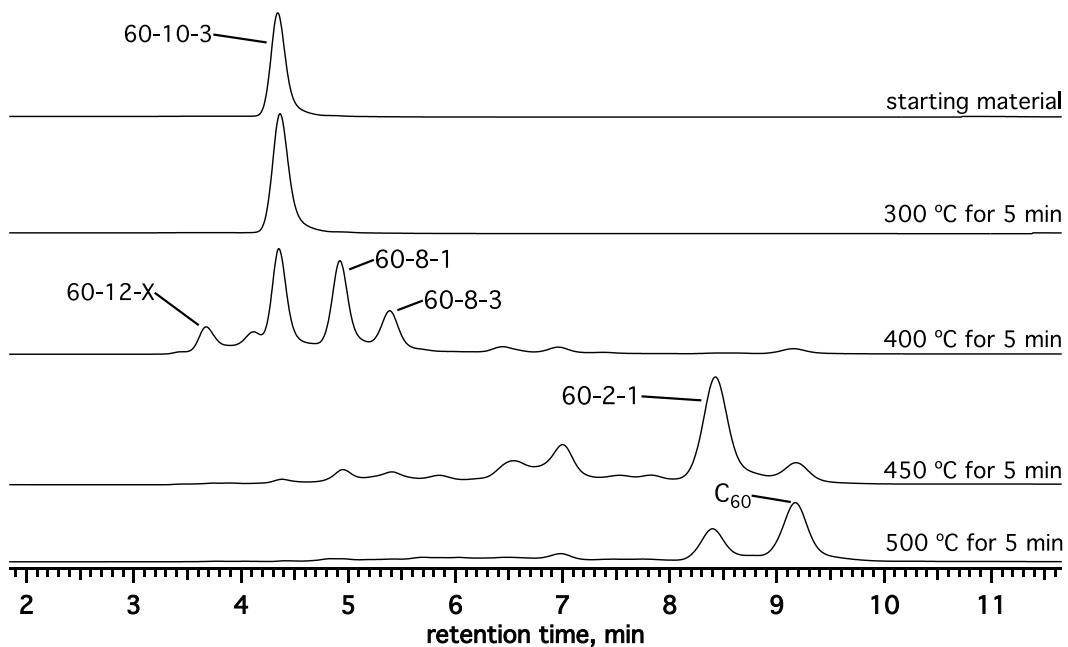
Figure 2.16. HPLC chromatograms of the resulting material after thermal treatment of 60-10-3 for 5 min at the temperature stated. The HPLC conditions were 100% toluene with a flow rate of 5 mL/min using a Buckyprep column.
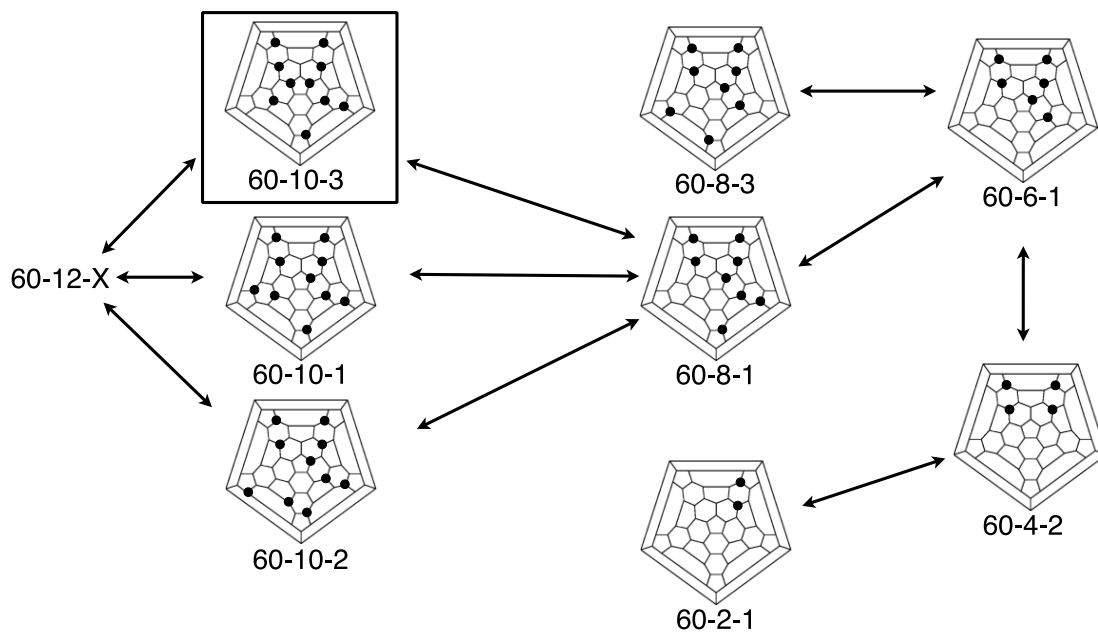
Figure 2.17. Schlegel diagrams of all the experimentally observed compounds after heating 60-10-3 (boxed) to 400 °C for 5 min. The arrows represent possible formation pathways between compounds by simple addition or removal of 2 CF$_3$ groups.
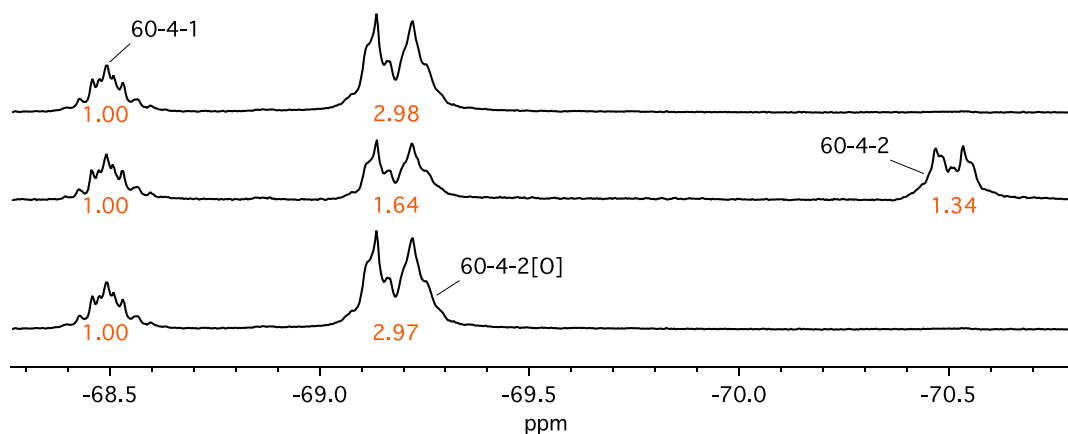
Figure 2.18. The ^{19}F NMR spectra from -68.2 to -70.8 ppm of (bottom) the mixture of starting material 60-4-2[O] and the internal standard 60-4-1, (middle) after heating to 300 °C for 30 min, and (top) the crude material in the middle spectrum after heating to 120 °C in the presence of 0.20 atm. of O_2. The numbers represent the integrated intensity relative to the internal standard that has been arbitrarily set to 1.00.

Table 2.1. Relative EA, $E_{1/2}$, $\Delta\Delta G_{sol}$, and E(LUMO) values for 1,7-$C_{60}(R_F)_2$ compounds.

cmpd.	EA[a], eV		$E_{1/2}$[b], V		$\Delta\Delta G_{sol}$[c], eV	E(LUMO), eV
	DFT	Exptl.	DFT	Exptl.	DFT	DFT
$C_{60}(CF_3)_2$	0	0	0	0	0	0
$C_{60}(C_2F_5)_2$	0.026	0.030(8)	0.004	0.002(10)	0.022	0.007
$C_{60}(n\text{-}C_3F_7)_2$	0.036	0.030(8)	−0.001	0.000(10)	0.037	−0.003
$C_{60}(i\text{-}C_3F_7)_2$	0.041	0.050(10)	0.001	0.000(10)	0.04	0.006
$C_{60}(n\text{-}C_4F_9)_2$	0.056	0.040(10)	−0.005	−0.021(10)	0.062	0.003
$C_{60}(s\text{-}C_4F_9)_2$	0.059	0.065(8)	0.005	0.000(10)	0.055	0.015
$C_{60}(n\text{-}C_8F_{17})_2$	0.075	0.090(8)	0.002	−0.005(10)	0.075	0.017

[a] EA= electron affinity; [b] $E_{1/2}$= 1st reduction potential (oDCB, 0.100 M TBABF$_4$, 100 mV/sec); $\Delta\Delta G_{sol}$= $\Delta G_{sol}(C_{60}(R_F)_2)$ − $\Delta G_{sol}(C_{60}(R_F)_2)^-$. Uncertainties for values shown in parentheses.

Table 2.2. Relative $E_{1/2}$ values for a series of 1,7-$C_{60}(R_F)_2$ compounds in different solvents.

cmpd.	DCM	oDCB	Benzonitrile
C_{60}	0	0	0
$C_{60}(CF_3)_2$	0.15	0.14	0.13
$C_{60}(C_2F_5)_2$	0.15	0.14	0.13
$C_{60}(n\text{-}C_3F_7)_2$	0.13	0.13	0.13
$C_{60}(i\text{-}C_3F_7)_2$	0.14	0.14	0.10
$C_{60}(n\text{-}C_4F_9)_2$	0.11	0.14	0.13
$C_{60}(s\text{-}C_4F_9)_2$	0.14	0.11	0.10
$C_{60}(n\text{-}C_8F_{17})_2$	0.15	0.13	0.13

References

(1)   Kareev, I. E.; Shustova, N. B.; Kuvychko, I. V.; Lebedkin, S. F.; Miller, S. M.; Anderson, O. P.; Popov, A. A.; Strauss, S. H.; Boltalina, O. V. *J. Am. Chem. Soc.* **2006**, *128*, 12268–12280.

(2)   Popov, A. A.; Kareev, I. E.; Shustova, N. B.; Stukalin, E. B.; Lebedkin, S. F.; Seppelt, K.; Strauss, S. H.; Boltalina, O. V.; Dunsch, L. *J. Am. Chem. Soc.* **2007**, *129*, 11551–11568.

(3)   Popov, A. A.; Shustova, N. B.; Boltalina, O. V.; Strauss, S. H.; Dunsch, L. *ChemPhysChem* **2008**, *9*, 431–438.

(4)   Takano, Y.; Herranz, M. Á.; Martin, N.; de Miguel Rojas, G.; Guldi, D. M.; Kareev, I. E.; Strauss, S. H.; Boltalina, O. V.; Tsuchiya, T.; Akasaka, T. *Chem. Eur. J.* **2010**, NA–NA.

(5)   Takano, Y.; Herranz, M. Á.; Kareev, I. E.; Strauss, S. H.; Boltalina, O. V.; Akasaka, T.; Martin, N. *J. Org. Chem.* **2009**, *74*, 6902–6905.

(6)   Popov, A. A.; Kareev, I. E.; Shustova, N. B.; Lebedkin, S. F.; Strauss, S. H.; Boltalina, O. V.; Dunsch, L. *Chem. Eur. J.* **2008**, *14*, 107–121.

(7)   Dorozhkin, E. I.; Ignat'eva, D. V.; Tamm, N. B.; Goryunkov, A. A.; Khavrel, P. A.; Ioffe, I. N.; Popov, A. A.; Kuvychko, I. V.; Streletskiy, A. V.; Markov, V. Y.; Spandl, J.; Strauss, S. H.; Boltalina, O. V. *Chem. Eur. J.* **2006**, *12*, 3876–3889.

(8)   Goryunkov, A.; Kuvychko, I.; Ioffe, I. *Journal of Fluorine Chemistry* **2003**.

(9)   Kareev, I. E.; Kuvychko, I. V.; Lebedkin, S. F.; Miller, S. M.; Anderson, O. P.; Seppelt, K.; Strauss, S. H.; Boltalina, O. V. *J. Am. Chem. Soc.* **2005**, *127*, 8362–8375.

(10)   Troyanov, S. I.; Dimitrov, A.; Kemnitz, E. *Angew. Chem. Int. Ed.* **2006**, *45*, 1971–
         1974.

(11)   Kareev, I. E.; Lebedkin, S. F.; Bubnov, V. P.; Yagubskii, E. B.; Ioffe, I. N.; Khavrel, P.
         A.; Kuvychko, I. V.; Strauss, S. H.; Boltalina, O. V. *Angew. Chem. Int. Ed.* **2005**, *44*,
         1846–1849.

(12)   Shustova, N. B.; Popov, A. A.; Mackey, M. A.; Coumbe, C. E.; Phillips, J. P.;
         Stevenson, S.; Strauss, S. H.; Boltalina, O. V. *J. Am. Chem. Soc.* **2007**, *129*, 11676–
         11677.

(13)   Troyanov, S. I.; Goryunkov, A. A.; Dorozhkin, E. I.; Ignat'eva, D. V.; Tamm, N. B.;
         Avdoshenko, S. M.; Ioffe, I. N.; Markov, V. Y.; Sidorov, L. N.; Scheurel, K.; Kemnitz,
         E. *Journal of Fluorine Chemistry* **2007**, *128*, 545–551.

(14)   Popov, A. A.; Tarábek, J.; Kareev, I. E.; Lebedkin, S. F.; Strauss, S. H.; Boltalina, O.
         V.; Dunsch, L. *J. Phys. Chem. A* **2005**, *109*, 9709–9711.

(15)   Fagan, P. J.; Krusic, P. J.; McEwen, C. N.; Lazar, J.; Parker, D. H.; Herron, N.;
         Wasserman, E. *Science* **1993**, *262*, 404–407.

(16)   Darwish, A. D.; Abdul-Sada, A. K.; Avent, A. G.; Lyakhovetsky, V. I.; Shilova, E. A.;
         Taylor, R. *Org. Biomol. Chem.* **2003**, *1*, 3102–3110.

(17)   Goryunkov, A.; Ioffe, I.; Kuvychko, I.; Yankova, T.; Markov, V.; Streletskii, A.; Dick,
         D.; Sidorov, L.; Boltalina, O.; Strauss, S. *Fullerene Nanot Carbon Nanostruct* **2004**, *12*,
         181–185.

(18)   Goryunkov, A. A.; Ignat'eva, D. V.; Tamm, N. B.; Moiseeva, N. N.; Ioffe, I. N.;
         Avdoshenko, S. M.; Markov, V. Y.; Sidorov, L. N.; Kemnitz, E.; Troyanov, S. I. *Eur. J.
         Org. Chem.* **2006**, 2508–2512.

(19)   Kareev, I. E.; Kuvychko, I. V.; Lebedkin, S. F.; Miller, S. M.; Anderson, O. P.; Seppelt,
        K.; Strauss, S. H.; Boltalina, O. V. *J. Am. Chem. Soc.* **2005**, *127*, 8362–8375.

(20)   Kareev, I. E.; Kuvychko, I. V.; Lebedkin, S. F.; Miller, S. M.; Anderson, O. P.; Strauss,
        S. H.; Boltalina, O. V. *Chem. Commun.* **2006**, 308.

(21)   Cardona, C. M.; Kitaygorodskiy, A.; Echegoyen, L. *J. Am. Chem. Soc.* **2005**, *127*,
        10448–10453.

(22)   Shu, C.; Cai, T.; Xu, L.; Zuo, T.; Reid, J.; Harich, K.; Dorn, H. C.; Gibson, H. W. *J.
        Am. Chem. Soc.* **2007**, *129*, 15710–15717.

(23)   Shustova, N. B.; Kuvychko, I. V.; Peryshkov, D. V.; Whitaker, J. B.; Larson, B. W.;
        Chen, Y.-S.; Dunsch, L.; Seppelt, K.; Popov, A. A.; Strauss, S. H.; Boltalina, O. V.
        Chem. Commun. **2011**, *47*, 875–877.

(24)   Shustova, N. B.; Kareev, I. E.; Kuvychko, I. V.; Whitaker, J. B.; Lebedkin, S. F.;
        Popov, A. A.; Dunsch, L.; Chen, Y.-S.; Seppelt, K.; Strauss, S. H. *Journal of Fluorine
        Chemistry* **2010**, *131*, 1198–1212.

(25)   Kuvychko, I. V.; Shustova, N. B.; Avdoshenko, S. M.; Popov, A. A.; Strauss, S. H.;
        Boltalina, O. V. *Chem. Eur. J.* **2011**, *17*, 8799–8802.

(26)   Kuvychko, I. V.; Whitaker, J. B.; Larson, B. W.; Folsom, T. C.; Shustova, N. B.;
        Avdoshenko, S. M.; Chen, Y. S.; Wen, H.; Wang, X.-B.; Dunsch, L.; Popov, A. A.;
        Boltalina, O. V.; Strauss, S. H. *Chem. Sci.* **2012**, *3*, 1399–1407.

(27)   Kuvychko, I. V.; Strauss, S. H.; Boltalina, O. V. *Journal of Fluorine Chemistry* **2012**,
        143, 103–108.

(28)   Chiu, M.-Y.; Jeng, U.-S.; Su, M.-S.; Wei, K.-H. *Macromolecules* **2010**, *43*, 428–432.

(29)   Olson, D. C.; Lee, Y.-J.; White, M. S.; Kopidakis, N.; Shaheen, S. E.; Ginley, D. S.;

Voigt, J. A.; Hsu, J. W. P. *J. Phys. Chem. C* **2008**, *112*, 9544–9547.

(30)   Cardona, C. M.; Li, W.; Kaifer, A. E.; Stockdale, D.; Bazan, G. C. *Adv. Mater.* **2011**, *23*, 2367–2371.

(31)   Matsuo, Y. *Pure Appl. Chem.* **2012**, *84*, 945–952.

(32)   Coffey, D. C.; Larson, B. W.; Hains, A. W.; Whitaker, J. B.; Kopidakis, N.; Boltalina, O. V.; Strauss, S. H.; Rumbles, G. *J. Phys. Chem. C* **2012**, *116*, 8916–8923.

(33)   Nardes, A. M.; Ferguson, A. J.; Whitaker, J. B.; Larson, B. W.; Larsen, R. E.; Maturová, K.; Graf, P. A.; Boltalina, O. V.; Strauss, S. H.; Kopidakis, N. *Adv. Funct. Mater.* **2012**, n/a–n/a.

(34)   Kadish, K. M.; Gao, X.; Caemelbecke, E. V.; Suenobu, T.; Fukuzumi, S. *J. Phys. Chem. A* **2000**, *104*, 3878–3883.

(35)   Murata, Y.; Shiro, M.; Komatsu, K. *J. Am. Chem. Soc.* **1997**, *119*, 8117–8118.

(36)   Kareev, I. E.; Quiñones, G. S.; Kuvychko, I. V.; Khavrel, P. A.; Ioffe, I. N.; Goldt, I. V.; Lebedkin, S. F.; Seppelt, K.; Strauss, S. H.; Boltalina, O. V. *J. Am. Chem. Soc.* **2005**, *127*, 11497–11504.

(37)   Balch, A. L.; Costa, D. A.; Noll, B. C.; Olmstead, M. M. *J. Am. Chem. Soc.* **1995**, *117*, 8926–8932.

(38)   Heymann, D.; Weisman, R. B. *C. R. Chimie.* **2006**, *9*, 1107–1116.

(39)   Weisman, R. B.; Heymann, D.; Bachilo, S. M. *J. Am. Chem. Soc.* **2001**, *123*, 9720–9721.

(40)   Tajima, Y.; Takeuchi, K. *J. Org. Chem.* **2002**, *67*, 1696–1698.

(41)   Matsuo, Y.; Ozu, A.; Obata, N.; Fukuda, N.; Tanaka, H.; Nakamura, E. *Chem. Commun.* **2012**, *48*, 3878–3880.

(42)   Matsuo, Y.; Nakamura, E. *J. Am. Chem. Soc.* **2005**, *127*, 8457–8466.

(43)   Kuvychko, I. V.; Streletskii, A. V.; Popov, A. A.; Kotsiris, S. G.; DREWELLO, T.; Strauss, S. H.; Boltalina, O. V. *Chem. Eur. J.* **2005**, *11*, 5426.

(44)   Dorozhkin, E. I.; Goryunkov, A. A.; Ioffe, I. N.; Avdoshenko, S. M.; Markov, V. Y.; Tamm, N. B.; Ignat'eva, D. V.; Sidorov, L. N.; Troyanov, S. I. *European Journal of Organic Chemistry* **2007**, *2007*, 5082–5094.

(45)   Isobe, H.; Tomita, N.; Nakamura, E. *Org. Lett.* **2000**, *2*, 3663–3665.

(46)   Kennedy, R. D.; Halim, M.; Khan, S. I.; Schwartz, B. J.; Tolbert, S. H.; Rubin, Y. *Chem. Eur. J.* **2012**, 7418–7433.

(47)   Shustova, N. B.; Kuvychko, I. V.; Popov, A. A.; Delius, von, M.; Dunsch, L.; Anderson, O. P.; Hirsch, A.; Strauss, S. H.; Boltalina, O. V. *Angew. Chem. Int. Ed.* **2011**, *50*, 5537–5540.

(48)   Hirsch, A.; Brettreich, M.; Wudl, F. *Fullerenes: Chemistry and Reactions*; 1st ed. Wiley-VCH, 2005.

(49)   Creegan, K.; Robbins, J.; Robbins, W. *J. Am. Chem. Soc.* **1992**.

(50)   Shigemitsu, Y.; Kaneko, M.; Tajima, Y.; Takeuchi, K. *Chem. Lett.* **2004**, *33*, 1604–1605.

(51)   Huang, S.; Xiao, Z.; Wang, F.; Zhou, J.; Yuan, G.; Zhang, S.; Chen, Z.; Thiel, W.; Schleyer, P. V. R.; Zhang, X.; Hu, X.; Chen, B.; Gan, L. *Chem. Eur. J.* **2005**, *11*, 5449–5456.

(52)   Huang, S.; Yang, X.; Zhang, X.; Hu, X.; Gan, L.; Zhang, S. *Synlett* **2006**, *2006*, 1266–1268.

(53)   Tajima, Y.; Hara, T.; Honma, T.; Matsumoto, S.; Takeuchi, K. *Org. Lett.* **2006**, *8*,

3203–3205.

(54)   Jia, Z.; Zhang, X.; Zhang, G.; Huang, S.; Fang, H.; Hu, X.; Li, Y.; Gan, L.; Zhang, S.; Zhu, D. *Chem Asian J* **2007**, *2*, 290–300.

(55)   Zhang, Q.; Pankewitz, T.; Liu, S.; Klopper, W.; Gan, L. *Angew. Chem. Int. Ed.* **2010**, *49*, 9935–9938.

(56)   Blackett, B. N.; Coxon, J. M.; Hartshorn, M. P.; Lewis, A. J.; Little, G. R.; Wright, G. J. *Tetrahedron* **1970**, *26*, 1311–1313.

(57)   Xiao, Z.; Yao, J.; Yang, D.; Wang, F.; Huang, S.; Gan, L.; Jia, Z.; Jiang, Z.; Yang, X.; Zheng, B.; Yuan, G.; Zhang, S.; Wang, Z. *J. Am. Chem. Soc.* **2007**, *129*, 16149–16162.

(58)   Xiao, Z.; Yao, J.; Yu, Y.; Jia, Z.; Gan, L. *Chem. Commun.* **2010**, *46*, 8365.

(59)   Jiang, Z.; Zhang, Y.; Gan, L.; Wang, Z. *Tetrahedron* **2008**, *64*, 11394–11403.

(60)   Gan, L.; Yang, D.; Zhang, Q.; Huang, H. *Adv. Mater.* **2010**, *22*, 1498–1507.

(61)   *Organic Photovoltaics: Materials, Device Physics, and Manufacturing Technologies*; Brabec, C.; Scherf, U.; Dyakonov, V., Eds. 1st ed. Wiley-VCH, 2008.

(62)   Shaheen, S. E.; Ginley, D. S.; Jabbour, G. E. *MRS bulletin* **2005**, *30*, 10–19.

(63)   Avdoshenko, S. M.; Ioffe, I. N.; Sidorov, L. N. *J. Phys. Chem. A* **2009**, *113*, 10833–10838.

(64)   Ignat'eva, D. V.; Mutig, T.; Goryunkov, A. A.; Tamm, N. B.; Kemnitz, E.; Troyanov, S. I.; Sidorov, L. N. *Russ Chem Bull* **2010**, *58*, 1146–1154.

(65)   Mutig, T.; Kemnitz, E.; Troyanov, S. I. *Mendeleev Communications* **2009**, *19*, 30–31.

(66)   Goryunkov, A. A.; Dorozhkin, E. I.; Tamm, N. B.; Ignat'eva, D. V.; Avdoshenko, S. M.; Sidorov, L. N.; Troyanov, S. I. *Mendeleev Commun.* **2007**, *17*, 110–112.

(67)   Rispens, M. T.; Meetsma, A.; Rittberger, R.; Brabec, C. J.; Sariciftci, N. S.; Hummelen,

J. C. *Chem. Commun.* **2003**, 2116.

(68)   Kennedy, R. D.; Ayzner, A. L.; Wanger, D. D.; Day, C. T.; Halim, M.; Khan, S. I.;

Tolbert, S. H.; Schwartz, B. J.; Rubin, Y. *J. Am. Chem. Soc.* **2008**, *130*, 17290–17292.

(69)   Niinomi, T.; Matsuo, Y.; Hashiguchi, M.; Sato, Y.; Nakamura, E. *J. Mater. Chem.*

2009, *19*, 5804.

(70)   Haddon, R. C.; Brus, L. E.; Raghavachari, K. *Chem. Phys. Lett.* **1986**, *125*, 459–464.

(71)   Xie, Q.; Perez-Cordero, E.; Echegoyen, L. *J. Am. Chem. Soc.* **1992**, *114*, 3978–3980.

(72)   Dubois, D.; Kadish, K. M.; Flanagan, S.; Wilson, L. J. *J. Am. Chem. Soc.* **1991**, *113*,

7773–7774.

(73)   Echegoyen, L.; Echegoyen, L. E. *Acc. Chem. Res.* **1998**, *31*, 593–601.

(74)   Lichtenberger, D. L.; Nebesny, K. W.; Ray, C. D. **1991**, *126*, 203–208.

(75)   Xie, Q.; Arias, F.; Echegoyen, L. *J. Am. Chem. Soc.* **1993**, *115*, 9818–9819.

(76)   Feldberg, S. W. *Journal of Electroanal. Chem.* **2008**, *624*, 45–51.

(77)   Tsierkezos, N. G. *J. Solution Chem.* **2007**, *36*, 289–302.

(78)   Zheng, M.; Li, F.-F.; Ni, L.; Yang, W.-W.; Gao, X. *J. Org. Chem.* **2008**, *73*, 3159–

3168.

(79)   Hammett, L. P. *Chemical Reviews* **1935**, *17*, 125–136.

(80)   Hansch, C.; Leo, A.; Taft, R. W. *Chemical Reviews* **1991**, *91*, 165–195.

(81)   Charton, M. *J. Am. Chem. Soc.* **1975**, *97*, 1552–1556.

(82)   Marzilli, L. G.; Bayo, F.; Summers, M. F.; Thomas, L. B.; Zangrando, E.; Bresciani-

Pahor, N.; Mari, M.; Randaccio, L. *J. Am. Chem. Soc.* **1987**, *109*, 6045–6052.

(83)   Bunten, K. A.; Chen, L.; Fernandez, A. L.; Poë, A. J. *Coordination chemistry reviews*

2002, *233*, 41–51.

(84)   Brown, T. L.; Lee, K. J. *Coordination chemistry reviews* **1993**, *128*, 89–116.

(85)   Simón-Manso, Y. *J. Phys. Chem. A* **2005**, *109*, 2006–2011.

(86)   Agrafiotis, D. K.; Shemanarev, M.; Connolly, P. J.; Farnum, M.; Lobanov, V. S. *J. Med. Chem.* **2007**, *50*, 5926–5937.

(87)   Do, J. Y.; Park, S. K.; Ju, J. J.; Park, S.; Lee, M. H. *Optical Materials* **2004**, *26*, 223–229.

(88)   Espeso, J.; Lozano, A. E.; la Campa, de, J. G.; de Abajo, J. *Journal of Membrane Science* **2006**, *280*, 659–665.

(89)   Babazadeh, M. *J. Appl. Polym. Sci.* **2006**, *102*, 633–639.

(90)   Justin Thomas, K. R.; Lin, J. T.; Tao, Y.-T.; Chuen, C.-H. *Chem. Mater.* **2004**, *16*, 5437–5444.

(91)   Brabec, C. J.; Gowrisanker, S.; Halls, J. J. M.; Laird, D.; Jia, S.; Williams, S. P. *Adv. Mater.* **2010**, *22*, 3839–3856.

(92)   Lemal, D. M. *J. Org. Chem.* **2004**, *69*, 1–11.

(93)   Corvaja, C.; Farnia, G.; Formenton, G.; Navarrini, W.; Sandona, G.; Tortelli, V. *The Journal of Physical Chemistry* **1994**, *98*, 2307–2313.

(94)   Combellas, C.; Kanoufi, F.; Thiébault, A. *J. Phys. Chem. B* **2003**, *107*, 10894–10905.

(95)   Yuan, Z.; Li, J.; Xiao, Y.; Li, Z.; Qian, X. *J. Org. Chem.* **2010**, *75*, 3007–3016.

(96)   Li, Y.; Li, C.; Yue, W.; Jiang, W.; Kopecek, R.; Qu, J.; Wang, Z. *Org. Lett.* **2010**, *12*, 2374–2377.

(97)   Ruoff, R. S.; Kadish, K. M.; Boulas, P.; Chen, E. *The Journal of Physical Chemistry* **2001**, *99*, 8843–8850.

(98)   Djurovich, P. I.; Mayo, E. I.; Forrest, S. R.; Thompson, M. E. *Organic Electronics*

2009, *10*, 515–520.

(99)   Doubois, D.; Moninot, G.; Kutner, W.; Jones, M. T.; Kadish, K. *The Journal of Physical Chemistry* **1992**, *96*, 7137.

(100)   Dixon, D. A.; Matsuzawa, N.; Fukunaga, T.; Tebbe, F. N. *The Journal of Physical Chemistry* **1992**, *96*, 6107–6110.

(101)   Kuvychko, I. V.; Strauss, S. H.; Boltalina, O. V. In *Efficient Preparation of Fluorine Compounds*; Wiley: New York, 2013; pp. 9–11.

(102)   Bonifazi, D.; Enger, O.; Diederich, F. O. *Chem. Soc. Rev.* **2007**, *36*, 390.

(103)   Matsuo, Y.; Iwashita, A.; Abe, Y.; Li, C.-Z.; Matsuo, K.; Hashiguchi, M.; Nakamura, E. *J. Am. Chem. Soc.* **2008**, *130*, 15429–15436.

(104)   Kennedy, R. D.; Ayzner, A. L.; Wanger, D. D.; Day, C. T.; Halim, M.; Khan, S. I.; Tolbert, S. H.; Schwartz, B. J.; Rubin, Y. *J. Am. Chem. Soc.* **2008**, *130*, 17290–17292.

(105)   Pope, M.; Swenberg, C. E. *Electronic processes in organic crystals and polymers*; Oxford University Press, USA, 1999.

(106)   Sawamura, M.; Kawai, K.; Matsuo, Y.; Kanie, K.; Kato, T.; Nakamura, E. *Nature* **2002**, *419*, 702–705.

(107)   Bashilov, V. V.; Dolgushin, F. M.; Tumanskii, B. L.; Petrovskii, P. V.; Sokolov, V. I. *Tetrahedron* **2008**, *64*, 11291–11295.

(108)   Ignat'eva, D. V.; Ioffe, I. N.; Troyanov, S. I.; Sidorov, L. N. *Russ. Chem. Rev.* **2011**, *80*, 631–645.

(109)   Green, M. A.; Emery, K.; Hisikawa, Y.; Warta, W. *Prog. Photovolt: Res. Appl.* **2007**, *15*, 425–430.

(110)   Green, M. A.; Emery, K.; Hishikawa, Y.; Warta, W.; Dunlop, E. D. *Prog. Photovolt:*

Res. Appl. **2011**, *19*, 565–572.

(111) Larson, B. W.; Whitaker, J. B.; Wang, X.-B.; Popov, A. A.; Rumbles, G.; Kopidakis, N.; Strauss, S. H.; Boltalina, O. V. *J. Phys. Chem. C* **2013**, *117*, 14958–14964.

(112) Kang, H.; Cho, C.-H.; Cho, H.-H.; Kang, T. E.; Kim, H. J.; Kim, K.-H.; Yoon, S. C.; Kim, B. J. *ACS Appl. Mater. Interfaces* **2012**, *4*, 110–116.

(113) He, Y.; Chen, H.-Y.; Hou, J.; Li, Y. *J. Am. Chem. Soc.* **2010**, *132*, 1377–1382.

(114) Brabec, C. J.; Cravino, A.; Meissner, D.; Sariciftci, N. S.; Fromherz, T.; Rispens, M. T.; Sanchez, L.; Hummelen, J. C. *Adv. Funct. Mater.* **2001**, *11*, 374–380.

(115) Li, G.; Shrotriya, V.; Huang, J.; Yao, Y.; Moriarty, T.; Emery, K.; Yang, Y. *Nat Mater* **2005**, *4*, 864–868.

(116) Wang, J.-C.; Weng, W.-T.; Tsai, M.-Y.; Lee, M.-K.; Horng, S.-F.; Perng, T.-P.; Kei, C.-C.; Yu, C.-C.; Meng, H.-F. *J. Mater. Chem.* **2010**, *20*, 862.

Chapter 3

Fullerenes in Organic Photovoltaics

Introduction

One of the most intriguing possible uses of novel derivatized fullerenes is as electron acceptors in organic photovoltaics (OPVs). The power conversion efficiencies (PCE) of bulk heterojunction OPV devices that employ fullerene derivatives has increased from 4 to 8.3% over the span of 4 years.[109,110] This remarkable improvement over a short period of time is attributed in large part to the facile tunability of electronic and physical properties (solubility, crystal packing, and thermal stability) of organic compounds. Even simple modifications to the molecular structure can have marked effects on the device properties. For example, going from $PC_{60}BM$ to $PC_{70}BM$ results in a higher performing device.[62] However, OPV science is still a young field and many aspects remain unexplored or poorly understood. For example, electrochemical effects of the purity purity and thermal stability of the most common fullerenes used in OPV devices (phenyl-C_{60}-butyric acid methylester and indene-C_{60} multiadducts) are for the most part unknown or not agreed upon.

This chapter will examine several of these aspects that have not been addressed in the vast literature on OPVs. The electrochemical behavior of PCBM will be discussed and the

solution phase $E_{1/2}$ value under carefully controlled conditions will be presented. The electrochemical consequence of both thermally depositing thin films of PCBM and using an isomeric and compositional mixture of indene-C_{60} multiadducts in OPV devices will be explored. Lastly, the data from the initial screening of OPV devices that incorporate PFAFs in the active layer that was done in collaboration with Dr. Nikos Kopidakis and Dr. Garry Rumbles from the National Renewable Energy Laboratory will be discussed.

3.1. Fullerenes in Organic Photovoltaics

3.1.1. Electrochemical Characterization of PCBM. PCBM has become the prototypical fullerene electron acceptor in organic photovoltaic devices (OPVs). Despite PCBM being one of the most common fullerenes acceptors used in OPVs as well as one of the best performing, there is very little agreement on the solution phase $E_{1/2}$ which is widely used to estimate the E(LUMO). In over 30 original cyclic voltammetry experiments conducted over the past 6 years, there has been a huge range of reported reduction potentials of PCBM. This discrepancy can be traced to several causes. First, simple variations in electrochemical conditions such as the solvent, electrolyte, or reference used, were either not accounted for or simply not reported. Second, the methods of extracting the reduction potential from the resulting cyclic voltammogram (i.e., onset of reduction or half-wave potentials) varied from source to source.

Therefore, an independent CV measurement of PCBM was conducted in this work and the solution phase $E_{1/2}$ was determined under controlled conditions. As shown in Figure 3.1 PCBM exhibits three quasi-reversible reductions in oDCB. The calculated $E_{1/2}$ (defined as $E_{1/2}$=

(E_{pa} + E_{pc})/2 where E_{pa} and E_{pc} are the anodic and cathodic peak potentials respectively) in oDCB is −1.15(1) V versus the $E_{1/2}$ of the internal standard ferrocene. The exact conditions of the electrochemical experiments can be found in the experimental section. This value is in good agreement with several literature values but is significantly different from other reports.[111] Detailed analysis of the experimental conditions in these reports reveals that variations in solvent composition, supporting electrolyte, and electrodes are the most likely sources of the observed discrepancies. It is therefore necessary to fully describe all electrochemical conditions used. A complete discussion of the effects of the experimental conditions on the solution phase $E_{1/2}$ can be found in Chapter 2. To alleviate some of the confusion, reporting the solution phase electrochemical potentials vs. the measured $E_{1/2}$ value of C_{60} under the exact same conditions and with the same electrochemical cell is recommended.

3.1.2. Electrochemical Consequences of the Termal Evaporation of PCBM. As discussed above, PCBM has become the prototypical fullerene acceptor in OPV devices. One of the methods of PCBM deposition in bi-layer OPV devices is thermal evaporation. In this method, a sample of PCBM is heated in a vacuum chamber until it sublimes and subsequently condenses on a substrate positioned above the PCBM. Typically, it is unknown what temperature the sample of PCBM is heated to. The graduate student Bryon Larson, as part of his graduate research, determined that films prepared from PCBM with this method undergo drastic changes to their molecular composition and only 50% of the sublimed material consists of PCBM.

Purity of the donor and acceptor components of an active layer is an important factor in the device performance. It has recently been shown that when found in the active layer, impurities with different reduction potentials can drastically affect the OPV device performance

by introducing so called "trap states" that can hinder electron mobility.[32] Therefore, all of the components of the thermally evaporated film of PCBM were isolated by Bryon Larson using HPLC; these samples were studied in this work by cyclic voltammetry to determine their solution phase electrochemical properties and compared to pristine PCBM.

As shown in the HPLC trace in Figure 3.2, the sublimate from a sample of pristine PCBM was separated into 3 fractions: A (retention time 5.5 – 6.0 minutes), B (retention time 6.0 – 6.8 minutes), and C (the rest of the material eluting at 2.8 – 5.5 min. and 6.8 – 12.0 min.). Fraction A was confirmed by ^{1}H NMR spectroscopy by Bryon Larson to be PCBM whereas fractions B and C were tentatively assigned as products of partial fragmentation or rearrangements. These 3 fractions, along with the pristine commercial PCBM sample, were then analyzed by cyclic voltammetry as shown in Figure 3.1. The voltammogram of fraction A was, as expected, identical to the voltammogram of pristine PCBM. Fraction B exhibited sharp quasi-reversible first and second reductions at the same potentials as PCBM. Fraction C exhibited much broader peaks but with potentials identical to that of pristine PCBM as well. Remarkably, considering how many different components are present in the crude mixture after thermal evaporation, there is no observable difference in the $E_{1/2}{}^{0/-}$ potentials of these three fractions as compared with pristine PCBM, within the ±10 mV experimental error. This evidence indicates that the electronic properties (as derived from CV measurements) of a thermally evaporated PCBM film, albeit partially decomposed, remain mostly unaltered.

3.1.3. Electrochemical Characterization of the OPV Acceptor Indene-C_{60} Adducts. It is generally accepted that the V_{OC} of OPV devices is proportional to the difference between the LUMO energy level of the acceptor and the HOMO energy level of the donor.[30,31,33,112-114]

Therefore, development of fullerenes with higher LUMO levels than PCBM has attracted a lot of attention. Three such fullerenes that have higher LUMO levels than PCBM are a series of three indene-C_{60} multi adducts including indene-C_{60} monoadduct (ICMA), indene-C_{60} bisadduct (ICBA), and indene-C_{60} trisadduct (ICTA) that differ by the number of indene groups bound to the cage. As a result, when these compounds are used as electron acceptors blended with P3HT as the electron donating polymer in OPV devices, the V_{oc} values are 0.65, 0.83, and 0.92 V respectively.[112] However, there was no mention of the compositional or isomeric purity of these three compounds and as previously discussed, both the number and addition pattern of addends can greatly affect the reduction potential of acceptor fullerenes. As part of his graduate research, Bryon Larson analyzed commercially purchased samples of ICMA, ICBA, and ICTA by HPLC chromatography, ^{1}H NMR spectroscopy, and APCI mass specrometery reveling that none of the samples were compositionally or isomerically pure. For example, ICMA contained several isomers of ICBA. Moreover, ICBA was comprised of at least 4 different isomers of ICBA. However, the least pure indene-C_{60} adduct examined was ICTA that contained numerous isomers of ICTA and ICBA.[33]

In this work, cyclic voltammetry was conducted on ICMA, ICBA, and ICTA that were commercially purchased and used without further purification (see Figure 3.3 for structures of indenes). The resulting voltammograms are shown in Figure 3.4. The measured $E_{1/2}$ values in oDCB are −0.21, −0.25, and −0.45 V vs. $C_{60}^{0/-}$ for ICMA, ICBA, and ICTA, respectively. For reference, PCBM measured in the same solvent has an $E_{1/2}$ value of −0.09 V vs. $C_{60}^{0/-}$. The voltammograms also indicate that the impurities in ICMA and ICBA do not greatly affect the solution phase reduction potential. However, the peaks in the voltammogram of ICTA are broadened. There are also some indications of shoulders and weak peaks between the main

peaks. These features in the voltammogram of ICTA are presumably present due to numerous components that are present in the crude material.

3.2. Use of PFAFs in Organic Photovoltaics

3.2.1. Introduction. The large class of trifluoromethyl fullerenes, that differ in the number and position of CF_3 groups and have a wide range of reduction potentials, offers an attractive opportunity to study how various TMFs affect the performance of organic photovoltaic devices because a systematic study can be conducted by tuning the fullerene properties and measuring the resulting device performance. Working in collaboration with Dr. Nikos Kopidakis at the National Renewable Energy Laboratory (NREL), a preliminary study was conducted were the prototypical fullerene acceptor, phenyl-C_{60}-butyric acid methylester (PCBM), was swapped out with different PFAFs. The goal of this study was to determine how the OPV device performance is affected by the number, type and addition pattern of R_F groups of various PFAFs.

In a control experiment, a device was fabricated using the prototypical fullerene acceptor PCBM and poly 3-hexylthiophene (P3HT) as the conjugated polymer electron donating material in a 1:1 by mass blend. A conventional architecture (described in the experimental section and shown in Figure 3.5) was used for this control device. The plot showing the current density (mA/cm^2) vs. applied voltage (V) of this device is shown in Figure 3.6. The power conversion efficiency (PCE) of this device is 4.0% which is expected for this type of device.[115] The open circuit voltage (V_{oc}), which is the voltage of the device without current, was measured to be 0.588 V. This figure is also comparable to published devices that were fabricated with the same

materials and techniques. The short circuit current density (J_{sc}), a measure of the current under no load (shorted), was 9.8 mA/cm^2. Again, this control device exhibits an experimental J_{sc} that is close to the highest performing devices made with these components.[115] The final figure of merit, the so-called fill factor (FF), is the ratio of the experimentally determined maximum power over the theoretical maximum power. The calculated theoretical maximum power is the product of the V_{oc} and J_{sc}. An ideal FF value would be 100%. The FF of the control device was calculated to be 66.5%, which is also comparable to the literature values of these types of devices.[115] The figures of merit of this control device confirm that the device is performing at the level of the highest preforming devices in the literature that were made with the same materials and that our fabrication methods are sound.

Eight different PFAFs were used in this initial screening and are shown in Table 3.1 along with the resulting figures of merit and fabrication methods of the devices that incorporated each PFAF. These PFAFs were chosen to determine if variations in the molecular structures such as the nature, number, or cage size affects the performance of the device. For example, three PFAFs, 1,7-$C_{60}(CF_3)_2$, 1,7-$C_{60}(i\text{-}C_3F_7)_2$, and 1,7-$C_{60}(CF_2C_6F_5)_2$, were chosen because they had the same addition pattern but varied in the length and bulkiness of the R_F groups bound to the cage. The number of CF_3 groups on C_{60} was examined by preparing devices with $C_{60}(CF_3)_2$, and $C_{60}(CF_3)_4$ (60-4-1). In addition, three C_{70} PFAFs were used including $C_{70}(CF_3)_{8,10}$ as well as $C_{70}(s\text{-}C_4F_9)_2$ to determine if the larger cage affected the device performance. In total, 23 devices were fabricated using a conventional architecture and tested.

All 23 conventional OPV devices that were made in this preliminary screening had very low PCE values and other figures of merit. The device which featured $C_{60}(i\text{-}C_3F_7)_2$ as the electron acceptor had a PCE of only 0.076%. The plot showing the current density (mA/cm^2) vs.

applied voltage (V) of this device is shown in Figure 3.7. Due to the multitude of variables associated with each device that could not be controlled or accurately accounted for (such as morphology of the active layer, quality of the thin-film active layer, miscibility of polymer/fullerene, wetting of the substrate, etc.) as well as the similarity of the device figures of merit, no conclusions about how the various fullerene characteristics affect the OPV device performance could be made from the initial trial.

One hypothesis as to why the efficiencies of the PFAF containing devices were so low could be due to the morphology of the active layer. It has been shown that phase separation of donor and acceptor materials in bulk heterojunction OPVs results in a higher concentration of the electron rich fullerenes near the hole transport layer.[116] This distribution of donor and acceptor domains could increase free charge carrier recombination and disfavor charge transport in the direction required in conventional architecture OPVs that were discussed above. The ideal morphology for a conventional OPV device would feature the hole-rich electron-donating material (the conjugated polymer) in contact with the hole transport layer, not the electron-rich fullerene layer.

In order to test this hypothesis, 9 devices were fabricated using an alternative architecture where the electrodes were reversed and is shown in Figure 3.8. In this inverted device architecture a layer of ZnO is deposited, via annealing Zinc acetate, directly on the ITO patterned slide. The active layer is then applied followed by the top electrode. This inverse architecture effectively reverses the electron flow through the device resulting in the ITO acting as the cathode. If the hypothesis about phase separation of donor and acceptor domains is true, then with the inverse design the electron rich PFAF layer would now be in direct contact with the electron transporting ZnO layer and the cathode.

We however did not see any appreciable increase in efficiency with the inverted devices. This result neither confirms nor refutes our hypothesis. Until proven otherwise, it is possible that the PFAFs form a layer on the bottom of the active layer, but other variables can affect the performance of inverted devices such as poor electrode contact, poor band gap offset, too small or too large domain formation, etc.

The results from this study do, however, merit further investigation because even the unoptimized devices with PFAFs in the active layers do function as solar cells, albeit poorly. These initial tests demonstrated the complexity of the design of organic-based solar cells and the need to apply a more systematic approach. Therefore, a more detailed fundamental study about the charge carrier dynamics of active layers containing PFAFs using time resolved microwave conductivity (TRMC) and with different electron donating polymers was conducted by the graduate student Bryon Larson as part of his graduate research.

Experimental for Section 3.2

OPV device fabrication. A PFAF sample and conjugated polymer (usually poly(3-hexylthiophene)) (P3HT) were dissolved in a common organic solvent in a glove box overnight. The solvent, concentration, and ratio of PFAF to polymer varied between tests. Indium tin oxide (ITO) patterned glass slides were first scrubbed with soap and water. The slides were then rinsed with distilled deionized water and placed in an acetone sonic bath for 5 minutes. The slide was then dried with compressed nitrogen and placed in an isopropyl alcohol sonic bath for another 5 minutes. The slides were again dried using compressed nitrogen and placed in an O_2 plasma

etching system for 5 minutes. The slides were covered by 250 uL of PEDOT:PSS and spin coated at 600 rpm with a ramp speed of 300 rpm/ second for 1 minute. This process was repeated another time in order to slightly thicken the PEDOT:PSS layer. The slides were then transferred to a glove box where the active layer was applied. A 250 uL sample of the active layer solution that was previously prepared and allowed to stir in the glove box overnight, was spin coated on the slide at 600 rpm for 1 min. Slides then went though a variety of different annealing procedures. Once the slides were annealed, the contacts were scraped clean of active layer using a razor blade. Slides were transferred in an inert atmosphere into a metal evaporation chamber. The desired electrode metal was loaded into a resistive heating boat. The chamber was evacuated until a pressure below 6.00×10^{-8} Torr had been reached. The metal was then heated and deposited on the active layer. Thickness and deposition rate of the metal was varied depending on electrode composition. The completed devices were immediately transferred into another glove box and characterized on a solar simulator. All devices made were 0.11 cm^2.

"Inverted" device fabrication. Preparation and cleaning of the slides was identical to previously described method. Once slides were cleaned, Zinc acetate was spin coated on an ITO patterned side of the slide. The slide was heated at 120° C for 1 hour to afford Zinc Oxide. The subsequent steps are identical to the previous method. The completed slides were allowed to age in the dark under an air atmosphere for up to 1 month and routinely tested to monitor device degradation.

OPV Device Measurement. The device performance of individual OPV cells was determeined on a home built solar simulator. This device consisted of a lamp that emitted a spectrum similar to the solar spectrum and had an intensity of 1 sun. The power input at the device level was equal to 100 mW/cm^2. The device contacts were connected to a potentiostat and

controlled by a Lab View program. Light and dark currents were measured while sweeping though a forward and reverse voltage bias of 1 volt with the solar lamp on and off respectively. The resulting light and dark current density (mA/cm^2) vs. voltage (V) plots were created. From this data the open circuit voltage (V_{oc}), the short circuit current density (J_{sc}), the fill factor (a ratio of the theoretical maximum power output to the experimental maximum power output), and the PCE was calculated. Power conversion efficiencies were calculated using the accepted formula (($V_{oc} \times J_{sc} \times FF$)/area of the device)/100 mW/cm^2.

Conclusions

Under carefully controlled conditions, an electrochemical study was conducted on PCBM and the solution phase $E_{1/2}$ value was determined. This value was compared to the multitude of values reported in the literature and it was determined that poor reporting of the electrochemical conditions used or simply interpreting the data incorrectly resulted in confusion about the electrochemical properties of PCBM. The electrochemical effects of thermally decomposed PCBM were studied revealing that although PCBM undergoes partial decomposition and fragmentation, the electrochemical properties remain largely unaffected. The commercially purchased indene-C$_{60}$ mono-, bis-, and tris- adducts exhibited varying reduction potentials that are 0.21, 0.25, and 0.45 V more negative than C$_{60}$ respectively. The Cyclic voltammetry data from the latter two compounds confirmed that they consisted of multiple components with slightly varying $E_{1/2}$ values. Lastly, a screening of 32 OPV devices fabricated with different

197

PFAFs in the active layer indicated that, although the devices prepared in this chapter exhibited a

low PCE, a more detailed fundamental study is warranted.
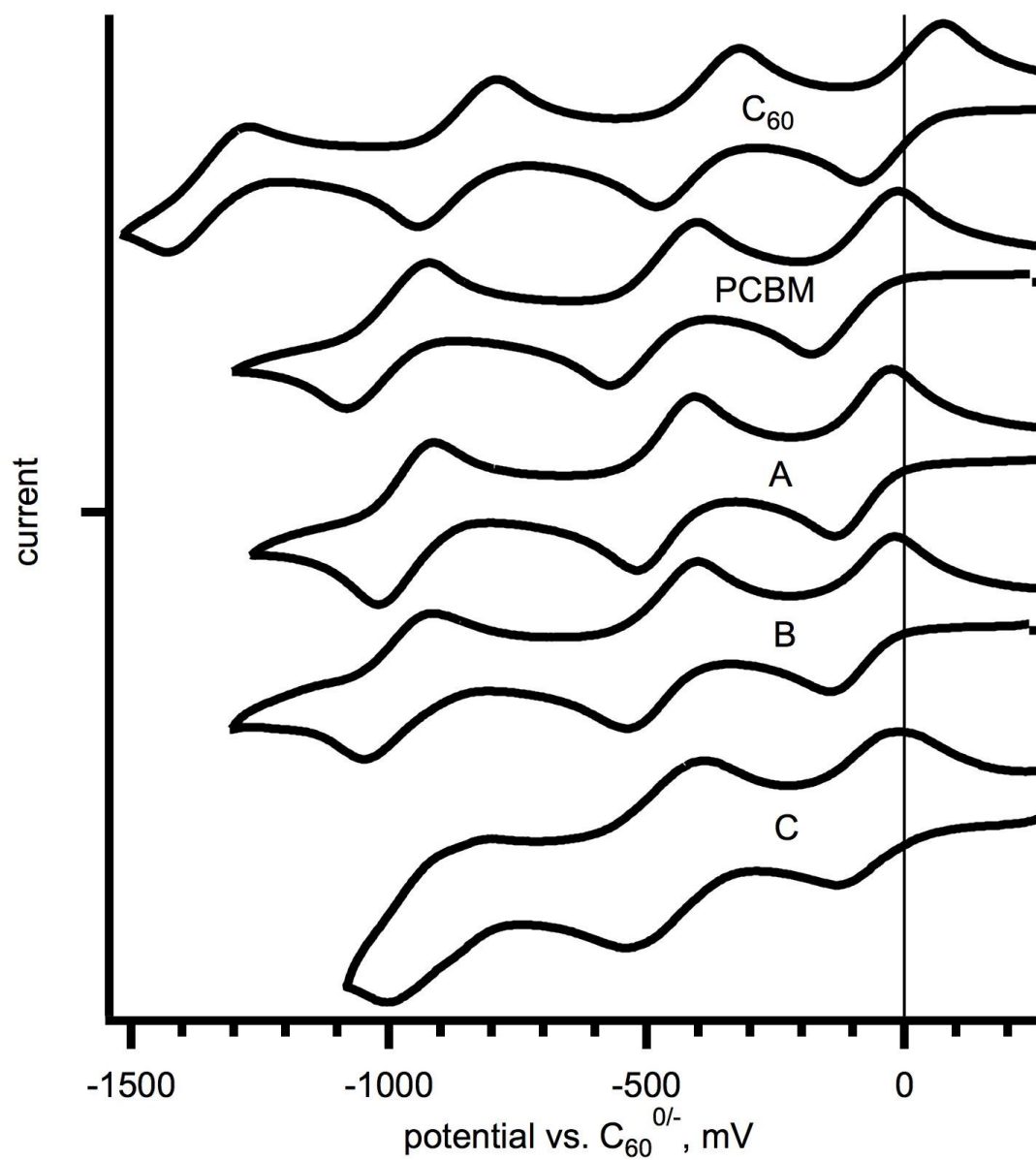
Figure 3.1. Cyclic voltammograms recorded in oDCB of PCBM and the HPLC isolated fractions A, B, and C. The supporting electrolyte was $TBABF_4$ and the scan rate for each voltammogram was 10 mV/sec.
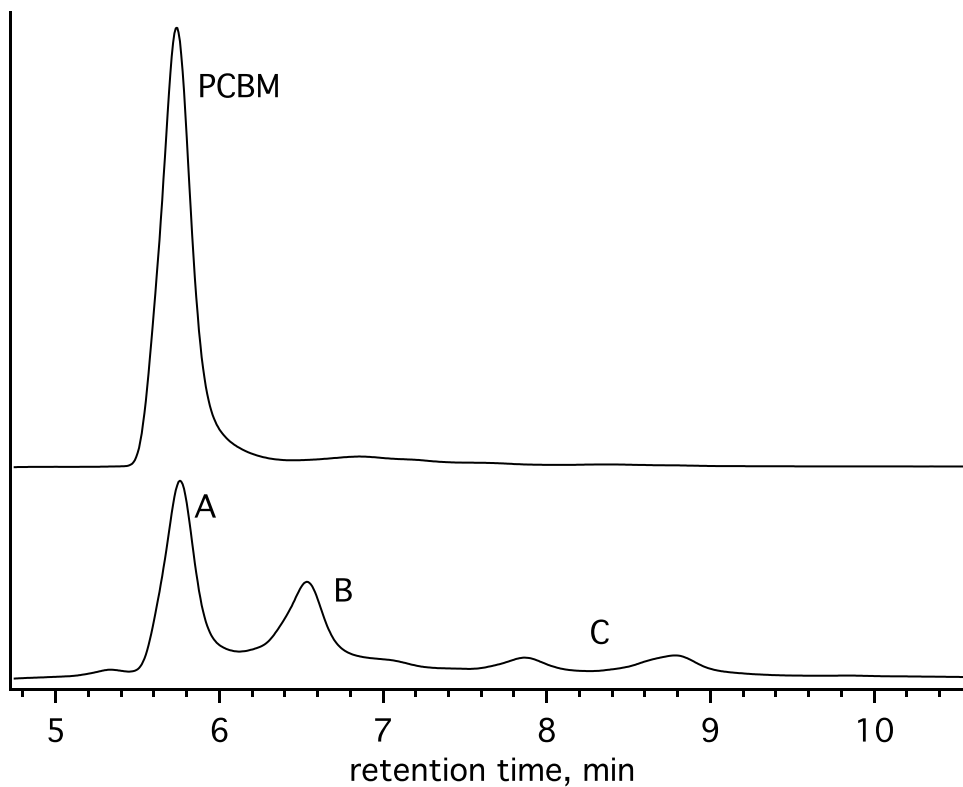
Figure 3.2. HPLC chromatograms (250 x 10mm. i.d. Cosmosil Buckyprep, 5 ml/min, 300 nm) of pristine PCBM (top) and the sublimed crude material collected after thermal evaporation of PCBM (bottom).
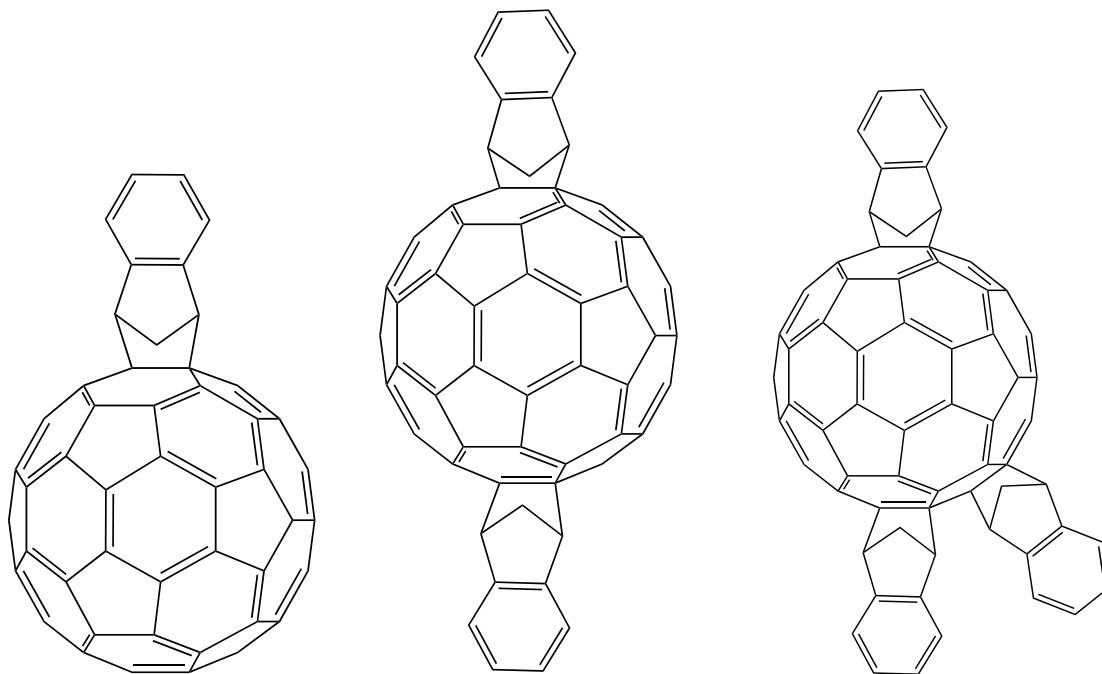
Figure 3.3. Structure of indene-C$_{60}$ mono-adduct (left), bis-adduct (middle) and tris-adduct (right). These structures represent only one of the possible isomers of each compound.
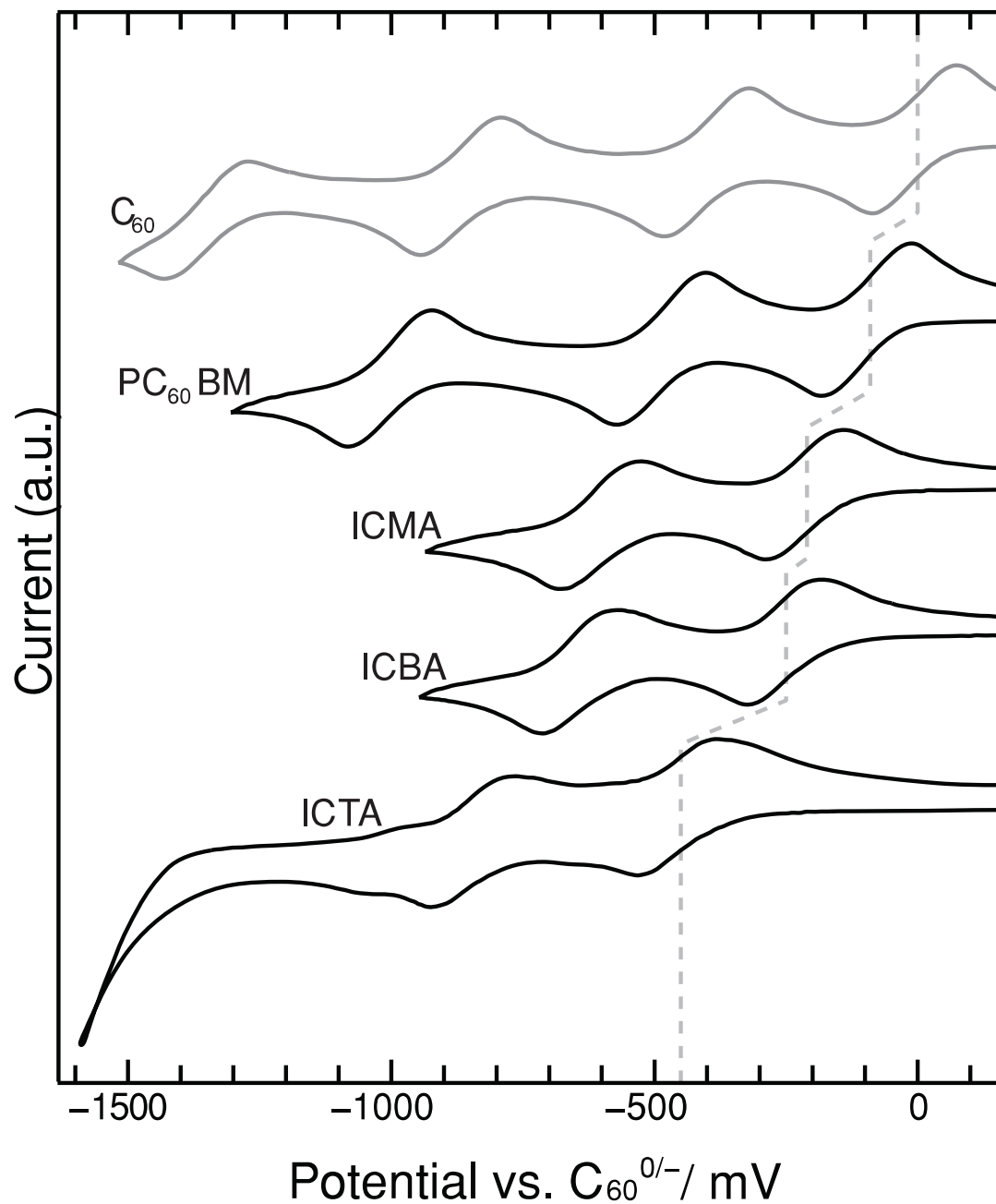
Figure 3.4. Cyclic voltammograms of C_{60}, PCBM, and three C_{60}-indene multi-adducts recorded in oDCB. Dashed line indicates the $E_{1/2}$ of each compound. The supporting electrolyte for each scan was $TBABF_4$ and the scan rate was 100 mV/sec.
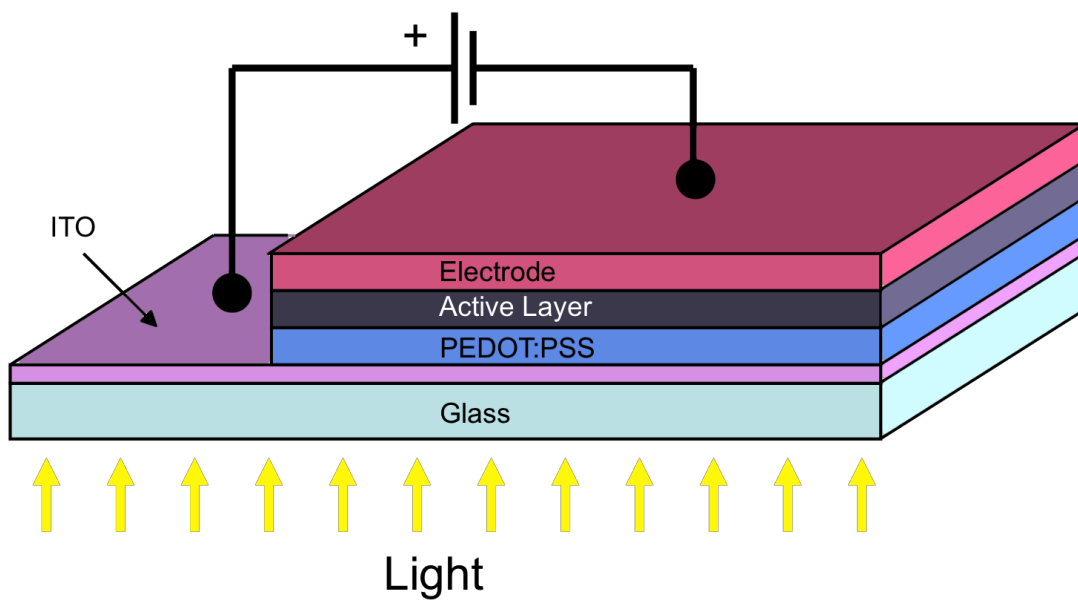
Figure 3.5. Architecture of a conventional OPV device.
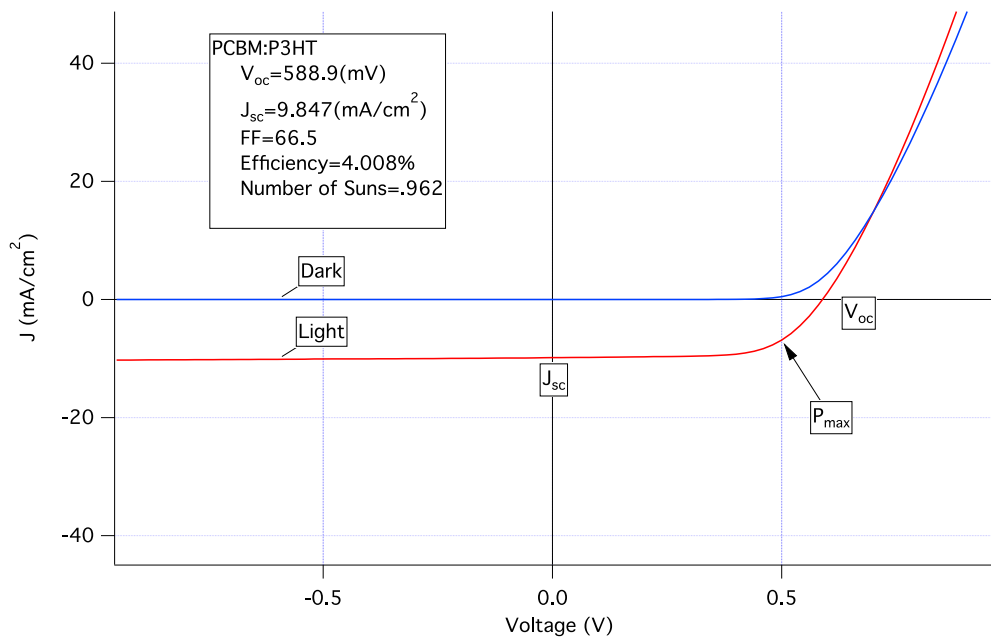
Figure 3.6. Plot of the current density (mA/cm^2) vs. the applied potential (mV) of a bulk heterojunction P3HT: PCBM OPV device.
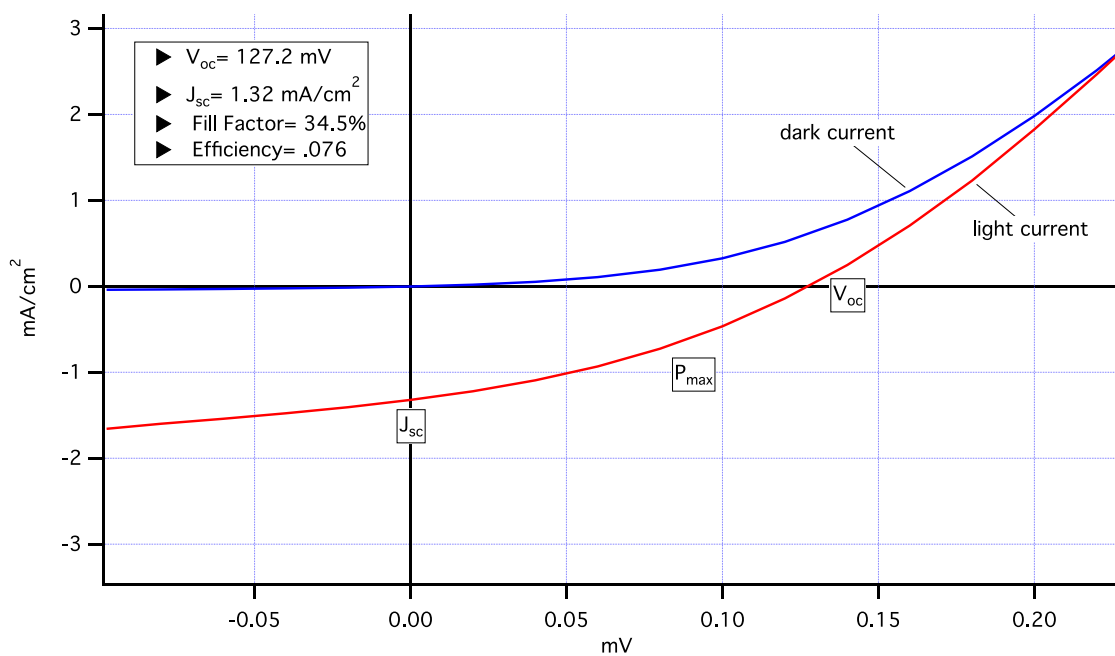
Figure 3.7. Plot of the current density (mA/cm^2) vs. the applied potential (mV) of a bulk heterojunction P3HT: C$_{70}$(CF$_3$)$_2$ OPV device.
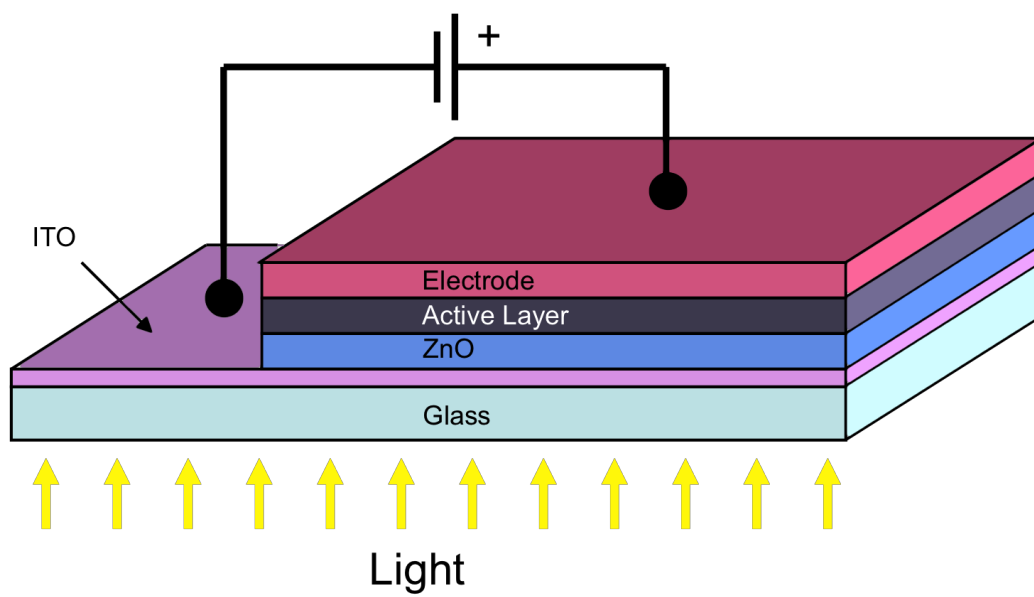
Figure 3.8. Architecture of an inverse OPV device.

Table 3.1

fullerene: polymer	V_{oc}, mV	J_{sc}, mA/cm^2	fill factor	Efficiency
$C_{60}(CF_3)_2$:P3HT	90.8	0.127	27	0.003
$C_{60}(CF_3)_4$:P3HT	37.6	0.264	27.7	0.003
$C_{60}(i\text{-}C_3F_7)_2$:P3HT	235.2	0.786	34.9	0.067
$C_{60}(i\text{-}C_3F_7)_4$:P3HT	60.7	0.163	28.1	0.003
$C_{60}(i\text{-}C_3F_7)_2$:P3HT	89.3	0.085	26.3	0.002
$C_{60}(i\text{-}C_3F_7)_2$:P3HT	128.3	1.11	31.1	0.044
$C_{60}(i\text{-}C_3F_7)_2$:P3HT	133.8	0.555	29.5	0.022
$C_{60}(i\text{-}C_3F_7)_2$:P3HT	67.6	0.065	28	0.001
$C_{60}(CF_3)_4$:P3HT	189.3	0.175	24	0.011
$C_{70}(i\text{-}C_4F_9)_2$:P3HT	127.2	1.321	34.5	0.076
$C_{60}(CF_3)_2$:P3HT	240.9	0.328	35.9	0.036
$C_{70}(CF_3)_8$:ZZ-50	47.1	0.036	24.9	0.001
$C_{70}(CF_3)_8$:ZZ-50	216.6	0.227	29.6	0.019
$C_{70}(CF_3)_{10}$:ZZ-50	61.5	0.155	23.7	0.003
PCBM:P3HT	66.3	0.057	29	0.001

References

(1)   Kareev, I. E.; Shustova, N. B.; Kuvychko, I. V.; Lebedkin, S. F.; Miller, S. M.;
       Anderson, O. P.; Popov, A. A.; Strauss, S. H.; Boltalina, O. V. *J. Am. Chem. Soc.* **2006**,
       128, 12268–12280.

(2)   Popov, A. A.; Kareev, I. E.; Shustova, N. B.; Stukalin, E. B.; Lebedkin, S. F.; Seppelt,
       K.; Strauss, S. H.; Boltalina, O. V.; Dunsch, L. *J. Am. Chem. Soc.* **2007**, *129*, 11551–
       11568.

(3)   Popov, A. A.; Shustova, N. B.; Boltalina, O. V.; Strauss, S. H.; Dunsch, L.
       ChemPhysChem **2008**, *9*, 431–438.

(4)   Takano, Y.; Herranz, M. Á.; Martin, N.; de Miguel Rojas, G.; Guldi, D. M.; Kareev, I.
       E.; Strauss, S. H.; Boltalina, O. V.; Tsuchiya, T.; Akasaka, T. *Chem. Eur. J.* **2010**,
       NA–NA.

(5)   Takano, Y.; Herranz, M. Á.; Kareev, I. E.; Strauss, S. H.; Boltalina, O. V.; Akasaka,
       T.; Martin, N. *J. Org. Chem.* **2009**, *74*, 6902–6905.

(6)   Popov, A. A.; Kareev, I. E.; Shustova, N. B.; Lebedkin, S. F.; Strauss, S. H.; Boltalina,
       O. V.; Dunsch, L. *Chem. Eur. J.* **2008**, *14*, 107–121.

(7)   Dorozhkin, E. I.; Ignat'eva, D. V.; Tamm, N. B.; Goryunkov, A. A.; Khavrel, P. A.;
       Ioffe, I. N.; Popov, A. A.; Kuvychko, I. V.; Streletskiy, A. V.; Markov, V. Y.; Spandl,
       J.; Strauss, S. H.; Boltalina, O. V. *Chem. Eur. J.* **2006**, *12*, 3876–3889.

(8)   Goryunkov, A.; Kuvychko, I.; Ioffe, I. *Journal of Fluorine Chemistry* **2003**.

(9)   Kareev, I. E.; Kuvychko, I. V.; Lebedkin, S. F.; Miller, S. M.; Anderson, O. P.; Seppelt,
       K.; Strauss, S. H.; Boltalina, O. V. *J. Am. Chem. Soc.* **2005**, *127*, 8362–8375.

(10)   Troyanov, S. I.; Dimitrov, A.; Kemnitz, E. *Angew. Chem. Int. Ed.* **2006**, *45*, 1971–
         1974.

(11)   Kareev, I. E.; Lebedkin, S. F.; Bubnov, V. P.; Yagubskii, E. B.; Ioffe, I. N.; Khavrel, P.
         A.; Kuvychko, I. V.; Strauss, S. H.; Boltalina, O. V. *Angew. Chem. Int. Ed.* **2005**, *44*,
         1846–1849.

(12)   Shustova, N. B.; Popov, A. A.; Mackey, M. A.; Coumbe, C. E.; Phillips, J. P.;
         Stevenson, S.; Strauss, S. H.; Boltalina, O. V. *J. Am. Chem. Soc.* **2007**, *129*, 11676–
         11677.

(13)   Troyanov, S. I.; Goryunkov, A. A.; Dorozhkin, E. I.; Ignat'eva, D. V.; Tamm, N. B.;
         Avdoshenko, S. M.; Ioffe, I. N.; Markov, V. Y.; Sidorov, L. N.; Scheurel, K.; Kemnitz,
         E. *Journal of Fluorine Chemistry* **2007**, *128*, 545–551.

(14)   Popov, A. A.; Tarábek, J.; Kareev, I. E.; Lebedkin, S. F.; Strauss, S. H.; Boltalina, O.
         V.; Dunsch, L. *J. Phys. Chem. A* **2005**, *109*, 9709–9711.

(15)   Fagan, P. J.; Krusic, P. J.; McEwen, C. N.; Lazar, J.; Parker, D. H.; Herron, N.;
         Wasserman, E. *Science* **1993**, *262*, 404–407.

(16)   Darwish, A. D.; Abdul-Sada, A. K.; Avent, A. G.; Lyakhovetsky, V. I.; Shilova, E. A.;
         Taylor, R. *Org. Biomol. Chem.* **2003**, *1*, 3102–3110.

(17)   Goryunkov, A.; Ioffe, I.; Kuvychko, I.; Yankova, T.; Markov, V.; Streletskii, A.; Dick,
         D.; Sidorov, L.; Boltalina, O.; Strauss, S. *Fullerene Nanot Carbon Nanostruct* **2004**, *12*,
         181–185.

(18)   Goryunkov, A. A.; Ignat'eva, D. V.; Tamm, N. B.; Moiseeva, N. N.; Ioffe, I. N.;
         Avdoshenko, S. M.; Markov, V. Y.; Sidorov, L. N.; Kemnitz, E.; Troyanov, S. I. *Eur. J.
         Org. Chem.* **2006**, 2508–2512.

(19)   Kareev, I. E.; Kuvychko, I. V.; Lebedkin, S. F.; Miller, S. M.; Anderson, O. P.; Seppelt, K.; Strauss, S. H.; Boltalina, O. V. *J. Am. Chem. Soc.* **2005**, *127*, 8362–8375.

(20)   Kareev, I. E.; Kuvychko, I. V.; Lebedkin, S. F.; Miller, S. M.; Anderson, O. P.; Strauss, S. H.; Boltalina, O. V. *Chem. Commun.* **2006**, 308.

(21)   Cardona, C. M.; Kitaygorodskiy, A.; Echegoyen, L. *J. Am. Chem. Soc.* **2005**, *127*, 10448–10453.

(22)   Shu, C.; Cai, T.; Xu, L.; Zuo, T.; Reid, J.; Harich, K.; Dorn, H. C.; Gibson, H. W. *J. Am. Chem. Soc.* **2007**, *129*, 15710–15717.

(23)   Shustova, N. B.; Kuvychko, I. V.; Peryshkov, D. V.; Whitaker, J. B.; Larson, B. W.; Chen, Y.-S.; Dunsch, L.; Seppelt, K.; Popov, A. A.; Strauss, S. H.; Boltalina, O. V. *Chem. Commun.* **2011**, *47*, 875–877.

(24)   Shustova, N. B.; Kareev, I. E.; Kuvychko, I. V.; Whitaker, J. B.; Lebedkin, S. F.; Popov, A. A.; Dunsch, L.; Chen, Y.-S.; Seppelt, K.; Strauss, S. H. *Journal of Fluorine Chemistry* **2010**, *131*, 1198–1212.

(25)   Kuvychko, I. V.; Shustova, N. B.; Avdoshenko, S. M.; Popov, A. A.; Strauss, S. H.; Boltalina, O. V. *Chem. Eur. J.* **2011**, *17*, 8799–8802.

(26)   Kuvychko, I. V.; Whitaker, J. B.; Larson, B. W.; Folsom, T. C.; Shustova, N. B.; Avdoshenko, S. M.; Chen, Y. S.; Wen, H.; Wang, X.-B.; Dunsch, L.; Popov, A. A.; Boltalina, O. V.; Strauss, S. H. *Chem. Sci.* **2012**, *3*, 1399–1407.

(27)   Kuvychko, I. V.; Strauss, S. H.; Boltalina, O. V. *Journal of Fluorine Chemistry* **2012**, *143*, 103–108.

(28)   Chiu, M.-Y.; Jeng, U.-S.; Su, M.-S.; Wei, K.-H. *Macromolecules* **2010**, *43*, 428–432.

(29)   Olson, D. C.; Lee, Y.-J.; White, M. S.; Kopidakis, N.; Shaheen, S. E.; Ginley, D. S.;

Voigt, J. A.; Hsu, J. W. P. *J. Phys. Chem. C* **2008**, *112*, 9544–9547.

(30)   Cardona, C. M.; Li, W.; Kaifer, A. E.; Stockdale, D.; Bazan, G. C. *Adv. Mater.* **2011**, *23*, 2367–2371.

(31)   Matsuo, Y. *Pure Appl. Chem.* **2012**, *84*, 945–952.

(32)   Coffey, D. C.; Larson, B. W.; Hains, A. W.; Whitaker, J. B.; Kopidakis, N.; Boltalina, O. V.; Strauss, S. H.; Rumbles, G. *J. Phys. Chem. C* **2012**, *116*, 8916–8923.

(33)   Nardes, A. M.; Ferguson, A. J.; Whitaker, J. B.; Larson, B. W.; Larsen, R. E.; Maturová, K.; Graf, P. A.; Boltalina, O. V.; Strauss, S. H.; Kopidakis, N. *Adv. Funct. Mater.* **2012**, n/a–n/a.

(34)   Kadish, K. M.; Gao, X.; Caemelbecke, E. V.; Suenobu, T.; Fukuzumi, S. *J. Phys. Chem. A* **2000**, *104*, 3878–3883.

(35)   Murata, Y.; Shiro, M.; Komatsu, K. *J. Am. Chem. Soc.* **1997**, *119*, 8117–8118.

(36)   Kareev, I. E.; Quiñones, G. S.; Kuvychko, I. V.; Khavrel, P. A.; Ioffe, I. N.; Goldt, I. V.; Lebedkin, S. F.; Seppelt, K.; Strauss, S. H.; Boltalina, O. V. *J. Am. Chem. Soc.* **2005**, *127*, 11497–11504.

(37)   Balch, A. L.; Costa, D. A.; Noll, B. C.; Olmstead, M. M. *J. Am. Chem. Soc.* **1995**, *117*, 8926–8932.

(38)   Heymann, D.; Weisman, R. B. *C. R. Chimie.* **2006**, *9*, 1107–1116.

(39)   Weisman, R. B.; Heymann, D.; Bachilo, S. M. *J. Am. Chem. Soc.* **2001**, *123*, 9720–9721.

(40)   Tajima, Y.; Takeuchi, K. *J. Org. Chem.* **2002**, *67*, 1696–1698.

(41)   Matsuo, Y.; Ozu, A.; Obata, N.; Fukuda, N.; Tanaka, H.; Nakamura, E. *Chem. Commun.* **2012**, *48*, 3878–3880.

(42)   Matsuo, Y.; Nakamura, E. *J. Am. Chem. Soc.* **2005**, *127*, 8457–8466.

(43)   Kuvychko, I. V.; Streletskii, A. V.; Popov, A. A.; Kotsiris, S. G.; DREWELLO, T.; Strauss, S. H.; Boltalina, O. V. *Chem. Eur. J.* **2005**, *11*, 5426.

(44)   Dorozhkin, E. I.; Goryunkov, A. A.; Ioffe, I. N.; Avdoshenko, S. M.; Markov, V. Y.; Tamm, N. B.; Ignat'eva, D. V.; Sidorov, L. N.; Troyanov, S. I. *European Journal of Organic Chemistry* **2007**, *2007*, 5082–5094.

(45)   Isobe, H.; Tomita, N.; Nakamura, E. *Org. Lett.* **2000**, *2*, 3663–3665.

(46)   Kennedy, R. D.; Halim, M.; Khan, S. I.; Schwartz, B. J.; Tolbert, S. H.; Rubin, Y. *Chem. Eur. J.* **2012**, 7418–7433.

(47)   Shustova, N. B.; Kuvychko, I. V.; Popov, A. A.; Delius, von, M.; Dunsch, L.; Anderson, O. P.; Hirsch, A.; Strauss, S. H.; Boltalina, O. V. *Angew. Chem. Int. Ed.* **2011**, *50*, 5537–5540.

(48)   Hirsch, A.; Brettreich, M.; Wudl, F. *Fullerenes: Chemistry and Reactions*; 1st ed. Wiley-VCH, 2005.

(49)   Creegan, K.; Robbins, J.; Robbins, W. *J. Am. Chem. Soc.* **1992**.

(50)   Shigemitsu, Y.; Kaneko, M.; Tajima, Y.; Takeuchi, K. *Chem. Lett.* **2004**, *33*, 1604–1605.

(51)   Huang, S.; Xiao, Z.; Wang, F.; Zhou, J.; Yuan, G.; Zhang, S.; Chen, Z.; Thiel, W.; Schleyer, P. V. R.; Zhang, X.; Hu, X.; Chen, B.; Gan, L. *Chem. Eur. J.* **2005**, *11*, 5449–5456.

(52)   Huang, S.; Yang, X.; Zhang, X.; Hu, X.; Gan, L.; Zhang, S. *Synlett* **2006**, *2006*, 1266–1268.

(53)   Tajima, Y.; Hara, T.; Honma, T.; Matsumoto, S.; Takeuchi, K. *Org. Lett.* **2006**, *8*,

3203–3205.

(54)   Jia, Z.; Zhang, X.; Zhang, G.; Huang, S.; Fang, H.; Hu, X.; Li, Y.; Gan, L.; Zhang, S.; Zhu, D. *Chem Asian J* **2007**, *2*, 290–300.

(55)   Zhang, Q.; Pankewitz, T.; Liu, S.; Klopper, W.; Gan, L. *Angew. Chem. Int. Ed.* **2010**, *49*, 9935–9938.

(56)   Blackett, B. N.; Coxon, J. M.; Hartshorn, M. P.; Lewis, A. J.; Little, G. R.; Wright, G. J. *Tetrahedron* **1970**, *26*, 1311–1313.

(57)   Xiao, Z.; Yao, J.; Yang, D.; Wang, F.; Huang, S.; Gan, L.; Jia, Z.; Jiang, Z.; Yang, X.; Zheng, B.; Yuan, G.; Zhang, S.; Wang, Z. *J. Am. Chem. Soc.* **2007**, *129*, 16149–16162.

(58)   Xiao, Z.; Yao, J.; Yu, Y.; Jia, Z.; Gan, L. *Chem. Commun.* **2010**, *46*, 8365.

(59)   Jiang, Z.; Zhang, Y.; Gan, L.; Wang, Z. *Tetrahedron* **2008**, *64*, 11394–11403.

(60)   Gan, L.; Yang, D.; Zhang, Q.; Huang, H. *Adv. Mater.* **2010**, *22*, 1498–1507.

(61)   *Organic Photovoltaics: Materials, Device Physics, and Manufacturing Technologies*; Brabec, C.; Scherf, U.; Dyakonov, V., Eds. 1st ed. Wiley-VCH, 2008.

(62)   Shaheen, S. E.; Ginley, D. S.; Jabbour, G. E. *MRS bulletin* **2005**, *30*, 10–19.

(63)   Avdoshenko, S. M.; Ioffe, I. N.; Sidorov, L. N. *J. Phys. Chem. A* **2009**, *113*, 10833–10838.

(64)   Ignat'eva, D. V.; Mutig, T.; Goryunkov, A. A.; Tamm, N. B.; Kemnitz, E.; Troyanov, S. I.; Sidorov, L. N. *Russ Chem Bull* **2010**, *58*, 1146–1154.

(65)   Mutig, T.; Kemnitz, E.; Troyanov, S. I. *Mendeleev Communications* **2009**, *19*, 30–31.

(66)   Goryunkov, A. A.; Dorozhkin, E. I.; Tamm, N. B.; Ignat'eva, D. V.; Avdoshenko, S. M.; Sidorov, L. N.; Troyanov, S. I. *Mendeleev Commun.* **2007**, *17*, 110–112.

(67)   Rispens, M. T.; Meetsma, A.; Rittberger, R.; Brabec, C. J.; Sariciftci, N. S.; Hummelen,

J. C. *Chem. Commun.* **2003**, 2116.

(68)   Kennedy, R. D.; Ayzner, A. L.; Wanger, D. D.; Day, C. T.; Halim, M.; Khan, S. I.;

Tolbert, S. H.; Schwartz, B. J.; Rubin, Y. *J. Am. Chem. Soc.* **2008**, *130*, 17290–17292.

(69)   Niinomi, T.; Matsuo, Y.; Hashiguchi, M.; Sato, Y.; Nakamura, E. *J. Mater. Chem.*
2009, *19*, 5804.

(70)   Haddon, R. C.; Brus, L. E.; Raghavachari, K. *Chem. Phys. Lett.* **1986**, *125*, 459–464.

(71)   Xie, Q.; Perez-Cordero, E.; Echegoyen, L. *J. Am. Chem. Soc.* **1992**, *114*, 3978–3980.

(72)   Dubois, D.; Kadish, K. M.; Flanagan, S.; Wilson, L. J. *J. Am. Chem. Soc.* **1991**, *113*,
7773–7774.

(73)   Echegoyen, L.; Echegoyen, L. E. *Acc. Chem. Res.* **1998**, *31*, 593–601.

(74)   Lichtenberger, D. L.; Nebesny, K. W.; Ray, C. D. **1991**, *126*, 203–208.

(75)   Xie, Q.; Arias, F.; Echegoyen, L. *J. Am. Chem. Soc.* **1993**, *115*, 9818–9819.

(76)   Feldberg, S. W. *Journal of Electroanal. Chem.* **2008**, *624*, 45–51.

(77)   Tsierkezos, N. G. *J. Solution Chem.* **2007**, *36*, 289–302.

(78)   Zheng, M.; Li, F.-F.; Ni, L.; Yang, W.-W.; Gao, X. *J. Org. Chem.* **2008**, *73*, 3159–
3168.

(79)   Hammett, L. P. *Chemical Reviews* **1935**, *17*, 125–136.

(80)   Hansch, C.; Leo, A.; Taft, R. W. *Chemical Reviews* **1991**, *91*, 165–195.

(81)   Charton, M. *J. Am. Chem. Soc.* **1975**, *97*, 1552–1556.

(82)   Marzilli, L. G.; Bayo, F.; Summers, M. F.; Thomas, L. B.; Zangrando, E.; Bresciani-

Pahor, N.; Mari, M.; Randaccio, L. *J. Am. Chem. Soc.* **1987**, *109*, 6045–6052.

(83)   Bunten, K. A.; Chen, L.; Fernandez, A. L.; Poë, A. J. *Coordination chemistry reviews*
2002, *233*, 41–51.

(84)   Brown, T. L.; Lee, K. J. *Coordination chemistry reviews* **1993**, *128*, 89–116.

(85)   Simón-Manso, Y. *J. Phys. Chem. A* **2005**, *109*, 2006–2011.

(86)   Agrafiotis, D. K.; Shemanarev, M.; Connolly, P. J.; Farnum, M.; Lobanov, V. S. *J. Med. Chem.* **2007**, *50*, 5926–5937.

(87)   Do, J. Y.; Park, S. K.; Ju, J. J.; Park, S.; Lee, M. H. *Optical Materials* **2004**, *26*, 223–229.

(88)   Espeso, J.; Lozano, A. E.; la Campa, de, J. G.; de Abajo, J. *Journal of Membrane Science* **2006**, *280*, 659–665.

(89)   Babazadeh, M. *J. Appl. Polym. Sci.* **2006**, *102*, 633–639.

(90)   Justin Thomas, K. R.; Lin, J. T.; Tao, Y.-T.; Chuen, C.-H. *Chem. Mater.* **2004**, *16*, 5437–5444.

(91)   Brabec, C. J.; Gowrisanker, S.; Halls, J. J. M.; Laird, D.; Jia, S.; Williams, S. P. *Adv. Mater.* **2010**, *22*, 3839–3856.

(92)   Lemal, D. M. *J. Org. Chem.* **2004**, *69*, 1–11.

(93)   Corvaja, C.; Farnia, G.; Formenton, G.; Navarrini, W.; Sandona, G.; Tortelli, V. *The Journal of Physical Chemistry* **1994**, *98*, 2307–2313.

(94)   Combellas, C.; Kanoufi, F.; Thiébault, A. *J. Phys. Chem. B* **2003**, *107*, 10894–10905.

(95)   Yuan, Z.; Li, J.; Xiao, Y.; Li, Z.; Qian, X. *J. Org. Chem.* **2010**, *75*, 3007–3016.

(96)   Li, Y.; Li, C.; Yue, W.; Jiang, W.; Kopecek, R.; Qu, J.; Wang, Z. *Org. Lett.* **2010**, *12*, 2374–2377.

(97)   Ruoff, R. S.; Kadish, K. M.; Boulas, P.; Chen, E. *The Journal of Physical Chemistry* **2001**, *99*, 8843–8850.

(98)   Djurovich, P. I.; Mayo, E. I.; Forrest, S. R.; Thompson, M. E. *Organic Electronics*

2009, *10*, 515–520.

(99)   Doubois, D.; Moninot, G.; Kutner, W.; Jones, M. T.; Kadish, K. *The Journal of Physical Chemistry* **1992**, *96*, 7137.

(100)   Dixon, D. A.; Matsuzawa, N.; Fukunaga, T.; Tebbe, F. N. *The Journal of Physical Chemistry* **1992**, *96*, 6107–6110.

(101)   Kuvychko, I. V.; Strauss, S. H.; Boltalina, O. V. In *Efficient Preparation of Fluorine Compounds*; Wiley: New York, 2013; pp. 9–11.

(102)   Bonifazi, D.; Enger, O.; Diederich, F. O. *Chem. Soc. Rev.* **2007**, *36*, 390.

(103)   Matsuo, Y.; Iwashita, A.; Abe, Y.; Li, C.-Z.; Matsuo, K.; Hashiguchi, M.; Nakamura, E. *J. Am. Chem. Soc.* **2008**, *130*, 15429–15436.

(104)   Kennedy, R. D.; Ayzner, A. L.; Wanger, D. D.; Day, C. T.; Halim, M.; Khan, S. I.; Tolbert, S. H.; Schwartz, B. J.; Rubin, Y. *J. Am. Chem. Soc.* **2008**, *130*, 17290–17292.

(105)   Pope, M.; Swenberg, C. E. *Electronic processes in organic crystals and polymers*; Oxford University Press, USA, 1999.

(106)   Sawamura, M.; Kawai, K.; Matsuo, Y.; Kanie, K.; Kato, T.; Nakamura, E. *Nature* **2002**, *419*, 702–705.

(107)   Bashilov, V. V.; Dolgushin, F. M.; Tumanskii, B. L.; Petrovskii, P. V.; Sokolov, V. I. *Tetrahedron* **2008**, *64*, 11291–11295.

(108)   Ignat'eva, D. V.; Ioffe, I. N.; Troyanov, S. I.; Sidorov, L. N. *Russ. Chem. Rev.* **2011**, *80*, 631–645.

(109)   Green, M. A.; Emery, K.; Hisikawa, Y.; Warta, W. *Prog. Photovolt: Res. Appl.* **2007**, *15*, 425–430.

(110)   Green, M. A.; Emery, K.; Hishikawa, Y.; Warta, W.; Dunlop, E. D. *Prog. Photovolt:*

Res. Appl. **2011**, *19*, 565–572.

(111)   Larson, B. W.; Whitaker, J. B.; Wang, X.-B.; Popov, A. A.; Rumbles, G.; Kopidakis, N.; Strauss, S. H.; Boltalina, O. V. *J. Phys. Chem. C* **2013**, *117*, 14958–14964.

(112)   Kang, H.; Cho, C.-H.; Cho, H.-H.; Kang, T. E.; Kim, H. J.; Kim, K.-H.; Yoon, S. C.; Kim, B. J. *ACS Appl. Mater. Interfaces* **2012**, *4*, 110–116.

(113)   He, Y.; Chen, H.-Y.; Hou, J.; Li, Y. *J. Am. Chem. Soc.* **2010**, *132*, 1377–1382.

(114)   Brabec, C. J.; Cravino, A.; Meissner, D.; Sariciftci, N. S.; Fromherz, T.; Rispens, M. T.; Sanchez, L.; Hummelen, J. C. *Adv. Funct. Mater.* **2001**, *11*, 374–380.

(115)   Li, G.; Shrotriya, V.; Huang, J.; Yao, Y.; Moriarty, T.; Emery, K.; Yang, Y. *Nat Mater* **2005**, *4*, 864–868.

(116)   Wang, J.-C.; Weng, W.-T.; Tsai, M.-Y.; Lee, M.-K.; Horng, S.-F.; Perng, T.-P.; Kei, C.-C.; Yu, C.-C.; Meng, H.-F. *J. Mater. Chem.* **2010**, *20*, 862.